Quasiclassical trajectory study of D+HH and H+HD

Glen J. McNamara

B.Sc., University of Northern British Columbia, 2004

Thesis Submitted in Partial Fulfillment of

The Requirements for the Degree of
Master of Science
in
Mathematical, Computer and Physical Sciences (Chemistry)

The University of Northern British Columbia

June 2010

Your file Votre référence
ISBN: 978-0-494-75112-1
Our file Notre référence
ISBN: 978-0-494-75112-1

Abstract

An examination of the dynamical behaviour of H + HD and D + H_2 in the ground electronic state is performed on the BKMP2 potential energy surface [J. Chem. Phys. **104**, 7139 (1996)] using the quasiclassical trajectory method. The complete set of state–to–state energy transfer and state–specific dissociative cross sections and thermal rate coefficients has been obtained for both systems. Comparisons are made to the H + H_2 system to investigate isotopic effects on reactivity and energy transfer. Collision–induced dissociation, exchange reactions, and non–reactive energy transfer are analyzed and compared to previous results on this system, when such are available.

As a prototypical three–body reactive system, H + H_2 and its isotopic analogues are interesting as benchmarks for both theoretical and experimental methods. The results of this work can be applied to the general field of molecular reaction dynamics, to interstellar physics and chemistry, to models of planetary atmospheres and stellar system formation, and to studies of the effects of isotopes on reaction rates. The work is motivated by astrophysical applications: in particular, the data may be used as inputs for master equation calculations for interstellar gases.

Contents

Tables

Figures

Chapter 1

Introduction

1.1 Molecular reaction dynamics

Molecular reaction dynamics is the study of how energy is distributed during collisions between molecules. This field emerged from the field of chemical kinetics, the study of rates of chemical processes, as researchers developed its theoretical underpinnings. In order to predict the rate at which a reaction will occur, it is necessary to know the probabilities of the elementary processes which contribute to it.

The study of reaction dynamics connects microscopic and macroscopic systems. By determining the properties of individual molecular collisions and averaging over all possible collisions, macroscopic behaviour may be predicted.

Reaction dynamics studies often determine values of importance to studies of chemical systems: cross sections and rate coefficients. Cross sections are values related to the probability of simple microscopic processes. In principle, a cross section can be calculated directly from first principles using quantum mechanics. Rate coefficients are bulk statistical quantities, useful in describing how populations of species change over time in chemical kinetics calculations. Rate coefficients are calculated by averaging cross sections over an appropriate distribution of translational or internal energy.

A cross section, as a measure of the probability of a given process, is a function of the relative motions and physical properties of two colliding species. A cross section given as a function of translational or total energy may be referred to as an excitation function. Two types

of cross section are commonly considered: differential (or scattering) and integral (or total) cross sections.

A differential cross section is a measure of the probability of scattering at a particular angle. It is expressed in units of area per solid angle unit. Differential cross sections can be determined by crossed beam scattering experiments. Observations of a particular product at each angle give rise to the differential cross section for the process leading to that product.

An integral cross section may be determined by integrating a differential cross section over all angles. As an average over all possible initial orientations of the target and collider, an integral cross section corresponds to the total probability of the occurrence of a particular process. Integral cross sections are expressed in units of area. An integral cross section may be considered as an effective area of the target molecule through which a colliding species must pass in order for the process of interest to take place.

Many processes will not occur unless certain conditions have been met. A transition from a state with energy E to a state with energy $E' > E$ will require at least $E' - E$ energy to be transferred during the collision. The energetic requirement $E' - E$ is the energetic threshold. Collision distance and geometry may also be factors in the amount of energy which must be transferred for a particular process to occur: for example, if a collider can not approach the target molecule closely enough to cause the process under consideration, then that process can not occur, even if the energetic requirement has been met. The same is true if a collider can not approach at the correct conformation for the process to occur. (This is perhaps most commonly recognized in reactions of organic molecules, for which a "steric factor" may be used to modify rate coefficients to account for geometrical restrictions.) If E'' is the amount of energy required for a collider to approach closely enough and in the correct geometry to cause a particular collisional outcome, then $E'' - E$ is the dynamical threshold. For a particlar process, if $E'' - E > E' - E$, or equivalently $E'' > E'$, then there is said to exist an elevation of the dynamical threshold for that process.

When describing a collision, it is helpful to use the variables which describe its initial

approach. One of these is the impact parameter (Figure 1.1), the distance of what would be the closest approach, if there were no interaction, from the collider's centre of mass to the target molecule's centre of mass.

An opacity function is the probability of a collisional process as a function of impact parameter b and translational energy E, usually denoted $P(b, E)$ (or sometimes simply as $P(b)$, when the translational energy is held constant). Opacity functions are useful in the analysis of excitation functions because they indicate which types of collisions are the most important contributors to the excitation function. The relationship between an opacity function and an associated integral cross section σ is

$$\sigma(E) = 2\pi \int_0^\infty bP(b, E)\mathrm{d}b. \tag{1.1}$$

A rate coefficient describes the rate at which a process occurs as a function of temperature. For instance, the rate of the elementary reaction

$$m\mathrm{A} + n\mathrm{B} \rightarrow \text{products} \tag{1.2}$$

at temperature T can be described by a rate coefficient $\gamma(T)$ with the formula

$$\frac{\mathrm{d}\,[\text{products}]}{\mathrm{d}\,t} = \gamma(T)[\mathrm{A}]^m[\mathrm{B}]^n, \tag{1.3}$$

for m, n the stoichiometric coefficients of A and B in the elementary reaction.

Experimentally, crossed beam experiments are the most common method of obtaining information about the dynamics of a collision and the associated cross sections. In these experiments, two beams of particles are crossed at a chosen angle, often with specific relative speeds and initial internal states selected, and the products are detected at various angles relative to the beams. Analysis of the distribution of scattered products is a sensitive way to probe the potential energy of systems (as in the study of N_2–N_2 of Aquilanti *et al.*, 2002 [1], or the study of Br–HBr by Meuwly and Hutson, 2000 [2]). Reactants with specific translational energies can be selected to determine the energy dependence of the various collisional outcomes. Some

selection of specific vibrational and rotational energies is possible (for instance, by use of tuned lasers), giving information about dynamics for specific initial and final states [3]. Dynamical data can be used to derive information about kinetics, which can then be compared to results from shock tube and other bulk experiments.

Considerable theoretical work has been done on a variety of systems, with treatments ranging from purely classical, through quasiclassical and semiclassical, to detailed quantum mechanical. Increases in computing power have rendered complex calculations feasible, allowing for detailed quasiclassical and semiclassical studies and somewhat limited (but more exact) quantum studies of many systems. The specific treatment used for any given system depends upon a number of factors, including the physical properties of the molecules involved, the parameter space to be probed, and the computational resources available. The theoretical aspect of the field has been developed to the point where in some cases theory is capable of guiding experiment [4].

Because of their simplicity, those systems with only three interacting atoms are of particular interest in the study of reaction dynamics. Calculations on small systems are relatively easy to perform, and there exists a large body of experimental and theoretical data pertaining to many of them. $H + H_2$ is the simplest open–shell three–body interaction; therefore, $H + H_2$ and its isotopic analogues form a basis for comparison of all open–shell systems.

1.1.1 The Born–Oppenheimer approximation

The Born–Oppenheimer approximation is the proposal that as the nuclei in a molecular system move, the electrons adjust immediately to correspond to the new configuration, so that the relative positions of the nuclei alone determine the potential energy of a molecular system. When the approximation is made, the nuclear and electronic motions of a system are separable, which allows the forces between atoms to be calculated as a function solely of the positions of the nuclei. The dependence of the potential energy on the positions of the nuclei alone allows for considerable savings in terms of the amount of time required to perform theoretical

calculations, often with little impact on the overall accuracy of results.

If all particles are treated as point masses, q_i are the positions of electrons, q_α are the positions of nuclei, and ψ is the wavefunction, the Born–Oppenheimer approximation assumes that the nuclear and electronic portions of the wavefunction are separable [5]

$$\psi(q_i, q_\alpha) = \psi_{\mathrm{el}}(q_i, q_\alpha)\psi_{\mathrm{N}}(q_\alpha). \tag{1.4}$$

This is a good approximation if

$$\left(\frac{m_i}{m_\alpha}\right)^{1/4} \ll 1. \tag{1.5}$$

Given the Born–Oppenheimer approximation, it is possible to create a potential energy surface (PES)—a single function of nuclear separation which returns a potential energy—which may then be used for each time step of each simulated collision. The use of a PES saves the computational expense of having to solve costly differential equations to evaluate the *ab initio* energy at each point of the calculation. PESs are specific to a system and electronic configuration: changing the number of protons in the nuclei, adding or removing nuclei, or changing the number or configuration of electrons will mean that a different PES is required. Because the nuclear and electronic motions are separated, a PES is independent of the nuclear masses: a system and its isotopologues may share the same PES. When the Born–Oppenheimer approximation is invoked, there may be a discontinuous jump in the PES where the electronic state is changed. In practice, PESs are derived from experimental data, from *ab initio* quantum calculations using various approximations, or from some combination of the two.

For H + HD and D + H_2, where H is ^{1}H and D is ^{2}H,

$$\left(\frac{m_i}{m_\alpha}\right)^{1/4} = \left(\frac{3m_e}{2m_H + m_D}\right)^{1/4} = 0.142. \tag{1.6}$$

For H + H_2,

$$\left(\frac{m_i}{m_\alpha}\right)^{1/4} = \left(\frac{3m_e}{3m_H}\right)^{1/4} = 0.152. \tag{1.7}$$

It is possible to invoke the Born–Oppenheimer approximation for these systems, but the results must be treated cautiously. In more sophisticated schemes, a correction is applied to account

for the approximation (for instance, the Born–Oppenheimer diagonal correction in quantum calculations [6]). It has been estimated that the approximation affects the potential energy of H + H_2 at the saddle point by as much as 0.21 kcal mol^{-1} [7]. For comparison, the potential for D+D_2 was estimated in the same study to be affected by 0.11 kcal mol^{-1}. It may be expected that cross sections and rate coefficients obtained with the Born–Oppenheimer approximation invoked may differ slightly from those obtained without the approximation or with corrections applied.

A PES for a system with more than two atoms may be considered as the sum of the 2–body potentials of each pair of atoms, plus correction terms. In the limit of infinite separation between two parts of the system, the correction terms become zero, and the potential energy of the system extrapolates to the sum of the internal energies of the two parts. When one atom of a 3–body system is moved far from the other two, the potential energy of the system depends only upon the 2–body potential between the two closest atoms, and the PES becomes the 2–body potential.

1.1.2 Theoretical methods

Purely classical methods are easy to implement and require relatively little computing time; however, they do not accurately describe systems in which quantum effects are important. Classical methods generate data by simulating trajectories: initial positions and momenta for the atoms involved are selected, then integrated over time steps until the collision is deemed complete. A number of trajectories are then used to determine values of interest. Such simulations are computationally efficient, and are faster for collisions with more translational energy. These are statistical methods, whose errors decrease as the number of trajectories is increased.

At the other extreme, detailed quantum calculations can in principle give very accurate results for all systems; however, these are prohibitively expensive to perform for all but the lowest energy states of the simplest systems, at best scaling with complexity $\mathcal{O}(E^6)$. Quantum calculations generate data (often cross sections) through the numerical solution of Schrödinger's

equation, yielding exact values within the limits of the basis set and approximation method chosen.

Quasiclassical and semiclassical methods seek to combine classical and quantum methods in order to increase accuracy but decrease computational expense. Semiclassical methods treat one or more degrees of freedom of a system as purely classical, while using quantum mechanical descriptions for the rest. Quasiclassical methods set up initial conditions according to quantum mechanical principles, with initial rotational and vibrational energies corresponding exactly to quantum numbers. The problem is then solved classically. The final vibrational and rotational energies calculated by a classical method can take on values other than those corresponding to any quantum state of the product molecule; however, quasiclassical and semiclassical trajectory methods can include a method to convert these classically–derived results into integral quantum numbers. These are not trivial conversions to perform [8]. Quasiclassical and semiclassical methods suffer inaccuracies in the form of the assumptions they make: for instance, quantum tunnelling may be important at very low temperatures, and quantum resonances (which do not occur classically) may exist. In a classical method, unlike a quantum method, the zero point energy of a molecule is not a constraint. For both quantum and classical methods, limitations to the potential energy function used for the calculation may exist, both in the form of approximations made in the calculation of the potential energy function, and in how intersecting potentials (for electronically excited states, for example) are treated[9].

1.1.3 The quasiclassical trajectory method

The quasiclassical trajectory (QCT) method is useful in that it both enables a model of collisional processes in terms of quantum states and allows for computationally efficient solutions.

While quantum and quasiclassical trajectory results will often match very closely for high energies, they tend to diverge, often significantly, at lower energies (c.f. Mandy and Martin, 1992 [9]). Quantum tunnelling may increase quantum rate coefficients over classical

ones by allowing for nuclear motions through potential energy barriers that can not be overcome classically. Quantum resonances may cause cross sections for some transitions to be enhanced relative to others. These resonances do not occur in classical calculations. Zero point energy leak may cause some classical cross sections to be overestimated as a result of the consideration of product molecules with internal energy less than that of the ground state. (Zero point energy may also be important thermodynamically, in a way which does not directly depend on the method: for example, HD has a lower zero point energy than does H_2, suggesting that if only thermodynamics were taken into consideration, an exchange reaction that produces HD would be favoured energetically over an exchange reaction that produces H_2.) The QCT method's accuracy depends on the number of trajectories computed, and accuracy increases slowly with the number of trajectories (scaling as $\mathcal{O}(1/\sqrt{n})$ for collisional outcomes with probability $p \gg 1/n$; and $\mathcal{O}(1/n)$ for collisional outcomes with $p \sim 1/n$—see Equation 2.8).

Despite their limitations, quasiclassical and semiclassical methods are currently the only feasible methods available for studies which seek a complete set of state–to–state cross sections. They are excellent for moderate to high energy collisions, and since the primary intended application of this work is in master equation studies of the interstellar medium (ISM), where temperatures are often high (particularly in shocked regions and the warm neutral medium), the low temperature deficiencies are less significant. For cold regions of the ISM, only the lowest energy states are important, and exact quantum cross sections exist for many of these already. Neither tunnelling through the exchange barrier nor tunnelling through the rotational barrier is accounted for in the QCT method; however, the H + H_2 surface is reactive, meaning that the dynamical thresholds for most processes are not highly elevated above their corresponding energetic thresholds, so that the cases in which tunnelling may have a significant impact are mostly limited to those exchange processes with small probabilities near the energetic threshold. As all quasibound states of H + H_2 and its isotopic analogues have large probabilities for collision–induced dissociation (CID) at all translational energies, and these states are unlikely to be populated at the lowest temperatures studied, the neglect of dissociative tunnelling is

not a problem in the study of CID. (Rate coefficients for low temperature exchange reactions calculated using the QCT method may suffer due to the existence of an energetic barrier to exchange.)

1.1.4 2–body potentials for the ground state of H + H_2 and its isotopic analogues

Because the species differ only by a neutron and the Born–Oppenheimer approximation is being made, the 2–body potential energy curves of H_2 and HD are the same. However, the difference in mass means that the spacing and number of internal energy levels differs. HD has 464 available energy levels, compared to 349 for H_2. These energetic states are denoted by their vibrational quantum number v and rotational quantum number j, as in $H_2(v, j)$.

The atomic harmonic oscillator solutions to the Schrödinger equations for H_2 and HD can be used to illustrate why there are more (v, j) states for HD than for H_2.

$$E_{H_2} = (v + \frac{1}{2})h\nu_{H_2}, E_{HD} = (v + \frac{1}{2})h\nu_{HD}, \tag{1.8}$$

where E is the energy of the state, v is the vibrational quantum number, h is Planck's constant, and the vibrational frequency ν is

$$\nu = \frac{1}{2\pi}\sqrt{\frac{k}{\mu}}, \tag{1.9}$$

for which k is a force constant and the mass of the diatom is μ. Because $\mu_{HD} > \mu_{H_2}$, there are more values of v which satisfy

$$\left(v + \frac{1}{2}\right) h\nu < E_{diss} \tag{1.10}$$

for the HD molecule than for the H_2 molecule, where E_{diss} is the dissociation energy.

The rotational contribution to internal energy is given by

$$E_r = \frac{j(j+1)\hbar^2}{2\mu R_e^2} \tag{1.11}$$

for equilibrium nuclear separation R_e, reduced mass μ, and rotational quantum number j. Increasing the μ in Equation 1.11 means that there are more j which satisfy

$$\frac{j(j+1)\hbar^2}{2\mu R_e^2} < E_{diss}. \tag{1.12}$$

Thus, HD has more rotational levels in each vibrational manifold than does H_2.

A commonly used 2–body potential for H_2 is that of Schwenke [10], which is used explicitly in the BKMP2 potential energy surface. It is used in this study to calculate the energies at which to initiate trajectories. Internal energies for all (v, j) states of HD and H_2 obtained from the Schwenke potential are displayed in Figure A.1 and Figure A.2 respectively in Appendix A. Energies for selected states are given in Table A.1 and Table A.2, while turning points for selected states are given in Table A.3.

1.2 H + H_2 and its isotopic analogues

The first electronically excited state of H_2 (and HD) has electronic energy approximately two–thirds that of the dissociation energy of the ground state. The transition between electronic states on the H + H_2 surface is difficult to deal with theoretically, as without relaxing the Born–Oppenheimer approximation, the electrons must make a sudden jump to a new energy surface, which makes the position and momentum derivatives discontinuous. Under thermal conditions at temperatures typical for neutral interstellar gas (under approximately 10000 K), H_2 and HD molecules will have sufficiently low internal energy that studies on the ground electronic state provide a reasonable description of the behaviour of hydrogen gas.

The spacings between low level vibrational and rotational states in H_2 and HD are large relative to those of most other diatomics. These spacings make experiments on H_2 relatively easy to perform and interpret. Extensive theoretical and experimental studies have been performed on H + H_2 and its isotopic analogues. Studies of these systems provide a point of departure for more complex studies. According to Aoiz *et al.* [4], "all major theoretical advances in the field of gas-phase kinetics and reaction dynamics have used the hydrogen-atom exchange reaction as a benchmark."

Hydrogen atom exchange in the H + H_2 reaction can not be measured directly in experiment, as the incoming and outgoing atoms are indistinguishable. Therefore, the related systems D + H_2 and H + HD, in which one of the ^{1}H atoms has been substituted with a ^{2}H

atom, are important for experimental work. (As in Equation 1.6, ^{1}H and ^{2}H are written as H and D, respectively.) Thus, measurements of exchange reactions in these isotopic systems may provide insights into the behaviour of H atoms in the H + H_2 reaction. These measurements also provide a valuable link between theory and experiment.

The dynamical behaviour of H + H_2 and its isotopic analogues are also of particular importance to astrophysical research, as molecular hydrogen is the major component of cold interstellar clouds, and atomic hydrogen is the dominant species in the interstellar medium. In nebulae, molecular hydrogen may act as a radiation shield, and the time evolution of a nebula depends in part upon the collisional behaviour of H_2. Both molecular and atomic hydrogen are important contributors to interstellar chemistry. Models of stellar outflows, galaxy formation, interstellar gas clouds and circumstellar disks all require knowledge of the dynamical behaviour of H_2 and its isotopic analogues [11, 12, 13, 14].

Among the differences between H + H_2 and its isotopic analogues, the most important difference from the perspective of interstellar chemistry is that of the selection rules for radiative transitions. HD has a (small) permanent dipole moment $\mu = 0.00059$ D, allowing electric dipole transitions with the rotational selection rule $\Delta J = \pm 1$ [15]. Due to the lack of a permanent electric dipole, the most probable radiative processes for H_2 are due to quadrupole transitions, with rotational selection rule $\Delta J = \pm 2$. The radiative transition probability from the lowest excited state of HD is about a thousand times that of H_2, meaning that the cooling rates of low density interstellar regions with deuterium may be sensitive to the HD population [16].

The energy levels of HD (Appendix A, Figure A.1) differ from those of H_2 (Figure A.2). Not only does a ground state HD molecule require more energy to undergo dissociation than does a ground state H_2 molecule, but the HD molecule has a larger energetic barrier to exchange. The lower zero point energy of HD compared to H_2 and the difference in moment of inertia also affect the quantum tunnelling rates. In addition, because the D/H mass ratio is large, there are significant differences in collision time between H + H_2, D + H_2 and H + HD at

a given translational energy. Some representative collision times are given in Appendix A, Table A.4. Because the probabilities of the collisional outcomes depend in part upon interaction time, especially at relatively large impact parameter, different mass combinations may exhibit different dynamical behaviour.

A kinetic isotope effect arises from the differences of rate coefficients that come from changing one atom in a reaction to a different isotope of the same element. Such a substitution has the effect of changing the mass of that nucleus without changing the potential energy surface (assuming the Born–Oppenheimer approximation). Isotopic substitutions may induce changes in equilibrium coefficients; such a change is called a thermodynamic isotope effect. D + H_2, H + HD, and H + H_2 can be compared for kinetic isotope effects. In some dynamical systems (particularly organic reactions involving proton exchange), because of the increased speed of a lighter atom, rate coefficients may be greater for reactions involving the movement of lighter isotopes. In others, a slower collision may be more likely to result in a particular collisional outcome.

The difference of the atomic masses of H and D means that an HD molecule is not symmetric about its centre of mass. The opacity functions for similar transitions involving H + H_2 and H + HD may appear different even if the overall cross sections for those transitions are similar. Reactions can occur at much higher values of the impact parameter in H + HD, because the H nucleus is farther from the centre of mass. However, the increase in opacity functions at greater impact parameters may be compensated for by a decrease in the opacity function just below the maximum impact parameter for H + HD relative to H + H_2 due to collisions which "miss" on the (geometrically smaller) D atom side.

HD is interesting in an astrophysical context because it can significantly affect the dynamics of interstellar gas clouds. Although D exists at small concentrations in most of the ISM, reactions on interstellar dust grains may lead to a high population of deuterated molecules relative to the population of atomic D. The closer spacing of energy levels in HD as opposed to H_2 means that HD can be excited by lower energy collisions than can H_2, which in turn may lead

to an enhancement of the population of excited molecules in HD gas over H_2 gas. Combined with a higher probability of photon emission due to the HD dipole, the higher population of excited molecules contributes to increased radiative cooling in interstellar regions containing HD [17].

In addition to studies of the interstellar medium, temperature–dependent rate coefficients are required for studies of deuterium chemistry in the Jovian thermosphere [18]. The abundance of atomic D and HD depend in large part upon these rate coefficients, as the main source of atomic D is via the reaction HD + H $\rightarrow$ H_2 + D, while the main loss of atomic D is via the reverse reaction. These rate coefficients are used in conjunction with deuterium Lyman α observations to calculate the H/D ratio of the early solar system, which is important in models of solar system formation [18].

1.3 Existing work on H + H_2, H + HD, and D + H_2

The H + H_2 reaction and its isotopic analogues have been studied since the late 1920s [4]. Although the major developments in H + H_2, D + H_2, and H + HD are discussed here, a full treatment of the history of these investigations is beyond the scope of this work. Further details of the work on these and other isotopic analogues of H + H_2 can be found in (for example) Mayne and Toennies, 1981 [19], Mayne *et al.*, 1990 [20], and a comprehensive and highly detailed review by Aoiz *et al.*, 2005 [4].

The concept of a potential energy surface was introduced by London, and with it the first H + H_2 PES [21]. The functional form of the surface was extremely simple, ignoring three body terms [20]. A lack of computing power in the 1930s made a large study too difficult to perform. The first trajectory attempted was trapped in an unphysical well in the exchange barrier of the potential, and it was abandoned after three years of calculations.

It would be another thirty years before Karplus, Porter and Sharma fitted experimental data to a LEPS–type potential energy surface, which had a more advanced functional form than London's surface [22]. (A LEPS surface is a sum of two–body terms, but does not contain

three-body terms and is relatively inflexible compared to modern functional forms.) They used quasiclassical trajectories to carry out the first comprehensive dynamical study. Results from this study did not match the predictions of transition state theory, and the rate coefficients were over–estimated relative to experimental values [23]. There were qualitative agreements between this study and experiment, however, such as the repulsiveness of regions of the surface, the energetic threshold barrier for the exchange reaction, and the lack of a stable intermediate species in the exchange reaction.

Early experiments were performed by LeRoy and co–workers (also see Aoiz *et al.* 1996 [23], and references 12–19 therein), mostly using fast flow systems [20]. These experiments were limited to temperatures below 750 K and the ground vibrational state, but they showed some important features. The effects of tunnelling were visible in the differences between $H + H_2$ rate coefficients and the corresponding $D + H_2$ rate coefficients [23].

The first *ab initio* $H + H_2$ surface was determined by Liu in 1973 [24]. It was state of the art for its time, though restricted to collinear geometries. It has since been discovered that the behaviour of collinear collisions is not representative of the behaviour of collisions in general, though attempts have been made to extend results on restricted dimensional systems to 3–dimensional systems [25].

The 2–dimensional [26] and 3–dimensional [27] quantum mechanical results of Kuppermann, Schatz and Baer published in 1976 were highly accurate for their time. The quasiclassical rate coefficients of Karplus *et al.* were closer to the experimental values than were the QM rate coefficients, and transition state theory calculations were the best of all in matching experiment. The accuracy of the TST calculations was later attributed to good luck rather than to any superiority in the method [23], as errors in creating the PES used in those calculations made the barrier height very close to the true value [20].

1.3.1 LSTH potential energy surface

To overcome the inadequacies of earlier PESs, the LSTH surface was developed [28, 29, 30]. It was the first fully 3–dimensional surface fitted primarily with *ab initio* quantum points. (Porter and Karplus had used experimental data for their surface, in addition to *ab initio* values.) Considered highly accurate at the time, it was fitted using 25 parameters, 267 *ab initio* data points (the 135 collinear points used by Liu, plus 132 new nonlinear points), and 4 empirical data points (one at the saddle point and 3 in the van der Waals well). It has an rms error of 6.83 kcal mol^{-1}, with a maximum deviation of 106 kcal mol^{-1}, performing about equally well (or poorly) on both bent and linear configurations. These errors are much less when only considering non–compact geometries, that is, those in which not all internuclear separations are small: the rms error is 0.45 kcal mol^{-1}, while the maximum error is 2.55 kcal mol^{-1}[31].

In addition to what are now regarded as high errors, the LSTH surface has a fundamental defect in that it is not well fitted around the region where the collider and target molecule are separated by about 2 Å. The defect is especially apparent at collinear geometries, where the collider closely approaches one of the target atoms, but it also occurs at other geometries. This defect leads to somewhat suspect results for some calculations [31, 32], although experimental rate coefficients for the exchange reaction D + H_2 $\rightarrow$ H + HD agreed well with quantum rate coefficients calculated on the LSTH surface at low temperature [33, 34].

Early theoretical studies on the LSTH surface yielded good results for the ground vibrational state. Early transition state studies by Garrett and Truhlar [35, 36] significantly underestimated the rate coefficients, but those studies led to corrections [37], culminating in successful application of the method [23]. Quasiclassical studies on D + H_2 [38] and H + H_2 [19] managed to accurately predict $v = 0$ exchange rate coefficients above 500 K, though the neglect of quantum tunnelling inherent in the method caused underestimation of rate coefficients at lower temperatures.

Despite these successes for the ground vibrational state of the target molecule, the rate

coefficients for the D + H_2(v=1) exchange reaction remained problematic. Similarly, rate coefficients for the H + HD(v=1) exchange reaction did not match experiments. Quasiclassical trajectory calculations of both cross sections and rate coefficients (c.f. [19, 38, 39]) varied considerably from the experimental values obtained from studies involving maser pumping of H_2 into an excited vibrational state [40, 41]; the QCT cross sections were too large by several orders of magnitude. To address the difference between theory and experiment, experiments involving both better maser tuning of the reactant vibrational state and better detection of products were performed in the late 1980s (c.f. [20] and references therein, [42]). These experiments measured smaller rate coefficients at low temperatures than did previous experiments, placing the experimental values closer to the theoretical ones. Measurements of the energetic threshold to dissociation in these experiments were also closer to theoretical values.

1.3.2 DMBE potential energy surface

By the time the experiments involving better maser tuning were carried out, a new PES was available, the double many–bodied expansion (DMBE) surface [43, 44]. Calculations on both DMBE and LSTH would allow for comparisons regarding the importance of features of the PES on the dynamics of trajectories on that surface.

The DMBE method, in general, was developed with a view to facilitating quantum calculations that permit strong bonds to be broken. It produces global analytical surfaces with physically motivated functional forms. The H + H_2 DMBE surface was fitted using 316 *ab initio* data points, 267 of which had been used for the LSTH surface. The relative errors on the DMBE surface are comparable to those of the LSTH surface in non–compact geometries and using the entire set of known *ab initio* points; however, DMBE is considerably better than LSTH for compact linear configurations [31].

The DMBE surface has a drawback similar to that of the LSTH surface in that the region of the surface in which the separation between target and collider is near 2 Å is not well fitted, especially for collinear geometries. These configurations form an important part of the surface,

especially for calculations involving low energy collisions. These poor fits at important geometries adversely affect both quantum and quasiclassical calculations at low temperature, causing overestimates of cross sections by as much as a factor of 30 relative to those obtained on more recent surfaces [31].

1.3.3 Calculations on the LSTH and DMBE potential energy surfaces

Even after DMBE was developed, quasiclassical calculations continued to be performed using the LSTH surface [45, 46, 47]. These studies on the LSTH surface investigated the formation of collision complexes, rotational distributions of products, and what were thought to be possible resonance effects observed in earlier quantum mechanical calculations. Experiments showed sharp increases of some cross sections relative to other cross sections with similar vibrational and rotational energies, which lead researchers to believe that they could be observing quantum resonance effects. Some of these were shown later to be real quantum effects [9]; others were shown to exist in classical studies as well [4], and thus could not be due exclusively to quantum processes.

Full quantum mechanical calculations proved to be challenging. As such, only very approximate (and semiclassical) results were initially available. When the first accurate QM results came out [48, 49, 50], it was noted, with some consternation, that they were further from the experimental values than were the results of very approximate methods [51, 52]. QCT and accurate QM rate coefficients were in general close to each other, but for vibrationally excited molecules, and even for some low rotational states in the $D + H_2(v = 0)$ exchange reaction [53], they differed considerably from the most recent and refined experiments [49, 54, 55, 56, 57, 58]. Later, approximate QM methods would produce results in good agreement with accurate QM [59], furthering the controversy. For instance, accurate QM calculations by Park and Light [33] for ground state exchange reactions agreed well with experiment up to 1000 K, but were off by a factor of two at 1500 K, well outside the experimental error bars.

Shortly after, the experiments and calculations of Adelman *et al.* [60, 61] were performed

at higher energies than previously possible, and are interesting not only in that they confirmed that experimental and theoretical studies were still far apart (and suggested that a better PES was needed), but also in that they suggested that the D + H_2 exchange reaction often conserves internal energy of the bound molecule: the product HD molecule may frequently have roughly the same internal energy as did the initial H_2 molecule.

1.3.4 BKMP potential energy surface

A number of possible approaches to resolving the difference between theory and experiment were considered. The first was to affirm that the theoretical methods used were valid. Since the theoretical results came from a variety of groups, and since the accurate QM and QCT results matched, Keogh *et al.* [53] discarded the idea that there was any problem with the calculations themselves. Because the experiments that led to the difference had been repeated with similar results, experimental artefacts were also discarded as an issue (though as discussed in Section 1.3.5, there was an unknown problem with the experiments which would not be discovered and resolved for another decade). Effort was therefore put into improving the potential energy surface, with the hope that inaccuracies in the existing PESs were the primary cause of the discrepancy between theory and experiment.

These efforts resulted in the BKMP surface [62]. The BKMP surface uses the points used to fit the LSTH surface in addition to newer points, totalling 770 *ab initio* points and covering a wider range of separations, fitted to a highly flexible function [62]. Like the LSTH and DMBE surfaces, its largest errors are inside the van der Waals region (around 3 Å), with the H–H_2 separation around 2–2.5 Å [34]. Unfortunately, calculations of cross sections (especially quantum calculations) may be highly sensitive to this part of the potential.

A study of both QCT and QM results on the BKMP surface [53] for the D + H_2 exchange reaction showed that it suffered many of the same problems as DMBE. A study by Mielke *et al.* [34] compared quantum results from LSTH, DMBE, and BKMP, concluding that BKMP was not good for calculations of cross sections for the exchange reaction below 200 K; this was

later shown to be largely due to an anomalous reaction barrier height [31].

This study by Mielke *et al.* also showed that part of the source of the previously poor agreement between quantum calculations and experimental results was the calculation method (at least for high temperature, where most of the deviation occurred), and not necessarily the potential energy surfaces. Nevertheless, even after correcting for methodological issues, there was still a significant difference (as much as 10% for the states studied) between experimental and theoretical results.

A similar work using quasiclassical trajectories for the $v = 0$ and $v = 1$ states by Aoiz *et al.* [23] presented cross sections and rate coefficients for $D + H_2 \rightarrow H + HD$, with v =0 or 1 and j =0–7. This was a computationally difficult problem at the time, especially since the calculations were performed on each of the LSTH, DMBE, and BKMP surfaces. Good agreement with quantum results was obtained, even at temperatures as low as 200 K for the lower j states, suggesting that the QCT method is generally suitable for the $H + H_2$ problem. The effect of rotational energy on reaction was highlighted, as well. Calculations of the cross sections at low collision energy were shown to be sensitive to the PES chosen, meaning that a very accurate PES is needed for good quantitative calculations [23].

1.3.5 BKMP2 potential energy surface

The anomalous height of the energetic barrier to exchange on the BKMP surface was corrected, new points were computed to further constrain the surface, especially in the van der Waal's well region, and a new fit was released as the BKMP2 surface [31]. The BKMP2 surface not only manages to replicate the symmetry and bonding issues that DMBE was developed to incorporate, but also ensures that the function has continuous derivatives for high energy complexes, where LSTH and DMBE did not. These derivatives are important for QCT calculations, enabling more efficient integration of the classical equations of motion.

The same highly flexible functional form used for BKMP was kept for BKMP2. The BKMP2 surface was fitted with a total of 8701 *ab initio* points, yielding a r.m.s. error of

0.17 kcal mol^{-1}, with the worst absolute error being 3.9 kcal mol^{-1}. These errors are an order of magnitude better than those of the BKMP and DMBE surfaces, and are correspondingly better than those of LSTH. When compact configurations are not considered, BKMP2 is better still [31].

With the advent of the BKMP2 surface, some of the extant theoretical problems were resolved, including those problems involving the difference in barrier height between surfaces. Once the BKMP2 surface was in use, most experimental data matched with both accurate QM and QCT calculations, but there were still problems below 200 K and above 1500 K [63]. For low temperatures, quantum D + H_2 rate coefficients calculated using BKMP2 were double those measured by experiments; above 1500 K, they were underestimated by as much as 25% [64]. This discrepancy was attributed mostly to a systematic error in the experimental method [53], but the idea remained that the difference was possibly due to the fact that the van der Waals well on the BKMP2 surface was still too deep [64, 65]. Despite these reservations, when Mielke *et al.* checked newly computed *ab initio* points against BKMP2 (and also BKMP), they found rms errors similar to the fitting errors, indicating that the systematic errors that arise from the correlation treatment and London basis set corrections used in these fits largely cancel out [64].

The remaining discrepancy between theory and experiment was at this time discovered to be due in large part to an issue in the experimental procedure. In prior experiments, free D (or H) atoms were created via flash photolysis of a DI or DBr molecule (or HI/HBr), a process which interfered with the measurements. A set of shock tube experiments which used instead the thermal decomposition of C_2H_5I or C_2D_5I, and corresponding accurate quantum calculations on the CCI surface, were performed by Mielke *et al.* [65] over the temperature range 167–2112 K for the $H+H_2 \rightarrow H_2+H$ exchange reaction. These changed the experimental values significantly, so that they now agree "perfectly, within experimental error, bringing [the resolution of] this 75-year-old scientific problem to completion" [65].

1.3.6 Mielke, Garrett, and Peterson's potential energy surfaces

The CCI surface used in Mielke *et al.*, 2003 [65] is part of a hierarchical family of PESs developed by Mielke, Garrett and Peterson [64]. The rationale for these surfaces is that prior surfaces used *ab initio* points from a variety of different and often old sources, and errors from those sources propagate into the surfaces. Thus, it makes sense to compute new *ab initio* points at higher accuracy, using updated methods. The hierarchical method was chosen so that accuracy depends primarily upon the basis set chosen.

All four of the surfaces (named A2, A3, A4, and an extrapolated surface called CCI) produced are superior to BKMP2 in terms of rms error and maximum absolute error (though A2 has some deficiencies, especially in terms of barrier height). Though the traditional form of the functions used to fit these surfaces does not have analytical derivatives, Mielke *et al.* introduced an optional small constant that ensures continous analytical derivatives exist. A3, A4 and CCI all fit the van der Waals region and longer ranges very well, though A2 is inaccurate. The most accurate of the surfaces is CCI, which has an rms error of 0.0023 kcal mol^{-1}, under 4% that of BKMP2, and a maximum error about 4.5% of the maximum error of BKMP2. Verifying the surfaces with points not used in the fit, Mielke *et al.* found that the rms error to these points is comparable to the rms error from each fit, indicating accurate fits.

The CCI and BKMP2 surfaces never differ by more than a small amount, both in terms of energy [64] and in terms of quantum mechanical integral cross sections [66]. Calculations using BKMP2 slightly overestimate the integral cross sections for the exchange reaction relative to those using CCI in some cases, while underestimating them in other cases, but for quantum calculations, it appears that an accurate estimation of the reaction barrier height is the most important factor in calculating integral cross sections, and the two surfaces agree closely in this aspect. Differential cross sections calculated with BKMP2 may be noticeably different from those of CCI [66].

It is reasonable to expect that sets of rate coefficients calculated using quasiclassical

trajectories on the CCI surface or a surface very much like it (e.g. BKMP2) will be accurate, within the limitations of the QCT method.

1.3.7 Other 3–body potentials for H + H_2

There exist several potential energy surfaces for H + H_2 other than the ones mentioned in Section 1.3. Some are very accurate in specific localized regions, such as the van der Waals well, and are useful only for studies in those areas, or as parts of a global PES. Because this study uses the QCT method, and the QCT method requires the use of a potential energy surface which covers a wide range of atomic separations, focus is given here to the available global PESs.

In addition to theoretically calculated surfaces, there exist empirical surfaces, LEPS–type [67] being the most popular. LEPS surfaces assume a collinear conformation, though there are "extended LEPS" surfaces which allow for bent configurations. Although collinear LEPS calculations have recently been used successfully to model the behaviour of bent configurations in Cl + HCl [68], it turns out for H + H_2 that collinear studies do not correspond well either with full 3 dimensional calculations nor with experiments.

It is preferable from a computational standpoint to have an *ab initio* surface with continuous analytic derivatives, so now that sufficient *ab initio* data can be produced, empirical surfaces are rarely used. Continuous derivatives are important because the most efficient algorithms for integration and quadrature require well–behaved derivatives, and integrations of the equations of motion which use these algorithms may not converge around solutions near discontinuous derivatives.

The exact quantum Monte Carlo (EQMC) surface of Wu *et al.* [69] was fitted largely with collinear points, though an extension using more MC points would probably provide an extremely accurate global PES. There was some uncertainty regarding the accuracy of Wu *et al.*'s fitted PES at the time this study began [64], so it was not considered for use.

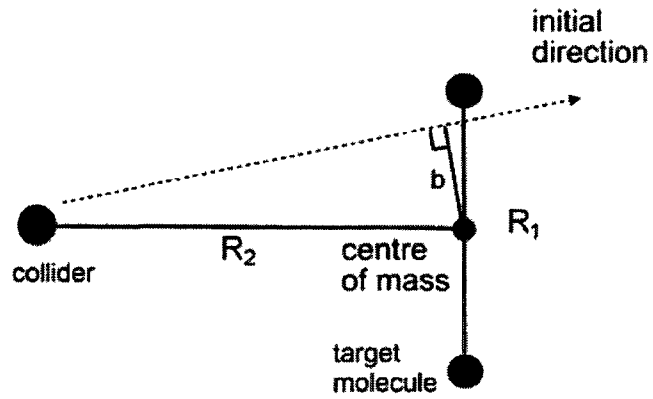

Figure 1.1: The impact parameter b is the minimum distance to which the collider would approach the centre of mass of the target if there were no interaction. R_2 is the initial separation of collider and the centre of mass of the target molecule. R_1 is the initial separation of the target molecule's atoms.

Chapter 2

Method

The quasiclassical trajectory method was used to calculate full sets of state–to–state and dissociative cross sections and rate coefficients for H + HD, D + H_2, and H + H_2.

2.1 Potential energy surface

Because the quantum mechanical integral cross sections for H + H_2 calculated using BKMP2 agree very closely with those of CCI [66], the most accurate available potential energy surface (PES), and because some previous results on BKMP2 are available for comparison and validation, BKMP2 was chosen for this study [31]. From a computational perspective, the existence of analytic derivatives built into the published BKMP2 code and the lack of such derivatives in the code distributed for the CCI surface makes BKMP2 a more attractive option, with integration of trajectories expected to be faster on BKMP2 by a factor of about 10.

A comparison of the BKMP2 and CCI surfaces is given in Figure 2.1. For most internuclear separations, the difference in potential energies is 0.2 kcal mol^{-1} or less. The largest differences come at very small internuclear separations, where the potential energy is greater than that required for dissociation; however, few trajectories will encounter these regions of the PES. The small differences between BKMP2 and CCI will likely become important only in detailed quantum calculations, so confidence in QCT results using the BKMP2 surface is justified.

2.2 Trajectories

Trajectories were computed using a modified version of the REAC program originally written by J. L. Schreiber [70]. Although a complete set of H + H_2 cross sections was available [71], the original trajectory data from that study was lost in a disk crash, so a new set of H + H_2 data was computed as well.

For each set of trajectories, the initial vibrational state, rotational state, relative translational energy, and impact parameter stratum were fixed. Batches were run for all initial vibrational and rotational (v, j) states. For each (v, j) state, a batch of trajectories was run for each translational energy on a 1 kcal mol^{-1} grid, up to 20 kcal mol^{-1} above the point at which the total energy of the system is the H_2 dissociation energy. Above that, the translational energy intervals were 5 kcal mol^{-1}, up to a maximum translational energy of 315 kcal mol^{-1}. Cross sections for many transitions are similar at all translational energies above 315 kcal mol^{-1}, and the low weight given to these cross sections in the computation of thermal rate coefficients at the temperatures chosen in this study means that the small differences in cross sections above 315 kcal mol^{-1} are unimportant. Due to the high energy of such configurations, the BKMP2 PES is not valid at internuclear separations less than 0.2 Å, which may occur during a collision at high translational energies. A cutoff of translational energy at 315 kcal mol^{-1} ensures that most trajectories do not reach internuclear separations less than 0.2 Å and subsequently fail.

Because the majority of collisions in which energy transfer occurs are at low impact parameter, stratified sampling was used to select the impact parameter. Stratified sampling focusses the computational effort on low impact parameter collisions, ensuring that the dynamics can be probed efficiently. For each (v, j) state and translational energy, the impact parameter was chosen using Monte Carlo selection from a minimum of 0 Å to a maximum of 7 Å, in intervals of 0.5 Å. At each (v, j), E_{trans}, and impact parameter range, a minimum of 1000 trajectories was run for H + HD and D + H_2. A minimum of 3000 trajectories was run for H + H_2, as more computational resources became available during the course of research.

For each trajectory, the initial distance between the colliding atom and the centre of mass of the target molecule was chosen to be 7 Å, a separation beyond which any interaction between the two species is less than the average error in the PES. The initial vibrational and rotational energies were selected to correspond to the initial vibrational and rotational quantum states. The initial angle of rotation and angle between the collider and target were Monte Carlo selected, as was the vibrational phase (which determines the initial separation between atoms in the target molecule).

Once the initial conditions for a trajectory were set up, the trajectory was determined by integrating Hamilton's equations of motion (for direction i, position q, momentum p and potential H)

$$\mathrm{d}q_i = \frac{\partial H}{\partial p_i}\mathrm{d}t \tag{2.1}$$

$$\mathrm{d}p_i = -\frac{\partial H}{\partial q_i}\mathrm{d}t \tag{2.2}$$

using a sixth order Runge–Kutta integrator. Each trajectory was deemed complete when the distance between any two of the atoms was greater than 7 Å. Checks for conservation of energy were made to ensure that the integration step size was appropriate. If a trajectory encountered a situation in which the energy derivatives were greater than a given tolerance, or if energy conservation was violated, then the trajectory was back–integrated to ensure correctness. In addition, every twenty-fifth trajectory was routinely back–integrated to ensure correctness in general. If a back–integration failed to reproduce the original configuration of the trajectory, then the trajectory was marked as a failure and discarded.

2.3 Outcomes

There are several possible outcomes to any given trajectory. The first possibility is that the bond of the target molecule is broken, and the three atoms all end up far apart, moving with enough momentum that they will not recombine. This is collision–induced dissociation (CID). The second possibility is nonreactive energy transfer: the collider adds energy to or

removes energy from the target molecule, which remains bound at the end of the process. The third possibility is an exchange reaction. For systems with more than one isotope, there is the possibility of multiple distinct exchange reactions.

To determine which process a trajectory has undergone, the two atoms closest together at the end of the trajectory are identified. The relative motion of that pair of atoms is used to calculate their angular momentum and total energy. The angular momentum L of the atom pair determines the rotational quantum number j:

$$L = \frac{h}{2\pi}\sqrt{j(j+1)}, \tag{2.3}$$

where h is Planck's constant. The maximum of the 2–body effective potential for this rotational quantum number is then found. If the internal energy determined from the relative motion of the atom pair is greater than the maximum of the 2–body potential, then CID is deemed to have occurred.

If the result of a trajectory is a bound product molecule (i.e. CID has not occurred), the identities of the atoms in the closest pair determine which of exchange and nonreactive energy transfer has occurred. For a bound atom pair, the effective potential is evaluated and used to partition the internal energy assigned to the atom pair into rotational energy (as determined by the rotational quantum number calculated from the angular momentum) and vibrational energy. From the vibrational energy and the effective potential, the vibrational quantum number is determined by quadrature.

For a general exchange reaction involving target AB and collider C, the two possible reactions are AB + C $\rightarrow$ AC + B and AB + C $\rightarrow$ BC + A. Although from a quantum mechanical perspective it is not possible to differentiate between two H atoms in this system, it is possible to do so classically. Thus, for H + HD, the two reactions are

$$\begin{aligned} \mathrm{H_\alpha D} + \mathrm{H_\beta} &\rightarrow \mathrm{H_\beta D} + \mathrm{H_\alpha}, \\ \mathrm{H_\alpha D} + \mathrm{H_\beta} &\rightarrow \mathrm{H_\beta H_\alpha} + \mathrm{D}, \end{aligned}$$

and for D + H_2,

$$H_\alpha H_\beta + D \rightarrow H_\alpha D + H_\beta,$$
$$H_\alpha H_\beta + D \rightarrow H_\beta D + H_\alpha.$$

For collisions of H + HD, classical vibrational and rotational quantum numbers are computed for $H_\beta D$ products in the first case, and for H_2 products in the second case (and similarly for the D + H_2 reactions).

A particular class of nonreactive collision is an elastic collision. This occurs when the target molecule remains intact, and does not change either its rotational or vibrational state. In QCT, every collision may result in some measure of energy transfer, so an elastic collision is defined as one in which the energy change in both vibrational and rotational quantum numbers is less than half that of an allowed transition. For H + HD, the allowed rotational transitions include $\Delta j = \pm 1$, so any trajectory with both $|\Delta v| < 0.5$ and $|\Delta j| < 0.5$ was considered to be elastic. For D + H_2, the allowed rotational transitions are those with Δj a multiple of 2, so any trajectory with both $|\Delta v| < 0.5$ and $|\Delta j| < 1$ was considered to be elastic. No data regarding elastic trajectories was recorded other than incrementing a counter to show how many such trajectories occurred.

A plot of final (v, j) states for the exchange reaction from D + H_2(2,14) from the lowest impact parameter stratum at $E_{\text{trans}} = 85$ kcal mol^{-1} is given on the left panel of Figure 2.2. Non–reactive, inelastic trajectories at the same parameters are shown in the right panel.

2.4 Opacity functions

The initial trajectory configurations were generated using a Monte Carlo selection of the impact parameter within successive strata at 0.5 Å increments. This is not fine enough resolution to obtain meaningful results from an opacity function. Therefore, to study opacity functions, the collisions are divided into 0.1 Å bins. However, because the trajectories were sampled from 0.5 Å strata and data from the elastic trajectories were not recorded (other than a

count of how many elastic trajectories occurred), the total number of trajectories in each 0.1 Å substratum was not recorded, and must instead be estimated.

Let N_{tot} be the number of trajectories run for an impact parameter range (b_{min}, b_{max}). Choosing a subrange (b_i, b_{i+1}), an estimate of the number of trajectories in that range may be obtained:

$$N_i = N_{\text{tot}} \frac{b_{i+1}^2 - b_i^2}{b_{\text{max}}^2 - b_{\text{min}}^2}. \tag{2.4}$$

The relative error is greatest in the 0.0–0.1 Å bin. For 1000 trajectories in the 0.0–0.5 Å stratum, it is expected that 40 will fall in the 0.0–0.1 Å range, yielding a relative error of 6.2×10^{-3}. This is sufficiently small that the predicted number of trajectories will be treated as an exact value.

Now the probabilities can be calculated. Let q_i be the number of observed (dissociative) events in range (b_i, b_{i+1}) for some fixed translational energy. Then the probability P_i is

$$P_i = \frac{q_i}{N_i} \tag{2.5}$$

with standard error

$$\mathrm{d}P_i = \sqrt{\frac{P_i(1-P_i)}{N_i}} \tag{2.6}$$

$$= \sqrt{\frac{\frac{q_i}{N_i}\left(1-\frac{q_i}{N_i}\right)}{N_i}} \tag{2.7}$$

. The limit of P_i as $b_{i+1} - b_i$ tends to 0 gives the value of the opacity function for impact parameter b_{i+1}. Because there are a finite number of events in each 0.1 Å bin, opacity functions are plotted in this work as functions of b_{i+1}; that is, $P(0.1\text{ Å}, E)$ corresponds to the impact parameter range 0.0–0.1 Å.

2.5 Cross sections

Integral cross sections with statistical errors have been calculated for state–to–state, exchange, and CID processes at each translational energy for all (v, j) states of H + H_2, D + H_2, and H + HD.

2.5.1 Assignment of final results to quantum states

A fundamental issue in the QCT method is in the assignment of quantum numbers to molecules after the classical integration is complete. The method of finding continuously valued quantum numbers from the angular momentum and internal energy of the molecule was described in Section 2.3. One common way of mapping these continuously valued quantum numbers to discrete quantum numbers is through histograms. The range of possible results is divided into bins according to the collisional selection rules particular to that process. Once the trajectories are binned, transition probabilities may be calculated as a function of the number of trajectories in the bin and total trajectories computed.

2.5.2 Calculation

Using the bin histogram method (rounding continuous quantum numbers to the nearest quantum state allowed by collisional selection rules), a contribution to the cross section can be computed for each impact parameter range. The sum over these cross section contributions is the total (integral) cross section. If P_i is the probability of the process in N_i trajectories, the cross section is [72]:

$$\sigma \pm \mathrm{d}\sigma = \sum_i P_i A_i \pm \sqrt{\sum_i A^2 \left(\frac{P_i(1-P_i)}{N_i} + \frac{1}{N_i^2} + \frac{1}{N_i^3} \right) / \left(\left(1+\frac{3}{N_i}\right)\left(1+\frac{2}{N_i}\right)^2 \right)}. \tag{2.8}$$

where A_i is the area covered by the impact parameter range $(b_{i,min}, b_{i,max})$, such that $A_i = \pi(b_{i,max}^2 - b_{i,min}^2)$. Note that Equation 2.8 allows for standard deviations to be calculated even when cross sections are null.

2.5.3 Microscopic reversibility

Classical dynamics is time reversible: any trajectory can be brought back to its initial position by changing the sign of the momenta of all the particles at any point in time, including at the end of the collision. This is the principle of microscopic reversibility. State–to–state

integral cross sections are related through microscopic reversibility:

$$\sigma(1 \rightarrow 2; E')g_1E_1 = \sigma(2 \rightarrow 1; E)g_2E_2, \tag{2.9}$$

or, rearranged to solve for $\sigma(1 \rightarrow 2; E)$,

$$\sigma(1 \rightarrow 2; E') = \sigma(2 \rightarrow 1; E)\frac{g_2}{g_1}\frac{E_2}{E_1}, \tag{2.10}$$

where g_i is the degeneracy, E_i is the energy of state i, and E and E' are translational energies such that the total energy of each side of Equation 2.9 is the same. For H_2 the degeneracy is given by

$$g_i = (2s_i + 1)(2j_i + 1), \tag{2.11}$$

where $s_i = 0$ for para states (j even), $s_i = 1$ for ortho states (j odd), and j_i is the rotational quantum number of state i. HD is heteronuclear, with all states having spin degeneracy 6, so

$$g_i = 6(2j_i + 1). \tag{2.12}$$

Due to the limited number of trajectories simulated and the difficulties associated with assigning continuously–valued quantum numbers to quantum states in the binning process—histograms systematically overestimate cross sections for endoergic processes and can predict nonzero cross sections below the energetic threshold [8]—this equation will not hold exactly for QCT data. Corrections to calculations involving binned trajectories can be made by using microscopic reversibility. Because of the limited number of trajectories, such a correction may yield different results when applied to the cross sections prior to calculation of rate coefficients as opposed to application to the rate coefficients directly. In this work, corrections are performed at the rate coefficient level of calculation rather than at the cross section level because of the intended use in interstellar applications: those performing calculations with nonthermal distributions of molecules may wish to use the cross sections directly, and it is left to those users to decide whether or not to perform corrections. Highly nonthermal distributions may also occur, for example, in crossed beam or shock tube experiments with state selection.

2.6 Rate coefficients

2.6.1 Calculation

Rate coefficients for thermal distributions of translational energy can be calculated from cross sections by

$$\gamma(T) = \left(\frac{8k_BT}{\pi\mu}\right)^{\frac{1}{2}} \int_{E_0}^{\infty} \left(\frac{E}{k_BT}\right) \sigma(E) e^{-\frac{E}{k_BT}} \left(\frac{\mathrm{d}E}{k_BT}\right), \tag{2.13}$$

where E_0 is the threshold energy of the process, μ the reduced mass, and k_B Boltzmann's constant.

Thermal rate coefficients were calculated from cross sections using a piecewise linear excitation function to represent the cross sections. Where appropriate, the energetic threshold of a process was taken into account by setting the cross section at threshold to 0 and ignoring unphysically nonzero cross sections.

The function connecting (E_i, σ_i) to (E_{i+1}, σ_{i+1}) is

$$\sigma(E) = b_i E + a_i \tag{2.14}$$

such that

$$b_i = \frac{\sigma_{i+1} - \sigma_i}{E_{i+1} - E_i}, \text{ and} \tag{2.15}$$

$$a_i = \frac{E_{i+1}\sigma_i - E_i\sigma_{i+1}}{E_{i+1} - E_i}. \tag{2.16}$$

Then the rate coefficient is given, for n pairs (E_i, σ_i) (where the first may be $(E_{\mathrm{thr}}, 0)$), by

$$\gamma(T) = \left(\frac{8k_BT}{\pi\mu}\right)^{\frac{1}{2}} \left(\sum_{i=0}^{n} \gamma_i(T)\right) \tag{2.17}$$

where

$$\gamma_i(T) = \int_{E_i}^{E_{i+1}} (b_i E + a_i) \left(\frac{E}{k_bT}\right) e^{-E/k_bT} \mathrm{d}\left(\frac{E}{k_bT}\right), \tag{2.18}$$

for $0 \leq i \leq n-1$, and

$$\gamma_n(T) = \int_{E_n}^{\infty} \sigma_n \left(\frac{E}{k_bT}\right) e^{-E/k_bT} \mathrm{d}\left(\frac{E}{k_bT}\right). \tag{2.19}$$

2.6.2 Temperature dependence and thresholds

Due to the exponential term in Equation 2.13, the rate coefficient for a process can be highly sensitive to cross sections near the energetic threshold of that process. Figure 2.3 shows the thermal distribution with which cross sections are weighted at 500 K, 1000 K, 2000 K, and 10000 K. Due to the exponential nature of the function, if the threshold for a process is located at a higher energy than that corresponding to the temperature at which the population distribution function peaks, contributions from the lowest energy non–zero cross sections will dominate the calculated rate coefficient.

2.6.3 Microscopic reversibility

Analogous to the case for cross sections, rate coefficients also obey microscopic reversibility (where $\Delta E = E_2 - E_1$):

$$\gamma(1 \rightarrow 2; T) = \frac{g_2}{g_1}\gamma(2 \rightarrow 1; T)e^{-\Delta E/k_B T}. \tag{2.20}$$

In principle, there is no difference in the rate coefficients obtained if the translational energy (temperature) distribution is adopted when computing cross sections as opposed to when computing rate coefficients; however, in trajectory studies there may be a small discrepancy due to the finite sample size. Endoergic or "upward" transitions are those transitions in which the final internal energy of the target molecule is greater than its initial internal energy, and exoergic or "downward" transitions are those in which the final internal energy is less than the initial internal energy. The binning method systematically overestimates state–to–state nonreactive and exchange cross sections for upward transitions, so a correction is made when computing rate coefficients. For state–to–state rate coefficients, Equation 2.20 was used to compute a second set of upward rate coefficients from the corresponding downward rate coefficients. Where both upward rate coefficients agreed within their standard errors, the average of the two was taken to be the final rate coefficient. Where not, the microscopic reversibility–derived rate coefficient replaced the rate coefficient derived directly from upward cross sections. Averaging tends to

occur at higher temperatures, while replacement of the rate coefficient is more likely at lower temperatures.

2.7 Reference states

To facilitate comparisons, nine states for each of H_2 and HD have been chosen for use as the bases for reference. The H_2 states coincide with those used in related studies [71, 73]. HD states are chosen to correspond closely in energy to H_2 states, as given in Appendix A, Table A.1. Most results will be presented using values derived from collisions involving molecules starting in these states. These states span a range of vibrational and rotational energies and are meant to give an overview of system behaviour. Energies for those states with internal energy < 1 eV are given in Table A.2, as these are also considered in some detail.

The ground state (0,0) is chosen for all three systems, as are the first pure vibrationally excited state (1,0), and a pure rotational state which has nearly the same energy as (1,0). The state HD(0,8) has slightly less internal energy than does H_2(0,8). Most results from HD(0,8) and HD(0,9), which more closely matches the energy of H_2(0,8), are quantitatively similar.

H_2 states (5,0), (2,14) and (0,20)—along with their HD counterparts (5,0), (2,16) and (0,24)—all have internal energy approximately half that required for dissociation. The $v = 2$ states have internal energy divided nearly equally between vibrational and rotational modes.

H_2 states (12,0), (5,24), and (0,32) are near the dissociation limit, as are the corresponding HD states (14,0), (8,24), and (0,37).

Turning points (Table A.3) may also be an important consideration, particularly the outer turning point, which is a measure of the size of a molecule. A molecule will spend a large portion of time with internuclear separation near the outer turning point, in part due to the anharmonicity of the 2–body potential. For the states under consideration, the only large difference between H_2 and HD in terms of molecular size is between H_2(5,24) and HD(8,24), where the HD molecule is 8% larger at its outer turning point and 11% smaller at its inner turning point than is H_2 at its respective turning points.

Of additional significance is the fact that HD is not symmetric about its centre of mass. This means that the opacity functions for H + HD are not directly comparable to those of H + H_2 and D + H_2. Of particular importance are collisions in which the collider hits the centre of the target molecule bond. It has been shown for H + H_2 that the configuration most likely to result in dissociation at threshold has the collider aimed at the centre of the bond in a perpendicular geometry [74]. For H + H_2 and D + H_2, this corresponds to $b = 0$. Due to the asymmetry of HD, the centre of the bond is at some impact parameter greater than 0.2 Å, depending upon the particular HD state.

For example, the outer turning point of HD(14,0) is at a separation of 2.38 Å, similar to the turning point of 2.37 Å for H_2(12,0). The impact parameter which corresponds to the centre of the H_2 bond at this separation is 0 Å. However, the impact parameter corresponding to the geometrical centre of the HD(14,0) bond is 0.395 Å. Similarly, when HD(8,24) is at its outer turning point, $b = 0.363$ Å. If the outer turning point of HD(8,24) were the same as that of H_2(5,24), the centre of mass would be at $b = 0.335$ Å, a small enough difference that the choice of HD(8,24) as a match for H_2(5,24) is appropriate.

2.8 Relative collision times

A contributing factor to differences between the isotopic analogues of H + H_2 is the differences in relative collision times. The collider and target molecule are initially 7 Å apart. Table A.4 gives the time it would take for the colliding species to reach the centre of mass in a head–on collision with no interaction, for selected translational energies. A typical collision lasts somewhat more than double this time. At a given translational energy, D + H_2 collisions occur over the greatest amount of time, approximately 1.22 times as long as H + H_2 collisions. H + HD collisions occur over time as long as 1.06 times that of H + H_2 collisions.

Figure 2.1: A comparison of the BKMP2 and CCI PESs. In the top left panel, the potential energy on the BKMP2 surface is plotted as contours for a perpendicular configuration. Dashed contours indicate potential energies below 109.5 kcal mol^{-1} at 25 kcal mol^{-1} intervals. Solid contours indicate potential energies of 109.5 kcal mol^{-1} and above at 25 kcal mol^{-1} intervals. R_1 is the distance between the collider and the centre of the diatom, while R_2 is the internuclear separation of the diatom. In the top right panel, the difference between the BKMP2 and CCI surfaces is plotted for a perpendicular configuration. Solid contours indicate that the potential energy of the BKMP2 surface is greater than that of the CCI surface, and are spaced at intervals of 0.1 kcal mol^{-1}, up to a limit of 1 kcal mol^{-1}. Dashed contours indicate that the potential energy of the CCI surface is greater than that of the BKMP2 surface, and are spaced at intervals of 0.1 kcal mol^{-1}. The first solid contour (that which separates the other solid contours from the dashed contours) represents those separations at which the BKMP2 and CCI surfaces have equal potential energies. The bottom left panel displays the difference between the BKMP2 and CCI surfaces for a 45° geometry, with the same contours as the upper right panel. The bottom right panel displays the difference between the BKMP2 and CCI surfaces for a collinear configuration, with the same contours as the upper right panel. The large differences observed along the diagonal in the bottom right panel correspond to small internuclear separations: the line connecting coordinate (0,0) to (6,3) corresponds to conformations in which two of the nuclei have the same position.

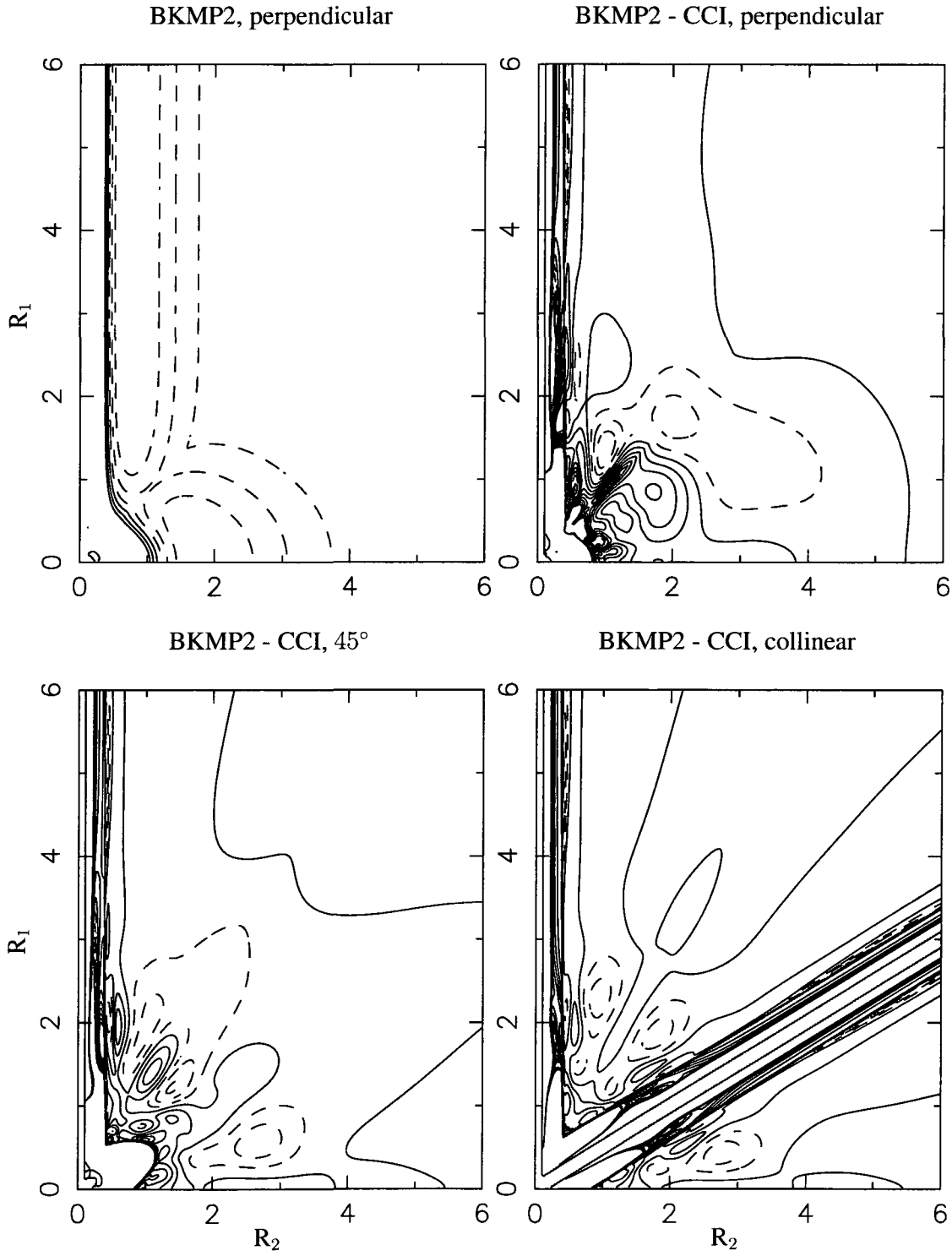

Figure 2.1: See text on previous page.

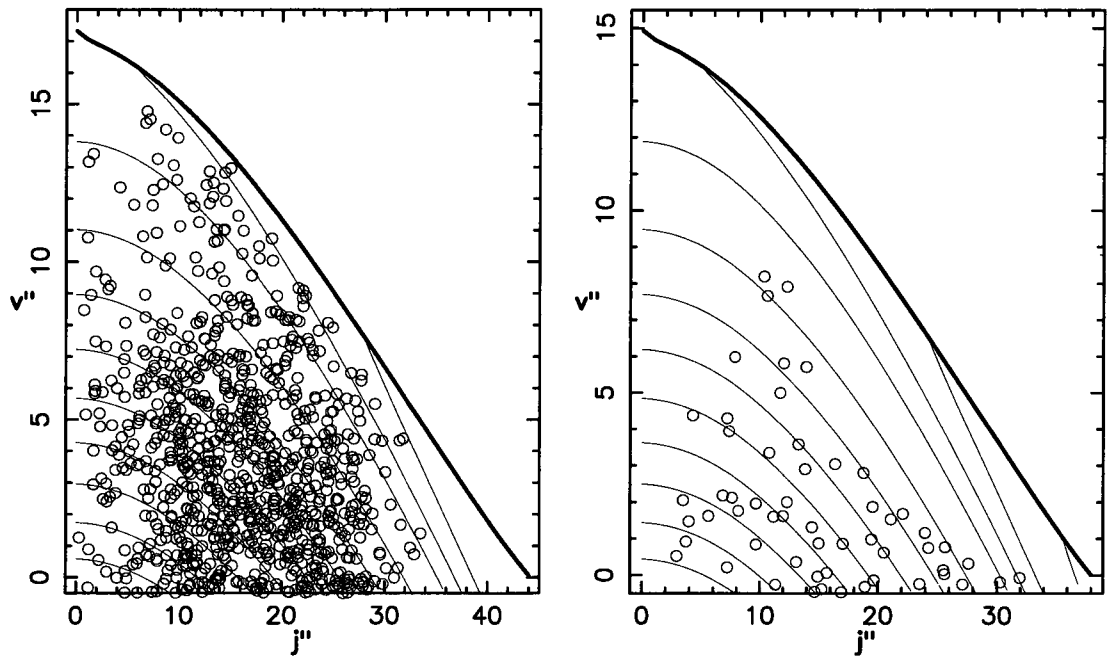

Figure 2.2: Final (classical) quantum numbers for trajectories from D + H_2(2,14), $0 \leq b \leq 0.5$ at $E_{\text{trans}} = 85$ kcal mol^{-1}. On the left is exchange to H + HD. On the right are the inelastic nonreactive trajectories. The final rotational quantum number j'' is given on the x–axis, and the final vibrational quantum number v'' is given on the y–axis. The bold line represents the classical dissociation limit. Each plot marker represents the result of a single trajectory from a batch of 1000.

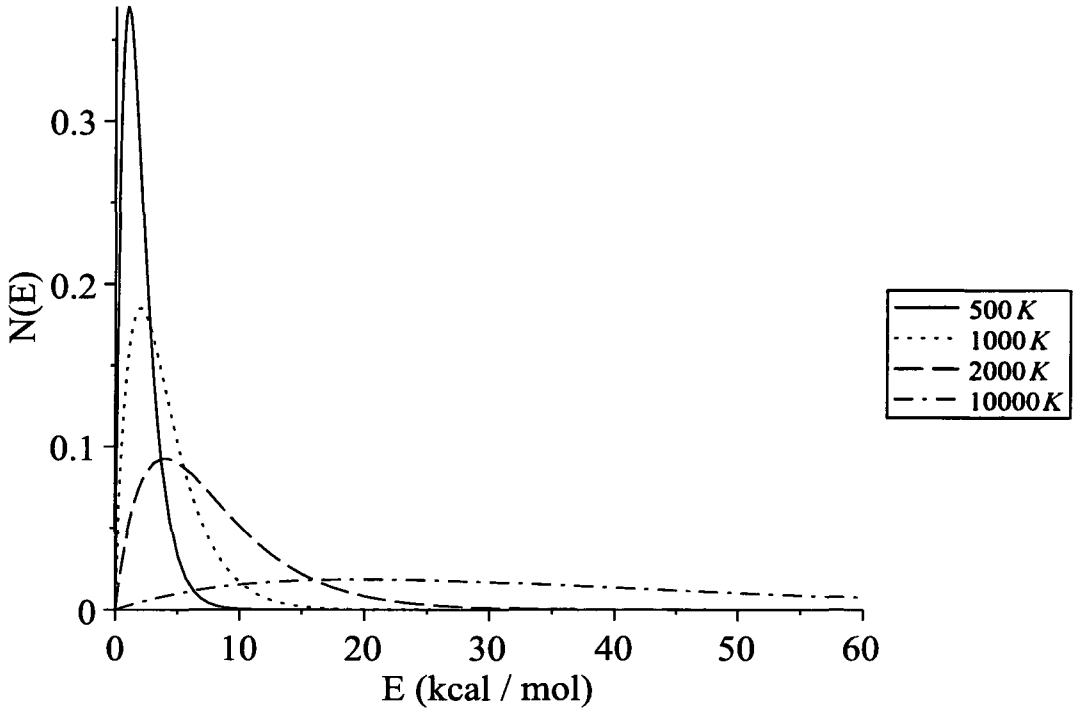

Figure 2.3: Population fraction $N(E)$ plotted against translational energy for a thermal (Boltzmann) distribution at 500 K, 1000 K, 2000 K and 10000 K.

Chapter 3

Collision–induced dissociation

Collision–induced dissociation (CID) is perhaps the simplest of the processes under consideration. There is only one outcome: all three atoms come apart as individual species. However, there are two possible mechanisms by which this can occur.

For trajectories with lower impact parameter, the insertion mechanism is possible. The collider is "inserted" between the atoms of the target molecule (possibly forming a relatively long–lived but unstable 3–body complex, though this is not usual). Insertion may occur when the target molecule is oriented such that the collider can move between the atoms of the target molecule. For each approach angle, there is a local saddle point in the potential. There exists a repulsive barrier leading up to this saddle point along the diatomic bond (see Figure 2.1, top left panel), but if this is overcome, the collider may be drawn toward the region surrounding the saddle point, and if the collision angle is not fixed, the entire system may move toward a conformation at an angle with a lower energy saddle point. A system which approaches a conformation near a saddle point may have a kinetic energy great enough that the collider will move up the repulsive wall toward a compact geometry, with the collider situated between the atoms of the target molecule. Due to the high potential energy of this conformation (relative to the state in which all three atoms are not in close proximity), one or both of the atoms of the target molecule may be ejected from the complex. Collision–induced dissociation occurs when the collider does not subsequently form a bond with either of the other atoms. (If a bond is formed, an exchange reaction results, and if the inserted atom is itself ejected, nonreactive

energy transfer may occur.)

The abstraction mechanism is possible for trajectories with impact parameters that make insertion impossible, as well as for those in which the insertion mechanism may occur. While the insertion mechanism relies upon the close–range repulsion of atoms to effect dissociation, processes involving the abstraction mechanism occur as a result of long–range attraction. In this mechanism, the collider passes close enough to attract one of the atoms of the target molecule. The original bond may be broken, resulting in either CID or exchange, depending upon the relative energy between the collider and the abstracted atom.

Each mechanism varies in effectiveness according to the translational energy. For collisions in which the collider ends up between the nuclei of the molecule (or close enough outside one to be effectively a direct hit—usually an insertion–type collision), an increase in translational energy means that the collider can make a closer approach, until the energy is reached at which the collider can penetrate the molecule entirely. The smaller internuclear separations that occur in higher energy collisions increase the repulsive force between the target molecule's nuclei, resulting in a promotion of this mechanism. Translational energy above that at which the collider can completely penetrate the molecule does not aid in promoting some processes which occur via the insertion mechanism due to a reduction in time available for interaction, though the additional available energy may, for instance, promote CID rather than exchange. Indeed, for some vibrational phases a quickly moving collider may pass right through the target molecule, leaving it (nearly) unaffected. In addition, a faster collider may have a smaller area to hit in order to cause a reaction, as the target molecule sweeps out less space in the limited interaction time.

The effectiveness of the abstraction mechanism also depends in part upon interaction time. A low translational energy means that there is more time for the attractive force to act upon the target molecule and break it apart. However, exchange is the preferred process at low translational energy. There are thus two competing factors for CID via the abstraction mechanism: there must be little enough translational energy to give enough time for the original

bond to be broken, but there must be enough translational energy for the collider to escape without having formed a new bond. The importance of each of these mechanisms to CID will be investigated through analysis of the opacity functions.

Microscopic reversibility can not be applied to the rate coefficients for CID because the rate coefficient for the process in which three unbound atoms come together to form a bound molecule can not be calculated directly. The initial phase space for such a process can not be precisely defined (though attempts at such calculations have been made: c.f. Schwenke, 1988 [10] and references therein). As binning is not required to calculate the rate coefficients for CID, the problems associated with binning are not encountered, so there is no need to apply microscopic reversibility.

The results of this study indicate that dissociative behaviour obeys relatively simple rules. At low temperature, dissociation occurs almost exclusively from high energy states and the rate coefficients are directly dependent upon the total internal energy. At very high temperature, the distribution of internal energy into vibrational and rotational modes makes a larger relative difference, but all states with similar internal energies have rate coefficients for dissociation which are within an order of magnitude of one another.

3.1 Opacity functions for CID

To study which types of collisions contribute most to CID cross sections, opacity functions are compared for each of H + H_2, H + HD and D + H_2 for each of the nine reference states introduced in Section 2.7. Although the corresponding HD and H_2 states chosen have slightly different internal energies (Table A.1), this is not expected to have a significant impact on the opacity functions. Low temperature rate coefficients are sensitive to cross sections for total energies immediately above the energetic threshold (total energy $\gtrsim$ 109.5 kcal mol^{-1}). However, at energies close to threshold, the relative errors in the opacity functions are too large to permit firm conclusions about the corresponding cross sections to be drawn from the opacity functions. To illustrate the role of the impact parameter, those opacity functions with

total energy of 130 kcal mol^{-1} and 205 kcal mol^{-1} are compared. The lowest energy at which the majority of probabilities are significantly nonzero is 130 kcal mol^{-1}, while 205 kcal mol^{-1} was chosen because the probabilities for the different systems are statistically distinct from one another in many cases, allowing further study of the differences between systems.

Opacity functions for the reference states are given in Figure 3.1 and Figure 3.2. In both figures, the first column contains the low internal energy states, the second column contains states with energy near 55 kcal mol^{-1}, and the third column contains high energy states. The first row contains states with rotational energy only, the middle row contains states with approximately equal amounts of vibrational and rotational energy, and the third row contains states with vibrational energy only. The total energy of systems displayed in Figure 3.1 is near 205 kcal mol^{-1}, while the total energy in Figure 3.2 is near 130 kcal mol^{-1}.

3.1.1 Opacity functions for CID from (0,0) states

From (0,0) at 205 kcal mol^{-1} total energy, trajectories with $b < 0.1$ are unlikely to cause dissociation, especially for D + H_2, which registered no dissociative events in 1000 trajectories (see Figure 3.1).

As impact parameter is increased, the opacity function for H + HD rises abruptly in the 0.2–0.3 Å range. The inner turning point of HD is 0.64 Å. However, since the centre of mass is one third of the way along the HD bond, an impact parameter of 0.21 Å potentially results in a trajectory with the collider aimed directly at the D atom. The functions for D + H_2 and H + H_2 rise more gradually, approaching the H + HD value in the 0.4–0.5 Å range. The inner turning point of 0.63 Å places the H nuclei of H_2 at an impact parameter of at most 0.32 Å. It appears from these opacity functions that dissociation is most likely to occur when the collider is aimed somewhat to the side of the target molecule, indicating that for this total energy, abstraction is the important mechanism.

The probabilities in Figure 3.2 have large relative errors, but there are significantly nonzero values for (0,0) above the first bin. It is interesting that no dissociative events are

observed at the lowest impact parameters, despite the fact that the most favourable conformation for CID is likely there [75]. One explanation may be that a very slight deviation from a perpendicular conformation drastically reduces the probability of CID. End–on collisions are the least likely to cause dissociation, and since the surface is attractive, an approaching collider will tug on the nearest atom of the target molecule, changing the orientation toward an end–on geometry. Since sampling is performed randomly over phase space, rather than selecting the specific most favourable geometry, this will happen in nearly all cases; consequently, there is little chance of CID at low impact parameter unless the translational energy is large enough that reorientation is unimportant. Such orientation effects have been discussed throughout the literature (c.f. Aoiz *et al.*, 1996 [23], and references 83–85 therein).

At a total energy of 130 kcal mol^{-1}, the opacity function for H + HD(0,0) peaks in the 0.7–0.8 Å bin. This is well outside the outer turning point, and may represent trajectories in which the target molecule has been abstracted, rather than undergoing the insertion mechanism, which occurs more commonly in low impact parameter collisions. A similar peak is observed for H + HD(0,8) in the 0.6–0.7 Å bin, though the error bars for these points are too large to draw firm conclusions. This peak represents 6 trajectories out of roughly 200, whereas the surrounding impact parameter ranges have only 1 or 2 CID events each. At these impact parameters, the other two systems show almost no dissociative behaviour at all: it would be interesting to do extremely large trajectory batches ($> 10^6$ trajectories) to see whether or not this is a real effect, and if so, whether or not the HD molecule is so much more prone to CID at this range. A more detailed look at single collisions for both H_2 and HD might also help to understand this behaviour, perhaps using a movie to visualize the collision.

Statistically, most collisions occur at high impact parameter, meaning that if the probabilities of a particular transition or dissociative process are separated into impact strata (as in an opacity function), those in the higher strata are given a higher weight in their contribution

to the value of the cross section, as in Equation 1.1

$$\sigma(E) = 2\pi \int_0^\infty bP(b, E)\mathrm{d}b.$$

Therefore, how rapidly the opacity function decreases as b is increased beyond the outer turning point greatly affects the total cross section. For the case of (0,0) at 205 kcal mol^{-1} total energy, CID events are observed for D + H_2(0,0) at impact parameters as much as 0.2 Å higher than for the other two systems. Thus, it can be expected that the D + H_2 cross section at 205 kcal mol^{-1} will be large compared to the other two, which should be similar to each other. This is borne out in Figure 3.3, where the CID cross section for D + H_2(0,0) at a translational energy of 200 kcal mol^{-1} is 0.311 ± 0.023 Å^2. The cross section for H + H_2(0,0) at this energy is 0.232 ± 0.011 Å^2, and the cross section for H + HD(0,0) is 0.220 ± 0.017 Å^2.

The difference in cross sections between D + H_2(0,0) and H + H_2(0,0) for collision–induced dissociation at 205 kcal mol^{-1} is most likely caused by a promotion of the abstraction mechanism as a result of the increased interaction time for D + H_2 relative to the other two systems. Times required for the movement of the colliding atom to the centre of mass of the diatomic in the absence of any interaction are given in Appendix A, Table A.4. At any translational energy, the ratio of the noninteractive time of movement to the centre of mass of D + H_2 to that of H + H_2 is 1.15 to 1. The ratio of the noninteractive time of movement to the centre of mass of H + HD to that of H + H_2 is 1.22 to 1. These ratios are also the ratios of the square roots of the reduced masses of the systems in question:

$$\sqrt{\frac{\mu_{D+HH}}{\mu_{H+HH}}} \simeq 1.15, \text{and} \tag{3.1}$$

$$\sqrt{\frac{\mu_{H+HD}}{\mu_{H+HH}}} \simeq 1.22. \tag{3.2}$$

If the increased interaction time were the primary cause of the difference in cross sections among these systems, one would expect to see the relation

$$\frac{\sigma_{\mathrm{CID},1}}{t_1} = \frac{\sigma_{\mathrm{CID},2}}{t_2} \tag{3.3}$$

or, substituting $\sqrt{m_i} \propto t_i$ and cancelling,

$$\sigma_{\mathrm{CID},1} = \sqrt{\frac{\mu_1}{\mu_2}} \cdot \sigma_{\mathrm{CID},2} \tag{3.4}$$

hold true. In particular,

$$\sigma_{\mathrm{CID,D+H_2}} = \sqrt{\frac{\mu_{\mathrm{D+H_2}}}{\mu_{\mathrm{H+H_2}}}} \cdot \sigma_{\mathrm{CID,H+H_2}}, \tag{3.5}$$

and

$$\sigma_{\mathrm{CID,H+HD}} = \sqrt{\frac{\mu_{\mathrm{H+HD}}}{\mu_{\mathrm{H+H_2}}}} \cdot \sigma_{\mathrm{CID,H+H_2}}. \tag{3.6}$$

When the cross section for CID of H + H_2(0,0) at 205 kcal mol^{-1} is multiplied by the factor 1.15 as in the right hand side of Equation 3.5, a modified cross section of 0.285 ± 0.014 Å^2 is obtained. The modified cross section calculated in this way for H + H_2 is a statistical match to the measured cross section for D + H_2, 0.311 ± 0.023 Å^2. When the cross section for CID of H + H_2(0,0) at 200 kcal mol^{-1} is multiplied by the factor 1.22 (corresponding to H + HD), a modified cross section of 0.254 ± 0.020 Å^2 is obtained, slightly larger than the measured 0.220 ± 0.017 Å^2 cross section for H + HD. The difference between cross sections for H + H_2 and H + HD may be in part because abstraction is an important contributor to the CID cross sections for low energy states. H + HD may experience less abstraction than does H + H_2 because the heavier D atom is more difficult to accelerate than an H atom, so trajectories in which the approaching H atom passes closest to the D atom in the HD molecule are less likely to result in CID than those passing by an H atom in the H_2 molecule. Another possibility is that the cross section for CID from H + HD(0,0) is less than that of H + H_2(0,0) because of the lower internal energy of H + HD(0,0); however, as the total energy of these systems (205 kcal mol^{-1}) is nearly twice that required for dissociation, the importance of the abstraction mechanism may be the more important factor in explaining the difference in cross sections.

3.1.2 Opacity functions for CID from (0,j) states

The effect on opacity functions of adding rotational energy may be seen by examination of the top rows of Figure 3.1 and Figure 3.2. Among the states with low internal energy

examined, for both translational energies studied, the opacity functions of D + H_2(0,8) are significantly nonzero at higher impact parameters than are those of H + H_2(0,8) and H + HD(0,8). Cross sections for D + H_2(0,8) may be larger than those of either H + H_2(0,8) or H + HD(0,8) in both cases.

At 205 kcal mol^{-1} total energy, the H + H_2(0,8) and H + HD(0,8) opacity functions decrease to 0 in the same impact parameter range; in this case, the greater values of the opacity function of H + H_2 at the impact parameter ranges immediately below this mean that the cross sections for H + H_2(0,8) will be the greater of the two, despite the almost complete absence of CID from H + H_2(0,8) at low impact parameter. The outer turning points of these states correspond to impact parameters which differ by less than 0.1 Å. Therefore, the region of phase space in which the insertion mechanism is available is similar in both cases; however, the lesser translational energy in the (0,8) systems should reduce the effect of insertion in promoting CID. This suggests that the increase in dissociation as a result of adding rotational energy is a result of the promotion of the abstraction mechanism.

At 130 kcal mol^{-1} total energy, the opacity function for H + HD(0,8) reaches its maximum at a lower impact parameter than do the opacity functions of H + H_2(0,8) and D + H_2(0,8). The opacity functions of H + H_2(0,8) and D + H_2(0,8) are largely similar to each another. At this total energy, because the opacity function of H + HD(0,8) declines with impact parameter more rapidly than do the opacity functions, the cross section for CID from H + HD(0,8) should be smaller than the corresponding cross sections for either H + H_2 or D + H_2.

The situation changes for H_2(0,20) and HD(0,24). At 205 kcal mol^{-1} total energy, the maximum value of the opacity function for CID from H + HD(0,24) is greater than the maximum values of the opacity functions of H + H_2(0,20) and D + H_2(0,20); however, the probabilities for H + HD(0,24) are less than those for H + H_2(0,20) and D + H_2(0,20) at the highest impact parameters in which CID is observed. The peak value of the opacity function for CID from H + HD(0,24) corresponds to an impact parameter range near the outer turning point, suggesting that the insertion mechanism may be important at a total energy of 205 kcal mol^{-1}.

For D + H_2(0,20) and H + H_2(0,20), at both 130 kcal mol^{-1} and 205 kcal mol^{-1} total energy, the opacity function peaks near 1.0 Å. This is far enough outside the outer turning point that abstraction is likely to be the dominant mechanism.

The opacity functions for all three of H + H_2(0,20), D + H_2(0,20) and H + HD(0,24) at 205 kcal mol^{-1} total energy are nonzero for impact parameters at which only the abstraction mechanism is likely: 1.7–1.8 Å for the H_2 systems and 1.8–1.9 Å for H + HD. For (0,8), the D + H_2 opacity function is much greater than the H + H_2 function at impact parameters above 0.8 Å. For high speed collisions at low internal energy, there may not be enough time to transfer sufficient energy to cause dissociation. As the initial internal energy is increased, less energy needs to be transferred to reach the dissociation limit, so the collision time decreases in importance.

At 130 kcal mol^{-1} total energy, the probability of CID for D + H_2(0,20) is in general greater than the probabilities of H + H_2(0,20) and H + HD(0,24), lending further credence to the hypothesis that abstraction is the dominant mechanism for CID. The enhanced values of the opacity function at 205 kcal mol^{-1} of D + H_2(0,20) over those of H + H_2(0,20) at the highest impact parameter ranges is also consistent with this hypothesis.

At a total energy of 205 kcal mol^{-1}, the opacity functions are similar among all of H + H_2(0,32), D + H_2(0,32) and H + HD(0,37). All three opacity functions approach 0 at impact parameters near 2.2 Å, and all are large between the turning points. The opacity functions for these states with 130 kcal mol^{-1} total energy reinforce the idea that a longer collision time promotes dissociation: the D + H_2(0,32) opacity function is much greater than the opacity functions of H + H_2(0,32) and H + HD(0,37) at most impact parameter ranges. In addition, CID events for 130 kcal mol^{-1} are observed for impact parameters as great as 2.5 Å, slightly greater than at 205 kcal mol^{-1}. Although the opacity functions at 205 kcal mol^{-1} are greater than those at 130 kcal mol^{-1} at most impact parameters due to the increased availability of energy, the higher collision speed leads to a lower probability at the outermost impact parameters, either because the collision does not last long enough to transfer sufficient energy to break the

molecule apart, or because there is not sufficient time for the target molecule to move into an orientation that favours dissociation.

3.1.3 Opacity functions for CID from $(v, 0)$ states

Dissociation from states with purely vibrational energy is similar in many respects to dissociation from those with purely rotational energy at a total energy of 205 kcal mol^{-1}; however, there are significant differences at 130 kcal mol^{-1}.

For (1,0) at 205 kcal mol^{-1}, a longer collision time makes for enhanced CID in D + H_2 as compared to H + H_2. H + HD(1,0) is more likely to undergo dissociation at low impact parameter, and less likely at high impact parameter, than is H + H_2(1,0). This is similar to what was observed in the case of (0,8). The opacity functions for the (5,0) states at 205 kcal mol^{-1} are all null at the same impact parameters, just as for the purely rotationally excited states; however, the opacity function for H + HD(5,0) is much less than the opacity functions for H + H_2(5,0) and D + H_2(5,0) at impact parameters between 1 Å and 2 Å. In all these cases, the probabilities of CID for D + H_2 are greater than those of H + H_2 and H + HD for most of the higher impact parameter values.

At 130 kcal mol^{-1} total energy, for both (1,0) and (5,0), CID is more likely for D + H_2 compared to H + H_2 and H + HD. At both energies compared, CID for D + H_2(12,0) is enhanced relative to H + H_2(12,0) over most of the impact parameters from 2.3–3.3 Å, but the opacity function of H + HD(14,0) is the greatest of those of all three isotopic analogues at the larger impact parameters at which CID occurs. The atomic separation of H_2(12,0) is 2.37 Å at its outer turning point, nearly the same as the 2.38 Å separation of HD(14,0). At 2.38 Å atomic separation, the centre of mass of HD is 0.4 Å from the geometric centre of the molecule; the centre of mass of H_2 is located at the geometric centre. The maximum impact parameter at which CID occurs for H + HD(14,0) at both 130 kcal mol^{-1} and 205 kcal mol^{-1} is approximately 0.4 Å greater than the maximum impact parameter at which CID occurs for either H + H_2(12,0) or D + H_2(12,0). This may indicate that the difference in opacity functions for

CID at the largest impact parameters at which CID occurs is due primarily to the difference in the impact parameter corresponding to the geometric centre of HD and of H_2.

3.1.4 Opacity functions for CID from $(v \neq 0, j \neq 0)$ states

The states with medium and high energy in both vibration and rotation have opacity functions that very closely resemble those of the corresponding purely vibrational states. As the fraction of energy in vibration is increased, the outer turning points of the molecules are increased, and dissociative events are observed at larger impact parameters. For any given impact parameter greater than that at which the opacity function peaks, the value of the opacity function is greater for states with higher vibrational energy. At low and moderate internal energies, the difference between H + HD and the other two systems is more pronounced when more of the internal energy is vibrational. The same is true for translational energy, meaning that as total energy is increased, regardless of its distribution, isotopic differences begin to vanish.

3.2 Thresholds to dissociation

Dynamical thresholds for CID were determined by running 9999 trajectories for ten batches with total energies near the energetic threshold for each (v, j) state, at the first eight energies above the energetic threshold, on a 1 kcal mol^{-1} (integer) grid. The two energies below the energetic threshold, when they existed, were also chosen for batches of 9999 trajectories, partly as a check to help verify that bound molecules would not be recorded as dissociated, and partly to obtain better statistics for some state–to–state transitions for which internal energy is nearly conserved. In contrast to He + H_2, a nonreactive system, for which a large dynamic elevation of threshold for CID exists [73], no significant elevation of threshold is observed in H + H_2 or its isotopic analogues, in accordance with previous studies (c.f. Dove *et al.*, 1986 [74]).

Calculations of rate coefficients using 1000 and 9999 trajectories gave results that sometimes differed by factors as great as 10^4 at 100 K, because the 1000 trajectory batches were not always large enough to find trajectories that would result in CID at the translational energies immediately above the energetic threshold. The differences were negligible or nearly so at temperatures of 1000 K and up. QCT results are in general expected to be valid only for temperatures above approximately 500 K, so there is confidence that the rate coefficients are precise for the temperature range within which the method is valid. The rate coefficients for CID near threshold, and therefore the rate coefficients for CID, could be improved with a smaller grid size (0.1 kcal mol^{-1} or less) and with more trajectories.

3.3 Cross sections and rate coefficients for dissociation from states with low internal energy

The left–hand column of Figure 3.3 shows CID cross sections from states with low internal energy plotted as a function of translational energy for H + H_2, H + HD and D + H_2. Within all three systems, cross sections from (0,8) and (1,0) are similar to each other below 120 kcal mol^{-1} translational energy. Above 120 kcal mol^{-1}, vibrational energy is more effective at promoting dissociation than is rotational energy. Cross sections from (0,0) are the smallest, due in part to the lower total energy of the system; however, even accounting for the difference in total energy, CID cross sections from (0,0) are lower than those from the other states, indicating that internal energy is more effective at promoting CID than is translational energy. This is in accordance with previous studies (c.f. Aoiz *et al.*, 2005 [4] and references therein).

D + H_2 and H + H_2 have similar energetic and dynamical thresholds to dissociation, but cross sections for CID on these systems differ at translational energies immediately above that. Cross sections for D + H_2 rise much more sharply as a function of E_{trans} than do those of H + H_2 and remain 10–15% higher at all energies. As discussed in Section 3.1.1, a larger reduced mass for D + H_2 at the same translational energy makes for a smaller relative velocity and a relatively

prolonged collision. The increase in interaction time may give a greater chance that energy will be transferred from the collider to the target molecule. Increased interaction time also appears to be important for exchange and nonreactive energy transfer, discussed in Sections 4 and 5, although the differences between the products of exchange reactions with H_2 and with HD complicate matters. This is shown in Appendix B, Table B.1, which contains trajectory counts for exchange and nonreactive energy transfer at different impact parameter strata.

The cross sections for CID from H + H_2(1,0) are 10–15% higher than are the corresponding cross sections for H + HD(1,0). As discussed in Section 3.1, cross sections are sensitive to events which occur at high impact parameter. Owing to this (see Figures 3.1 and 3.2), at both 205 kcal mol^{-1} and 130 kcal mol^{-1} total energy, the H + H_2(1,0) system has a higher probability for dissociation than does the H + HD(1,0) system at the uppermost impact parameters.

Given the differences in cross sections at most energies, one might hypothesize that the rate coefficients for these processes would differ significantly. However, this is not the case. These rate coefficients are displayed in the right–hand column of Figure 3.3. For all systems at any given lower to middle-range temperature, the rate coefficient for (0,0) is an order of magnitude lower than those of (0,8) and (1,0), which are closer in magnitude to each other, generally within a factor of two. For example, at 1000 K, the rate coefficients for CID of H + H_2 are

$$\begin{aligned}
\gamma((0,0) \rightarrow \text{CID}) &= 1.672 \times 10^{-13} \pm 1.9 \times 10^{-15} \ \text{cm}^3\text{s}^{-1}\text{molec}^{-1}, \\
\gamma((0,8) \rightarrow \text{CID}) &= 5.424 \times 10^{-13} \pm 4.9 \times 10^{-15} \ \text{cm}^3\text{s}^{-1}\text{molec}^{-1}, \\
\gamma((1,0) \rightarrow \text{CID}) &= 8.344 \times 10^{-13} \pm 6.5 \times 10^{-15} \ \text{cm}^3\text{s}^{-1}\text{molec}^{-1}.
\end{aligned}$$

The rate coefficient for H + H_2(0,8) is 3.2 times that of the rate coefficient for H + H_2(0,0), while the rate coefficient for H + H_2(1,0) is 5.0 times as great. The relative difference is more pronounced at lower temperatures. In this temperature regime, the most important contribution to the rate coefficients comes from cross sections near threshold; since (0,8) and (1,0) have similar thresholds to dissociation, their rate coefficients are more similar to each other than to

the rate coefficients for (0,0).

At higher temperatures, the relative difference between the rate coefficients of (1,0) and (0,8) is greater than at 1000 K, while the relative difference between the rate coefficients for each of these two states and those for (0,0) is less. As temperature increases, rate coefficients depend more upon the cross sections at high energy and less upon the threshold energy. The increased dependence upon high energy cross sections explains the separation of (1,0) and (0,8). The (0,0) rate coefficients become relatively more similar to the (1,0) and (0,8) rate coefficients as temperature increases despite the difference in cross sections: this is due to the importance of threshold energy to the value of rate coefficients in the low temperature regime.

Between isotopic analogues, corresponding rate coefficients are also similar to each other at most temperatures despite the large differences in higher energy cross sections. Around 1000 K, H + HD rate coefficients are just slightly larger than the corresponding $H + H_2$ or $D + H_2$ rate coefficients. This occurs even though the dependence of rate coefficients on the threshold energy suggests that the opposite should be the case. An analysis of the trajectory data shows why this is. There are few CID events near threshold, so the ones that do occur contribute greatly to the rate coefficients. The H + HD events may occur at a larger impact parameters than the $H + H_2$ or $D + H_2$ events, resulting in larger cross sections at the lowest energies at which CID is observed.

In summary, rate coefficients for low energy states depend mostly upon the internal energy of the state and the threshold, with only minor adjustments imposed by the specific energy distribution or masses of the reactants. A large number of trajectories near threshold are necessary to get highly accurate low to medium temperature rate coefficients, but results with more limited batches are still reasonable for all but the lowest temperatures.

3.4 Cross sections and rate coefficients for dissociation from states with internal energy near 55 kcal mol^{-1}

At an internal energy about half of that required for dissociation, cross sections and rate coefficients exhibit the same trends as were seen for lower internal energies. The left–hand column of Figure 3.4 shows cross sections plotted against translational energy for H + H_2 and D + H_2 states (5,0), (2,14) and (0,20), as well as for H + HD states (5,0), (2,16) and (0,24). As laid out in Appendix A, Table A.1, the H_2 states all have nearly the same internal energies as each other (within 4 kcal mol^{-1} of each other), while the HD states vary more (within 11 kcal mol^{-1} of each other). As seen previously, for each system an increase in vibrational energy at the expense of rotational energy increases the cross sections at most translational energies.

All cross sections for D + H_2 are larger than their corresponding H + H_2 values. For states with low internal energy, cross sections continue to rise as translational energy is increased to 315 kcal mol^{-1}; however, most CID cross sections from states with internal energy near 55 kcal mol^{-1} have a maximum value below this. The cross sections of D + H_2(0,20) and D + H_2(2,14) do not decrease, but rather achieve nearly constant values at higher translational energies. For both H + H_2 and D + H_2, the (5,0) cross sections are distinct from the cross sections of the rotationally excited states almost immediately above threshold, while the rotationally excited states remain similar to one another at translational energies below 100 kcal mol^{-1}.

The excitation functions for each of the H + HD states are more similar in value to one another than to those of any state of H + H_2. The internal energy of HD(0,24) is 10 kcal mol^{-1} greater than that of the other two states, which accounts in part for why CID cross sections from HD(0,24) are greater than those of HD(2,16). The excitation functions for H + HD for all these states decrease dramatically as translational energy is increased above 200 kcal mol^{-1}.

For rate coefficients, it is notable that the internal energy of H_2(2,14) is 2 kcal mol^{-1} less than that of H_2(5,0), which is in turn 2 kcal mol^{-1} less than that of H_2(0,20). It could be

expected that because of the dependence of rate coefficients on the threshold energy, the rate coefficients for these states, given in the right–hand column of Figure 3.4, should be ordered correspondingly at low temperature. For both $H + H_2$ and $D + H_2$, although rate coefficients for CID from (2,14) are markedly smaller than the others up to 3000 K, the rate coefficients for CID from (5,0) and (0,20) are similar to each other. Above 3000 K, where cross sections at higher translational energies become important contributors to the rate coefficients, the rate coefficients from (5,0) are the greatest, while those for the other two states have comparable values, with all values converging near 100000 K. The cross sections for (5,0) near threshold are large enough compared to those of (0,20) to compensate for the greater energetic requirement for dissociation at most of the temperatures studied.

The same trends hold for H + HD rate coefficients as for $H + H_2$. At 780 K, a larger internal energy corresponds directly to a larger rate coefficient. At 100000 K, all the rate coefficients are nearly identical, as expected from the similarity of the cross sections at high E_{trans}.

In summary, CID rate coefficients for states with internal energies near 55 kcal mol^{-1} are most strongly dependent upon the internal energies of the species, rather than upon the specific internal energy distribution or masses.

3.5 Cross sections and rate coefficients for dissociation from states with internal energy near 109.5 kcal mol^{-1}

The left–hand column of Figure 3.5 shows cross sections for CID from selected states with internal energy near that required for dissociation. The most obvious feature of these curves is the difference in cross sections at low translational energy. Rapidly rotating molecules are shielded against dissociation at low translational energy: for most collision geometries, the collider can not penetrate the molecule to force it apart, as rapid rotation almost ensures that the collider will encounter one of the other atoms directly. Long range interactions for rapidly rotating molecules are more likely to result in deexcitation or exchange than for slowly rotating

molecules.

Corresponding states of H + H_2 and D + H_2 exhibit very similar behaviour at these energies. The only large difference is for (12,0), where the D + H_2 cross section curve has a steeper rise from threshold as translational energy is increased, with larger cross sections across most translational energies. This rise may be due in part to the longer time (approximately 122%) for a D + H_2 collision and the corresponding promotion of abstraction at higher impact parameters. In both systems, cross sections from (12,0) and (5,24) begin to converge at high translational energy.

The rate coefficients for these states are shown in the right–hand column of Figure 3.5. At high temperature, the three systems exhibit relatively similar rate coefficients; near 100 K, the (5,24) and (8,24) rate coefficients may vary by a factor of 100. H + HD(8,24) has larger rate coefficients that either H + H_2(5,24) or D + H_2(5,24), despite having a lower internal energy. These two states have internal energy above threshold, so it is to be expected that low temperature rate coefficients will be determined primarily by the cross sections at 1 kcal mol^{-1}, which in turn are influenced heavily by the high impact parameter ranges of the opacity functions. The larger outer turning point of HD(8,24) means that slightly larger impact parameter collisions should be able to cause dissociation, which eventually translates into a larger rate coefficient. For high energy states of D + H_2 at low temperatures, the increased importance of high impact parameter collisions combined with the increased importance of the abstraction mechanism (as a result of the slower collision speed) leads to a larger rate coefficient than from the same states of H + H_2.

For H + H_2 and D + H_2, the rate coefficients for (12,0) are much less than are the rate coefficients for (5,24) at the lower temperatures because of the difference in internal energy between the states. In the 1000–2000 K range, the CID rate coefficients from (12,0) become greater than those of (5,24) for both H + H_2 and D + H_2. In terms of the contribution to the rate coefficients at these temperatures, the most important cross sections are those with translational energies in the 10–20 kcal mol^{-1} range. The (12,0) cross sections are greater than the (5,24)

cross sections around 10 kcal mol^{-1} in both H + H_2 and D + H_2. For both systems, these cross sections (and those at higher translational energies) contribute enough to the rate coefficients at 2000 K to make the rate coefficients from (12,0) greater than those of (5,24).

As observed for states near 55 kcal mol^{-1}, excitation functions for CID from $(v, 0)$ states begin to decline as translational energy is increased beyond a certain point. The declines in the opacity functions begin at lower translational energies for states with purely vibrational energy than those for states with purely rotational energy. This trend is most pronounced in the H + HD system. Below a translational energy of 10 kcal mol^{-1}, the mixed energy state H + HD(8,24) has cross sections greater than those of the purely vibrational state H + HD(14,0). Between 10 kcal mol^{-1} and 20 kcal mol^{-1}, the cross sections for CID from H + HD(14,0) are greater than are those from H + HD(8,24), but between 30 kcal mol^{-1} and 60 kcal mol^{-1}, the cross sections for H + HD(8,24) are again the greater of the two, above which the H + HD(14,0) cross sections are the greater. At translational energies around 100 kcal mol^{-1}, the excitation functions for H + HD(14,0) first begin to decline with increasing translational energy, such that the H + HD(8,24) cross sections are greater than the H + HD(14,0) cross sections at translational energies above 150 kcal mol^{-1}.

These observations help to explain the behaviour of the rate coefficients for high energy states. Because the CID cross sections for H + HD(8,24) are greater than those of H + HD(14,0) at the lowest translational energies, the rate coefficients for H + HD(8,24) are less than those of H + HD(14,0) at low temperature. The CID cross sections for H + HD(14,0) are greater than those of H + HD(8,24) between 10 kcal mol^{-1} and 20 kcal mol^{-1} and near 100 kcal mol^{-1}; however, because the Boltzmann distribution curve (with which the cross sections are convolved to obtain the rate coefficients) is very broad for temperatures at which these cross sections are important, the CID rate coefficients from (8,24) are as great as or greater than those from (14,0) at all temperatures.

3.6 Overall trends for CID

Figures 3.6, 3.7, and 3.8 contain contour plots of rate coefficients for CID from all states at selected temperatures. The greatest rate coefficient on each plot is indicated by a solid square marker. In each case, this is for dissociation from the highest rotational state in the highest vibrational manifold, either H_2(14,4) or HD(17,1). Each system under consideration behaves similarly to the others at the same temperature.

For low and medium energy states, the contours in each diagram match up well with contours representing constant internal energy, especially at the lower temperatures. This supports the idea that for all three systems with thermal E_{trans} distributions, the extent of CID is governed more by total internal energy than by the specific distribution of that energy. At higher internal energies, rotation imposes a small barrier to dissociation, making vibrationally excited molecules more prone to undergo CID than rotationally excited molecules with the same energy. Previous studies and theoretical considerations predict this behaviour for reactive surfaces [75].

At the highest temperatures, all states have rate coefficients with a maximum relative difference between the highest and lowest rate coefficients around 10^3 at 20000 K, compared to a relative difference greater than 10^{20} at 1000 K. At 1000 K, larger variations (indicated by more closely spaced contours) occur among low energy states than among highly excited states. As temperature increases, the fastest changes in rate coefficients come among the highly rotationally excited states.

Displayed in the right–hand column of Figure 3.9 is a series of cuts through the contour plots along the $v = 0$ axis for the above and additional temperatures. The rate coefficients rise smoothly as v increases, with no abrupt changes in the slopes of the lines connecting the data points. In the right–hand column of Figure 3.10, a series of cuts through the contour plots along the $v = 0$ axis are displayed for the same temperatures as in Figure 3.9. For H + H_2 and D + H_2, there is a small, but sharp, jump in the rate coefficients at 20000 K as j approaches

its maximum value. This leads to the compression of contours at high j and low v observed in Figure 3.8. Lesser such jumps occur at all temperatures, but may not be as noticeable for the lower temperatures in Figure 3.9 because the difference in rate coefficients from one value of j to the next is already large. For the relatively level curve of the function at 20000 K, however, the small absolute increase in rate coefficient from one j to the next is a large relative increase.

As the contours in Figures 3.6, 3.7, and 3.8 are on a logarithmic scale, the relative change in rates represented by the two lower temperature contour plots is large. For a system at 1000 K, for example, only states above the first few contours—those with a certain amount of internal energy—will contribute to CID at any great rate. On the other hand, at 20000 K all states will contribute to CID with similar rate coefficients, with at most a relative difference of 10^3. These rate coefficients are further studied in Chapter 6.

3.6.1 v-dependence of CID

The left–hand column of Figure 3.9 displays cross sections for $(v, 0)$ states as a function of v at several translational energies. Of particular interest are those instances in which the CID cross sections from the higher energy states decrease as translational energy increases. This was seen in Figure 3.5, for instance, but Figure 3.9 gives a different view of this phenomenon. As the collision speed is increased, there is less time for interaction. Therefore, the abstraction of the molecule by a collider which passes outside the outer turning point is increasingly unlikely. Since the cross sections are more sensitive to the values of the opacity functions at higher impact parameters than at low impact parameters, cross sections can be greatly influenced by even a small change in probability of dissociation at these distances, due to either a change in the outer turning point or the relative speed of the reactants.

In Figure 3.9, it can be seen from the data for $v = 7$ that the advantage of more translational energy is offset by the decrease in interaction time between 150 kcal mol^{-1} and 200 kcal mol^{-1}: the cross sections at 150 kcal mol^{-1} and 200 kcal mol^{-1} are nearly equal, implying that the maximum cross section from H + H_2(7,0) occurs at a translational energy near

or between the two. For H + H_2(7,0), the maximum value of the excitation function, 5.42 Å^2, occurs at 175 kcal mol^{-1}. The value of the excitation function at 150 kcal mol^{-1} is 5.25 Å^2, and the value at 200 kcal mol^{-1} is 5.18 Å^2, with relative errors on the order of 1%. Similar behaviour occurs for D + H_2(8,0) and H + HD(7,0). The curves of the cross sections as functions of v appear to cross each other at most once, and the gap between cross sections grows or remains constant with increasing v, suggesting that each of the excitation functions for these states has a single local maximum. (The gap between H + HD(14,0) and H + HD(15,0) from 20 kcal mol^{-1} to 200 kcal mol^{-1} is an exception, but such exceptions appear to occur only between states with large internal energy differences and at high translational energy.)

The cross sections as represented in Figure 3.9 are functions of the vibrational state and translational energy. For each pair of translational energies E_1 and E_2, where $E_1 < E_2$, there exist cross sections $\sigma((v,0);E_1)$ and $\sigma((v,0);E_2)$ which are functions of v only. Let $v^\star$ be the smallest v for which $\sigma((v,0);E_1) \geq \sigma((v,0);E_2)$, and let $E_v^\star$ be the internal energy of the molecule in state $(v^\star,0)$. For any given pair of translational energies E_1 and E_2, each of H + H_2, H + HD, and D + H_2 may have a different $v^\star$, which for H + H_2 may be written as $v^\star = v^\star$(H + H_2), and similarly for the other isotopic systems. As a result of increased collision times for D + H_2, for most pairs E_1 and E_2 it is true that $v^\star$(D + H_2) $\geq v^\star$(H + H_2), so that $E^\star_{v(\mathrm{D}+\mathrm{H_2})} \geq E^\star_{v(\mathrm{H}+\mathrm{H_2})}$. For $E_1 = 150$ kcal mol^{-1} and $E_2 = 200$ kcal mol^{-1}, it is also true that $v^\star$(H + HD) $\geq v^\star$(H + H_2); however, because of the difference in the energy levels of H_2 and HD, $E^\star_{v(\mathrm{H}+\mathrm{HD})} \leq E^\star_{v(\mathrm{H}+\mathrm{H_2})}$. This result for H + HD compared to H + H_2 holds for most pairs of translational energies E_1 and E_2.

The reduction in $E^\star_{v(\mathrm{H}+\mathrm{HD})}$ relative to $E^\star_{v(\mathrm{H}+\mathrm{H_2})}$ occurs even though collisions of H + HD occur over a longer time on average than do those of H + H_2. With the exception of those involving the highest vibrational states, high impact parameter collisions make less important contributions to the cross sections of H + HD than to those of H + H_2, as discussed in Section 3.1 and illustrated in Figure 3.1. The reduction of high impact parameter CID events caused by a decreased collision time leads to a corresponding reduction of cross sections. This

reduction is greater for H + H_2 more than for H + HD, meaning that for rotationally unexcited states, there exists a translational energy above which the excitation functions for H + HD continue to increase, but above which the excitation functions for H + H_2 are nearly constant.

As can be seen in Figure 3.9, at any given temperature the values of the rate coefficients for CID for H + $H_2(v,0)$, D + $H_2(v,0)$, and the H + HD(v',0) state with the closest amount of internal energy are within an order of magnitude of one another. At high temperature, the population distribution of the molecules of a gas among the (v,0) states is relatively unimportant in determining the total rate at which CID occurs: the rate coefficients are similar for all states. At low temperature, however, dissociation occurs significantly only from highly excited states, in line with the ladder mechanism of dissociation (described, for instance, by Dove and Teitelbaum [76]).

3.6.2 j-dependence of CID

The left–hand column of Figure 3.10 shows cross sections for CID out of $(0, j)$ states at several translational energies, and the right–hand column of Figure 3.10 shows the corresponding rate coefficients. The rate coefficients for states in different systems with similar internal energy are nearly independent of the system under consideration, varying by at most a half order of magnitude. For purely rotational states, different mass combinations appear to have little effect on CID.

For the highest energy states, cross sections for H + HD are less than the corresponding cross sections of H + H_2, while cross sections for D + H_2 are slightly enhanced at low translational energy, but are similar to or reduced compared to those of H + H_2 at high translational energy. Because of this, for high energy states, H + H_2 has the greatest rate coefficients among the three systems, while H + HD has the least. However, the differences in CID rate coefficients between systems, are small relative to the difference between CID rate coefficients and those of nonreactive energy transfer or exchange reactions.

In contrast to the (v, 0) case, the excitation functions at different translational energies

spanning the range of validity of the PES do not cross at any j. For the states with energy near 55 kcal mol^{-1} (Figure 3.4), the purely rotational cross sections for both H + H_2 and H + HD decline slightly as the translational energy approaches 315 kcal mol^{-1}. This is not the case for either the low or high internal energy cases; however, the cross sections are nearly constant at high translational energy for initial states with internal energy near 109.5 kcal mol^{-1}, and the behaviour of the cross sections for initial states with energy near 55 kcal mol^{-1} suggests that the initial states with low energy may peak at some translational energy above 315 kcal mol^{-1} and decline as translational energy is increased above that. Another possible explanation for the absence of crossing of excitation functions as functions of j is that this behaviour is specific to purely rotational states and exists across all translational energies. For (v, 0), it was suggested here that the crossing of excitation functions was due mainly to a reduction in the number of high impact parameter collisions that lead to dissociation. Rotationally excited molecules are less likely to be abstracted in these collisions at any energy (Figure 3.1), meaning that the effect which causes crossing of the excitation functions for CID of the (v, 0) states is greatly diminished for excitation functions for CID of the (0, j) states.

3.7 CID from states with energy less than 1 eV

The left–hand column of Figure 3.11 displays CID cross sections from selected states with internal energy less than 1 eV. The H + H_2 cross section data increases almost linearly with translational energy for the lowest energy states. For states with internal energy near 1 eV, the cross sections display a sharp rise with increasing translational energy near threshold, but at higher translational energy, a near–linear but less steep rise is observed, similar what is observed for the lowest energy states. The relative errors of the D + H_2 cross sections are greater than those of H + H_2 because of the smaller number of trajectories run. The D + H_2 cross sections themselves are qualitatively similar to those of H + H_2, but are larger than the corresponding H + H_2 cross sections by approximately one quarter to one third. As discussed for (0,0) in Section 3.1.1, the relative difference in cross sections for the $v = 0$ states for the

systems H + H_2 and D + H_2 is close to the square root of the ratio of reduced masses (generally within standard error). The relative difference in cross sections for the $v = 1$ states is somewhat greater than the square root of the ratio of reduced masses of D + H_2 and H + H_2, suggesting that if the cross sections do scale with the square roots of the reduced masses for these states, it is not a linear scaling.

The cross sections of H + HD in this energy range are generally smaller than those of H + H_2. This is observed for all states with internal energies below 1 eV: the CID cross sections of a state of H + H_2 with a similar internal energy to that of a state of H + HD will have approximately 25% larger cross sections than those of the H + HD state. As for H + H_2 and D + H_2, the cross sections for two systems with similar internal energy H + $H_2(0,j)$ and H + HD$(0,j')$ appear to scale with the square root of their reduced masses, while the vibrationally excited states exhibit a slightly larger relative difference.

As seen in Figures 3.6, 3.7, and 3.8, the rate coefficients of states with similar internal energy (less than 1 eV) display little variation with state at any T. The right–hand column of Figure 3.11 shows the rate coefficients for states with internal energy less than 1 eV. Above 1000 K, the rate coefficients of H + $H_2(0,1)$ and H + $H_2(1,3)$ have a relative difference which is at most a factor of 10. At 100000 K, the relative difference between H + $H_2(0,1)$ and H + $H_2(1,3)$ is closer to a factor of 2. The H + H_2 and D + H_2 rate coefficients are quantitatively similar (though the D + H_2 rate coefficients at high temperature are slightly larger). High temperature rate coefficients for H + HD are marginally smaller than those for H + H_2, but near 1000 K, the rate coefficients for H + HD are larger than those for H + H_2 by a factor as great as 2. The difference in high temperature rate coefficients between H + H_2 and H + HD is due to larger high energy cross sections for H + H_2, while the difference around 1000 K is likely due in part to the slightly larger energetic thresholds for dissociation from HD states.

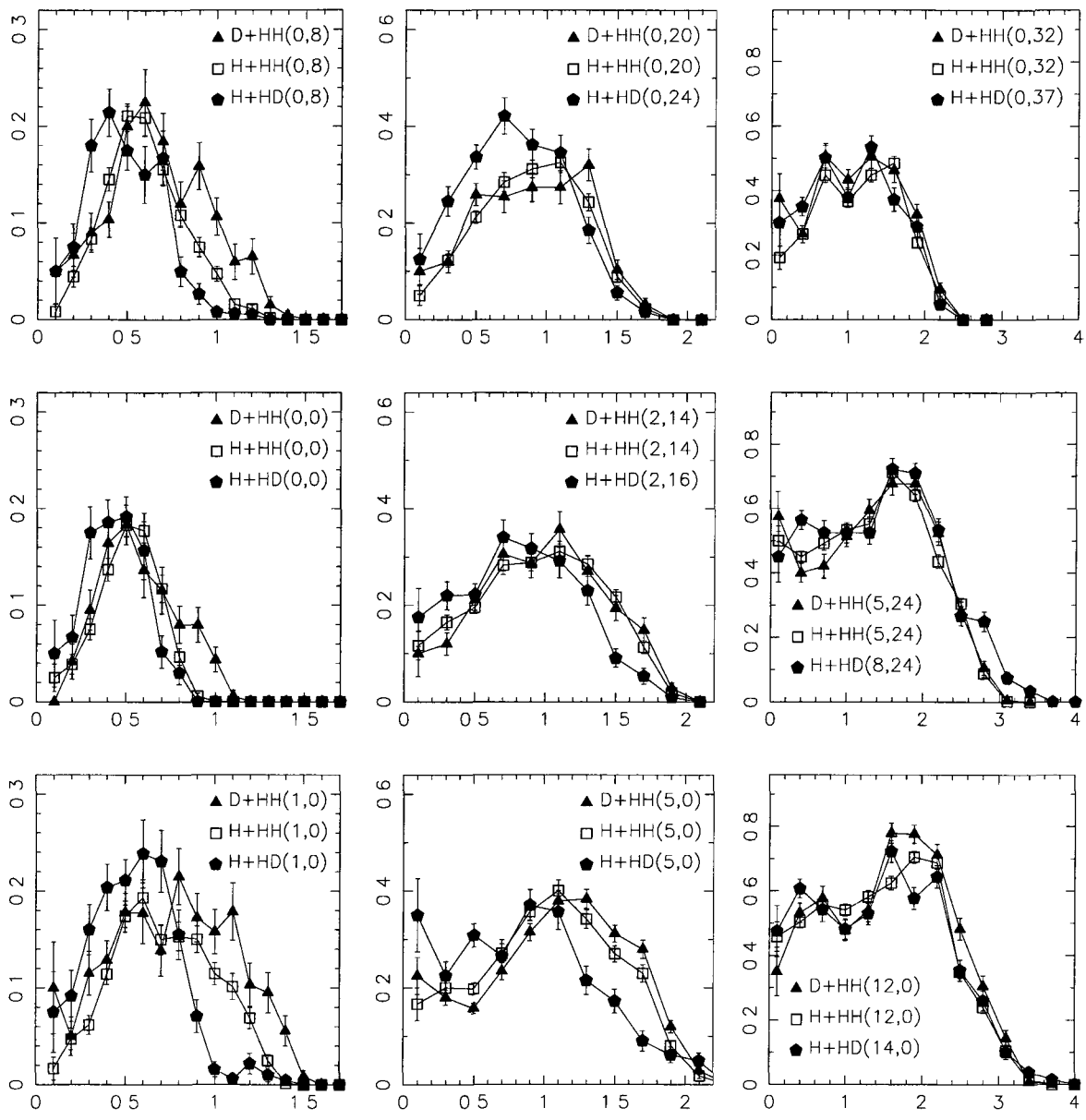

Figure 3.1: Opacity functions for CID from selected states of H + HD, H + H_2, and D + H_2 with total energy (internal plus translational) near 205 kcal mol^{-1}. The y axis is the probability of CID $P(b)$. The x axis is the impact parameter b. HD states are chosen to closely match the internal energy and turning points of the corresponding H_2 states. The first column contains the reference states with low internal energy, the second column contains states with energy near 55 kcal mol^{-1}, and the third column contains high energy states. The first row contains states with rotational energy only, the middle row contains states with approximately equal amounts of vibrational and rotational energy, and the third row contains states with vibrational energy only. Each column has a different y axis scale: the centre column is twice the leftmost, while the rightmost column is three times the leftmost.

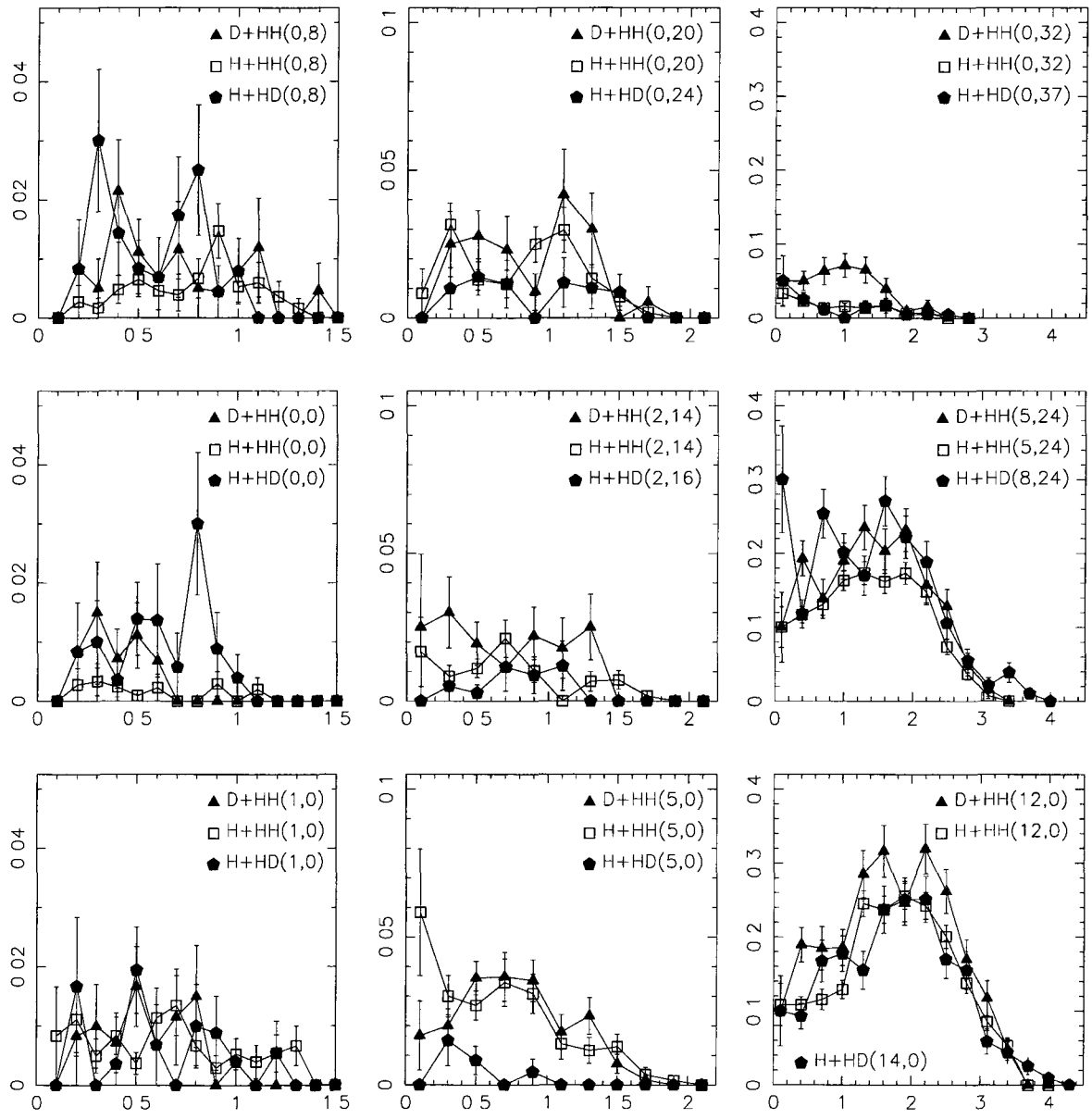

Figure 3.2: As in Figure 3.1, but for total energy near 130 kcal mol^{-1}. Note the changes of scale on the vertical axes.

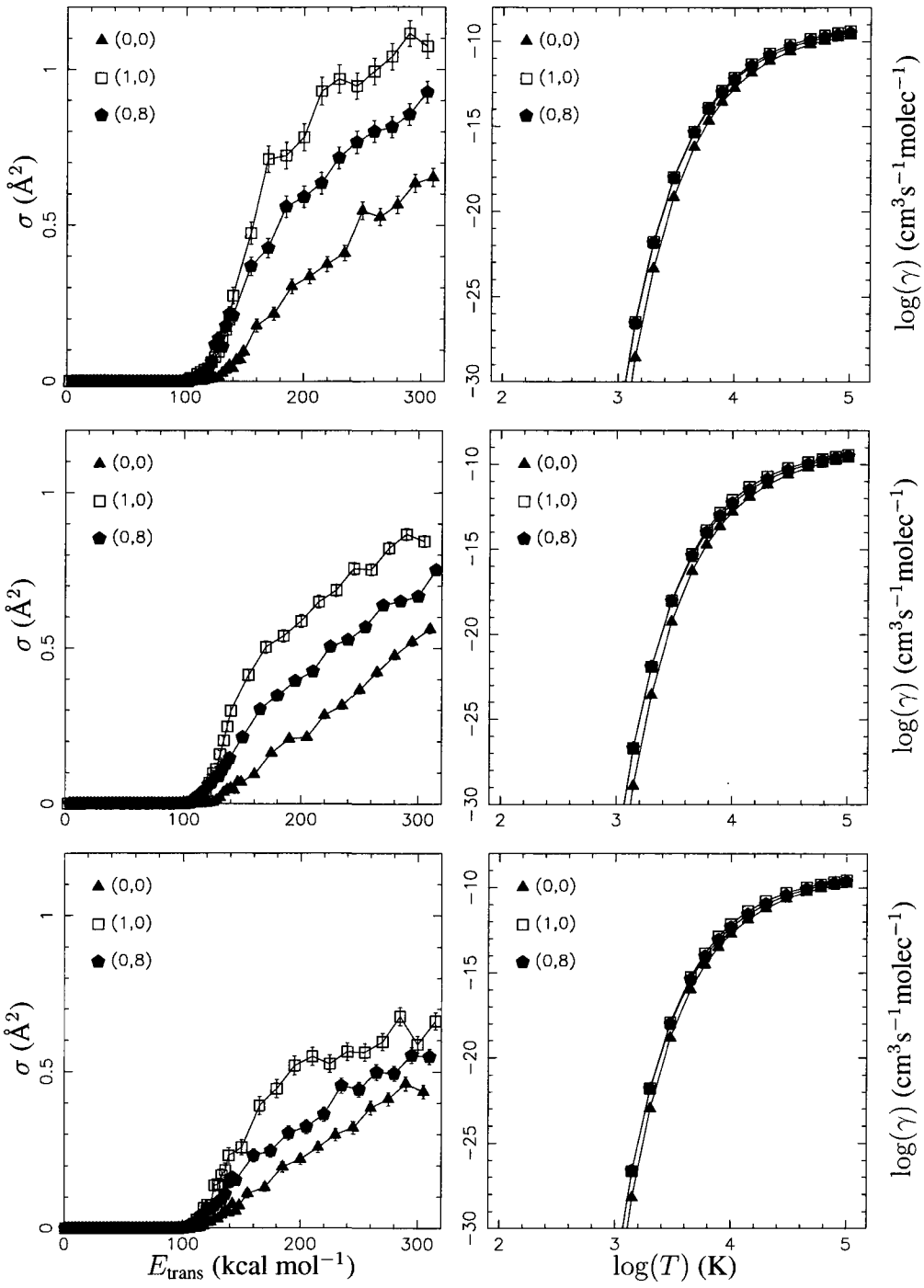

Figure 3.3: In the left–hand column, CID cross sections are plotted against translational energy for selected low energy states. In the right–hand column, corresponding thermal rate coefficients are plotted against temperature. The top row is D + H_2, the centre row is H + H_2, and the bottom row is H + HD. H_2(1,0) and H_2(0,8) are roughly isoergic. HD(0,8) has 10% less internal energy than does HD(1,0).

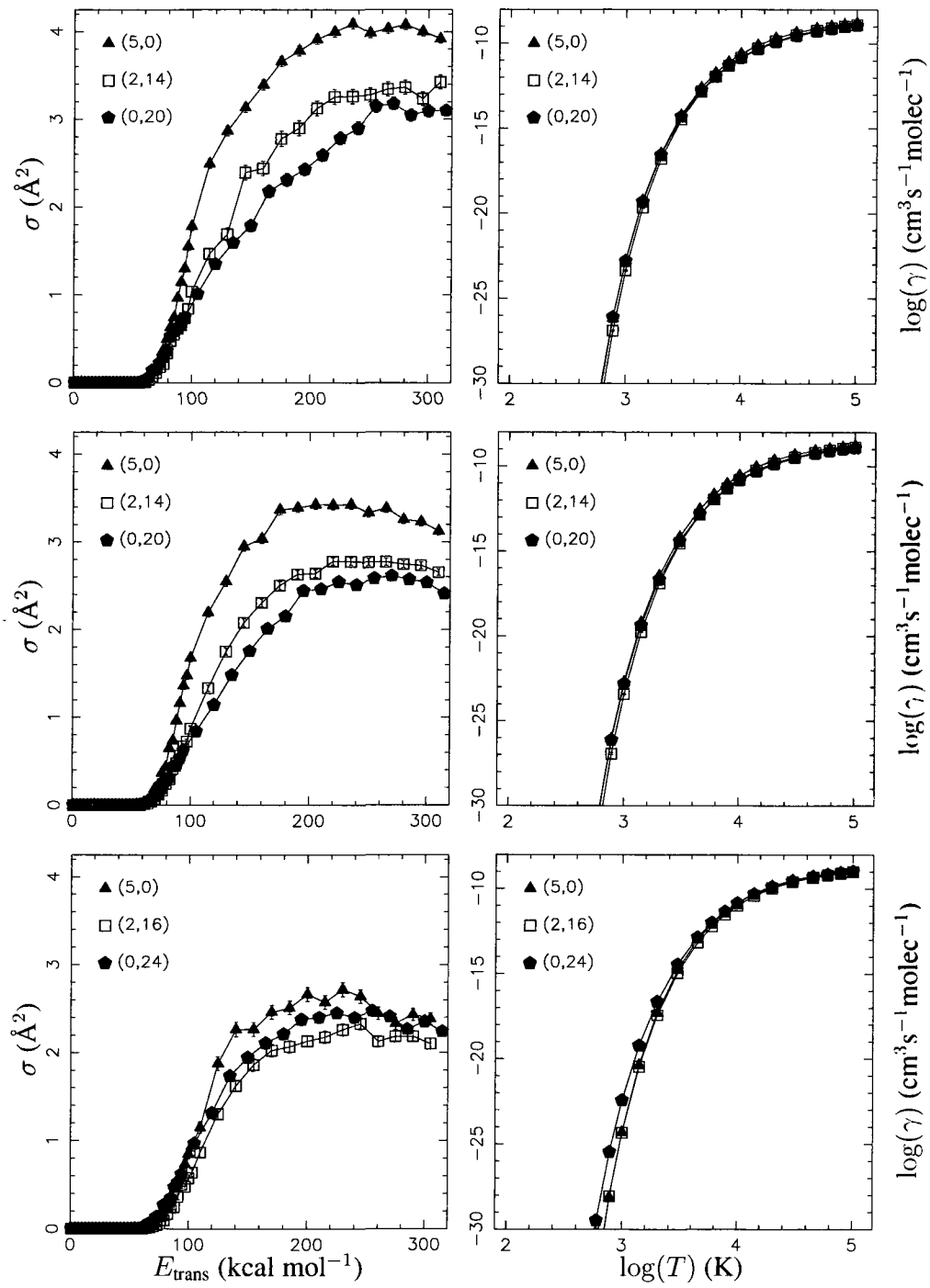

Figure 3.4: In the left–hand column, CID cross sections are plotted against translational energy for selected states with internal energy approximately half that required for dissociation. In the right–hand column, corresponding thermal rate coefficients are plotted against temperature. The top row is D + H_2, the centre row is H + H_2, and the bottom row is H + HD. The internal energy in H_2(2,14) and HD(2,16) is nearly equally distributed between rotational and vibrational modes.

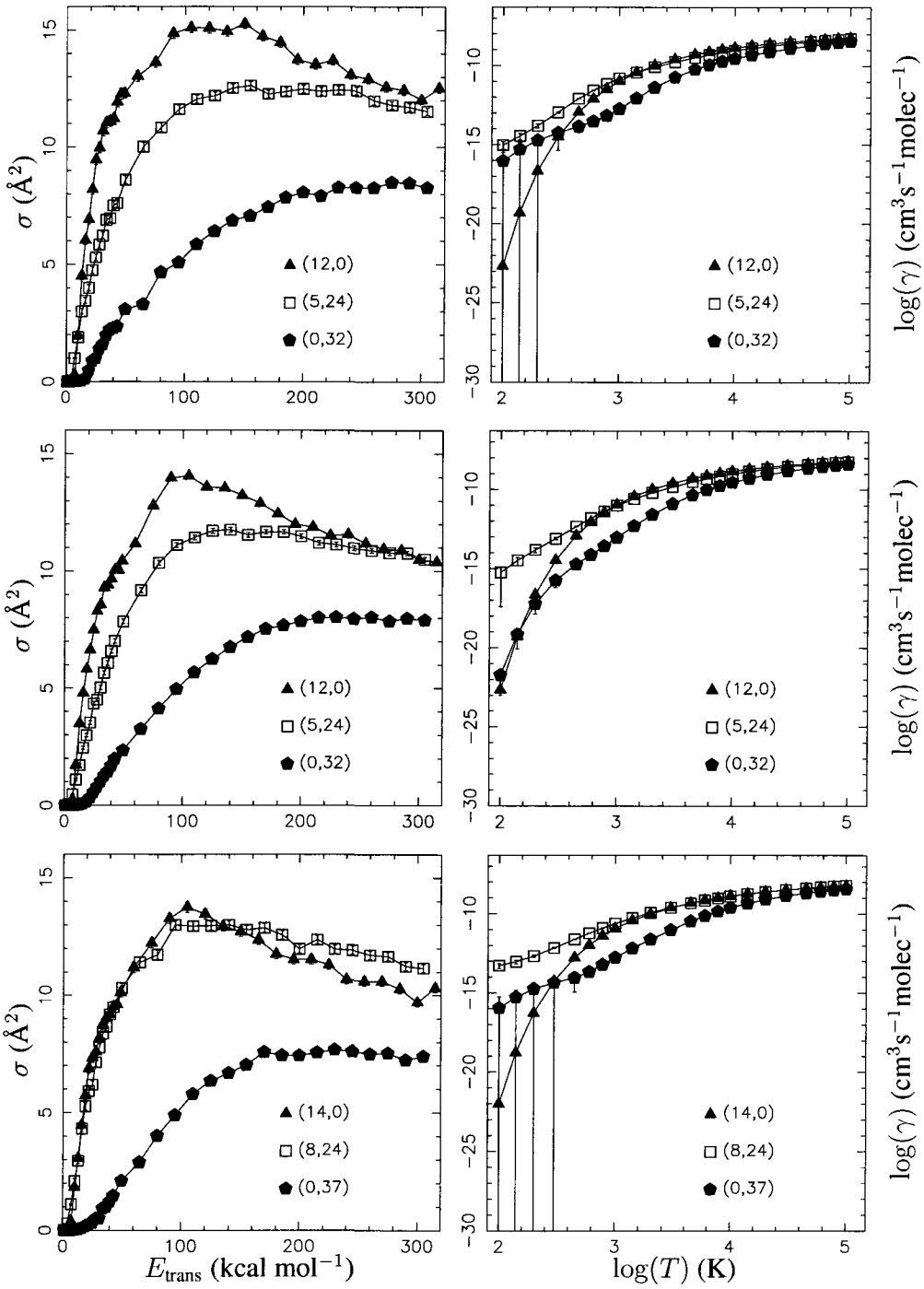

Figure 3.5: In the left–hand column, CID cross sections are plotted against translational energy for states with internal energy near 109.5 kcal mol^{-1}. In the right–hand column, corresponding thermal rate coefficients are plotted against temperature. The energy in H_2(5,24) and HD(8,24) is nearly equally distributed between rotational and vibrational modes. The top row is D + H_2, the centre row is H + H_2, and the bottom row is H + HD.

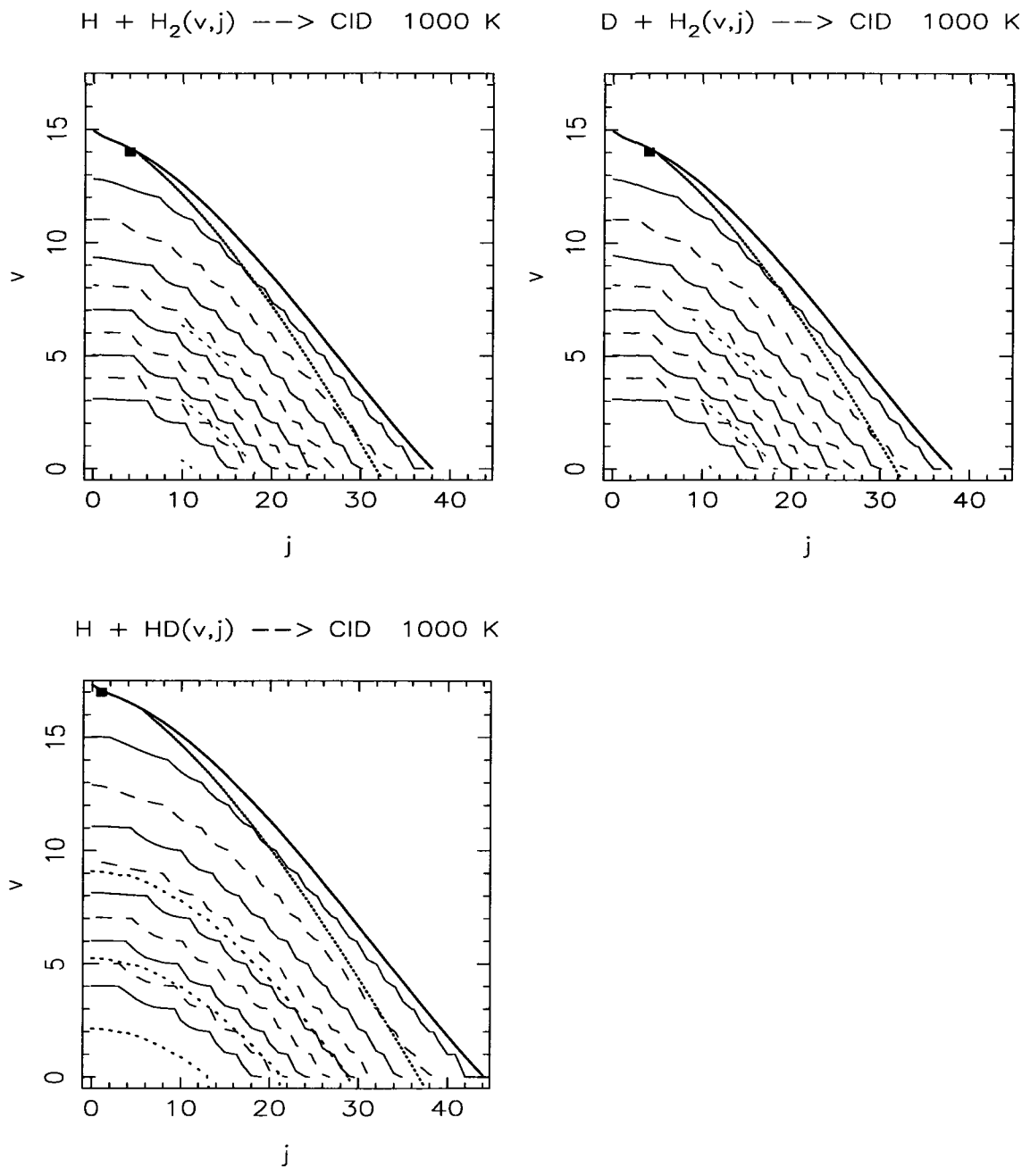

Figure 3.6: Thermal rate coefficients for CID at 1000 K. The bold solid line (topmost contour) is the dissociation limit. The bold dotted is 109.5 kcal mol^{-1}, while the lighter dotted lines are one quarter, half, and three quarters of that. The solid and dashed contours represent rate coefficients on a log scale. The uppermost dashed contour is at 10^{-10} cm^3 s^{-1}, and contours are located at every second power of ten. A solid square marker denotes the greatest rate coefficient in each panel.

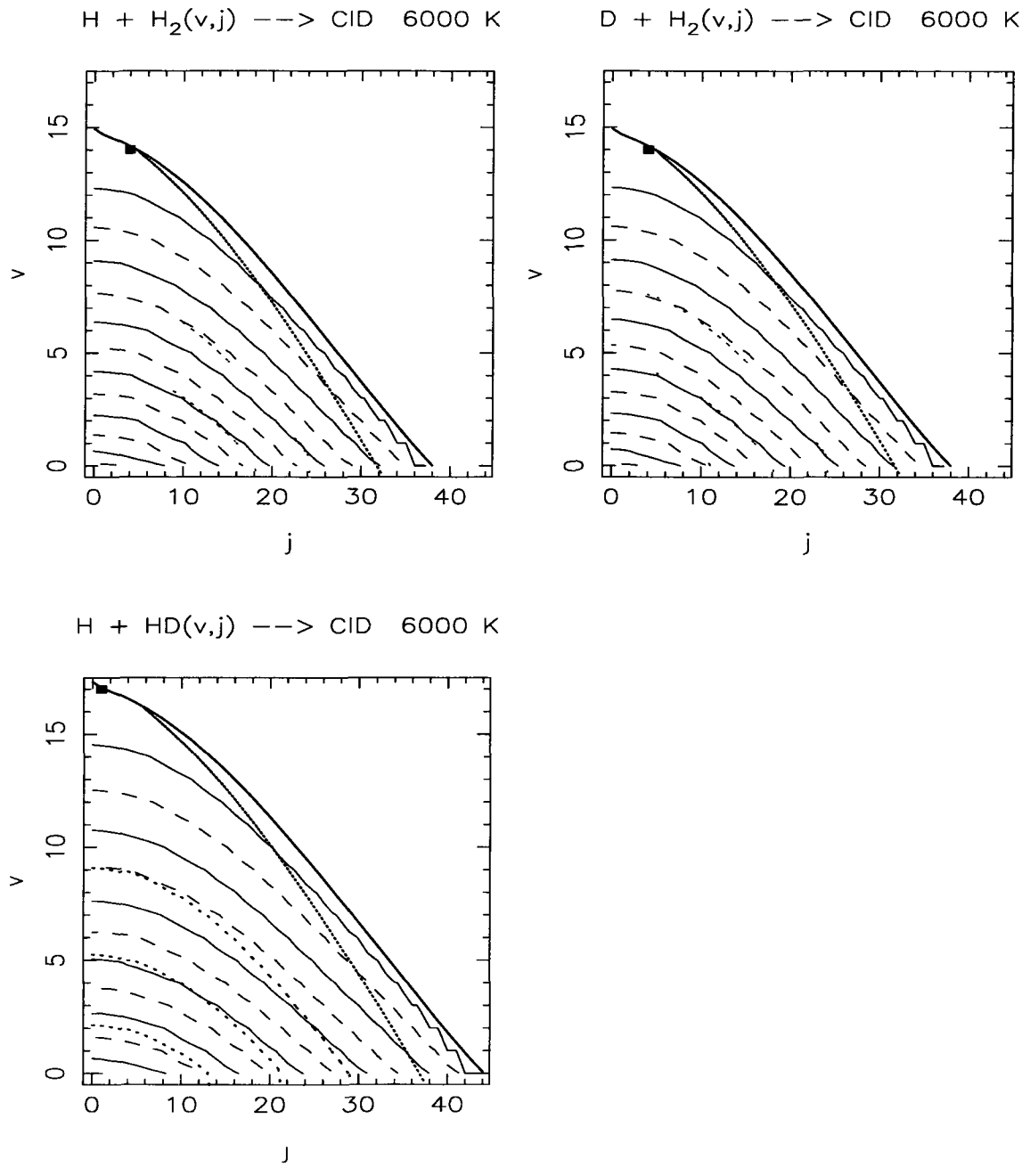

Figure 3.7: Thermal rate coefficients for CID at 6000 K, as in Figure 3.6. In this figure, the uppermost solid contour is at 10^{-9} cm^3 s^{-1}, and contours are spaced every half power of ten.

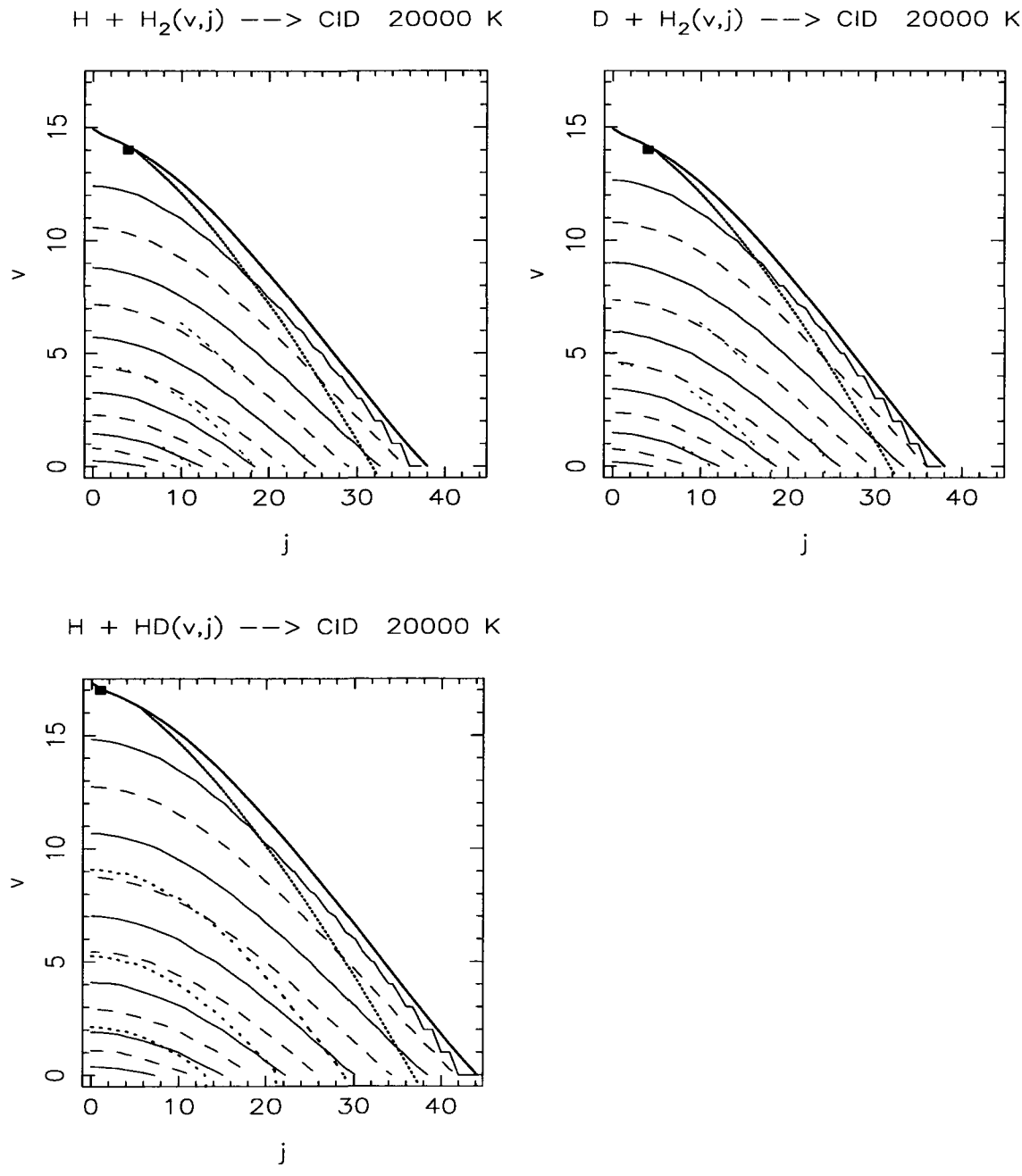

Figure 3.8: Thermal rate coefficients for CID at 20000 K, as in Figure 3.6. The uppermost solid contour is at $10^{-8.5}$ cm^3 s^{-1}, and contours are spaced every quarter power of ten.

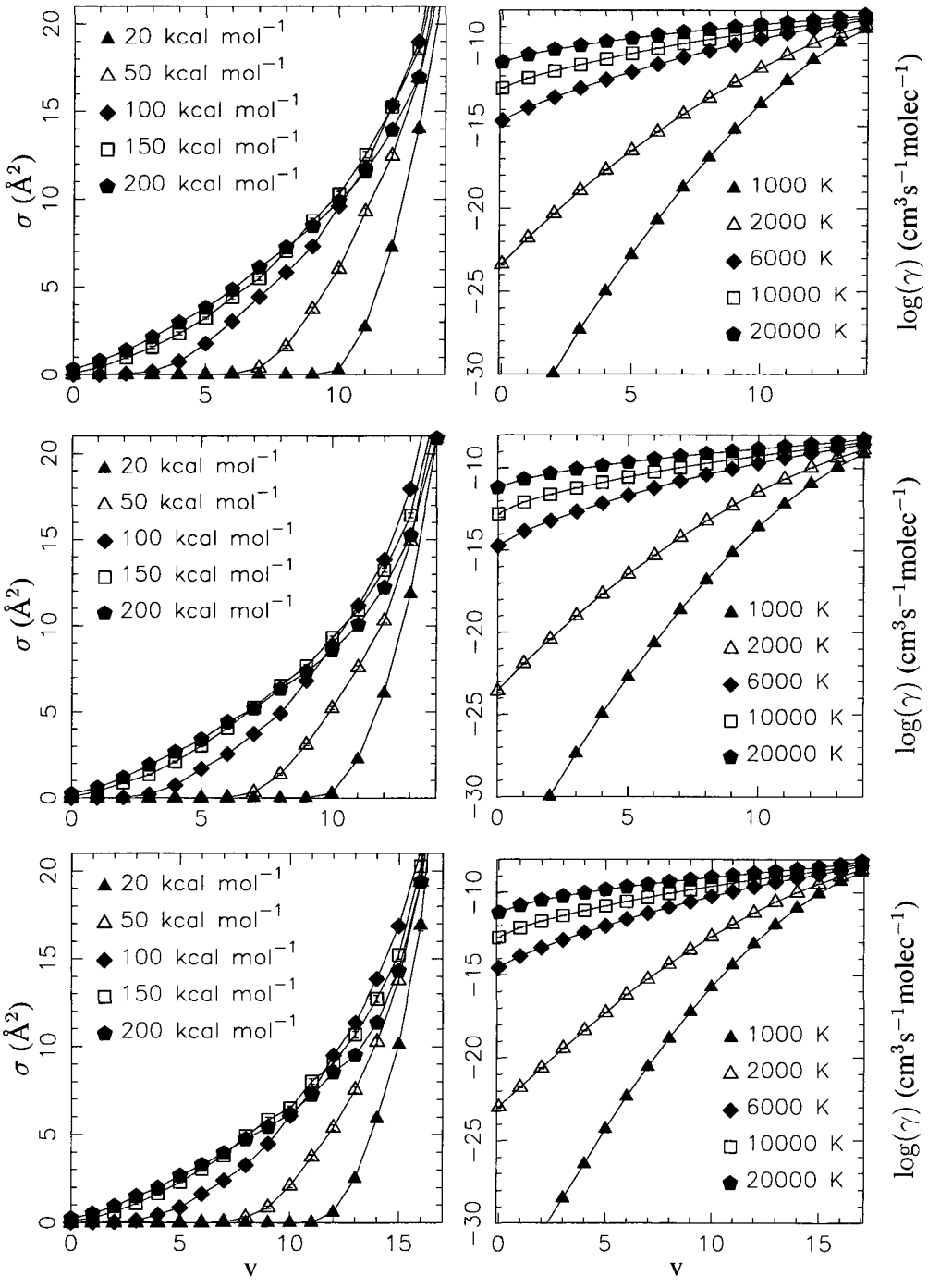

Figure 3.9: In the left–hand column, CID cross sections are plotted against v for $j = 0$ at selected translational energies. In the right column, CID rate coefficients are plotted against v at selected temperatures. The top row is D + H_2, the centre row is H + H_2, and the bottom row is H + HD.

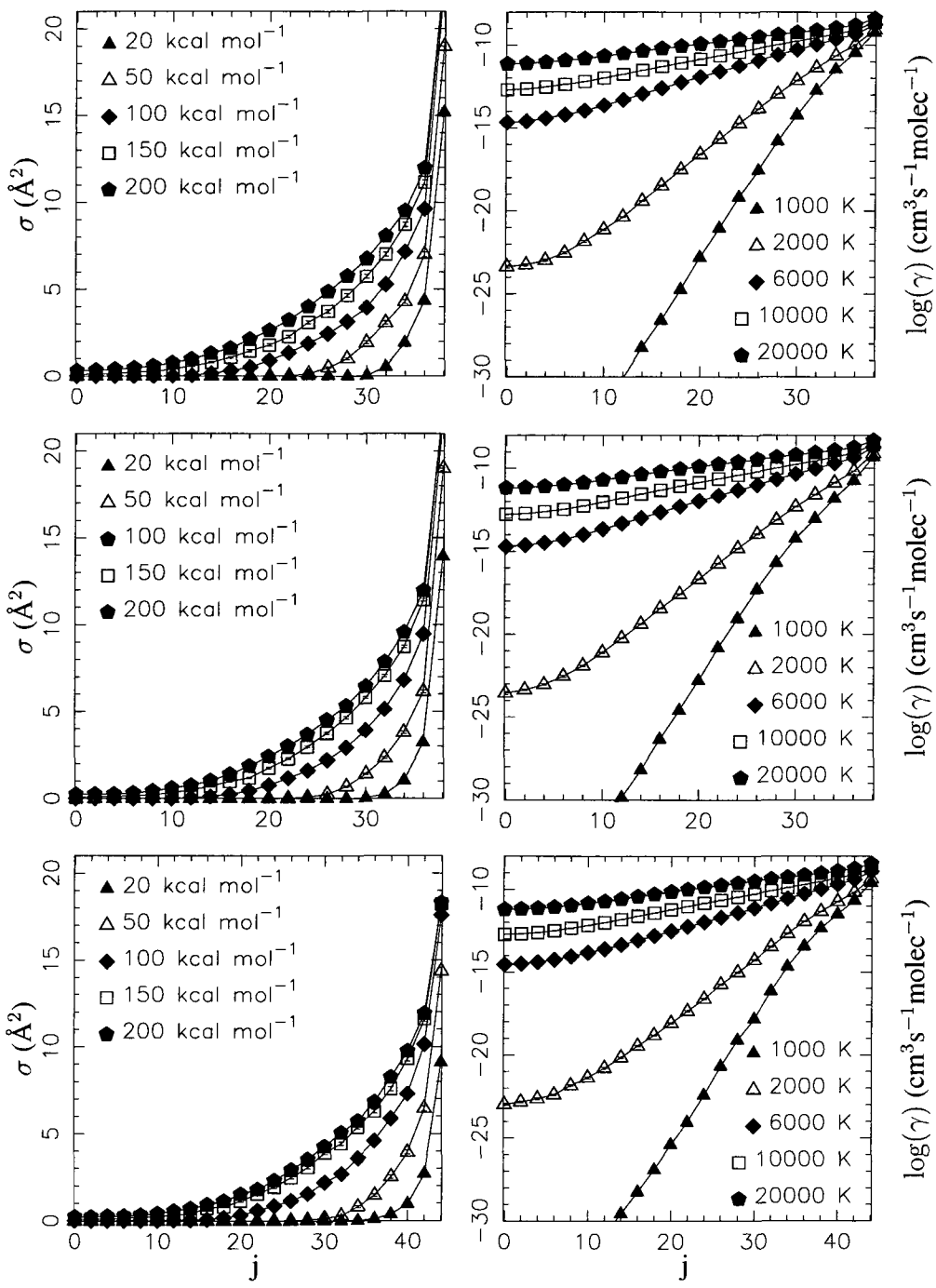

Figure 3.10: In the left–hand column, CID cross sections are plotted against j for $v = 0$ at selected translational energies. In the right column, CID rate coefficients are plotted against j at selected temperatures. The top row is D + H_2, the centre row is H + H_2, and the bottom row is H + HD.

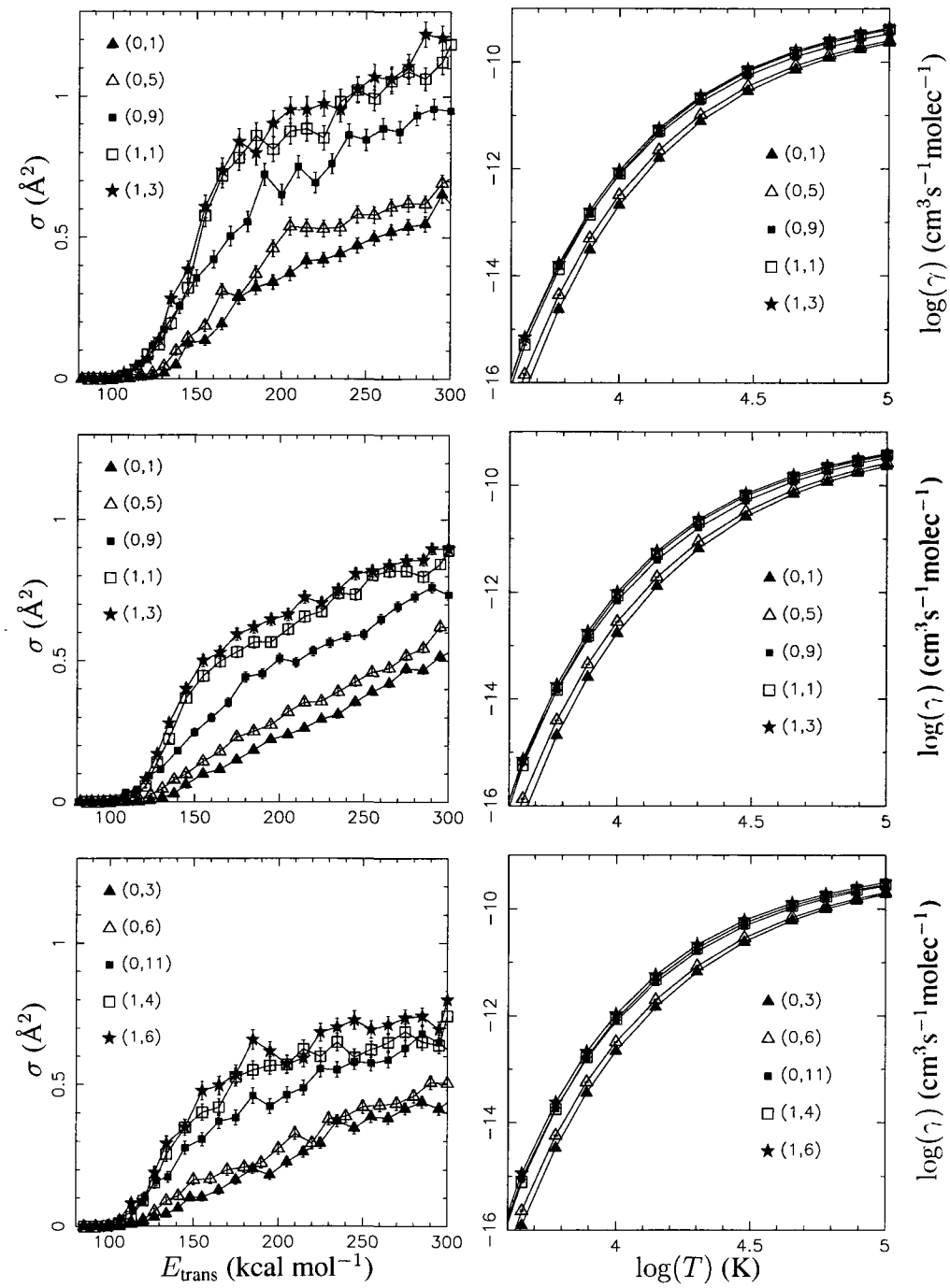

Figure 3.11: In the left–hand column, CID cross sections are plotted against translational energy for selected states of H + H_2, D + H_2, and H + HD with internal energy less than 1 eV. In the right–hand column, thermal rate coefficients for CID are plotted against temperature for the same states. The top row is D + H_2, the centre row is H + H_2, and the bottom row is H + HD. The H + H_2 and D + H_2 states are chosen to span the range of energies available between 0 eV and 1 eV, while the H + HD states are chosen to correspond energetically to the selected H + H_2 and D + H_2 states.

Chapter 4

Nonreactive energy transfer

Unlike the cross sections and rate coefficients for collision–induced dissociation (CID), for which rate coefficients depend primarily upon the internal energy of the initial state, it may be expected that the cross sections and rate coefficients of nonreactive energy transfer will be highly dependent not only upon the total amount of internal energy, but also upon its distribution. Considered here will be "upward" transitions, those transitions in which the final internal energy of the target molecule is greater than its initial internal energy (endoergic), and "downward" transitions, those in which the final internal energy is less than the initial internal energy (exoergic). At low translational energy, the most probable nonreactive upward transitions may naturally be expected to be those with the smallest changes in internal energy, those in which a gain of vibrational energy is largely offset by a loss of rotational energy, and *vice versa*. Such transitions will be referred to as "diagonal" transitions, as on a (v, j) scatter plot they lie roughly on a diagonal to the axes, from the top left to the bottom right. Although there is no energetic barrier to downward transitions, it is known that the most probable nonreactive downward transitions at low translational energy tend to be diagonal transitions or small transitions which are purely rotational in nature (c.f. [76]). In other words, for nonreactive collisions with little translational energy available, the internal energy of the colliding species tends to be preserved.

Figure 4.1 illustrates this point. It contains scatter plots of final states resulting from nonreactive energy transfer and exchange reactions from D + H_2(2,14). The final vibrational

quantum number is on the y axis, and the final rotational quantum number is on the x axis. Each plot marker represents a single trajectory outcome. The same trend of near–conservation of internal energy in nonreactive collisions holds strongly at higher impact parameters, but not at low impact parameters (as seen in Figure 2.2); however, there are fewer nonreactive trajectories at low impact parameters, and they each bear less statistical weight during the calculation of cross sections than do each of the higher impact parameter trajectories.

Accordingly, the study of state–to–state transitions will focus initially upon two classes of transitions. The first includes the purely vibrational and rotational transitions which lead to the smallest internal energy change. The second includes those transitions which lead to changes in both vibrational and rotational energy, with emphasis on the diagonal transitions.

Then, the importance of the different transition types (purely vibrational, purely rotational, mixed) and how these vary according to isotopic combinations will be considered. From this, it may be possible to draw conclusions about overall nonreactive behaviour. The average overall energy transfer for nonreactive transitions and its relation to energy transfer for exchange are discussed in Chapter 5, and a comparison of rate coefficients for nonreactive transitions with those of CID and exchange is made in Chapter 6.

4.1 Thresholds to nonreactive energy transfer

Energetic and dynamical thresholds play the same role in determining rate coefficients for upward nonreactive transitions as they do for CID. Because state–to–state energetic thresholds vary, it is not feasible to run additional trajectories to determine dynamical thresholds for every state as accurately as was done for CID. However, through the application of microscopic reversibility, upward rate coefficients and cross sections can be obtained from downward ones (which have no energetic threshold), eliminating the "barely in the box" problem.

Low temperature rate coefficients for an upward transition will thus depend most heavily on the lowest energy cross sections of the reverse process. For downward transitions, with no activation energy, the lowest energy cross sections are also the most important. Thus, to

most accurately determine rate coefficients for nonreactive transitions at lower temperatures, large numbers of trajectories could be run at the lowest translational energies at which any transitions are observed. However, these are the most computationally expensive trajectories, as trajectories at lower translational energies require more integrative steps. In addition, the rate coefficients most affected by this issue are those which are not likely to be highly accurate due to the assumptions of QCT. For these reasons, no additional trajectories to help determine thresholds for nonreactive energy transfer were run.

Although little or no elevation of the dynamical threshold was observed for CID, there appears to be an elevation of the dynamical threshold for nonreactive energy transfer for the smallest available transitions from some states of H + H_2 and D + H_2, but not H + HD. There is a 1.013 kcal mol^{-1} difference between H_2(0,0) and H_2(0,2); however, inelastic nonreactive trajectories for both H + H_2(0,0) and D + H_2(0,0) are not observed at translational energies below 6 kcal mol^{-1}. For H_2(0,8), the availability of downward transitions makes energy transfer possible even at 1 kcal mol^{-1}, but only a single instance of energy transfer in 1000 trajectories is observed for H + H_2(0,8) at $E_{trans} = 5$ kcal mol^{-1}, while the lowest energy at which D + H_2 engages in nonreactive energy transfer is $E_{trans} = 6$ kcal mol^{-1}. From H + H_2(1,0) and D + H_2(1,0), no inelastic trajectories are observed at 2 kcal mol^{-1}.

This is not to say that a dynamical threshold elevation definitely exists for nonreactive energy transfer; however, the existence of elevated thresholds across a number of low energy states of H + H_2 and D + H_2, but not H + HD, is suggestive that this warrants further investigation. An in–depth analysis is beyond the scope of the present work. It may be that low energy transitions are too improbable to show up in this study, but would show up if enough trajectories were run. It may also be that low energy transitions are more favourable for a particular collision geometry, as is the case with CID. If that geometry involves an impact parameter greater than 0.5 Å, then the program used to simulate collisions will end before reaching it. Although a small number of tests indicate tentatively that this is not the case, this would help explain why energy exchange takes place at all translational energies for H + HD(0,0), but not

for H + H_2(0,0) or D + H_2(0,0). An examination of the opacity functions for these collisions may yield insights into the question of the existence or nonexistence of dynamical threshold elevation for nonreactive energy transfer.

4.2 Microscopic reversibility

In Figure 4.2, rate coefficients are plotted against temperature for nonreactive energy transfer in H + H_2 for selected states. The corrections required to make the rate coefficients obey microscopic reversibility are largest at the lowest temperatures, where the "barely in the box" problem is manifested the most, and at the highest, where the rate coefficients depend more heavily upon cross sections calculated at translational energy intervals of 5 kcal mol^{-1}, rather than the 1 kcal mol^{-1} interval used for low translational energy cross sections.

In any case, the corrections made for the nonreactive transitions described in this study are rarely large. In this chapter, the rate coefficients presented are all corrected to obey microscopic reversibility, but the cross sections which correspond to those rate coefficients and are displayed alongside them have not been corrected. The small magnitude of most corrections means that they will not have a signficant impact upon the conclusions reached.

4.3 State–to–state behaviour of nonreactive transitions

4.3.1 Nonreactive rotational transitions from ground state

Cross sections for nonreactive energy transfer for transitions involving small changes in internal energy are expected to be (and are observed to be) greater for H + HD than for H + H_2 or D + H_2 due to the availability of $\Delta j = \pm 1$ transitions. Even when comparing transitions with the same Δj values, H + HD nonreactive transfer cross sections may be larger than those of H + H_2, in part because of the closer spacing of HD energy levels relative to H_2, and in part because of the longer collision time for H + HD. It will be seen that even at high translational energies, this trend persists, though it is more marked at the lower translational energies.

Cross sections are plotted as functions of translational energy for nonreactive energy transfer involving transitions from the lowest energy states in the left–hand column of Figure 4.3. The nonreactive cross sections for D + H_2 are greater than the corresponding cross sections for H + H_2, with a larger relative difference at high E_{trans} than at low E_{trans}. This could be attributed to the longer interaction time for D + H_2. The excitation function for the $\Delta j = +1$ transition of H + HD(0,0) displays a much sharper peak near threshold than does that of H + H_2(0,0). The excitation function of H + HD is nearly constant across the higher translational energies, while the excitation function for H + H_2 declines as E_{trans} is increased.

Despite the lower energetic requirement, the cross sections for $\Delta v = 0$, $\Delta j = +2$ for H + HD are smaller than are the corresponding cross sections for H + H_2 at almost all translational energies. This is because the bin size into which continuously–valued quantum numbers fall in H + H_2 transitions is twice that of H + HD transitions. Suppose each system had a trajectory with $\Delta j = 1.3$, where j is here a continuously–valued quantum number. For H + H_2, this trajectory would contribute to the cross section for $\Delta v = 0$, $\Delta j = +2$, but it would not count for the $\Delta v = 0$, $\Delta j = +2$ cross section of H + HD, having been binned instead as $\Delta v = 0$, $\Delta j = +1$. A similar situation occurs at the top end of the bin, where a trajectory with $\Delta j = 2.7$ counts toward the cross section for $\Delta v = 0$, $\Delta j = +2$ in H + H_2, but counts instead for $\Delta v = 0$, $\Delta j = +3$ in H + HD.

Corrected rate coefficients for purely rotational transitions for the lowest energy states, derived from the downward cross sections, are shown in the right–hand column of Figure 4.3. The rate coefficients for D + H_2 are generally greater than those of H + H_2, but tend to be at most 10% greater than those of H + H_2 in the 10^4 K to 10^6 K range, with larger differences at lower temperatures. The rate coefficients for H + HD are generally two to three times larger than those of H + H_2 above 10^4 K, and are many orders of magnitude larger than those of H + H_2 at lower temperatures. As expected from analysis of the cross sections, at high temperature the $\Delta j = +1$ rate coefficients for H + HD are larger than those of the $\Delta j = +2$ transitions of H + H_2.

The $\Delta j = +2$ rate coefficients for H + HD are greater than the corresponding rate coefficients for H + H_2 at low temperature because of the values of the cross sections at the two lowest translational energies. At high temperature, larger cross sections are observed for H + H_2 at the highest translational energies than for H + HD, resulting in rate coefficients for the $\Delta j = +2$ transition of H + H_2 that are higher than those for H + HD.

Cross sections for downward transitions involving the same states are given in the left–hand column of Figure 4.4. These cross sections for H + H_2 and D + H_2 agree within their standard errors at many translational energies, with a small overall elevation observed for D + H_2. The D + H_2(0,4) $\rightarrow$ D + H_2(0,2) transition has a notably larger peak than the corresponding H + H_2 transition.

Purely rotational downward cross sections from states with low internal energy are also highly elevated for H + HD compared to H + H_2, again due to the $\Delta j = \pm 1$ transition. For equal Δj, cross sections for H + HD are generally less than cross sections for H + H_2.

Downward rate coefficients to (0,0), in the right–hand column of Figure 4.4, are greater than the corresponding upward rate coefficients at low temperature, but are less than those rate coefficients at high temperature. Results mirror those for upward transitions: the $\Delta j = -1$ transitions for H + HD have the largest rate coefficients at all temperatures. The rate coefficients for the $\Delta j = -2$ transitions of H + H_2 and D + H_2 are larger than those of the $\Delta j = -2$ transitions for H + HD at high temperature, but are much smaller at low temperature. This is to be expected from detailed balance: the degeneracies of the higher energy states are greater than those of the low energy states. At high temperature, where the exponential term of Equation 2.20 is near 1, the rate coefficients are related simply as the ratio of degeneracies. At low temperature, the exponential term $e^{-\Delta E/k_B T}$ is more important than the degeneracies.

4.3.2 Nonreactive rotational transitions from low energy states

Figure 4.5 shows cross sections plotted against translational energy for purely rotational nonreactive transitions from states (0,0), (0,8) and (1,0). The cross sections from H + H_2(0,8)

to both (0,6) and (0,10) are quantitatively similar to those of D + H_2 at all energies. Although cross sections for the (1,0) $\rightarrow$ (1,2) and (0,0) $\rightarrow$ (0,2) transitions are similar for the two systems at high translational energy, the cross sections for D + H_2 are greater below about 200 kcal mol^{-1}.

As expected, upward cross sections for H + HD are elevated relative to those for H + H_2. It is to be noted that the downward H + HD(0,8) $\rightarrow$ H + HD(0,7) transition has much larger cross sections than does the H + H_2(0,8) $\rightarrow$ H + H_2(0,6) transition. This reflects the tendency of nonreactive collisions to conserve the translational energy of the collider at many translational energies.

Corrected thermal rate coefficients for purely rotational transitions from low energy states are plotted in Figure 4.6. At high temperature, the rate coefficient is influenced primarily by the initial rotational energy of the target molecule; more rotationally excited molecules are less likely to undergo a rotational transition. This is likely because of two factors which act in conjunction: the conservation of angular momentum and detailed balance. The total angular momentum of the system can be divided into two parts: that internal to the target molecule, and that of the target and collider about the centre of mass. In order to change the rotational energy of the target molecule, its angular momentum must also be changed. In low impact parameter collisions, the angular momentum of the collider about the centre of mass is small, so it is not possible to add much angular momentum to the target molecule. For collisions at higher impact parameters, a fast collider may have enough angular momentum about the centre of mass to cause a large increase in the rotational quantum number, but the relatively short interaction time means that whatever torque is applied will not much change the angular momentum of the target. A slow collider at higher impact parameter is not likely to add much rotational energy to a quickly rotating molecule simply because it is not moving fast enough to do so. There is no combination of impact parameter and translational energy which heavily favours the rotational excitation of a H_2 or HD molecule which is already in a high rotational state. Applying the principle of detailed balance (Equation 2.10), it can be seen that if an upward cross section

involving two states is very small, then the deexcitation cross section involving those states is also small.

At low temperature, the rate coefficients depend more upon the initial total internal energy of the target molecule, with downward transitions favoured heavily over upward.

In both H + H_2 and D + H_2, the (0,8) $\rightarrow$ (0,6) transition has higher rate coefficients than does the (0,0) $\rightarrow$ (0,2) transition. This is due to small but nonzero cross sections for the (0,8) $\rightarrow$ (0,6) transitions for both H + H_2 and D + H_2 at low translational energies. The cross sections for the (0,0) $\rightarrow$ (0,2) transitions in these systems at the same and lower energies are zero. This is not the case for the corresponding H + HD transitions; the energy difference between (0,0) and (0,1) is small relative to the difference between H_2(0,0) and H_2(0,2), meaning that the first nonzero cross section will occur at a lower translational energy for H + HD than for H + H_2.

Roueff and Flower [77] used a PES derived from BKMP2 to calculate state–to–state rate coefficients for rotational transitions of H + HD(0,j), applying the rigid rotor approximation to make quantum calculations feasible. These match the current results within an order of magnitude; however, there are some key differences. Table 4.1 contains some values for comparison. The rate coefficients calculated in this study tend to be smaller than those of Roueff and Flower at 100 K. The (0,0)$\rightarrow$(0,1) rate coefficients at 100 K nearly match within standard error, but the size of the discrepancy between the QCT and QM rate coefficients increases as the energy gap between states increases. At 300 K, the QCT rate coefficients also tend to be smaller than the QM rate coefficients, with the exception of the (0,0)$\rightarrow$(0,1) transition, for which the QCT rate coefficient is slightly larger. At 1000 K, the QCT rate coefficients are typically larger than the QM rate coefficients, with greater relative differences occurring for the transitions with larger energy differences between the states.

There are several considerations which may explain these differences in cross sections. First, the "barely in the box" problem, the phenomenon in which a classical trajectory may end up being assigned to a state which is energetically inaccessible given the total energy of the collision, may lead to overestimates of upward cross sections. Although corrections for

this problem have been made through the application of microscopic reversibility, the binning method itself may cause overestimates of some rate coefficients and underestimates of others. Second, the inability to account for tunnelling leads to underestimates of reactive quasiclassical cross sections; it may also influence nonreactive cross sections because of the exclusion of trajectories which tunnel into a configuration that would lead to exchange, then quickly tunnel back to form the original molecule. (The probability of this process may be low enough that it can be safely neglected.) Third, the rigid rotor approximation holds the atoms of the target molecule a fixed distance apart. This means that there is no vibration: in particular, the molecule is never at its outer turning point. From a classical perspective, some of the trajectories at the greatest impact parameters which would result in inelastic trajectories for a nonrigid rotor would for a rigid rotor system result in elastic trajectories. Because cross sections are sensitive to these trajectories, it can be expected that the rigid rotor approximation will underestimate cross sections.

4.3.3 Nonreactive vibrational transitions from low energy states

As seen in the left–hand column of Figure 4.7, for states with low internal energy, cross sections for purely vibrational transitions are markedly different than those for purely rotational transitions. Not only are they are of lesser magnitude, but there is less relative difference as a result of changing the internal energy of the target molecule. For all systems, the (0,8) $\rightarrow$ (1,8) transition has the highest probability across most of the translational energy range, while (0,0) $\rightarrow$ (1,0) and (1,0) $\rightarrow$ (2,0) are the least likely. For these states, the addition of internal energy in the form of vibration does promote state–to–state transitions, but rotational energy is more effective at promoting vibrational excitation than is a similar amount of vibrational energy.

In addition, vibrational deexcitation from (1,0) is more probable than vibrational excitation from (1,0) at most translational energies for all three systems, although the statistics for D + H_2 and H + HD make this conclusion tentative in those cases.

The rate coefficients for purely vibrational transitions from states with low internal energy, shown in the right–hand column of Figure 4.7, are similar across all systems. In all cases, the sole downward transition is the most probable at temperatures below 3200 K, and is the most probable by more than an order of magnitude at temperatures below 1000 K. This is because the upward transitions all have energetic thresholds in the range of 10–15 kcal mol^{-1}; the average translational energy for a collision at 3200 K is 6.4 kcal mol^{-1}, and the average translational energy at 4500 K is 8.9 kcal mol^{-1}. It is therefore not until a temperature of 4500 K is reached that a large proportion of collisions have enough energy to effect an upward vibrational transition. The enhancement of cross sections for translational energies between 20 kcal mol^{-1} and 100 kcal mol^{-1} for the rotationally excited states carries through to the rate coefficients at 10000 K, at which a roughly tenfold enhancement over the other upward transitions is seen for $H + H_2$ and $D + H_2$, with a lesser enhancement observed for H + HD. In all three systems at low temperature, the ladder climbing mechanism of dissociation will likely initiate primarily through the rotational excitation of molecules, with vibrational modes becoming more important at higher internal energies.

4.3.4 Nonreactive rotational transitions from states with internal energy near 55 kcal mol^{-1}

Cross sections for upward rotational transitions from selected states with internal energy near half that required for dissociation are shown in the left–hand column of Figure 4.8. In all cases, states which are rotationally excited are less likely to gain rotational energy than are vibrationally excited states; however, among the rotationally excited states it is not true that more rotational energy leads to a larger rotational excitation cross section.

As at lower internal energy, because of the closer energy level spacing, the excitation functions for H + HD peak sharply at low translational energy, relative to the other excitation functions. The excitation functions for $D + H_2$ and $H + H_2$ for corresponding transitions are similar to one another, with a slight enhancement for $D + H_2(5,0) \rightarrow D + H_2(5,2)$ over

$H + H_2(5,0) \rightarrow H + H_2(5,2)$.

Cross sections for downward rotational transitions from the same states are shown in the left–hand column of Figure 4.9. Each of these is comparable in magnitude to the cross section of its corresponding upward transition in Figure 4.8, for most translational energies. The similarity of corresponding upward and downward cross sections can be accounted for by a microscopic reversibility argument. For two states with high rotational quantum numbers, the ratio of degeneracies

$$\frac{g_2}{g_1} = \frac{2j_2 + 1}{2j_1 + 1} \tag{4.1}$$

will be near 1. Thus, rearranging Equation 2.10 and letting $\frac{g_2}{g_1} \simeq 1$,

$$\sigma(1 \rightarrow 2; E) \simeq \sigma(2 \rightarrow 1; E)\frac{E_2}{E_1}. \tag{4.2}$$

In addition, the two states have similar internal energies. Letting $E_2 \simeq E_1$,

$$\sigma(1 \rightarrow 2; E) \simeq \sigma(2 \rightarrow 1; E). \tag{4.3}$$

(It should be noted that the downward cross sections shown in Figure 4.9 are not the cross sections used to correct the rate coefficients corresponding to the transitions in Figure 4.8; however, they are similar in magnitude.)

The largest relative differences in upward and downward cross sections occur at the lowest translational energies. For instance,

$$\sigma(\mathrm{H} + \mathrm{HD}(0,24) \rightarrow \mathrm{H} + \mathrm{HD}(0,25); 1 \text{ kcal mol}^{-1}) = 0.38 \text{ Å}^2,$$

while

$$\sigma(\mathrm{H} + \mathrm{HD}(0,25) \rightarrow \mathrm{H} + \mathrm{HD}(0,24); 1 \text{ kcal mol}^{-1}) = 0.52 \text{ Å}^2.$$

This has a significant effect on low temperature rate coefficients for both these downward transitions and for the (upward) reverse processes.

Corrected rate coefficients for upward rotational transitions from states with internal energy near 55 kcal mol^{-1} can be seen in the right–hand column of Figure 4.8. Despite

the slight enhancement of cross sections for $D + H_2(5,0) \rightarrow D + H_2(5,2)$ relative to those for $H + H_2(5,0) \rightarrow H + H_2(5,2)$, the $H + H_2$ rate coefficients are the greater at low temperature. This is due to the correction for microscopic reversibility, as the cross sections for $(5,2) \rightarrow (5,0)$ at low translational energy are greater for $H + H_2$ than for $D + H_2$.

Rate coefficients for the same downward transitions are given in the right–hand column of Figure 4.9. Like the rate coefficients for upward transitions, low temperature rate coefficients for $H + H_2$ exceed those for $D + H_2$ for the downward transitions. In this case it is possible to see directly how this comes about: the $H + H_2$ cross sections at the lowest translational energies are greater than the $D + H_2$ cross sections at those same energies.

The enhancement of rate coefficients for purely rotational transitions involving H + HD over those involving $H + H_2$ is not entirely due to the greater cross sections for H + HD, but at low temperature is also due to lower energetic threshold of the H + HD transitions relative to the $H + H_2$ transitions. For example, although the cross sections for the nonreactive transition $H + HD(5,0) \rightarrow H + HD(5,2)$ are about two–thirds as great those of the nonreactive transition $H + H_2(5,0) \rightarrow H + H_2(5,2)$ at all translational energies, the rate coefficients for the H + HD transition are enhanced relative to those of the corresponding $H + H_2$ transition at low temperatures by several orders of magnitude. The rate coefficients for $H + H_2$ are greater than those for H + HD at temperatures above 1000 K, where the vast majority of collisions have translational energy greater than the energetic threshold for these transitions.

4.3.5 Nonreactive vibrational transitions from states with internal energy near 55 kcal mol^{-1}

State–to–state cross sections for vibrational transitions from states with internal energy near 55 kcal mol^{-1}, given in the left–hand columns of Figure 4.10 and Figure 4.11, are similar in magnitude to the cross sections for vibrational transitions from low energy states.

At low translational energy in all systems, the $(5,0) \rightarrow (6,0)$ cross sections are significantly smaller than the cross sections for the other upward vibrational transitions, despite having the

smallest energy gap. The upward cross sections of D + H_2 are generally smaller than those of H + H_2, in contrast to what is observed for the low internal energy cross sections. There are exceptions at high translational energy, where the cross sections for (2,14)→(3,14) are greater for D + H_2 than for H + H_2, and where cross sections for each corresponding transition for the three systems are all similar to one another.

The excitation functions for downward transitions are qualitatively similar to those of the upward transitions: there exist translational energies for each system above which the cross sections for each $v \rightarrow v - 1$ transition are similar, and the states in which more internal energy is rotational than vibrational have larger cross sections at most translational energies below those thresholds. There is a large difference, however, at the lowest few translational energies. At a translational energy of 1 kcal mol^{-1}, the rotationally unexcited states of H + H_2 and D + H_2 have cross sections near 0.1 $Å^2$, about ten times the value of those cross sections at a translational energy of 10 kcal mol^{-1}. A similar enhancement also occurs for H + HD, but the effect is not as pronounced.

The relatively large low energy cross sections in the (5,0)→(4,0) transitions are reflected in odd behaviour in the rate coefficients, with each function exhibiting a local minimum near 4500 K (Figure 4.11, right–hand column).

The rate coefficients for (5,0)→(6,0) show a lesser but qualitatively similar reduction in this temperature range (Figure 4.10, right–hand column). This is because these rate coefficients are derived from the application of microscopic reversibility to (6,0)→(5,0) cross sections, which also have enhanced cross sections at low translational energy. The effect of including these lowest energy cross sections is an enormous change in rate coefficients near and below 1000 K. It would be an interesting study (and likely beneficial in providing highly accurate rate coefficients) to probe the dynamics of these slow collisions more sensitively, perhaps computing trajectories for downward transitions using a 0.1 kcal mol^{-1} or finer grid.

4.3.6 Nonreactive rotational transitions from states with internal energy near 109.5 kcal mol^{-1}

Cross sections for upward rotational transitions from high energy states, shown in the left–hand column of Figure 4.12, display the same trends as the cross sections for states with internal energy near 55 kcal mol^{-1}. The cross sections for D + H_2(12,0)→D + H_2(12,2) are greater than the cross sections for H + H_2(12,0)→H + H_2(12,2) below 40 kcal mol^{-1}, and are similar at higher translational energies. For the rotationally excited states, cross sections for D + H_2 are smaller than the corresponding ones for H + H_2 below 40 kcal mol^{-1}, but they are similar at higher translational energies.

Cross sections for the $\Delta j = +1$ transitions of H + HD are greater than the corresponding H + H_2 transitions at all translational energies, as was the case for the lower energy states; however, the relative difference in this case is not as great. As seen in Chapter 6, the tendency for a nonreactive collision to conserve internal energy is reduced as internal energy is increased from 55 kcal mol^{-1} to 109.5 kcal mol^{-1}. This is due to the ready accessibility of the dissociative channel, as well as the accessibility of (and consequent spread of collisional outcomes into) more final states, both of which reduce the probability of achieving a small rotational excitation. Although this is true for both H + HD and H + H_2, the effect is more pronounced in H + HD, for which there are more accessible final states.

The downward rotational transitions at high internal energy, given in the left–hand column of Figure 4.13, are markedly different for H + H_2 and H + HD. The cross sections for the (0,32)→(0,30) transition for both H + H_2 and D + H_2 are negligible above 15 kcal mol^{-1}.

The excitation functions for the (5,24)→(5,22) transition of H + H_2 and D + H_2 do not qualitatively resemble the excitation functions for (2,14)→(2,12). In the case of (2,14), the excitation functions peak at translational energies around 100 kcal mol^{-1}, but for (5,24) the excitation functions continue to increase with translational energy up to 315 kcal mol^{-1}.

As the internal energies and degeneracies are similar, detailed balance suggests that the

upward and downward cross sections between two high energy states with similar rotational energies should be similar to each other. However, if $E_1 > E_2$ and $g_1 > g_2$, then detailed balance suggests that the downward cross sections ought to be small relative to the upward cross sections from states at lower energies.

$$\sigma_{1\to 2} = \sigma_{2\to 1}\frac{E_2}{E_1}\frac{g_2}{g_1} \tag{4.4}$$

This is observed in Figure 4.13. It is surprising then that the H + HD cross section for the transition H + HD(8,24)→H + HD(8,23) at 1 kcal mol^{-1} is small, while the upward transition H + HD(8,24)→H + HD(8,25) at 1 kcal mol^{-1} has a cross section nearly seven times as large, especially in light of the fact that the average internal energy change at 1 kcal mol^{-1} is about -4 kcal mol^{-1} for H + HD(8,24). The average internal energy change is nearly -20 kcal mol^{-1} for transitions from H + HD(0,37), but the cross sections for H + HD(0,37)→H + HD(0,38) and H + HD(0,37)→H + HD(0,36) are similar to each other across the whole translational energy range. Nonreactive downward transitions from highly excited HD states, when they do occur, must tend to involve transfer of a large amount of energy, while for nonreactive upward transitions, those with small energy changes are the most probable. This may be due in part to the limited amount of energy that can be transferred in an upward collision because of the proximity of the dissociative threshold.

Rate coefficients for upward rotational transitions from states with high internal energy are displayed in the right–hand column of Figure 4.12. In all cases, having more of the initial internal energy assigned to vibration increases the rate coefficient at temperatures below 10000 K. However, at the highest temperatures studied, rotational energy is more effective at promoting small upward transitions than is the same amount of energy split evenly between vibrational and rotational modes.

The rate coefficients for H + H_2 and D + H_2 for states with high internal energy are similar to each other at most temperatures. At the lowest temperatures studied, the rate coefficients of D + H_2 are greater than those of H + H_2, because D + H_2 has greater cross sections than

does H + H_2 at low translational energies.

The downward rate coefficients, given in the right–hand column of Figure 4.13, show significant differences between H + H_2 and D + H_2 at and below 600 K, where the rate coefficients for both processes are smaller for D + H_2 than for H + H_2. When compared to those of the other systems, the downward transitions for H + HD studied have relatively high rate coefficients across all temperatures, with the exception of H + HD(0,37)→H + HD(0,35), which has rate coefficients comparable to those of H + H_2(0,32)→H + H_2(0,30). (The former transition is not displayed in Figure 4.13.)

4.3.7 Nonreactive vibrational transitions from states with internal energy near 109.5 kcal mol^{-1}

The smallest vibrational transitions, both upward and downward, from high energy states tend to occur at low probability in this simulation, with the majority of events contributing to these cross sections occurring at high impact parameter, leading to large standard deviations on the cross sections. The left–hand column of Figure 4.14 displays cross sections for upward vibrational transitions from highly excited states, while the left–hand column of Figure 4.15 displays cross sections for downward vibrational transitions.

The excitation functions of corresponding high energy states of H + H_2 and D + H_2 are similar to each other across all translational energies. Although the cross sections for (12,0)→(13,0) are nearly identical to those of (12,0)→(11,0), the upward cross sections from (5,24) differ from the downward from (5,24) above 20 kcal mol^{-1}. (A similar result is seen for exchange from these states in Section 6.3.)

The major differences between the cross sections of H + H_2 and H + HD are in the downward transitions from states with both vibrational and rotational energy. The cross sections for the H + HD(8,24) →H + HD(7,24) transition are statistically indistinguishable from those of the H + HD(8,24) →H + HD(9,24) transition. For states with high internal energy mostly in either vibration or rotation, the cross sections for H + H_2 are generally greater than those of

H + HD, in part due to a difference in the number of dynamically available final states, but also due to the greater total nonreactive transfer cross sections for nonreactive energy transfer observed for H + H_2 than for H + HD (discussed in Section 4.4).

The rate coefficients for these transitions are given in the right–hand columns of Figure 4.14 and Figure 4.15. Relative to the rotationally excited states, the rate coefficients for downward transitions from the purely vibrational states are large at low temperature due to relatively large cross sections for the collisions with translational energy of 1 kcal mol^{-1}. For H + H_2 and D + H_2, the rate coefficients for downward transitions from (5,24) are much smaller than the rest of the rate coefficients for transitions from high energy states at high temperature: all other rate coefficients converge toward a common value as the temperature is increased to 100000 K. At 4500 K, the ordering of states by rate coefficient differs from the orderings at 100 K or 100000 K. The precise ordering and relative sizes of comparable rate coefficients are different for H + HD as compared to H + H_2 and D + H_2 (which are very nearly the same), but an absence of a general ordering exists nonetheless.

4.3.8 Mixed vibrational and rotational transitions for nonreactive energy transfer

In competition with transitions that are purely vibrational or rotational are the "diagonal" transitions. These are transitions in which internal energy is nearly conserved, and is exchanged between the vibrational and rotational modes. In the left–hand panel of Figure 4.1, the trajectories that will be binned as diagonal transitions can be seen as those close to the contour line that runs nearly through the centre of the (elastic) bin for H_2(2,14), but which are not directly above, below, or to the side of that bin.

The cross sections displayed in the left–hand column of Figure 4.16 are for transitions from H_2(2,14) and HD(2,16) to diagonally adjacent states: H_2(2,14) to states H_2(1,14) and H_2(3,12), and HD(2,16) to states HD(1,17), HD(1,18), HD(3,15), and HD(3,14). The peak values of the excitation functions observed are about two thirds of the peak values found for

the excitation functions of the purely rotational upward transitions in Figures 4.8, but are generally greater than the peak values for the excitation functions of the downward transitions in Figure 4.9.

At low translational energy, the probabilities of diagonal transitions for H + HD are about half the probabilities of diagonal transitions for H + H_2; at higher translational energy, the cross sections of H + HD(2,16)→H + HD(1,17) are similar to the corresponding H + H_2 cross sections. At a translational energy of 1 kcal mol^{-1}, there is an exception: the transition H + HD(2,16)→H + HD(3,14) has a cross section of about 0.3 $Å^2$, a value large relative to the cross sections of the other diagonal transitions and of the purely rotational transitions of H + H_2 and D + H_2. The cross section for H + HD(2,16)→H + HD(3,14) is nevertheless small compared to the purely rotational transitions from H + HD(2,16) for which Δj is +1 or -1. The large cross section for H + HD(2,16)→H + HD(3,14) at a translational energy of 1 kcal mol^{-1} leads to large rate coefficients at low temperature, relative to the cross sections and rate coefficients of the other H + HD transitions displayed in Figure 4.16.

Of note here is a difference in the cross sections for D + H_2 and H + H_2. The relationship between the different isotopic systems with regards to mixed vibrational and rotational transitions is similar to the relationship between systems for the upward rotational transitions from states with internal energy near 55 kcal mol^{-1}: for translational energies slightly above that corresponding to the maximum of the excitation function for the H + H_2(2,16)→H + H_2(3,14) transition, the cross sections for D + H_2(2,16)→D + H_2(3,14) are slightly greater than the cross sections for H + H_2(2,16)→H + H_2(3,14). The peak values of the excitation functions of these two systems are nearly the same for both transitions displayed; however, the location of those peaks along the translational energy axis has a large effect on the rate coefficients below 1000 K, with H + H_2 rate coefficients being between 2 and 10 times as great as the corresponding H + HD values.

Cross sections for diagonal transitions from high energy states with mixed vibrational and rotational energy are displayed in Figure 4.17. These are similar to the lower energy plots,

except that in this case, an abnormally high 1 kcal mol^{-1} cross section for H + HD occurs for the $\Delta v = -1$, $\Delta j = +1$ transition as opposed to the $\Delta v = +1$, $\Delta j = -1$ transition. At high internal energy, the cross sections for diagonal transitions of H + H_2 and D + H_2 are similar to one another, while the cross sections for H + HD vary considerably from those of H + H_2.

4.3.9 Summary of state–to–state nonreactive energy transfer

For states with internal energy well below the dissociative threshold, low temperature state–to–state nonreactive rate coefficients tend to be many orders of magnitude greater than CID rate coefficients from the same states. For purely vibrationally excited molecules with high internal energy, the rate coefficients for CID and those for rotational transitions tend to be similar at all temperatures, while for other states near threshold, CID may be the more important process. In all cases, the rate coefficients of the most probable nonreactive processes are within an order of magnitude of the CID rate coefficients at 10000 K and greater, generally in the range 10^{-10} to 10^{-9} $cm^3s^{-1}molec^{-1}$. The hard–sphere collision frequency may be given as [78]

$$\gamma(T)_{\mathrm{HS}} = \left(\frac{8\pi k_b T}{\mu}\right)^{1/2} d^2, \tag{4.5}$$

for spheres with diameter d and mass μ at temperature T. At 10000 K, assuming a molecular diameter of 1.236 Å (half the separation of the nuclei at the outer turning point in a H_2(5,0) molecule, plus one Bohr radius) and an atomic radius of 0.529 Å (one Bohr radius), $\gamma(T)_{\mathrm{HS,\,H+H_2}} = 5.52 \times 10^{-10}$. The hard sphere collision rate coefficients are comparable at higher temperatures to the rate coefficient of the most probable nonreactive processes.

It is typical for purely vibrational transitions that the H + H_2 rate coefficients at 100000 K are greater than the corresponding H + HD rate coefficients. For rotational transitions, the H + HD rate coefficients tend to be the greater. In cases involving purely rotational or vibrational transitions, the rate coefficients for H + H_2 and D + H_2 are similar except at the lowest temperatures studied. For diagonal transitions, H + H_2 and D + H_2 differ more noticeably, but

are more similar to one another than H + H_2 is to H + HD. This implies that the increase in interaction time at constant translational energy caused by an increase in mass is not a dominating factor in these processes; rather, the difference in behaviour from H + H_2 to H + HD indicates that the asymmetry of the HD molecule may significantly influence nonreactive processes.

4.4 Total nonreactive energy transfer

The total cross sections for nonreactive transitions illustrate the importance of transitions that have not been previously discussed. For simple vibrational and rotational excitations and deexcitations, it is observed that at constant internal and translational energies, cross sections for D + H_2 are almost always at least as great as those of H + H_2, while cross sections for the corresponding H + HD transitions tend to be smaller than either. The exceptions are for those upward transitions at low translational energy in which a smaller energy gap exists for the HD transition than for the H_2 transition. However, for transitions involving an exchange of vibrational and rotational energy, the cross sections for H + HD tend to be of similar magnitude as the corresponding transitions for H + H_2 or D + H_2.

There are more final states available for nonreactive H + HD collisions. Thus, which of H + H_2 and H + HD has the greatest overall nonreactive cross section for a given translational energy will be determined by whether or not the increase in the number of available states for H + HD is enough to compensate for the smaller cross sections for each state–to–state transition. The question now becomes: for a given H_2 state, the corresponding HD state, and a given translational energy, what is the relative number of final states available to each system, and how does that number compare to the relative cross sections for state–to–state transitions within those systems?

At low internal and translational energies, H + HD has an advantage for promoting nonreactive transfer on two counts: not only are the cross sections for $\Delta j = +1$ transitions much larger than those of the corresponding $\Delta j = +2$ transitions of H_2, but the $\Delta j = +2$ transition of HD is also available to contribute significantly to the total. In addition, there are few diago-

nal transitions available at low internal energy, so the purely rotational excitations will tend to dominate the overall process. It may be expected in these cases that the total nonreactive cross section for H + HD will be much greater than that of H + H_2 or D + H_2.

The data in Figure 4.18 support this hypothesis. At translational energies of 1 kcal mol^{-1}, 2 kcal mol^{-1}, and 3 kcal mol^{-1}, the total nonreactive cross sections from H + HD(0,0) are 3.40 ± 0.09 Å^2, 6.32 ± 0.11 Å^2, and 7.58 ± 0.11 Å^2, respectively. The contributions to the cross sections at these translational energies due to the transition H + HD(0,0)→H + HD(0,1) are 3.02 ± 0.09 Å^2, 5.63 ± 0.11 Å^2, and 6.71 ± 0.11 Å^2. For comparison, the total nonreactive cross sections for H + H_2 are 0 at these translational energies: the lowest energy nonzero cross section from H + H_2(0,0), at 6 kcal mol^{-1}, is 0.067 ± 0.004 Å^2.

At higher translational and internal energies, although the total number of energetically accessible states for transitions (whether diagonal and not) increases for H + HD, it also increases for H + H_2. The number of accessible states may be described in terms of the density of states. If the number of states with internal energy less than E is given by $G(E)$, then the density of states with energy in the range (E, dE) may be given as $N(E) = \frac{G(E+\mathrm{d}E)-G(E)}{\mathrm{d}E}$ [78]. In absolute terms, there is a higher density of states for HD at high internal energies than there is for H_2, but the relative difference in the density of states for the two is greater at low internal energies. This may best be seen by referring to Appendix A: the number of states between two points on the y–axis in Figure A.1 is at least as great as than the number of states between the same two points in Figure A.2. Therefore, a total inelastic cross section for H + H_2 under a set of high energy conditions ought to be closer to the corresponding cross section of H + HD than it would at lower total energy.

For example, if there are 5 H_2 states in an (arbitrary) energy range dE at low energy, then there might be 10 HD states in that same range. The ratio of the density of states of H_2 to the density of states of HD in the range dE is $\frac{1}{2}$. At a higher energy, there could be 40 H_2 states in an energy range of the same magnitude, but 50 HD states. The ratio of the density of states in the higher energy range is $\frac{4}{5}$. Although the absolute difference in states is 10 for both

ranges, the relative difference in density of states is much less for the high energy states than for the low energy states. This translates into a number of available diagonal transitions for the high energy H_2 state much closer (relatively) to that of the high energy HD state, compared to the low energy case. This in turn means that any dynamical threshold limitations that the $H + H_2$ cross sections might suffer are not as important for transitions involving states with high internal energies as they are for states with low internal energies.

In Figure 4.18, it can be seen that the totals of the nonreactive cross sections for $H + H_2$ and $D + H_2$ are similar at all translational energies. For all low energy states, these cross sections increase as translational energy is increased, until some (state–dependent) translational energy is reached above which the total cross sections are nearly constant. The total nonreactive cross sections of H + HD are greater than those of $H + H_2$ at all translational energies. The total excitation functions of H + HD peak at a relatively low translational energy, reflecting the lower energetic threshold for excitation, and decrease sharply as translational energy increases over a range of 40 kcal mol^{-1}, decreasing slowly as translational energy increases above that. The peak in the excitation function is noticeably less pronounced for the rotationally excited H + HD(0,8).

Which of $H + H_2$ and $D + H_2$ has the greater total inelastic cross sections depends upon whether or not the differences in cross sections for the few significant nondiagonal transitions are large enough to clearly differentiate the two. If so, then it may be expected that the $D + H_2$ total cross sections will be larger. If instead these differences do not make a large relative contribution to an overall cross section, it may be expected that the $H + H_2$ and $D + H_2$ cross section will be dominated by the diagonal transitions and thus similar in magnitude, as in Figure 4.21.

Below 50 kcal mol^{-1} in Figure 4.18, the small number of available final states means that only a few transitions are important. The enhancement of nonreactive cross sections for $D + H_2$ for these few transitions means that the overall nonreactive cross section is similarly enhanced. At higher translational energies, however, more final states are available, and the

influence of individual transitions on the total cross section is diminished, leading to similar total nonreactive cross sections for D + H_2 and H + H_2.

The enhancement of total cross sections for nonreactive energy transfer in D + H_2(0,8) over the total cross sections for H + H_2(0,8) seen in Figure 4.18 exists over a much smaller range of translational energies than it does for (0,0) and (1,0). The cross sections in Figure 4.5 do not tell the whole story; at high translational energies, both D + H_2(0,8) $\rightarrow$ D + H_2(0,10) and D + H_2(0,8) $\rightarrow$ D + H_2(0,6) have cross sections greater than those of the corresponding H + H_2 transitions. Due to the small size of these cross sections, contributions from other nonreactive transitions, such as vibrational excitation (Figure 4.10) are important.

For the total nonreactive cross sections of H + H_2(0,0) and D + H_2(0,0), and for those of H + H_2(0,8) and D + H_2(0,8), the greatest differences between isotopic analogues come at translational energies slightly lower than those at which the cross sections approach a constant value. However, for H + H_2(1,0) and D + H_2(1,0) there is also a significant difference between cross sections at high translational energies, in addition to differences a lower translational energies.

Among the reference states, although the purely rotationally excited molecules behave differently from the others at low internal energy, the purely vibrationally excited molecules differ from the others for the states with internal energy near 55 kcal mol^{-1} and states with internal energy near 109.5 kcal mol^{-1}. For translational energies below 50 kcal mol^{-1}, Figure 4.19 shows that there are much higher transition probabilities from (5,0) than from either of the rotationally excited states with similar internal energy. The difference is even more pronounced at translational energies near 1 kcal mol^{-1}, and is most pronounced of all in the H + HD case. The addition of rotational energy at the expense of vibrational energy in all systems reduces the total nonreactive cross section, except at very high translational energies. This is possibly due to orientation effects, as discussed for CID in Section 3.1.1; rotationally excited molecules are resistant to penetration by slow colliders.

At high internal energy, the cross sections for H + H_2 and D + H_2, shown in Figure 4.20,

are not similar at any translational energy. There is no low energy peak for (12,0) as there is for (5,0). These excitation functions otherwise share the same trends as those at 55 kcal mol^{-1}: the rotationally unexcited states have relatively large cross sections at low translational energy, and vibrational energy is more likely to cause nonreactive energy transfer than is an equivalent amount of rotational energy.

4.5 Relative importance of different transition types to nonreactive energy transfer

As observed in Figure 4.1, trajectory outcomes for nonreactive energy transfer tend to cluster among states with internal energy similar to that of the initial state. This behaviour is pronounced at low translational energy, but becomes less so as translational energy is increased. It is desirable to know how important these diagonal transitions are relative to ones which change the internal energy of the target molecule.

Figures 4.21, 4.22, and 4.23 display plots of total rate coefficients against temperature for diagonal, upward, and downward processes from each of the reference states. The definition of a diagonal transition is somewhat arbitrary, but was chosen in this case to be a transition to a state with internal energy within 12% of the initial state's energy. This cutoff was chosen mostly to ensure that HD(1,0) and HD(0,8) are considered diagonal to one another. A cutoff of 3.5% might be more appropriate for low to mid–temperature H + H_2(12,0) rate coefficients, for which the rate coefficients for diagonal transitions are halfway between those of the upward and downward transitions on a log scale; for the sake of consistency, the 12% value was used for all states. It is important to note that for an initial state with high internal energy there will be many other states within the 12% range, but that for low energy states there will be few. The choice of cutoff constrains the size of the diagonal rate coefficients much more for low states than for high ones, and permits some purely rotational transitions to contribute to the diagonal rate coefficients of the higher energy states. The number of final states which contribute to the diagonal rate coefficients for low internal energy states will be restricted much more for D + H_2 and H + H_2 than for H + HD.

Figure 4.21 contains the rate coefficients for total nonreactive transfer from low energy states. The rate coefficients for corresponding transition types of H + H_2 and D + H_2 are similar to each other. For H + HD, diagonal transitions are the most probable up to about 20000 K, while upward and downward transitions become significant at higher temperatures. For H + H_2 and D + H_2, the shapes of the graphs suggest that diagonal transitions are the most likely at low temperature, but if so, the temperatures at which diagonal transitions are the most probable are low, around 100 K The rate coefficients at these temperatures are both small and of limited validity due to quantum considerations.

There is a temperature for each initial state of each system above which an upward nonreactive transition is more likely than a downward one. In all three of H + H_2, D + H_2, and H + HD, this temperature is near 780 K for (1,0), and near 7800 K for (0,8).

At moderate internal energy (Figure 4.22), with more available states for diagonal transitions, there is greater opportunity for diagonal rate coefficients to be large. In all three systems, the diagonal rate coefficients are larger than either the upward or downward rate coefficients at all but the highest temperatures, and for transitions from (5,0) at low temperature.

For high internal energy states (Figure 4.23), the rate coefficients of H + H_2 and D + H_2 at low temperature differ, for some processes, by factors as great as 10. The rate coefficients at these temperatures are not expected to be highly accurate, however, so these differences are not exceptional. Upward transitions from high energy states are improbable at low temperature, likely because of the readily accessible CID channel, while the rate coefficients of all diagonal and downward transitions at the same temperature are within a factor of 100 of each other. At most temperatures, the total upward and downward nonreactive rate coefficients do not differ greatly between isotopic systems, nor do they differ by more than a factor of 10 between states with different internal energy distributions.

Table 4.1: A comparison of rotational energy transfer in H + HD calculated by QCT with quantum results. Rate coefficients are given in $cm^3\ s^{-1}\ molec^{-1}$. QCT data from this study is labelled QCT. QM data from Roeuff and Flower are labelled RF99, and have estimated errors "within 10 %, generally much better"[77]. All QCT rate coefficients presented have been corrected to obey microscopic reversibility.

	100 K	
transition	QCT	RF99
(0,0) → (0,1)	$8.9 \pm 0.4 \times 10^{-12}$	1.3×10^{-11}
(0,0) → (0,2)	$1.4 \pm 0.2 \times 10^{-17}$	5.8×10^{-14}
(0,0) → (0,8)	$0.8 \pm 2.0 \times 10^{-46}$	1.8×10^{-36}
(0,1) → (0,2)	$1.89 \pm 0.06 \times 10^{-12}$	2.6×10^{-12}
(0,1) → (0,8)	$0.9 \pm 3.4 \times 10^{-42}$	9.0×10^{-36}
(0,4) → (0,8)	$0.8 \pm 1.1 \times 10^{-37}$	3.1×10^{-29}
	300 K	
transition	QCT	RF99
(0,0) → (0,1)	$8.2 \pm 0.2 \times 10^{-11}$	7.0×10^{-11}
(0,0) → (0,2)	$3.7 \pm 0.3 \times 10^{-13}$	2.8×10^{-12}
(0,0) → (0,8)	$2.0 \pm 1.1 \times 10^{-23}$	1.0×10^{-22}
(0,1) → (0,2)	$4.09 \pm 0.07 \times 10^{-13}$	3.2×10^{-11}
(0,1) → (0,8)	$1.9 \pm 1.2 \times 10^{-22}$	2.2×10^{-22}
(0,4) → (0,8)	$9.9 \pm 2.0 \times 10^{-21}$	3.6×10^{-19}
	1000 K	
transition	QCT	RF99
(0,0) → (0,1)	$2.72 \pm 0.03 \times 10^{-10}$	2.5×10^{-10}
(0,0) → (0,2)	$2.78 \pm 0.07 \times 10^{-11}$	3.5×10^{-11}
(0,0) → (0,8)	$3.9 \pm 0.9 \times 10^{-15}$	2.1×10^{-16}
(0,1) → (0,2)	$1.88 \pm 0.01 \times 10^{-10}$	1.5×10^{-10}
(0,1) → (0,8)	$8.1 \pm 0.7 \times 10^{-15}$	4.1×10^{-16}
(0,4) → (0,8)	$4.1 \pm 0.2 \times 10^{-14}$	2.5×10^{-14}

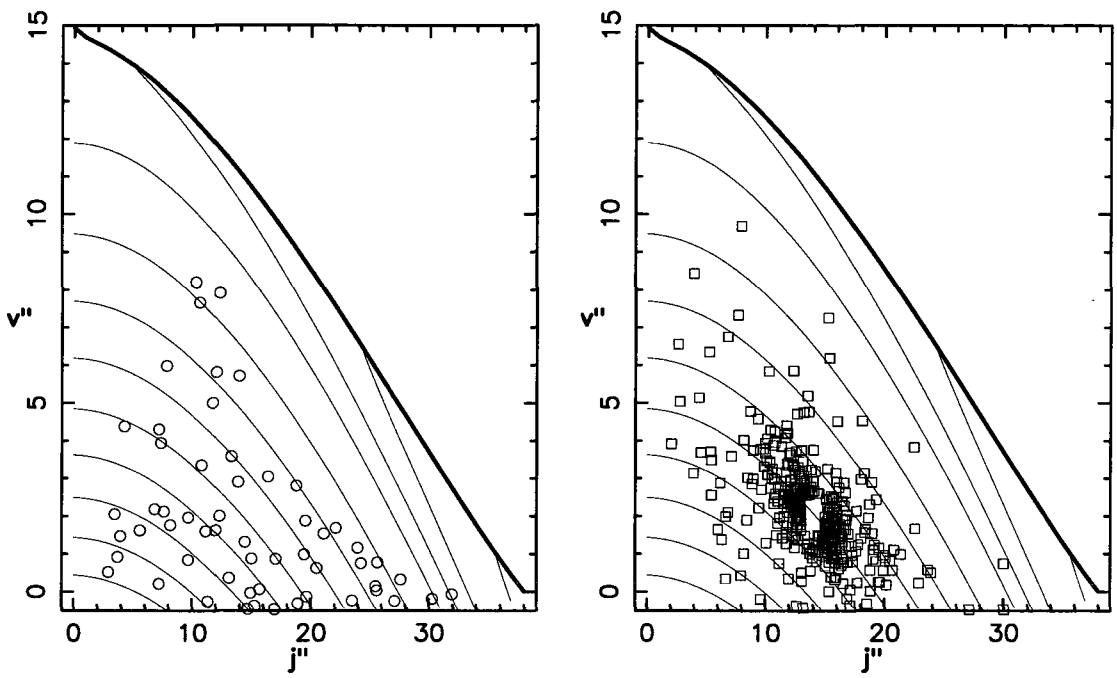

Figure 4.1: Scatter plots of nonreactive trajectories from D + H_2(2,14) in the impact parameter ranges 0–0.5 Å (left) and 1.5–2 Å (right) at a translational energy of 85 kcal mol^{-1}. Solid lines are energy contours at 10 kcal mol^{-1} intervals. The uppermost (bold) line is the energy contour representing the dissociation limit. Elastic trajectories are excluded, so that bin (2,14) is empty in both panels. In the higher impact parameter range, the final states of the nonreactive trajectories cluster around the initial state, and there is a tendency to interconvert vibrational and rotational energy for higher impact parameter collisions. These trends are not present in the trajectories at low impact parameters.

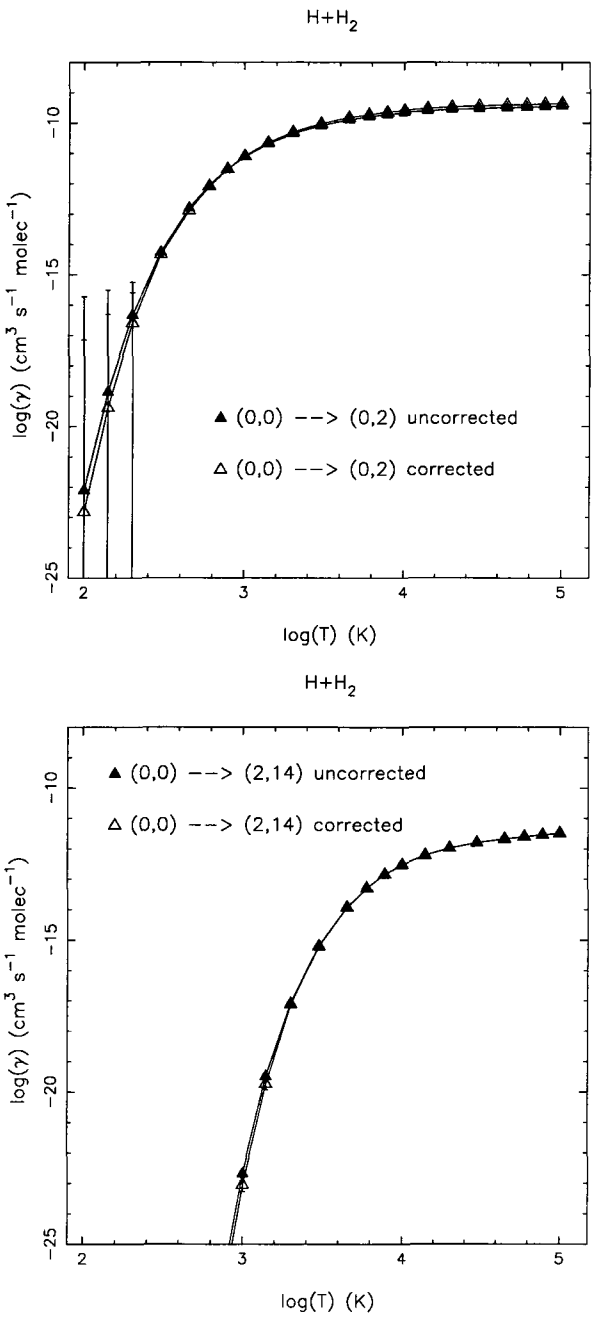

Figure 4.2: Corrected and uncorrected rate coefficients for selected H + H_2 nonreactive upward transitions.

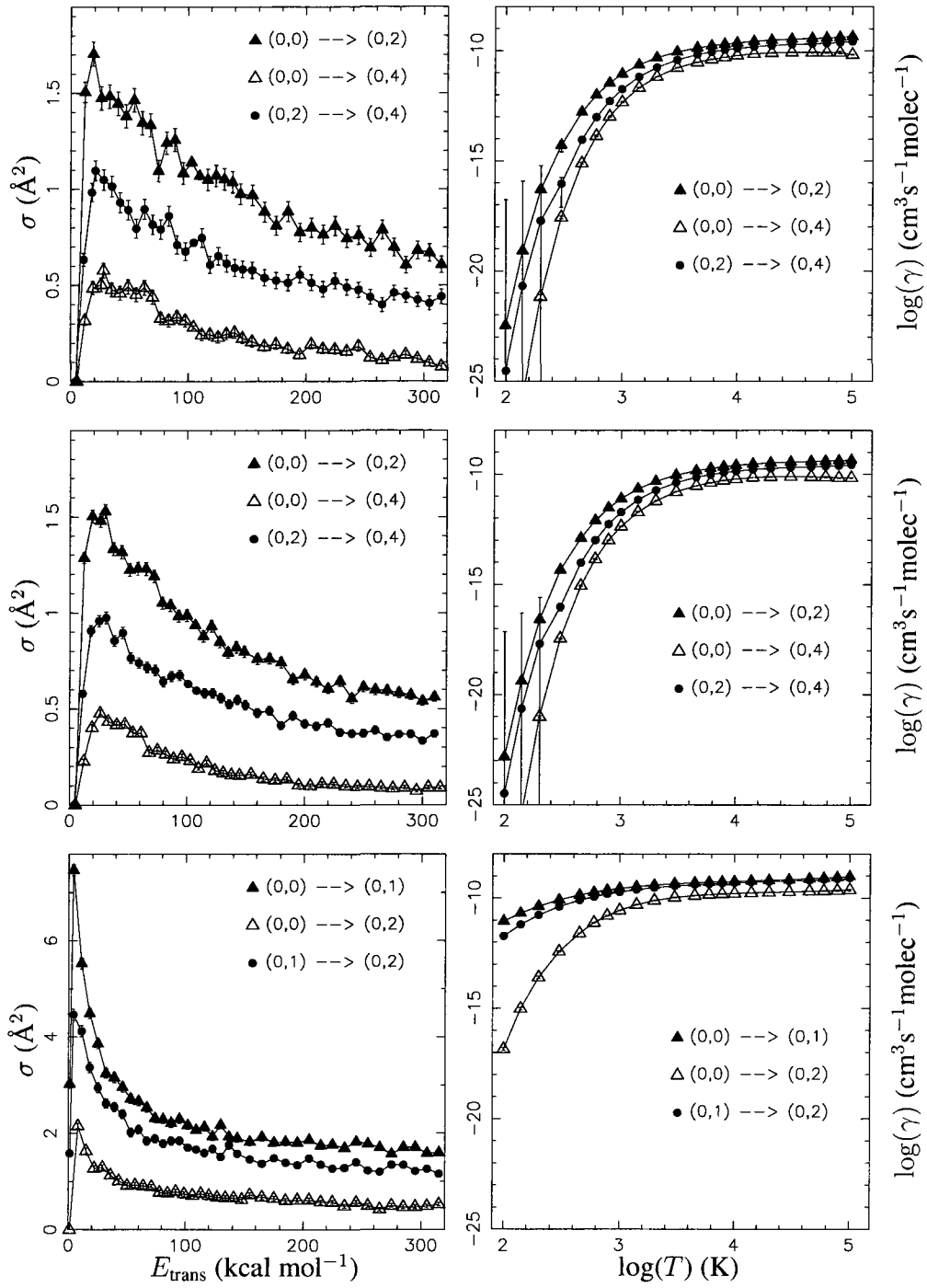

Figure 4.3: Left column: cross sections plotted against translational energy for upward nonreactive rotational transitions involving states (0,0), (0,2), and (0,4). Right column: thermal rate coefficients plotted against temperature for the same. The top row is D + H_2, the middle row is H + H_2, and the bottom row is H + HD.

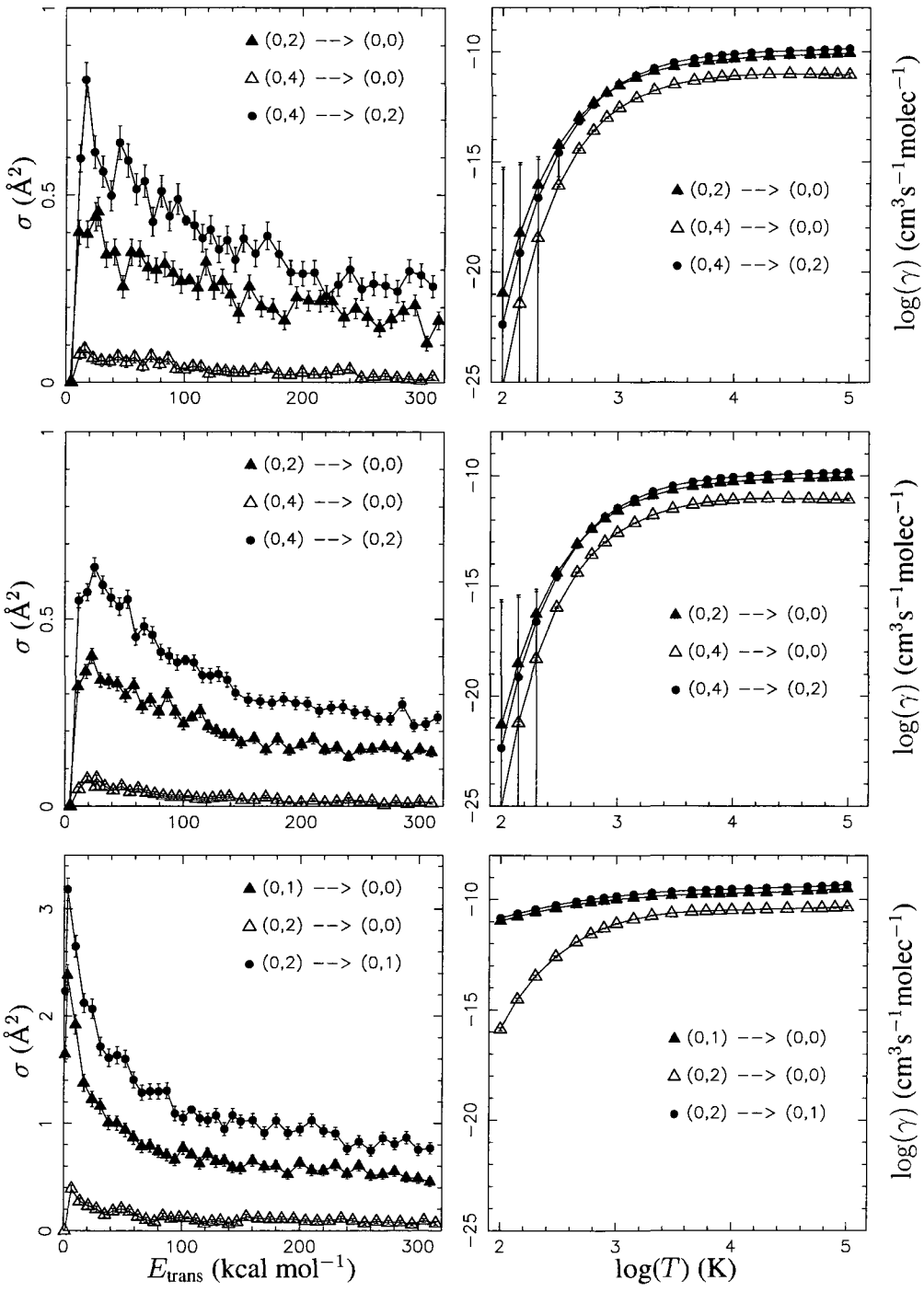

Figure 4.4: Left column: cross sections plotted against translational energy for downward nonreactive rotational transitions involving states (0,0), (0,2) and (0,4). Right column: thermal rate coefficients plotted against temperature for downward nonreactive rotational transitions involving states (0,0), (0,2) and (0,4). The top row is D + H_2, the middle row is H + H_2, and the bottom row is H + HD.

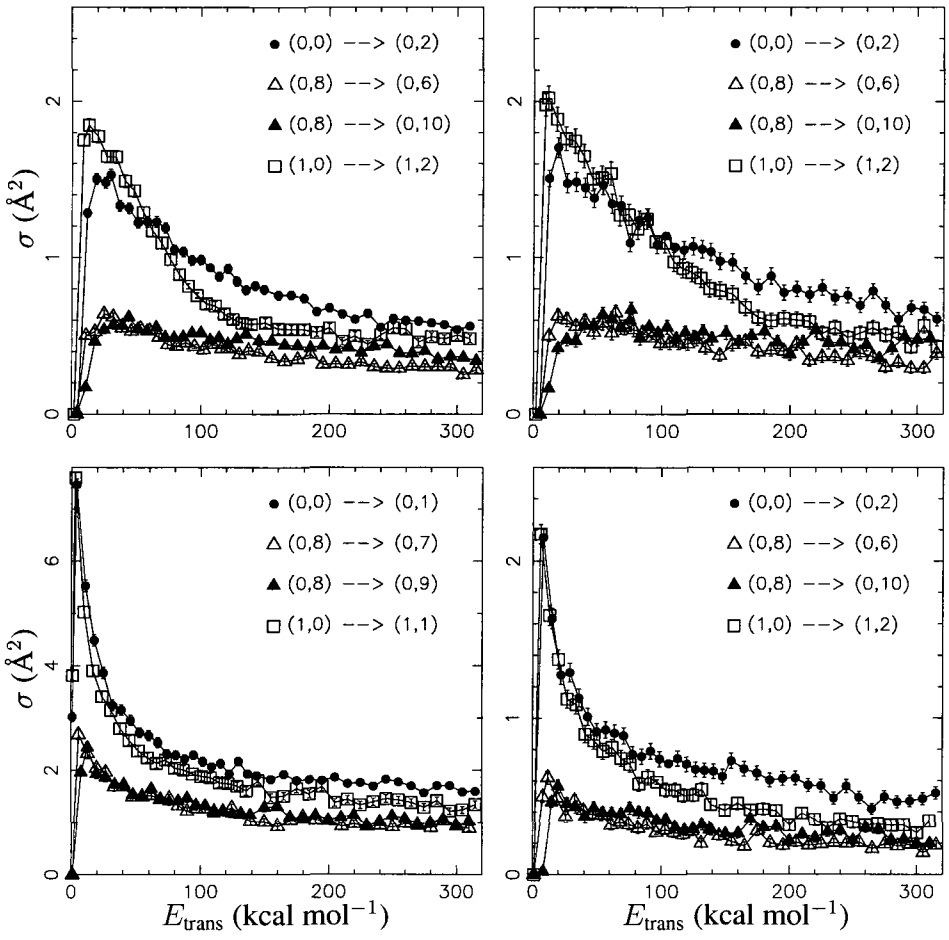

Figure 4.5: Cross sections plotted against translational energy for nonreactive rotational transitions between selected low energy states. The top left panel is H + H_2, the top right is D + H_2, and the bottom two are H + HD.

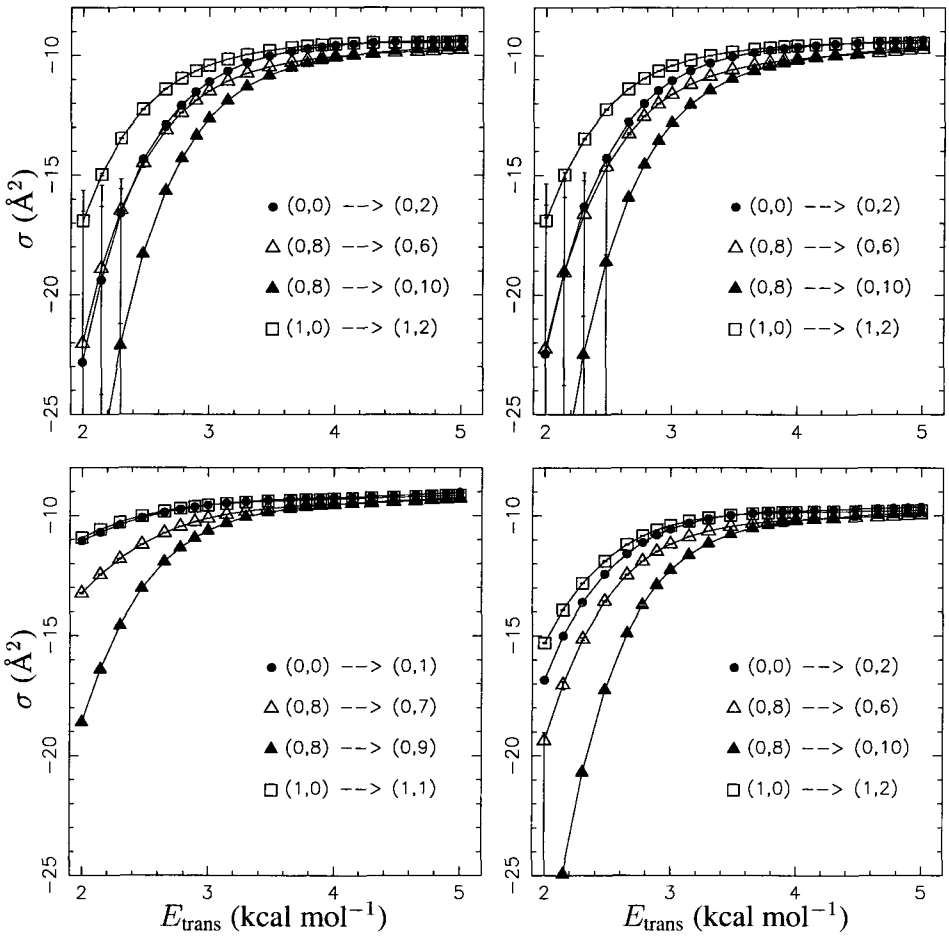

Figure 4.6: Thermal rate coefficients plotted against temperature for nonreactive rotational transitions between selected low energy states. The top left panel is H + H_2, the top right is D + H_2, and the bottom two are H + HD.

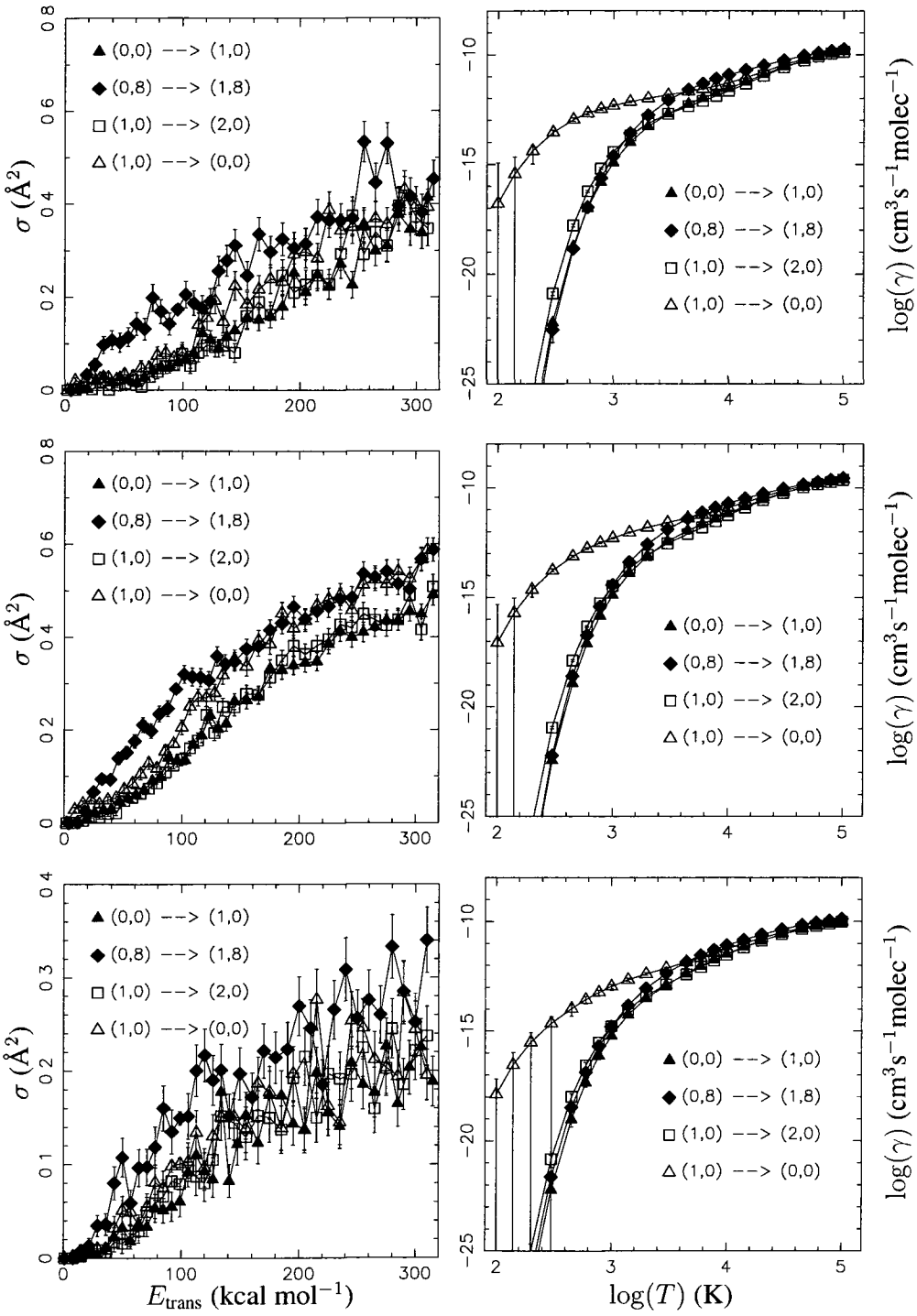

Figure 4.7: Left column: cross sections plotted against translational energy for nonreactive vibrational transitions between selected low energy states. Right column: thermal rate coefficients plotted against temperature for the same transitions. The top row is D + H_2, the middle row is H + H_2, and the bottom row is H + HD.

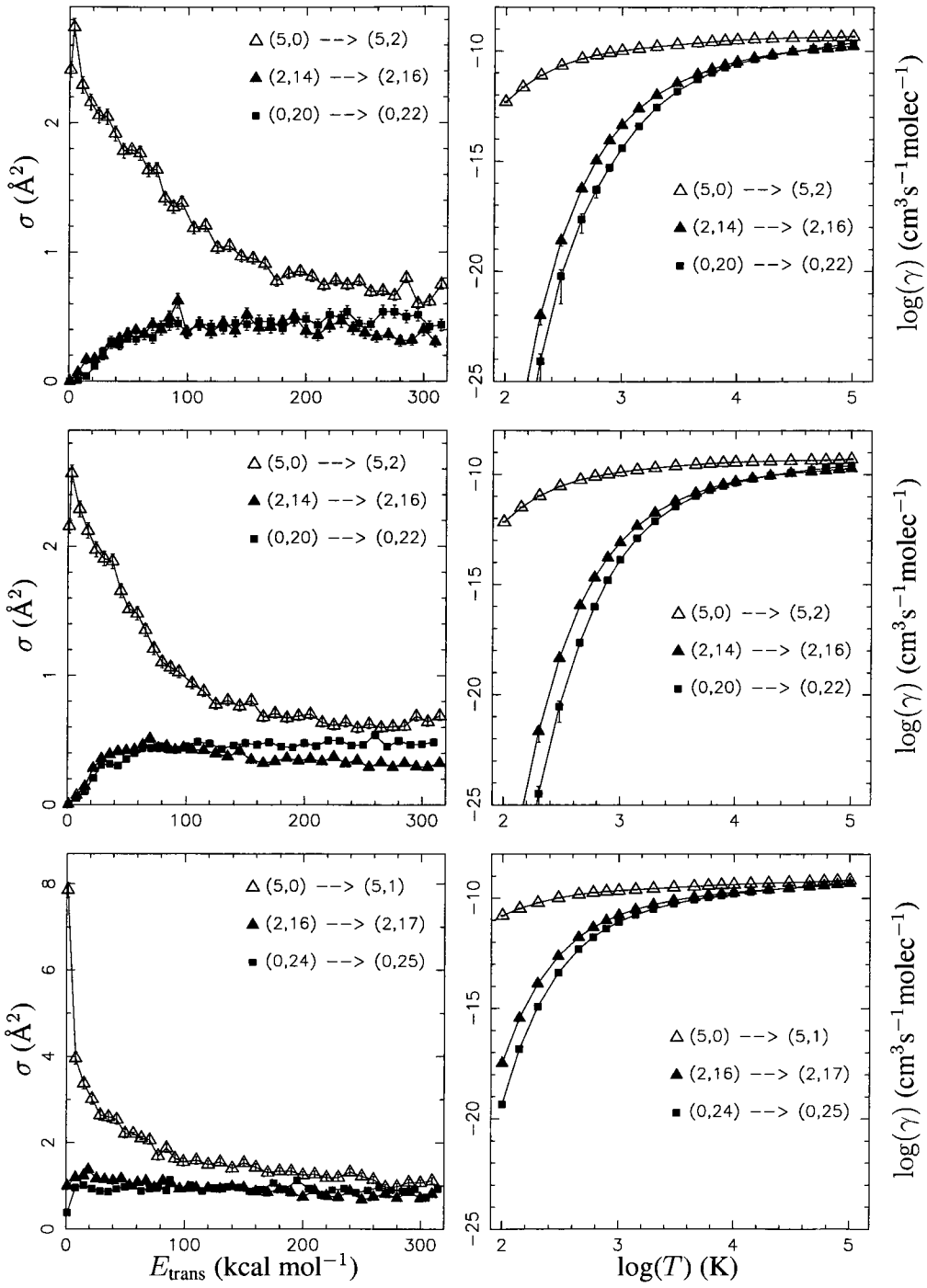

Figure 4.8: Left column: cross sections plotted against translational energy for upward non-reactive rotational transitions between selected states with internal energy near 55 kcal mol^{-1}. Right column: thermal rate coefficients plotted against temperature for the same transitions. The top row is D + H_2, the middle row is H + H_2, and the bottom row is H + HD.

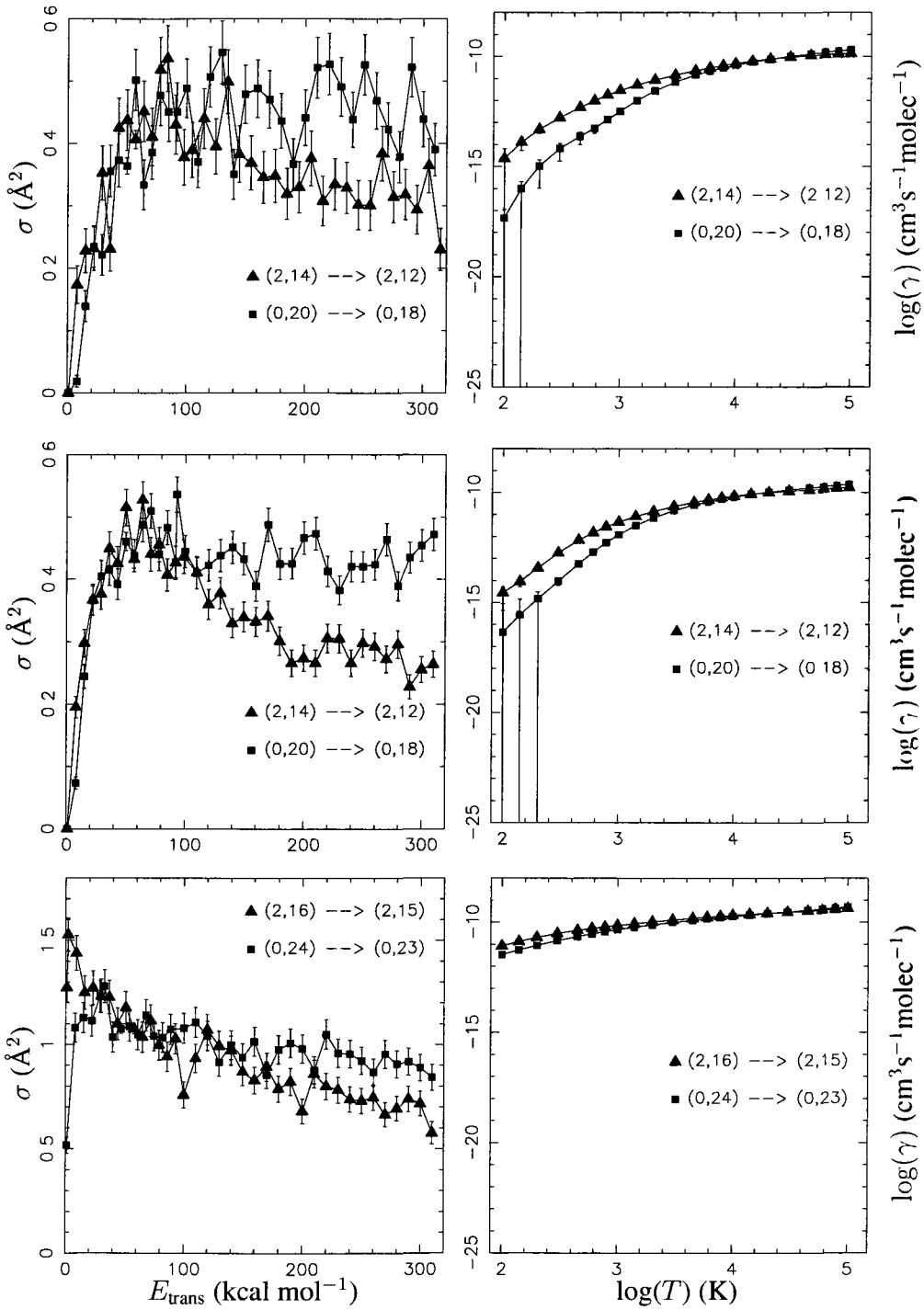

Figure 4.9: Left column: cross sections plotted against translational energy for downward non-reactive rotational transitions between selected states with internal energy near 55 kcal mol^{-1}. Right column: thermal rate coefficients plotted against temperature for the same transitions. The top row is D + H_2, the middle row is H + H_2, and the bottom row is H + HD.

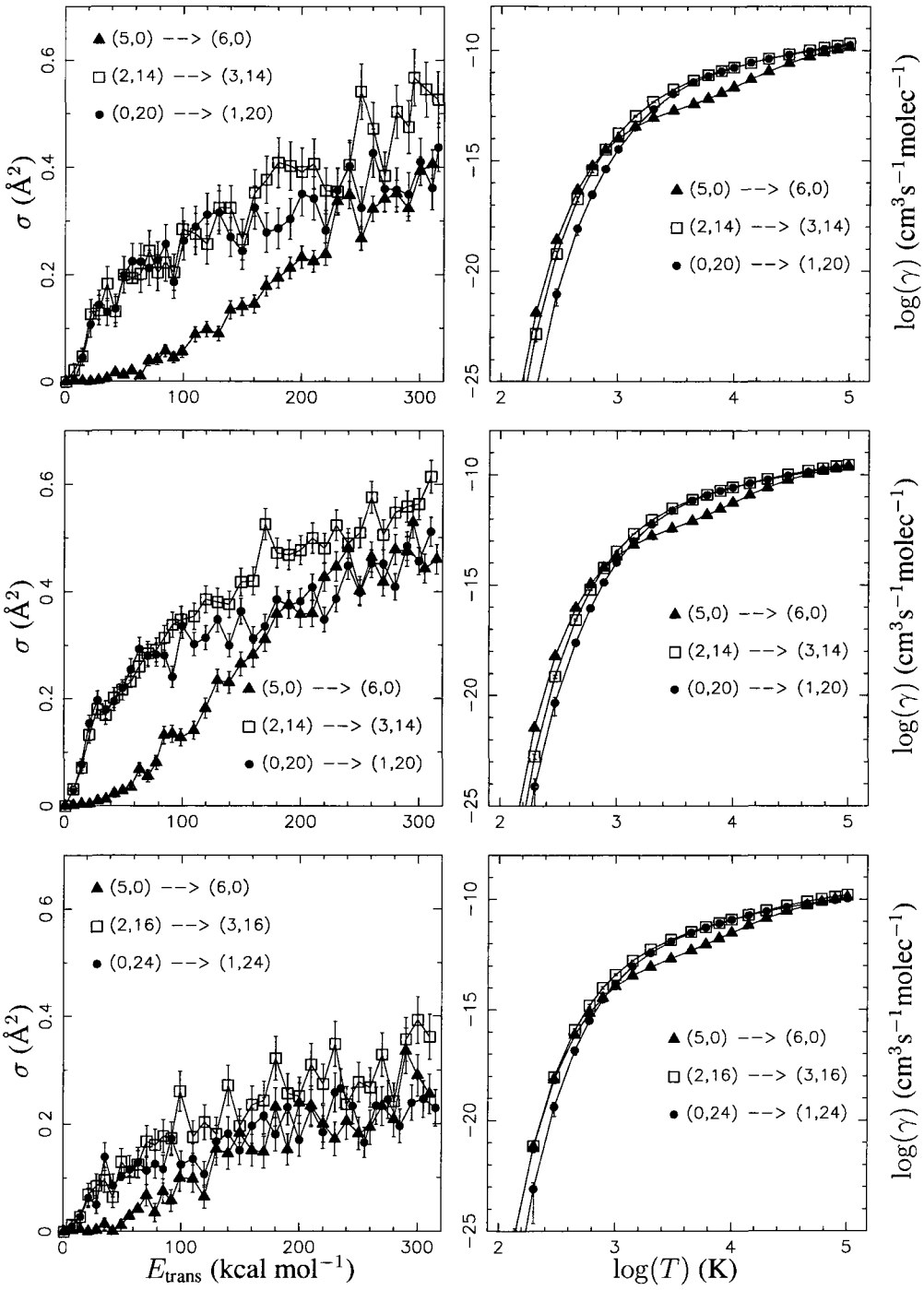

Figure 4.10: Left column: cross sections plotted against translational energy for upward nonreactive vibrational transitions between selected states with internal energy near 55 kcal mol^{-1}. Right column: thermal rate coefficients plotted against temperature for the same transitions. The top row is D + H_2, the middle row is H + H_2, and the bottom row is H + HD.

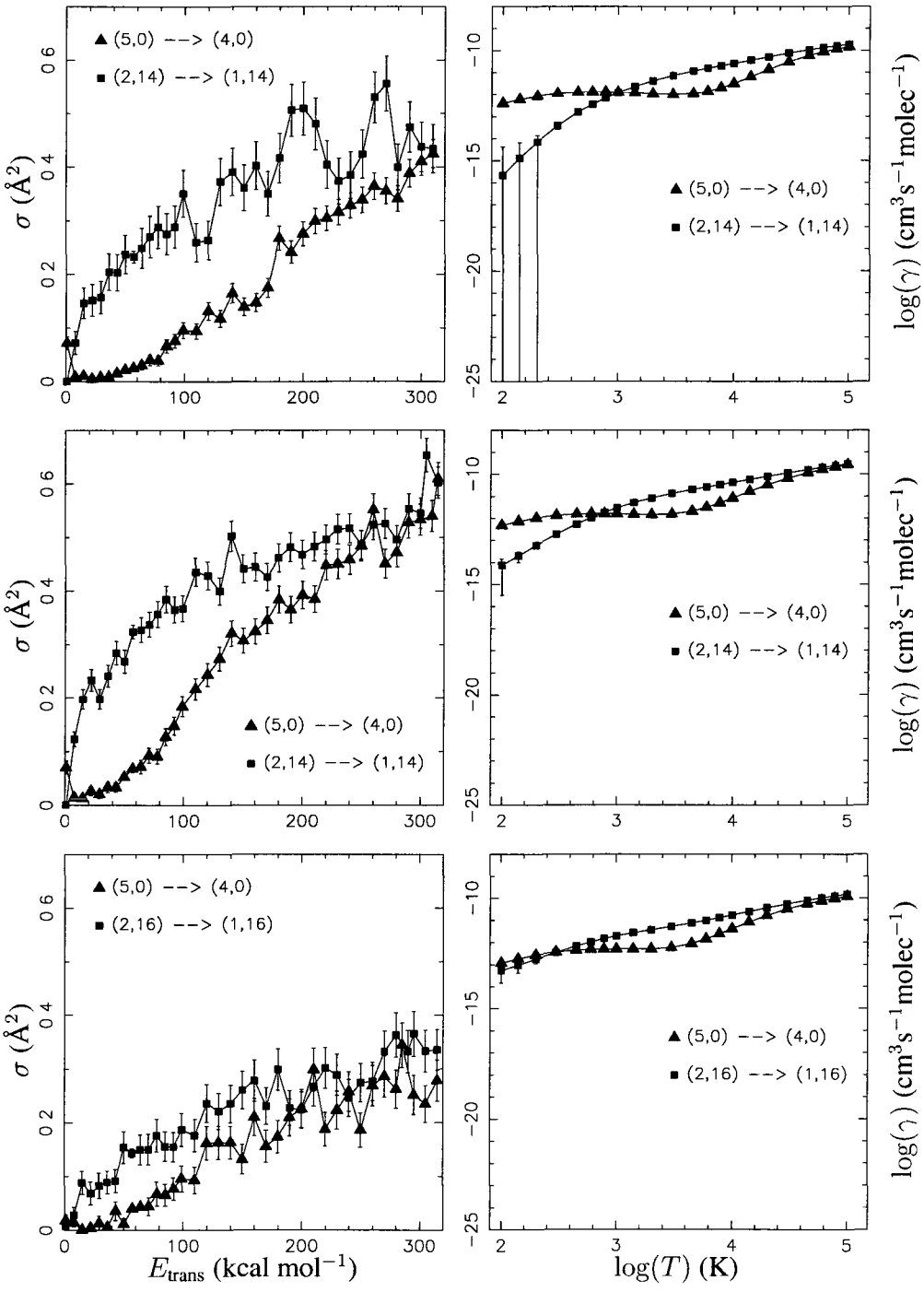

Figure 4.11: Left column: cross sections plotted against translational energy for downward nonreactive vibrational transitions between selected states with internal energy near 55 kcal mol^{-1}. Right column: thermal rate coefficients plotted against temperature for the same transitions. The top row is D + H_2, the middle row is H + H_2, and the bottom row is H + HD.

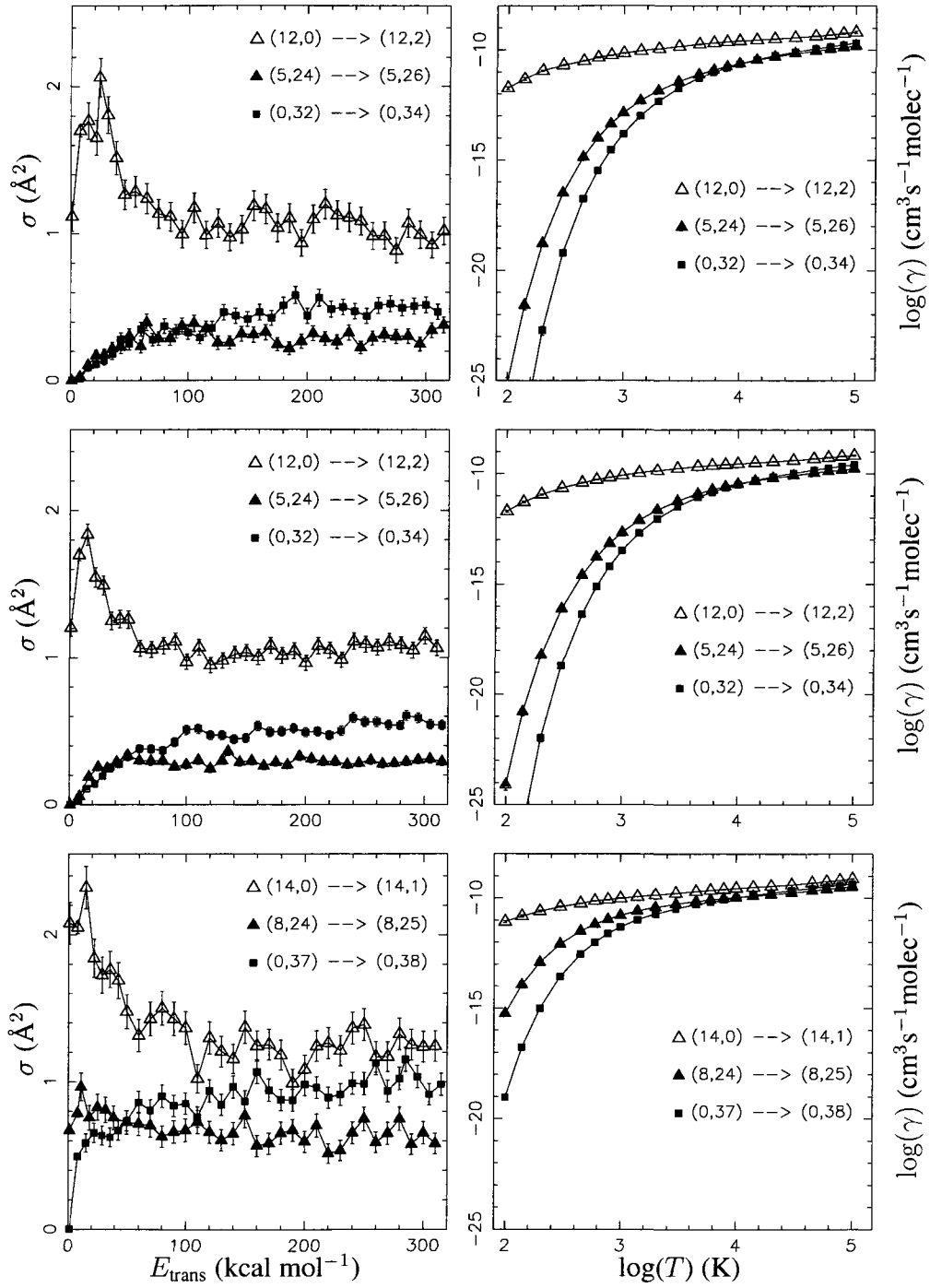

Figure 4.12: Left column: cross sections plotted against translational energy for upward non-reactive rotational transitions between selected high energy states. Right column: thermal rate coefficients plotted against temperature for the same transitions. The top row is D + H_2, the middle row is H + H_2, and the bottom row is H + HD.

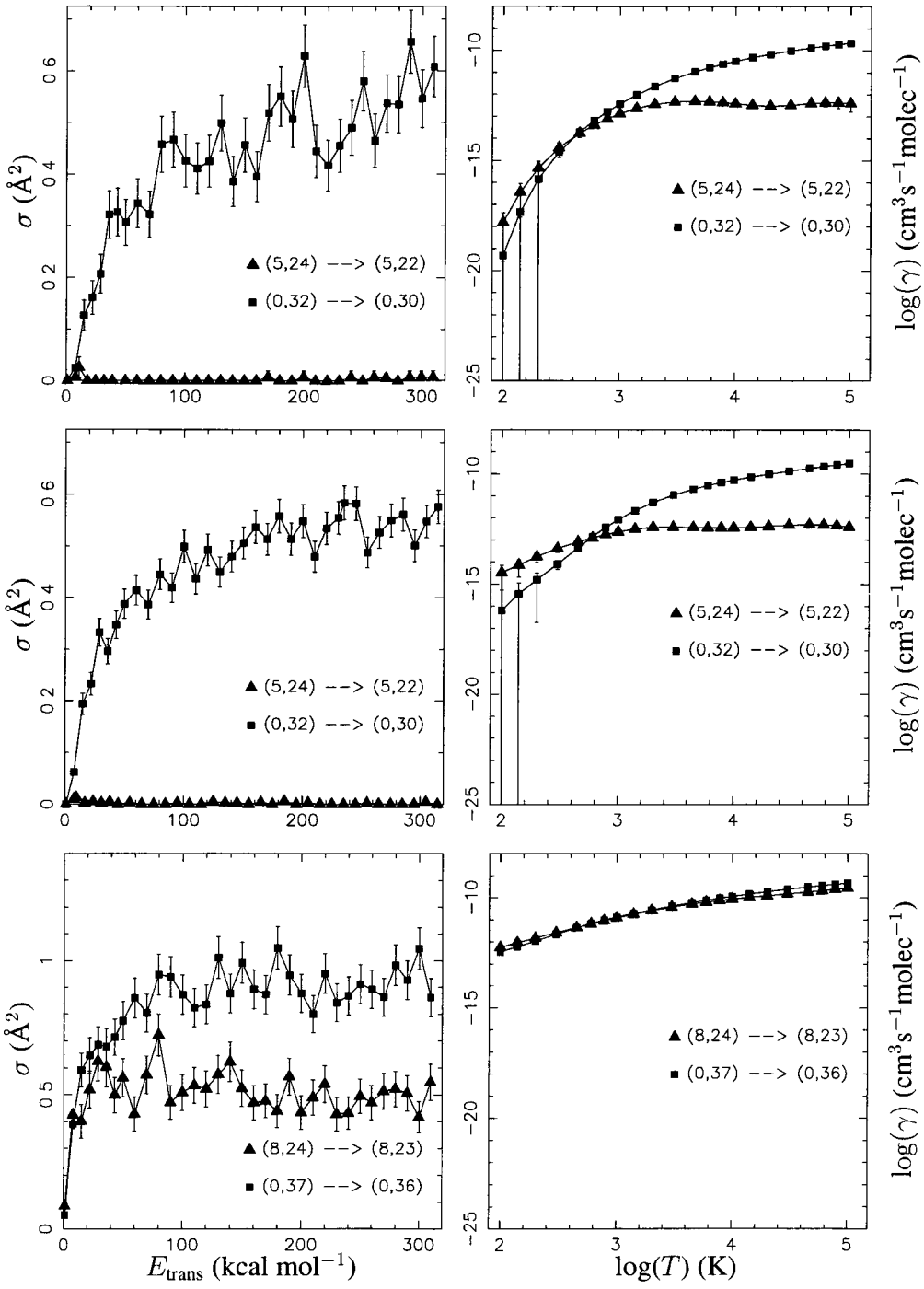

Figure 4.13: Left column: cross sections plotted against translational energy for downward nonreactive rotational transitions between selected high energy states. Right column: thermal rate coefficients plotted against temperature for the same transitions. The top row is D + H_2, the middle row is H + H_2, and the bottom row is H + HD.

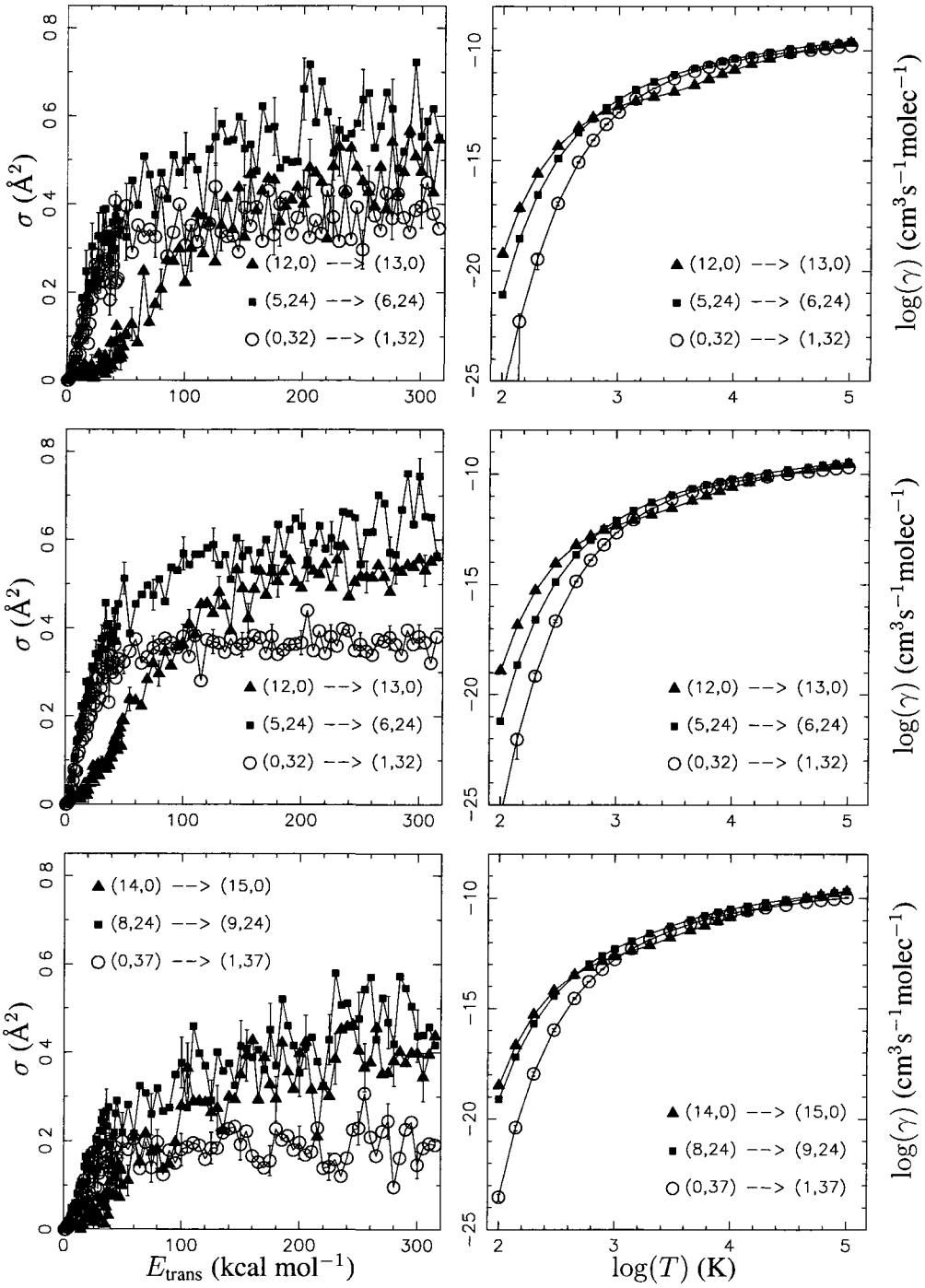

Figure 4.14: Left column: cross sections plotted against translational energy for nonreactive vibrational transitions between selected high energy states. Right column: thermal rate coefficients plotted against temperature for the same transitions. The top row is D + H_2, the middle row is H + H_2, and the bottom row is H + HD.

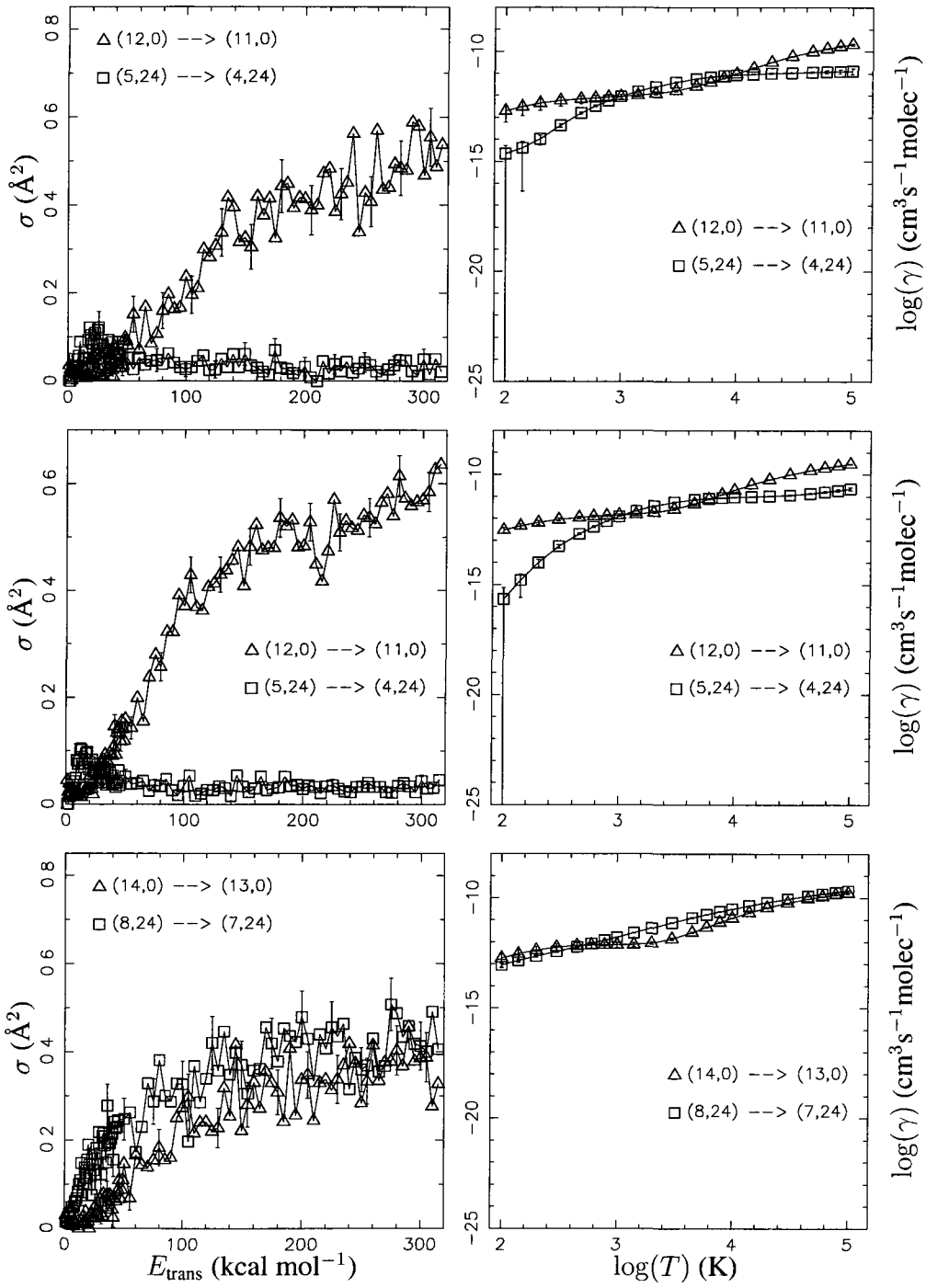

Figure 4.15: Left column: cross sections plotted against translational energy for nonreactive vibrational transitions between selected high energy states. Right column: thermal rate coefficients plotted against temperature for the same transitions. The top row is D + H_2, the middle row is H + H_2, and the bottom row is H + HD.

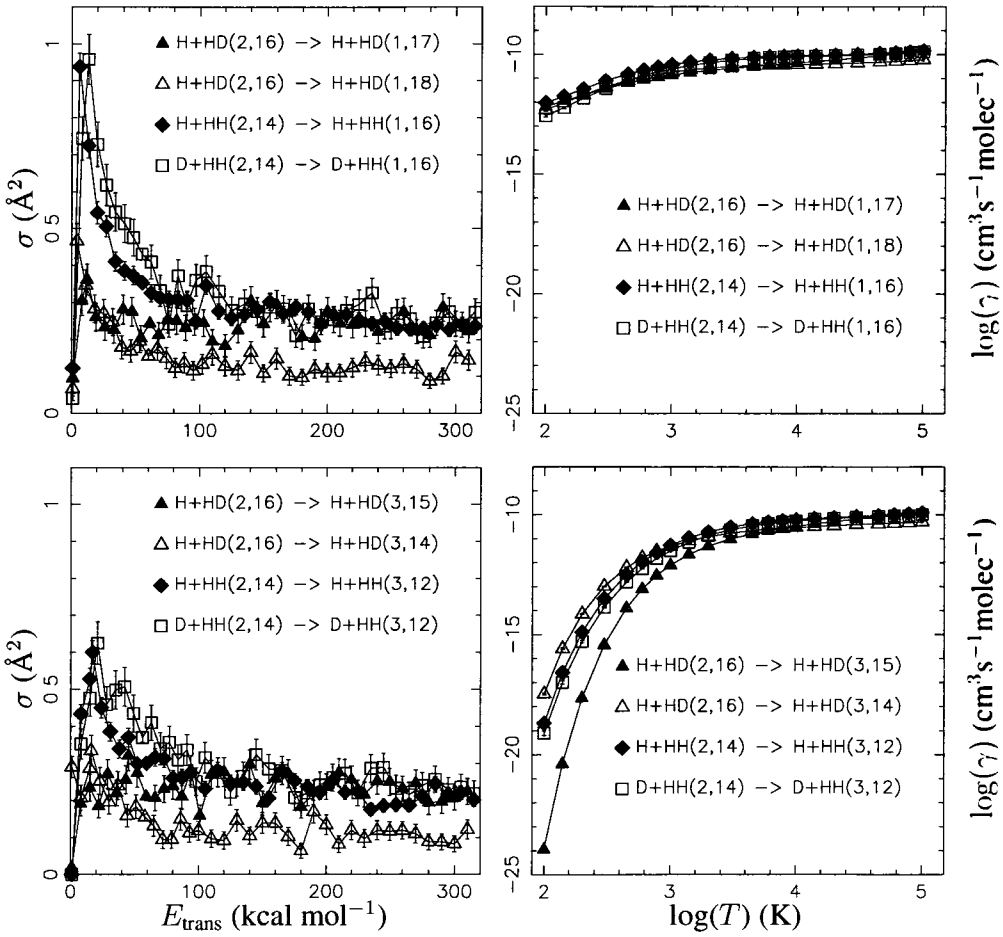

Figure 4.16: Left column: cross sections for vibrational/rotational energy interconversion plotted against translational energy for selected transitions from H_2(2,14) and HD(2,16). Right column: thermal rate coefficients plotted against temperature for the same transitions.

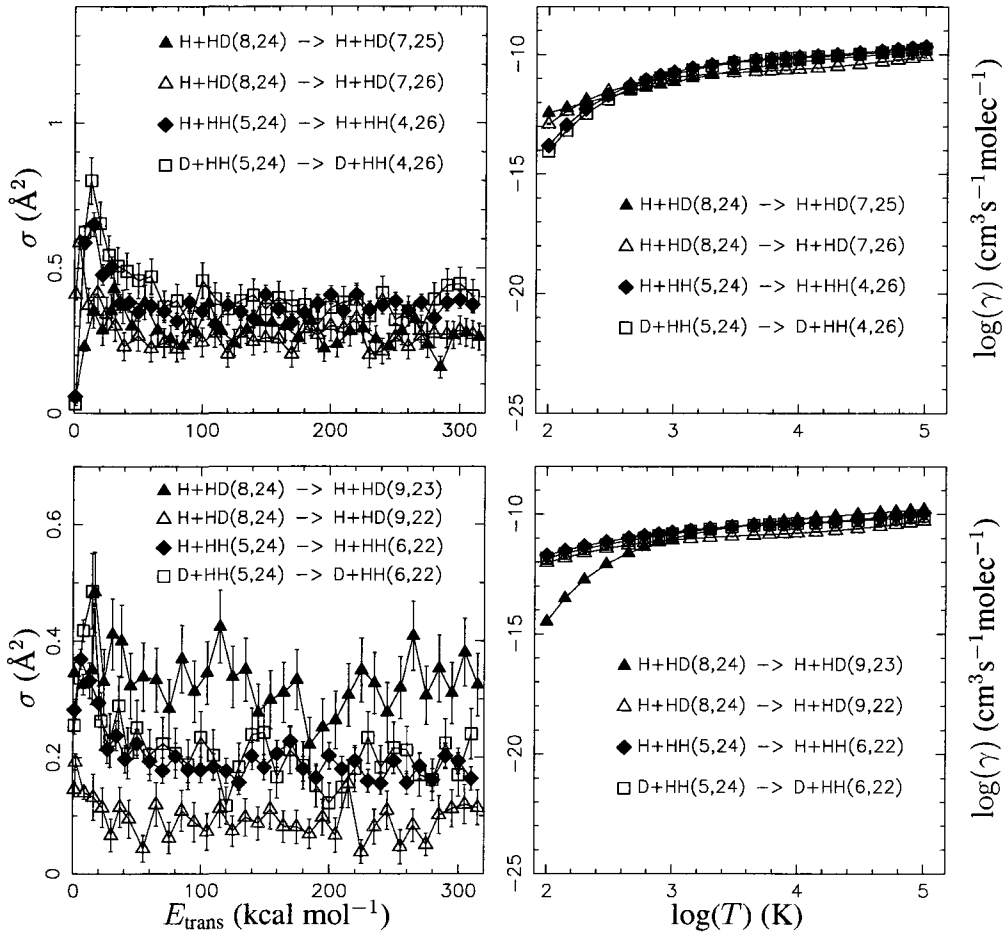

Figure 4.17: Left column: cross sections for vibrational/rotational energy interconversion plotted against translational energy for selected transitions from H_2(5,24) and HD(8,24). Right column: thermal rate coefficients plotted against temperature for the same transitions.

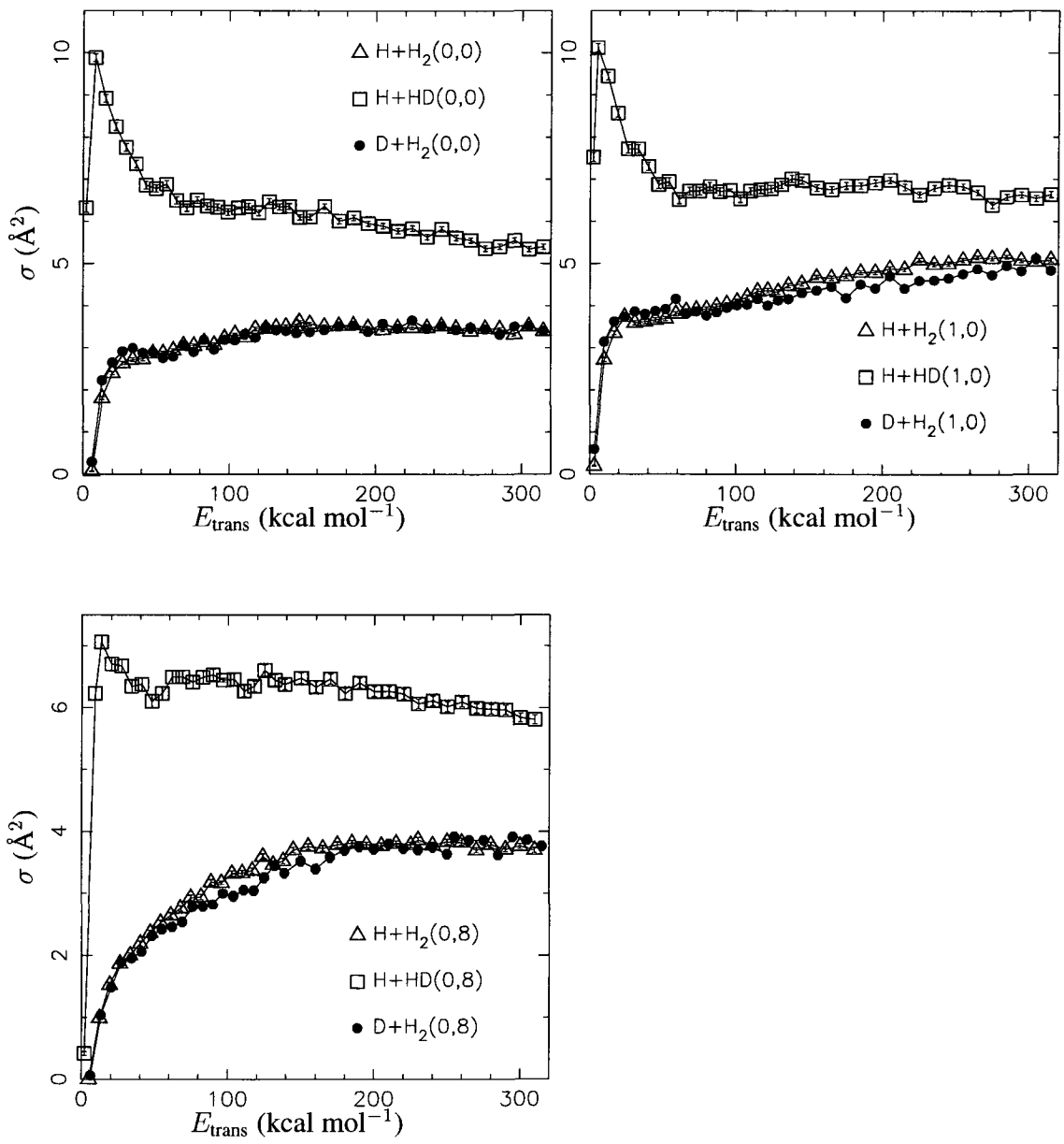

Figure 4.18: Total nonreactive inelastic cross sections plotted against translational energy from (0,0), (1,0), and (0,8).

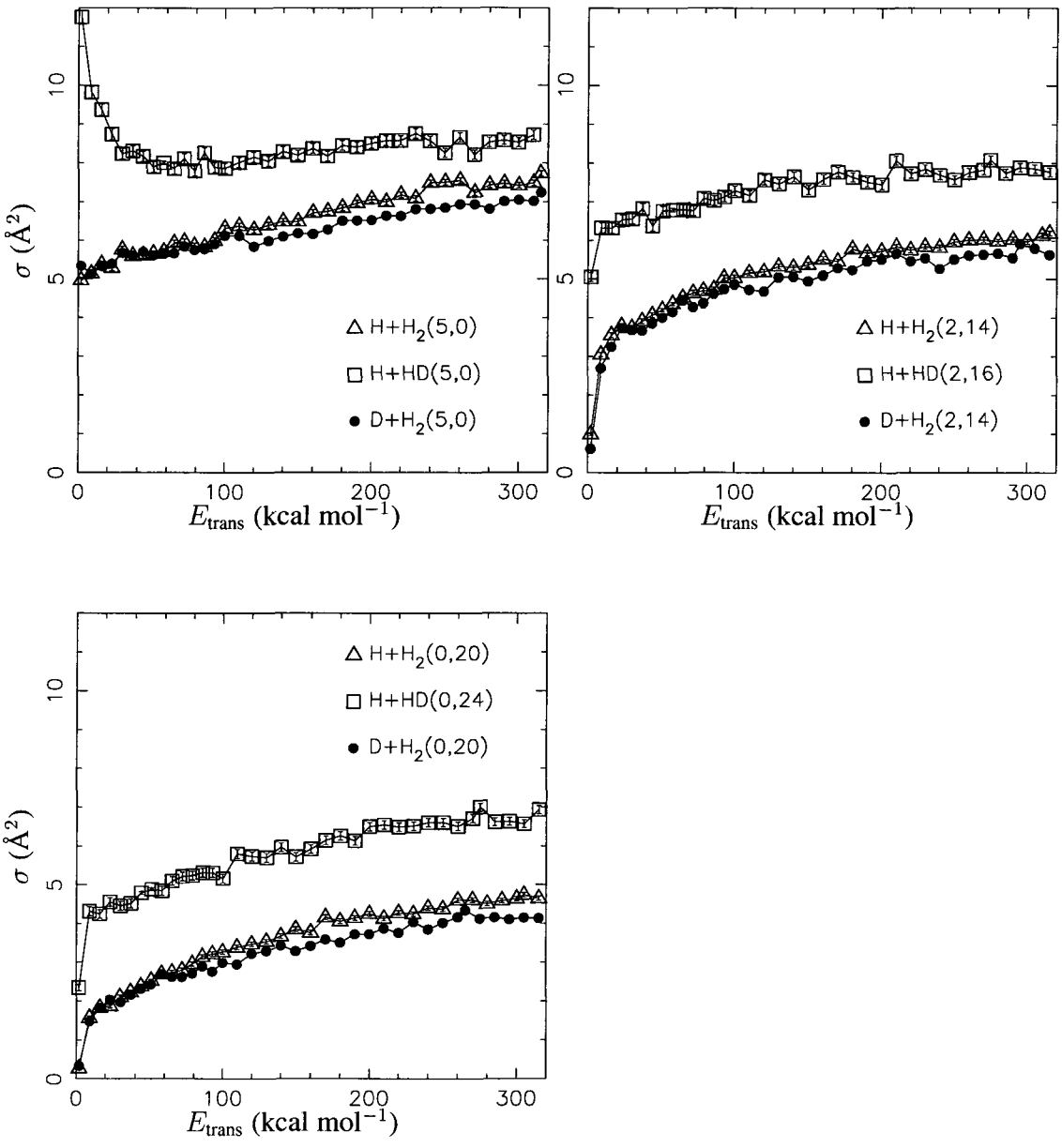

Figure 4.19: Total nonreactive inelastic cross sections plotted against translational energy from (5,0), (2,14/16), and (0,20/24).

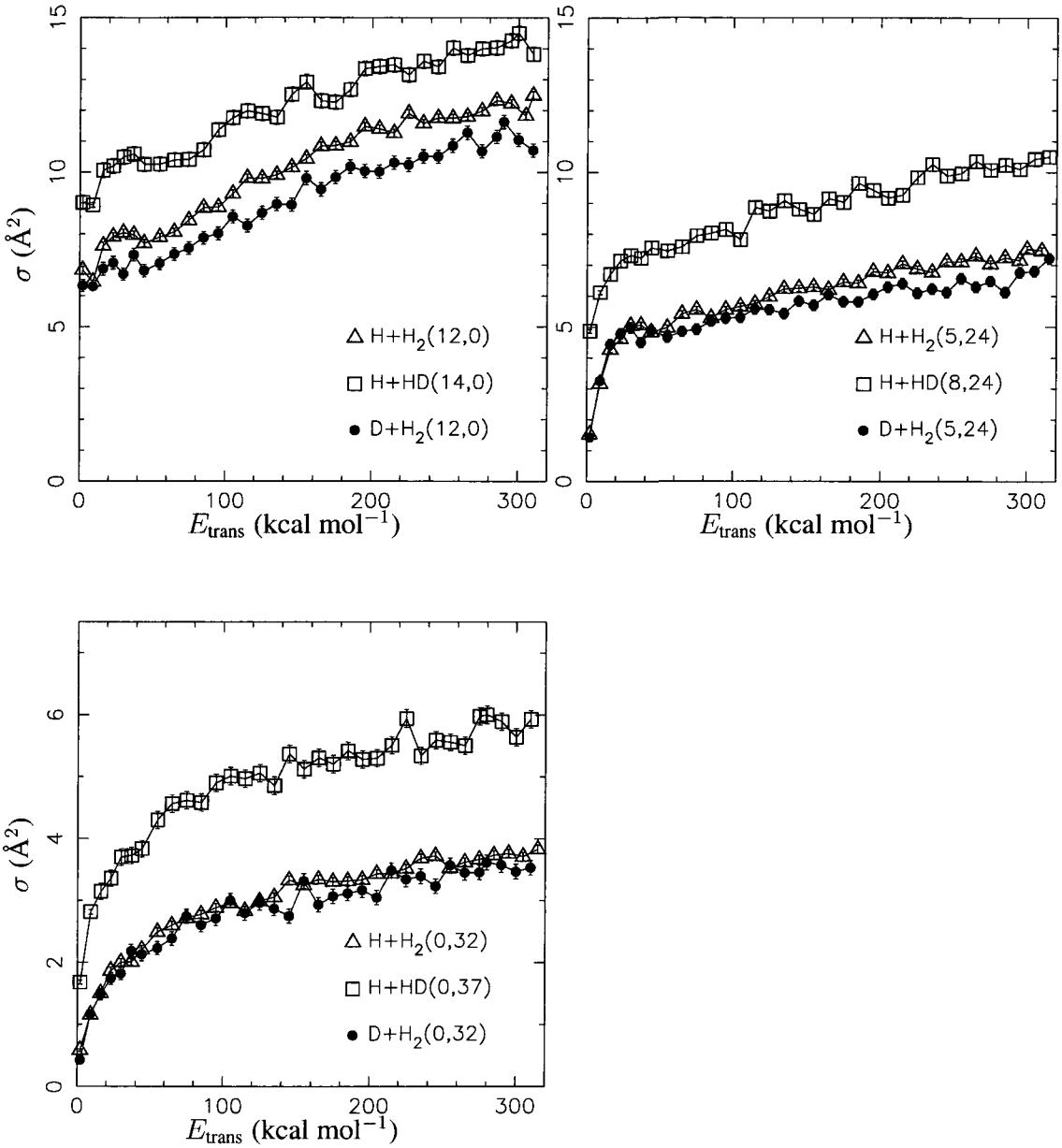

Figure 4.20: Total nonreactive inelastic cross sections plotted against translational energy from (12/14,0), (5/8,24), and (0,32/37).

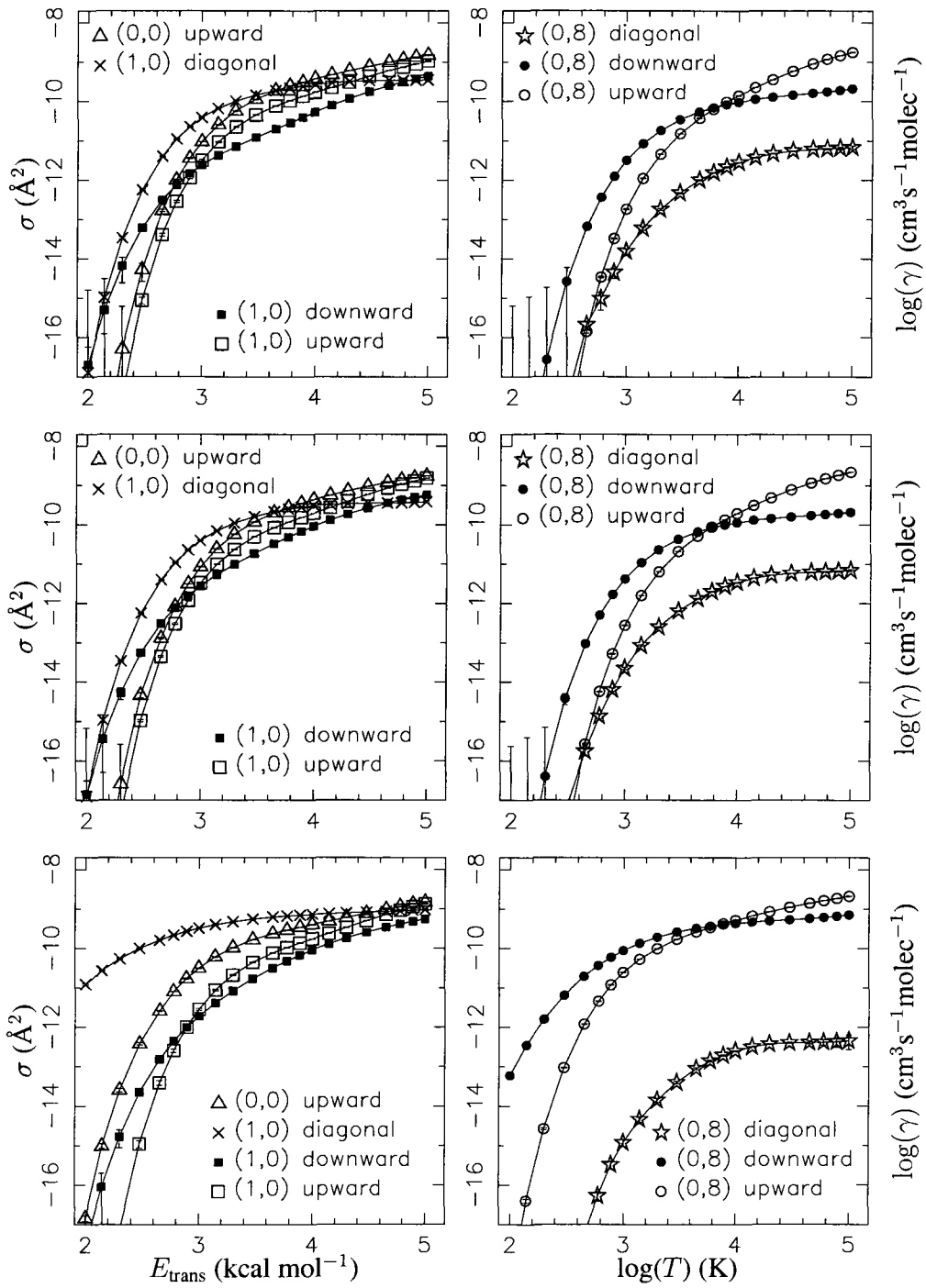

Figure 4.21: Nonreactive rate coefficients for nearly isoergic, upward, and downward transitions plotted against temperature from reference states with low internal energy. Nearly isoergic transitions are defined as transitions to final states with internal energy within 12% that of the initial state, and are labelled "diagonal." The top row is D + H_2, the middle row is H + H_2, and the bottom row is H + HD.

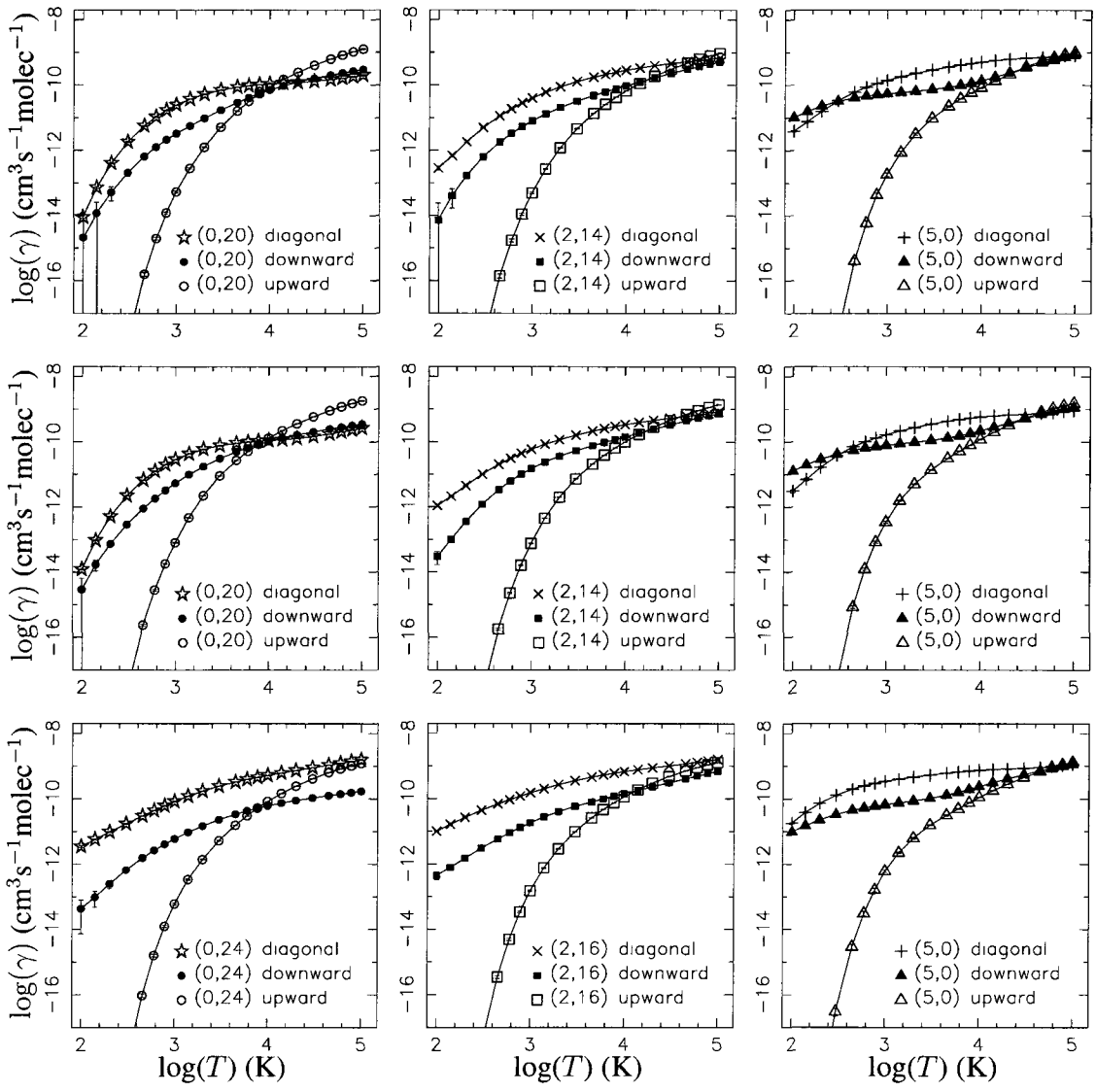

Figure 4.22: As in Figure 4.21, but for reference states with internal energy near 55 kcal mol^{-1}. The top row is D + H_2, the middle H + H_2, and the bottom H + HD.

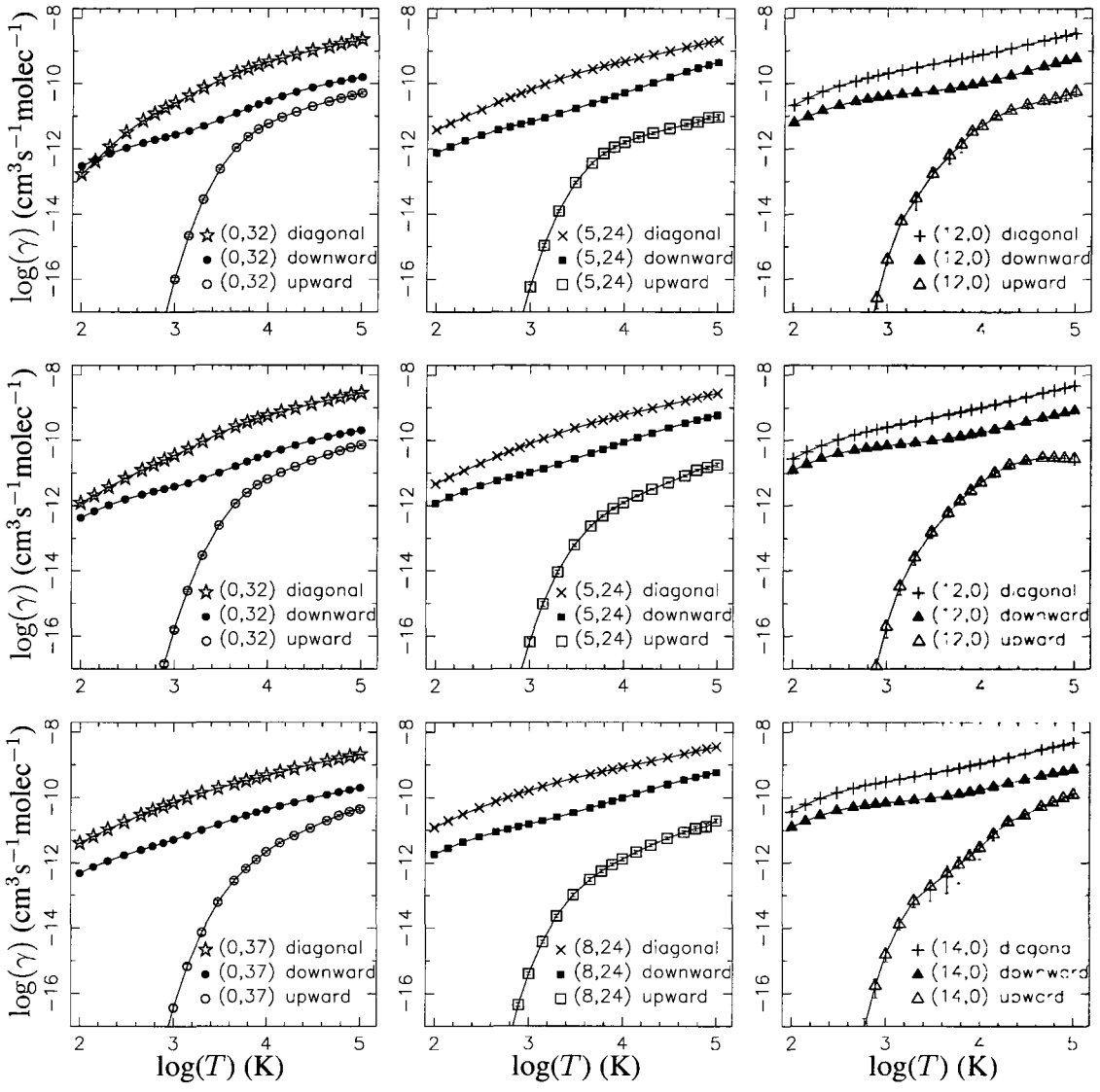

Figure 4.23: As in Figure 4.21, but for reference states with high internal energy. The top row is D + H_2, the middle H + H_2, and the bottom H + HD.

Chapter 5

Exchange reactions

5.1 Thresholds to the exchange reaction

There exists an energetic barrier to exchange which is 3.38 kcal mol^{-1} above the zero point energy of H_2, and 4.21 kcal mol^{-1} above the zero point energy of HD. For states with internal energy less than that required to overcome the energetic barrier, exchange reactions are not possible unless there is sufficient translational energy in the collision to overcome the energetic barrier.

In addition, there is observed in this study what may be a dynamical elevation of the threshold for exchange. For all three systems, the lowest translational energy at which exchange is observed from the ground state is 7 kcal mol^{-1}. From H + H_2(0,8) and D + H_2(0,8), the lowest translational energy is again 7 kcal mol^{-1}; however, exchange is observed at 5 kcal mol^{-1} for H + HD(0,8), despite the fact that HD(0,8) has lower internal energy than H_2(0,8). From (1,0), all three systems do not undergo exchange reactions at or below a translational energy of 2 kcal mol^{-1}.

This is similar to the dynamical thresholds observed for nonreactive energy transfer (Section 4.1), in that greater elevations of the dynamical threholds were observed for the H_2 systems than were observed for H + HD. It is also similar in that vibrational energy is more effective at promoting the process under consideration than is rotational energy in both the reactive and non–reactive processes.

5.2 State–to–state transitions for exchange

As in the case of nonreactive energy transfer, the collisions that make the greatest contributions to the state–to–state cross sections for exchange are those which occur at large impact parameter. However, as can be seen in Appendix B, Table B.1 and Table B.2, exchange occurs at a more limited set of impact parameters than does nonreactive energy transfer when the total energy of the system is enough to allow for a significant degree of collision–induced dissociation (CID). There is exchange from H + HD(0,0) to HD at any impact parameter greater than 1.0 Å in only one of the five translational energies displayed in Table B.1, and there are trajectories which result in exchange to H_2 for only two of those translational energies; one may contrast this with nonreactive energy transfer, for which contributing trajectories may occur with impact parameters as high as 2.0 Å. Of the data displayed in Table B.2, all three of H + H_2(5,0), D + H_2(5,0), and H + HD(5,0) exhibit only two exchange transitions with an impact parameter above 1.0 Å at a translational energy of 300 kcal mol^{-1}, while nonreactive energy transfer occurs at this translational energy for collisions with impact parameter greater than 2.0 Å.

For nonreactive energy transfer, it was seen in Figure 4.1 that from any given initial state, there is a small number of final states dynamically available to a trajectory relative to the total number of states which are energetically available. It may be seen from Figure 5.1 that there is no such restriction for exchange reactions. As a consequence, the products of exchange may be distributed across the full range of energetically available final states.

The large number of available final states, in combination with the fact that most transitions occur at relatively lower impact parameters when compared to nonreactive energy transfer, means that for many state–to–state exchange transitions, few trajectories contribute to the state–to–state cross section, resulting in smaller cross sections with larger relative errors. Figure 5.2 contains plots of exchange cross sections against translational energy for selected transitions involving states with low internal energy. The opacity functions vary by system, but

these cross sections are significantly nonzero only at lower translational energies, for which few final states are energetically available. Even when state–to–state exchange cross sections are statistically significant, they are typically at least a factor of 10 smaller than inelastic non-reactive cross sections involving the same state–to–state transitions. Therefore, the behaviour of exchange reactions is examined not by studying trends among state–to–state transfers, but instead through analysis of total exchange cross sections and average energy transfer.

There is a slight tendency for exchange products to be excited more rotationally than vibrationally. The large number of points near the $(0,j)$ axis in the right panel of Figure 5.1 is typical for exchange reactions, except for those with enough total energy to permit a significant degree of CID. The tendency toward rotational excitation is consistent with the formation of exchange products via collisions at impact parameters near or outside the outer turning point of the target molecule.

5.2.1 Comparison of state–to–state exchange cross sections to prior results

Keogh *et al.* calculated state–to–state integral cross sections for the exchange transition $D + H_2(1,1) \rightarrow H + HD(1,j)$ at translational energies of 23.5 kcal mol^{-1} and 18.9 kcal mol^{-1}, using both quantum and quasiclassical calculations, and noted agreement with the experiments of Kliner, Adelman, and Zare [54] when taking into account the difficulties associated with using DBr as a source of D atoms [53]. Some of these cross sections are given in Table 5.1. They agree qualitatively and within a factor of 2 with the results calculated here. The greatest absolute difference is the peak value of the QM results, for which the cross section is 150% that of the current QCT cross section.

The only large disagreement in the results presented in Table 5.1 occurs for $j' = 10$, with a smaller difference at $j' = 12$. There may be a quantum resonance effect which elevates the QM cross section for $j' = 10$, or it may be a statistical fluctuation in the QCT results. The difference in potential energy surfaces may play a role in explaining the difference for $j = 10$, though the fact that the current QCT and QM cross sections are similar for both $j = 8$ and

$j = 12$ indicates that this is probably not the case. The current QCT results match the QCT results of Keogh *et al.* well for this reaction.

5.3 Overall energy transfer in the exchange reaction

Cross sections for total exchange from low energy states as a function of translational energy are displayed in Figure 5.3.

The cross sections for the H + HD(0,0)→D + H_2 exchange reaction are consistently about 1 $Å^2$ smaller than are the cross sections for the H + HD(1,0)→D + H_2 reaction at comparable translational energies, due to the difference in internal energy, but the general shape of the excitation function is the same. Even though the peak value of the excitation function for the H + HD(0,8)→D + H_2 is diminished compared to that of the H + HD(0,0)→D + H_2 reaction, at translational energies above 50 kcal mol^{-1} the cross sections for exchange from H + HD(0,0) are only about 10% smaller than those from H + HD(0,8).

For low energy states, the excitation functions for each exchange process are qualitatively similar to each other, and in some cases are quantitatively similar, despite differences in the energy distribution or internal energy of the initial state. The excitation functions for H + HD(v, j)→D + H_2, where (v, j) is (0,0), (0,8), or (1,0), peak sharply at a low translational energy, and are nearly constant at high translational energies. The excitation functions for the H + H_2→H + H_2 exchange reactions from low energy states increase sharply with translational energy up to 20 kcal mol^{-1}, but have no sharp peak, and are nearly constant at translational energies above those corresponding to their peak values. The excitation functions D + H_2→H + HD for low energy states peak near 40 kcal mol^{-1} and decrease as translational energy is increased, as do the excitation functions for the H + HD→H + HD exchange reaction; however, from low energy states at a given translational energy, a cross section for exchange to H + HD products is greater for the D + H_2 reaction than for the H + HD reaction.

The similarity of energy dependence within systems regardless of internal energy means that for low energy states at a fixed translational energy, there is a rough ordering of cross

sections by system:

$$\sigma(H + HD \rightarrow D + H_2) > \sigma(H + H_2 \rightarrow H + H_2) \quad (5.1)$$

$$> \sigma(D + H_2 \rightarrow H + HD) \quad (5.2)$$

$$> \sigma(H + HD \rightarrow H + HD). \quad (5.3)$$

For H + HD, the exchange of H atoms for each other is less likely than the exchange of H for D because of the mechanism of exchange at wide impact parameter. For collisions near or beyond the outer turning point, the colliding H atom may abstract an atom from the target molecule. Due to the greater mass of D, more interaction time is required to accelerate a D atom sufficiently to break the molecular bond. At some translational energies, an H atom may be abstracted more easily than a D atom, making exchange to H_2 the more likely option for these collisions. This is a prototypical kinetic isotope effect, and is consistent with the decline of cross sections for HD products as translational energy increases. This explanation is supported by the opacity functions for these collisions, given as trajectory counts in Appendix B. Table B.1 contains counts of trajectories (per 1000) leading to each of nonreactive energy transfer, exchange to H_2, exchange to HD, and CID from H + H_2(0,0), D + H_2(0,0), and H + HD(0,0). Table B.2 contains the same type of data from H + H_2(5,0), D + H_2(5,0), and H + HD(5,0).

In order to achieve exchange to HD, the colliding H atom must either push the other H atom off (via the insertion mechanism) and replace it directly, or enter into a relatively long-lived complex which eventually ejects the other H atom. Although a trajectory can become temporarily trapped in the saddle point region of the potential (where all three atoms are approximately 1.5 Å apart), these trajectories are relatively rare. At impact parameters greater than that corresponding to the outer turning point of the target molecule, the insertion mechanism can not occur with any great frequency, leading to lesser cross sections for exchange reactions resulting in HD products compared to those resulting in H_2 products.

In this way, the exchange process is similar to that of CID, for which it was observed that

the opacity functions were greatest at or just above the impact parameters that corresponded to the outer turning points of the target molecules. In Table B.1 and Table B.2, it can be seen that the number of exchange trajectories decreases as total energy is increased above 109.5 kcal mol^{-1}, and that this decrease is matched closely by an increase in the number of CID trajectories. For example, the outer turning point of HD(0,0) is 0.87 Å. Although exchange to HD may be more common at smaller impact parameters (note particularly the data at translational energies of 55 kcal mol^{-1} and 110 kcal mol^{-1}in Table B.1), exchange to H_2 nearly always dominates at higher impact parameter. At very high translational energies, exchange to H_2 dominates exchange to HD at all impact parameters because the interactions at low impact parameter which may permit the acceleration of D are more likely to lead to dissociation instead.

For similar translational energies, exchange from D + H_2 for states with low internal energy is always less likely than exchange from H + H_2 for the same states. The cross sections for the exchange reaction of D + H_2 decrease at high translational energy in the same way that those for the H + HD→H + HD exchange reaction do. For the exchange reaction of H + HD→H + HD, it was hypothesized that this is because direct exchange of the H atom is not possible at the impact parameters which contribute most to the cross section, making collisions for which the collider passes outside the outer turning point unlikely to result in exchange. The same logic can not apply to D + H_2: the interaction times for D + H_2 are greater than those of H + H_2, meaning that if those considerations are the most important, collisions at large impact parameter should be more likely to result in exchange for D + H_2 than for H + H_2. The difference here is that high energy D + H_2 collisions are more likely to result in dissociation, especially at high impact parameter, as illustrated by the opacity functions for CID, Figure 3.1 and Figure 3.3.

The relationship between the exchange reactions from (0,0) and (0,8) warrants further investigation. Although the total exchange cross sections from (1,0) are greater than those from (0,0) for all systems, the cross sections for H + H_2(0,8)→H + H_2 and H + HD(0,8)→D + H_2

are smaller than the corresponding cross sections for (0,0) at translational energies below 100 kcal mol^{-1}. At a translational energy of 55 kcal mol^{-1}, for instance, although trajectory counts for exchange reactions at low impact parameter in these two systems are similar, the counts of exchange trajectories for $H + H_2$ in the 1.0–1.5 Å impact parameter range are nearly double those for $D + H_2$. For rotationally excited molecules, trajectories in which the collider penetrates the target molecule are the greatest contributors to cross sections for exchange: trajectories at higher impact parameters, trajectories at lower translational energies, and trajectories involving species with more massive colliding atoms are less likely to result in exchange. The total exchange cross sections for $H + H_2(0,8) \rightarrow H + H_2$ are less than those for $H + H_2(0,0) \rightarrow H + H_2$ because the addition of rotational energy makes penetration of the target molecule less likely at low translational energy.

While cross sections for total exchange from low energy states are more dependent upon the type of exchange than upon internal energy, the distribution of the internal energy is more important for states with internal energy near 55 kcal mol^{-1}. In Figure 5.4, it can be seen that although cross sections for corresponding exchange products are similar for the two rotationally excited states with internal energy near 55 kcal mol^{-1}, exchange from (5,0) is far more likely at low translational energy, and equally or slightly less likely at high translational energy. The reason for the large cross sections of the (5,0) reactions at low energy can be seen in Table B.2, in which trajectory counts indicate that for this state, exchange occurs with frequency greater than or equal to that of nonreactive energy transfer even at impact parameters above 2.0 Å. Although exchange does occur at impact parameters above 1 Å at a translational energy of 55 kcal mol^{-1} in the (0,0) reactions, it does not occur for impact parameters greater than 1.5 Å, and the trajectory counts in the 1.0–1.5 Å bin are less for the (5,0) reactions than for the (0,0) reactions. Thus, it may be concluded that vibrational energy is more effective at promoting exchange than is translational energy; however, by comparing the cross sections with similar total energies, at translational energy of 1 kcal mol^{-1} in Figure 5.4 and at translational energy of 55 kcal mol^{-1} in Figure 5.3, it can be seen that this is not necessarily the case for rotational

energy. At 55 kcal mol^{-1} total energy, translational energy is more effective than initial rotational energy at promoting exchange, but at 109.5 kcal mol^{-1} total energy, initial rotational energy is at least as effective as translational translational energy. At total energies greater than 109.5 kcal mol^{-1}, initial rotational energy is more effective for promoting exchange to H_2 than is translational energy.

The general shapes of the excitation functions for exchange from states with internal energy near 55 kcal mol^{-1} are the same as those of the excitation functions for states with lower internal energy. The most important difference is in the relative values of these functions; although there is a fairly strict ordering at low internal energy, where H_2 products were always favoured over HD products for exchange from H + HD, for states with total energy near 55 kcal mol^{-1} it may be that the excitation functions for processes which produce HD are the greater at low translational energies.

Some of the trends observed for the excitation functions for the exchange reactions from states with low and moderate internal energies also hold for states with high internal energies, which are shown in Figure 5.5. Cross sections for exchange to HD products are extremely large at high internal energy and low translational energy relative to any other cross sections for exchange for this system. The peaks in the excitation functions observed at low translational energy in the H + HD$\rightarrow$D + H_2 reaction for states with low internal energy are not present for states with high internal energy; rather, the excitation functions rise only slowly with translational energy after an initial steep rise, similar to those of the rotationally excited states with internal energy near 55 kcal mol^{-1}.

In contrast to the states with internal energy near 55 kcal mol^{-1}, the inclusion of rotational energy in high energy states does not in itself modify cross sections relative to the purely vibrational states. The magnitudes of the excitation functions at any particular translational energy differ between isotopic analogues, but the excitation functions for purely vibrational states with high internal energy are qualitatively similar between the isotopic analogues, as are those of the mixed energy states. The excitation functions of the purely rotational states differ

both quantitatively and qualitatively from those of the states with vibrational energy. While the excitation functions for HD products from vibrationally excited states decrease rapidly from a maximum value at a translational energy near 1 kcal mol^{-1}, the maxima of the excitation functions occur at slightly larger translational energies for HD products from D + H_2(0,32) and H + HD(0,37). In addition, the excitation functions for the purely rotational states do not decline as rapidly as translational energy is increased as they do for the vibrationally excited states.

5.3.1 Comparison of total exchange rate coefficients to previous results

Aoiz *et al.* calculated exchange cross sections and rate coefficients using the QCT method on the LSTH, DMBE, and BKMP surfaces for D + $H_2(v, j)$, where $v = 0, 1$ and j =0–7 [23]. For states with $j = 0$, they determined rate coefficients which matched within standard error the accurate quantum mechanical results of Zhang and Miller at temperatures as low as 250 K. For states with rotational energy, the results of Aoiz *et al.* diverged from experiment and accurate quantum mechanical results at temperatures below 1000 K. To calculate rate coefficients for the exchange reaction of D + H_2 for a thermal distribution of H_2 at temperatures up to 2000 K from the current QCT results, the method of Aoiz *et al.* was used, averaging over a thermal distribution of states with $v = 0$ or 1 and j in the range 0–7. This limitation to low energy (v, j) states will lead to a small underestimate of rate coefficients for temperatures at which higher energy states become signficantly populated; however, the states included represent more than 99% of the total population at 1000 K, and over 95% at 1500 K.

The quantum rate coefficients calculated by Mielke *et al.* on the CCI PES for the D + H_2 exchange reaction agree almost exactly with recent shock tube experiments between 170 K and 2000 K[65]. In Table 5.2, the rate coefficients calculated on the BKMP2 surface are compared with those of Aoiz *et al.* [23] on the DMBE surface and with the QM results of Mielke *et al.* on both the DMBE and CCI surfaces.

The QCT rate coefficients for the D + H_2 exchange reaction calculated BKMP2 surface

overestimate the experimental rate coefficients above 450 K, whereas the results of Aoiz *et al.* on the DMBE and LSTH surfaces underestimated the rate coefficients relative to the same experimental data. The difference may be due to the use of the more accurate BKMP2 PES, or it may be due to the greater number of trajectories run in this study, which could result in a determination of a lower value for the dynamical threshold to exchange.

It may also be that the ZPE effect is small and that tunnelling does not contribute significantly to the exchange process: this conclusion is consistent with the observation of an apparent elevated (dynamical) threshold to exchange in D + H_2(0,0). Aoiz *et al.* observed that the greatest differences between QCT and quantum mechanical rate coefficients occur for rotationally excited states, because there is an enhancement of tunnelling as the initial j of the target molecule is increased. Although there is a classical dynamical threshold to exchange, no such threshold exists for quantum calculations, leading to an underestimate of rate coefficients by QCT calculations even at higher temperatures. Although a larger relative difference is observed at higher temperatures than at lower temperatures between experimental rate coefficients and the QCT rate coefficients from the BKMP2 surface, the rate coefficients for the BKMP2 surface are greater than the quantum mechanical rate coefficients. Enhancement of tunnelling with increasing j is not the most important factor in the difference. There may be some difference from the surfaces, but it is likely that the biggest difference is due to the Born–Oppenheimer corrections employed in the calculation of the QM rate coefficients. This correction raises the energetic barrier to exchange of the D + H_2 reaction by 0.139 kcal mol^{-1}[65], which should lead to smaller rate coefficients relative to calculations involving an uncorrected barrier.

Mielke *et al.* give the relative size of the correction to be 34% at 167 K, 7% at 1000 K, and 3% at 2000 K. At 1000 K and 2000 K, the current QCT rate coefficients and the uncorrected QM rate coefficients on the CCI surface differ by a factor of 1.2, with the QM rate coefficients being larger. At 200 K, assuming a 34% reduction due to the Born–Oppenheimer correction, the difference between the current QCT results and the uncorrected QM results is a factor of 2.2, with the QM rate coefficients again being the larger. The corresponding relative differences

between the CCI calculations with the Born–Oppenheimer corrections and the BKMP2 QCT calculations are 1.47, 0.795, and 0.790, for 200 K, 1000 K, and 2000 K respectively. The fact that the corrected and uncorrected QM results bracket the current QCT results both indicates the importance of the Born–Oppenheimer approximation and suggests that QCT cross sections calculated on the BKMP2 PES may be as close to the "true" values as possible, given the limitations of the QCT method.

5.4 Average energy transfer in exchange and nonreactive collisions

The average energy transferred per collision was calculated for both the exchange and nonreactive collisional outcomes at each translational energy by weighting trajectory outcomes according to impact parameter range in the manner of Equation 2.4. By "nonreactive collisions," it is meant here that elastic trajectories are ignored; otherwise, the average energy transferred would always be zero, owing to the infinite range of impact parameters over which elastic trajectories occur. As used elsewhere in this study, an "upward" energy transfer is defined as one in which the target molecule gains internal energy on average (endoergic); a "downward" transfer is one in which the target molecule loses energy (exoergic).

The average energy transferred for all processes from ground state is in the upward direction. It can be seen in Figure 5.6 that from the ground state, more energy is transferred in the average exchange process than in the average nonreactive process, with exchange reactions at translational energies over 100 kcal mol^{-1} leaving a product molecule with an average of greater than half the energy required for dissociation. Exchange reactions leading to H_2 products transfer a similar amount of energy for all systems, but H + HD→H + HD exchanges tend to transfer more energy than do H + HD→D + H_2 exchanges at translational energies in the range 100–250 kcal mol^{-1}. At all translational energies, nonreactive transitions involving HD have less average energy transfer than those involving H_2.

Average energy transfer, given in Figure 5.7, is less for exchange reactions from (0,8) than for exchanges reactions from (0,0). There is a downward average at the bottom of the

translational energy scale; the exchange reactions for H + H_2 average a greater downward transfer of energy than does that of D + H_2, which in turn averages a greater average transfer of energy than does the exchange reaction of H + HD. Otherwise, the trends observed for the ground state hold for (0,8) and (1,0). The existence of downward transitions changes the energy transfer behaviour for transitions from (1,0) compared to the other low energy states, reducing the average amount of energy transferred by 10–20% (Figure 5.8).

The energy transferred for collisions involving (5,0) is less on average than for the low energy states, as seen in Figure 5.9. This is in part because of the existence of downward transitions, and in part because of the limit to how much internal energy a molecule can have. The systems H + H_2 and D + H_2 had sizeable differences in energy transfer behaviour for low energy states, but are more similar in this case. The magnitude of the energy transferred is greater for the exchange reactions than for nonreactive transitions at most translational energies. In all systems below about 100 kcal mol^{-1}, nonreactive collisions from the (5,0) states tend to be downward on average; above that, the average energy exchange is upward. Collisions which lead to exchange tend to be upward at translational energies above 20 kcal mol^{-1}. H + HD exchange to HD has a strong downward trend at very low translational energy relative to the other exchanges in Figure 5.9, but exchange from H + HD to H_2 is similar to the exchanges to H_2 in the other two systems, if a little more in the upward direction.

Notable differences are observed for H_2(2,14) and HD(2,16), shown in Figure 5.10. The translational energies at which the average nonreactive energy transfer changes from downward to upward, for all of H + H_2(2,14), D + H_2(2,14) and H + HD(2,16), are close to 60 kcal mol^{-1}, as opposed to the 100 kcal mol^{-1} energies observed for systems in state (5,0). The corresponding translational energies for the exchange reactions are near 40 kcal mol^{-1}.

The average amount of energy transferred from purely rotational states with internal energy near 55 kcal mol^{-1} (Figure 5.11) is similar to that of the other states with the same energy in that nonreactive collisions preserve internal energy more than do collisions resulting in exchange, which have potentially large ($\langle \Delta E \rangle \simeq 20$ kcal mol^{-1}) downward changes at transla-

tional energies below 50 kcal mol^{-1}, and upward changes similar in magnitude at translational energies above 50 kcal mol^{-1}. The translational energy at which the average energy transfer goes from downward to upward for the exchange reactions is also near 50 kcal mol^{-1}. There is a clear trend for these states: as the fraction of internal energy which is rotational is increased, the translational energy at which the average energy transferred is nearest to 0 increases for exchange reactions and decreases for nonreactive transitions.

The major difference in the behaviour of exchange trajectories for purely rotational states compared to purely vibrational states, all with internal energy near 55 kcal mol^{-1}, is that a large downward transfer of energy is more likely for a wider range of translational energies in more rotationally excited molecules. Nonreactive collisions tend to transfer slightly more energy to these molecules than for less rotationally excited ones. For example, the functions $\langle \Delta E \rangle (E_{\text{trans}})$ for D + H_2(5,0), D + H_2(2,14) and D + H_2(0,20) are qualitatively similar, but are shifted upward by approximately 4 kcal mol^{-1} from one to the next. That is,

$$\begin{aligned} \langle \Delta E \rangle (E_{\text{trans}}; 0, 20) &\simeq \langle \Delta E \rangle (E_{\text{trans}}; 2, 14) + 4 \text{ kcal mol}^{-1} \\ &\simeq \langle \Delta E \rangle (E_{\text{trans}}; 5, 0) + 8 \text{ kcal mol}^{-1}. \end{aligned}$$

For all states with internal energy near 55 kcal mol^{-1}, there is a downward trend for exchange trajectories at low energy. At low temperature, the probability of exchange is similar to the probability of nonreactive energy transfer. This implies that excited molecules in low temperature regimes will on average be converted to molecules in lower energy states, and that collisions resulting in exchange contribute far more to the process of deexcitation than do nonreactive collisions. This is significant also in that the atom ejected from the newly formed molecule may have a relatively high kinetic energy, enabling it to excite the low energy molecules around it.

Thus, a single excited molecule in a cold atomic gas would not gradually lose its internal energy through repeated collisions with other atoms, each of which gains a small amount of that energy. It is more likely (neglecting radiative cooling, which may be significant in low

density gases) that the energy loss is sudden, with the resulting molecule losing a third or more its internal energy, and the remaining atom moving out to either distribute its energy amongst other atoms or to excite a nearby ground state molecule by 5–10 kcal mol^{-1}, as in Figure 5.6.

The greatest contributions to deexcitation of HD come from the more rotationally excited states. A collision involving H + HD(0,24) at 5 kcal mol^{-1} can result in an HD or H_2 molecule with 20 kcal mol^{-1} less internal energy, and a free atom moving at 25 kcal mol^{-1}. If this atom then collides with another HD(0,24) or a H_2(0,20) molecule, the same amount of energy transfer will occur (on average), leading to another large downward transfer of energy (and an even faster free atom). Even at 45 kcal mol^{-1}, the average collision of an atom with molecular hydrogen will result, on average, in a 10 kcal mol^{-1} downward energy transfer.

The difference in energy transfer between exchange from H + HD to HD and exchange from H + HD to H_2 is worthy of mention. While the two averages tend to be similar below a translational energy of 60 kcal mol^{-1}, where the average is near 0, they diverge quickly as translational energy is increased above this, with exchange to HD generally leading to a greater amount of energy transfer. This is true for all states with low and moderate internal energy, but it is not true for states with higher internal energies.

The proximity of the dissociative threshold to the high energy states means that the average energy transfer is nearly universally downward for these states.

For H + H_2(12,0) and its analogues, nonreactive transfer tends to be predominantly isoergic, with at most a 5 kcal mol^{-1} average exchange across all three systems. All functions describing average energy transfers for exchange reactions from high energy states with purely vibrational energy (Figure 5.12) have two peaks—a local maximum near 5 kcal mol^{-1}, a local minimum near 50 kcal mol^{-1}, and another local maximum near 80 kcal mol^{-1}—with a large downward average at translational energies above 100 kcal mol^{-1}. Where the cross sections for exchange to HD are the greatest, the average energy transferred is small; where the cross sections for exchange to H_2 are greatest, the average energy transferred is large. Despite the large amount of energy which may be transferred in the exchange reactions, the average energy

transferred for H + H_2(12,0) and its analogues in nonreactive collisions is relatively small. The data are noisy at high translational energies due to the small number of exchange trajectories (the majority of collisions result in CID) and the large energy transfers involved in many of those trajectories which do undergo exchange.

The average energy transfer behaviour of highly excited states with both vibrational and rotational energy differs from that of states with high, purely vibrational energy in that there is no feature corresponding to the pair of local maxima observed for the excitation functions of H + H_2(12,0). Energy transfer from H + H_2(5,24) is downward for more translational energies than from H + H_2(12,0) (and similarly for the isotopic analogues). This can be seen in Figure 5.13. The average energy exchanges for nonreactive collisions from states with both vibrational and rotational energy are similar to those of the states with purely vibrational energy, being in the 2–5 kcal mol^{-1} downward range at most translational energies. The exchange reactions for the states with both high vibrational and rotational energy have average energy transfers of 10 kcal mol^{-1} or more in the downward direction at nearly all translational energies, in contrast to the upward averages observed for the states with high, purely vibrational energy.

The average energy transferred for collisions involving states with high, purely rotational energy (Figure 5.14) also differ significantly from those of the other states with high internal energy. Nonreactive energy transfer differs in that there is a large downward average exchange of energy (near 35 kcal mol^{-1} for the H_2 systems, 20 kcal mol^{-1} for H + HD) at low translational energy, in contrast to a smaller (approximately 10 kcal mol^{-1}) average for the vibrationally excited states. In addition, the averages for H_2(0,32) and HD(0,37) approach 0 as translational energy increases, whereas they are closer to 4 kcal mol^{-1} downward for the other states at these energies. Exchange reactions for the lowest energy collisions involving H_2(0,32) and HD(0,37) result in products which have an average of 30 kcal mol^{-1} less internal energy than the initial state have; this may be contrasted with the net upward energy exchange of H_2(12,0) and HD(14,0), and the small downward averages of H_2(5,24) and HD(8,24) at low translational

energies. For purely rotationally excited states with high internal energy, the average amount of energy transferred decreases as translational energy is increased; this is also in contrast to the vibrationally excited states.

5.5 Summary of exchange reactions

State–to–state exchange cross sections tend to be small and have large relative errors. More meaningful conclusions about exchange reactions in H + H_2 may be drawn through consideration of the total exchange cross sections from specific states.

Vibrational energy is more efficient at promoting exchange than is rotational energy or translational energy. Exchange trajectories resulting in H_2 products have excitation functions which increase as translational energy is increased, but those trajectories resulting in HD products become less likely as translational energy is increased. Processes producing HD products are highly likely only at high internal energy and low translational energy, or for low speed collisions of medium energy states with most of their internal energy partitioned into the rotational mode. For translational energies over 10 kcal mol^{-1}, total cross sections for exchange to H_2 products are consistently in the 5–10 $Å^2$ range. The new QCT cross sections and rate coefficients match existing quantum and experimental data within a factor of two, likely differing mostly because of the invocation of the Born–Oppenheimer approximation.

For most initial states, translational energies, and for the three isotopic analogues of H + H_2 studied, the average energy transferred between target and collider is greater for (both channels of) the exchange process than it is for the nonreactive, inelastic process. The exception is collisions at low translational energy involving states with high internal energy. For collisions of H + HD, there are no consistent trends observed regarding the average energy transferred and the exchange of a D atom rather than an H atom.

Table 5.1: A comparison of cross sections for the exchange reaction D + $H_2(1,1) \rightarrow H + HD(1,j')$. The results of this study are labelled QCT, BKMP2 and are for a translational energy of 23 kcal mol^{-1}. The quasiclassical and quantum results of Keogh *et al.*[53] on the BKMP PES, taken from Figure 3 in that paper, are labelled Keogh QCT and Keogh QM, respectively. These are for a translational energy of 1.02 eV (23.5 kcal mol^{-1}), and are rounded to the nearest 0.005. All cross sections are in $Å^2$.

j'	0	2	4	6
QCT, BKMP2	0.0016 ± 0.0014	0.031 ± 0.006	0.058 ± 0.011	0.11 ± 0.02
Keogh QCT	0.005	0.035	0.055	0.085
Keogh QM	0.005	0.035	0.070	0.100
j'	8	10	12	
QCT, BKMP2	0.14 ± 0.02	0.16 ± 0.02	0.13 ± 0.02	
Keogh QCT	0.120	0.165	0.135	
Keogh QM	0.145	0.215	0.10	

Table 5.2: A comparison of rate coefficients for the exchange reaction of D + H_2. The quantum mechanical results of Mielke *et al.*, 2003, on the CCI surface are essentially identical to those of recent shock tube experiments [65]. The QCT rate coefficients for the DMBE surface are from Aoiz *et al.*, 1996 [23]. The QM rate coefficients for the DMBE surface are from Mielke *et al.*, 1994 [34]. Both sets of QCT rate coefficients given here are averaged values, weighted by population for states with $v = 0$ or 1 and $j = 0$–7. These rate coefficients are underestimates: for a more complete calculation, the full set of QCT rate coefficients could be thermally averaged; however, at 1000 K, the states included represent over 99% of the total population, and at 1500 K, they represent over 95% of the population. All rate coefficients are in $cm^3s^{-1}molec^{-1}$.

T (K)	QCT, BKMP2	QM, CCI	QM, DMBE	QCT, DMBE
200	$1.27 \pm 0.12 \times 10^{-18}$	1.86×10^{-18}	1.64×10^{-18}	$5.20 \pm 6.30 \times 10^{-19}$
450	$1.64 \pm 0.07 \times 10^{-14}$	1.48×10^{-14}		$1.07 \pm 0.23 \times 10^{-14}$
1000	$2.39 \pm 0.04 \times 10^{-12}$	1.90×10^{-12}	1.83×10^{-12}	$1.54 \pm 0.06 \times 10^{-12}$
1400	$1.01 \pm 0.01 \times 10^{-11}$		7.13×10^{-12}	$5.76 \pm 0.11 \times 10^{-12}$
2000	$3.10 \pm 0.03 \times 10^{-11}$	2.45×10^{-11}		

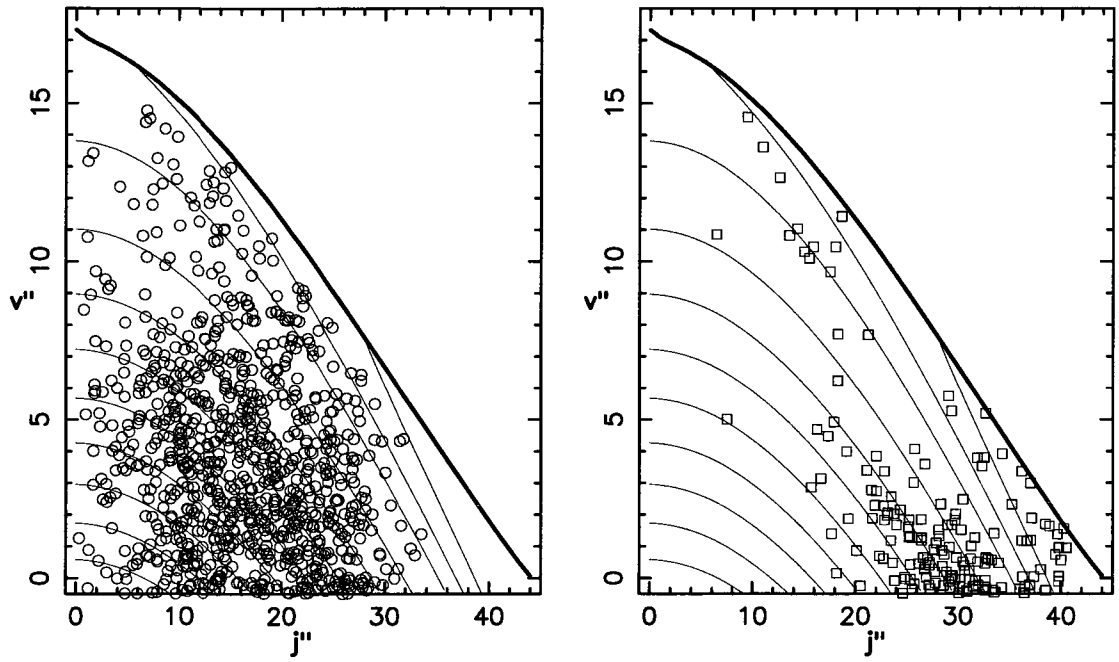

Figure 5.1: Scatter plots of exchange trajectories from D + H_2(2,14) in the impact parameter ranges 0–0.5 Å (left) and 1.5–2 Å (right) at a translational energy of 85 kcal mol^{-1}. Solid lines are energy contours at 10 kcal mol^{-1} intervals. The uppermost bold line is the energy contour representing the dissociation limit.

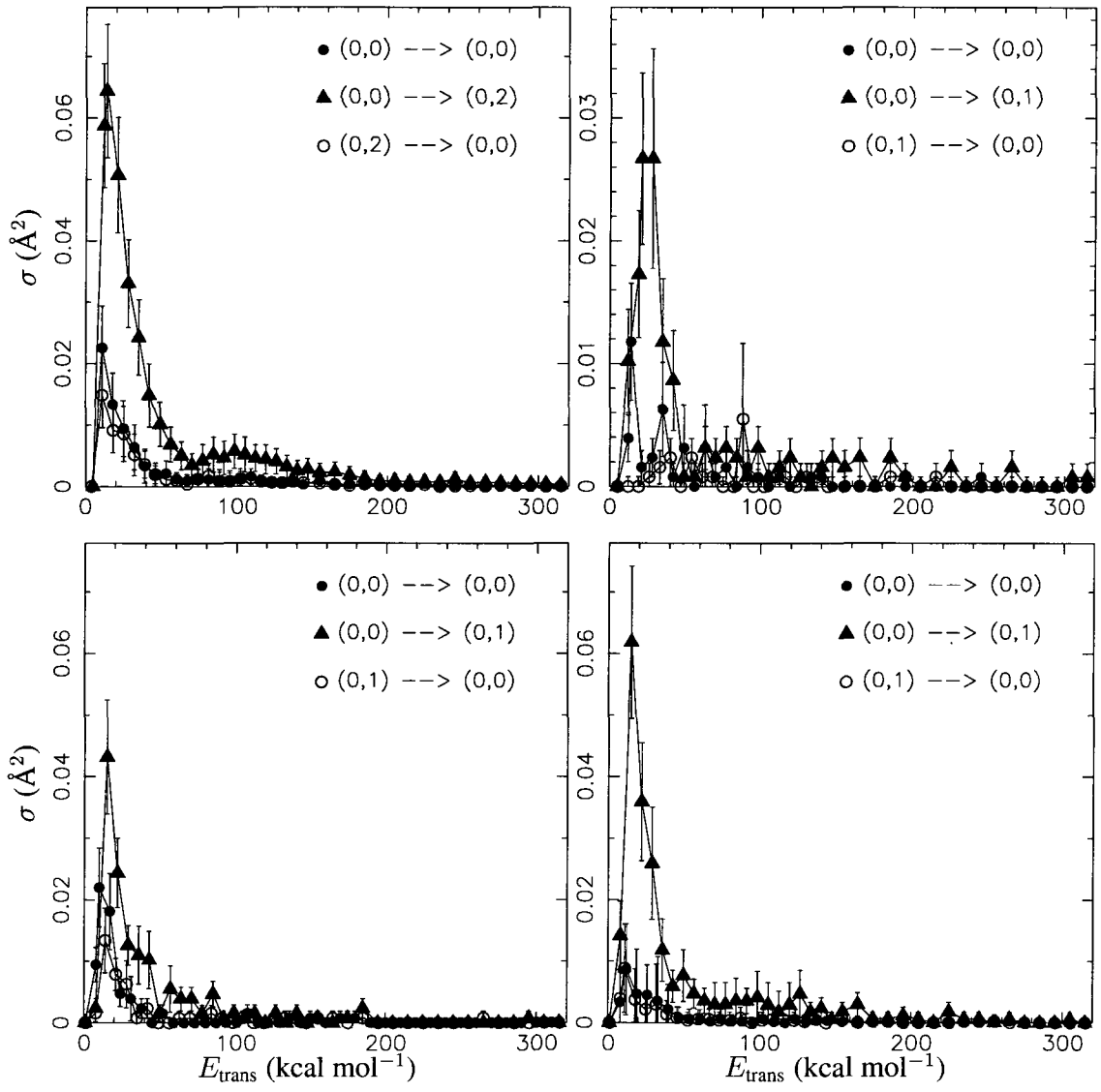

Figure 5.2: State–to–state cross sections for exchange versus translational energy for $v = 0, j = 0/1$. The top left panel is H + H_2, the top right panel is D + H_2, the bottom left panel is the H + HD→H + HD exchange reaction, and the bottom right panel is the H + HD→D + H_2 exchange reaction. Note the change of scale on the y–axis for D + H_2.

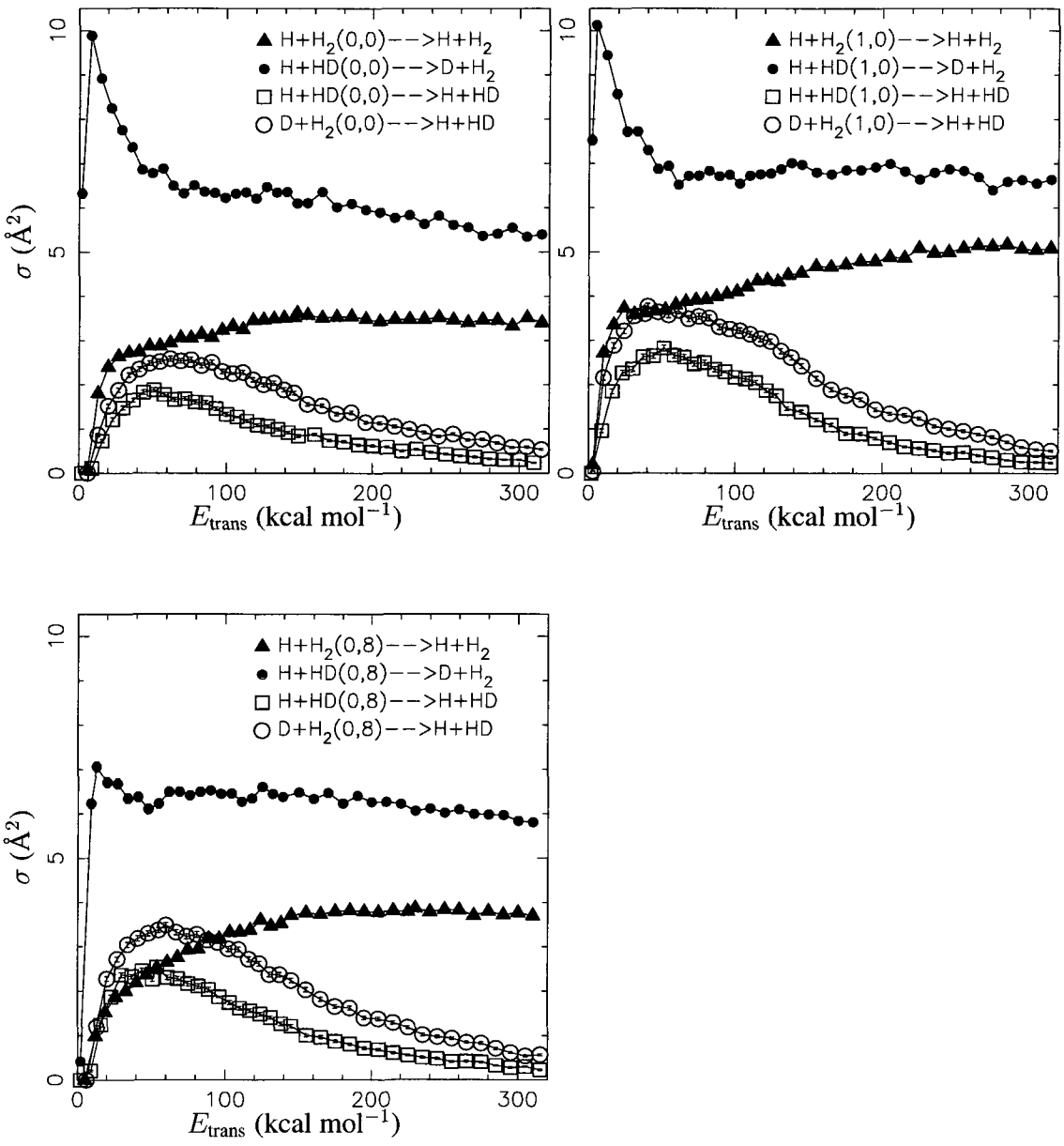

Figure 5.3: Total exchange cross sections plotted against translational energy for low energy states.

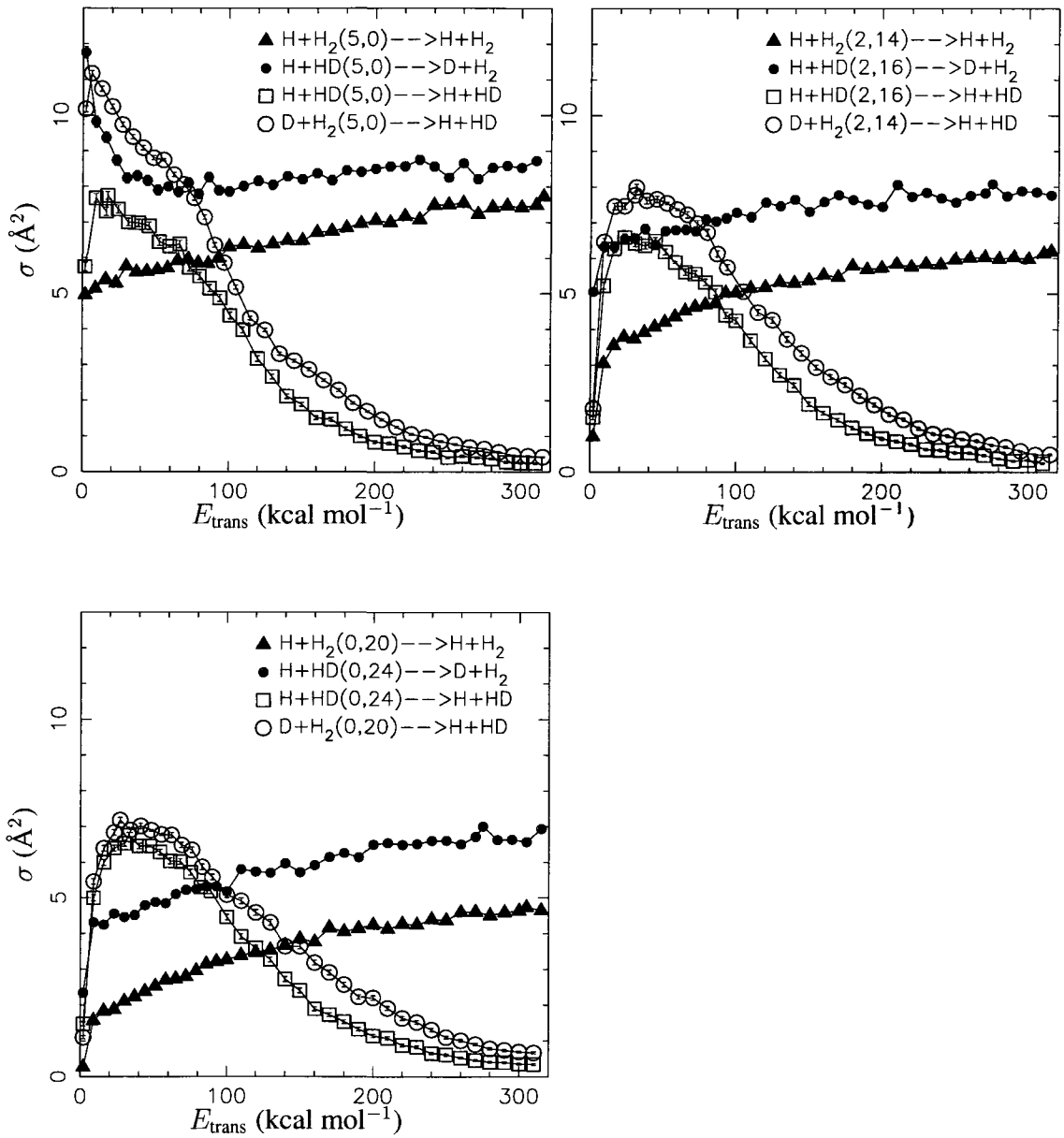

Figure 5.4: Total exchange cross sections plotted against translational energy for states with internal energy near 55 kcal mol^{-1}.

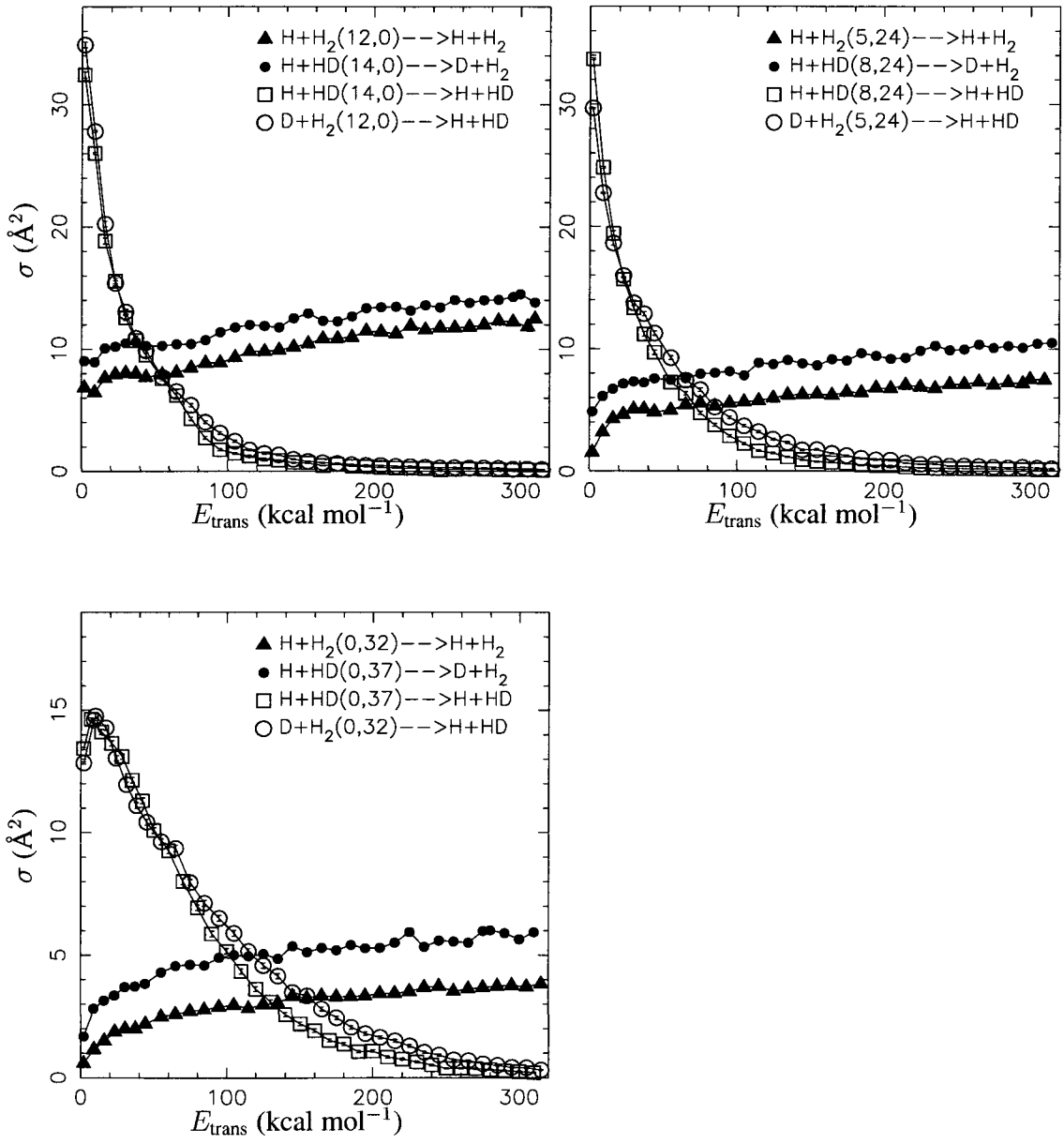

Figure 5.5: Total exchange cross sections plotted against translational energy for states with internal energy near that required for dissociation. Note the difference in scales on the y-axis.

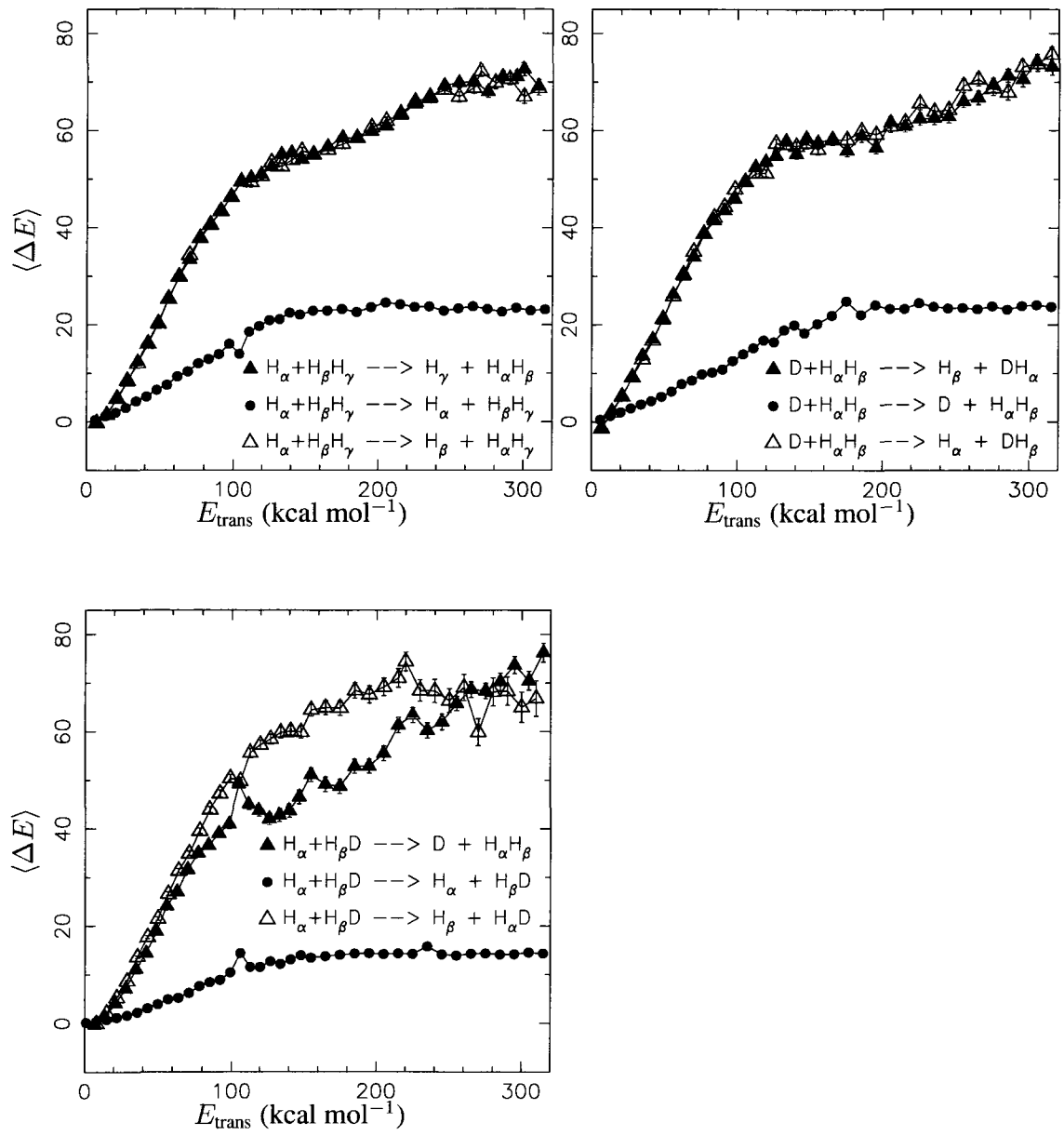

Figure 5.6: Average energy transfer for collisions resulting in exchange and nonreactive energy transfer from H + H_2(0,0), D + H_2(0,0), and H + HD(0,0). The two exchange channels for H_2 are chemically equivalent, but they are displayed as separate series in this figure to facilitate comparison with H + HD.

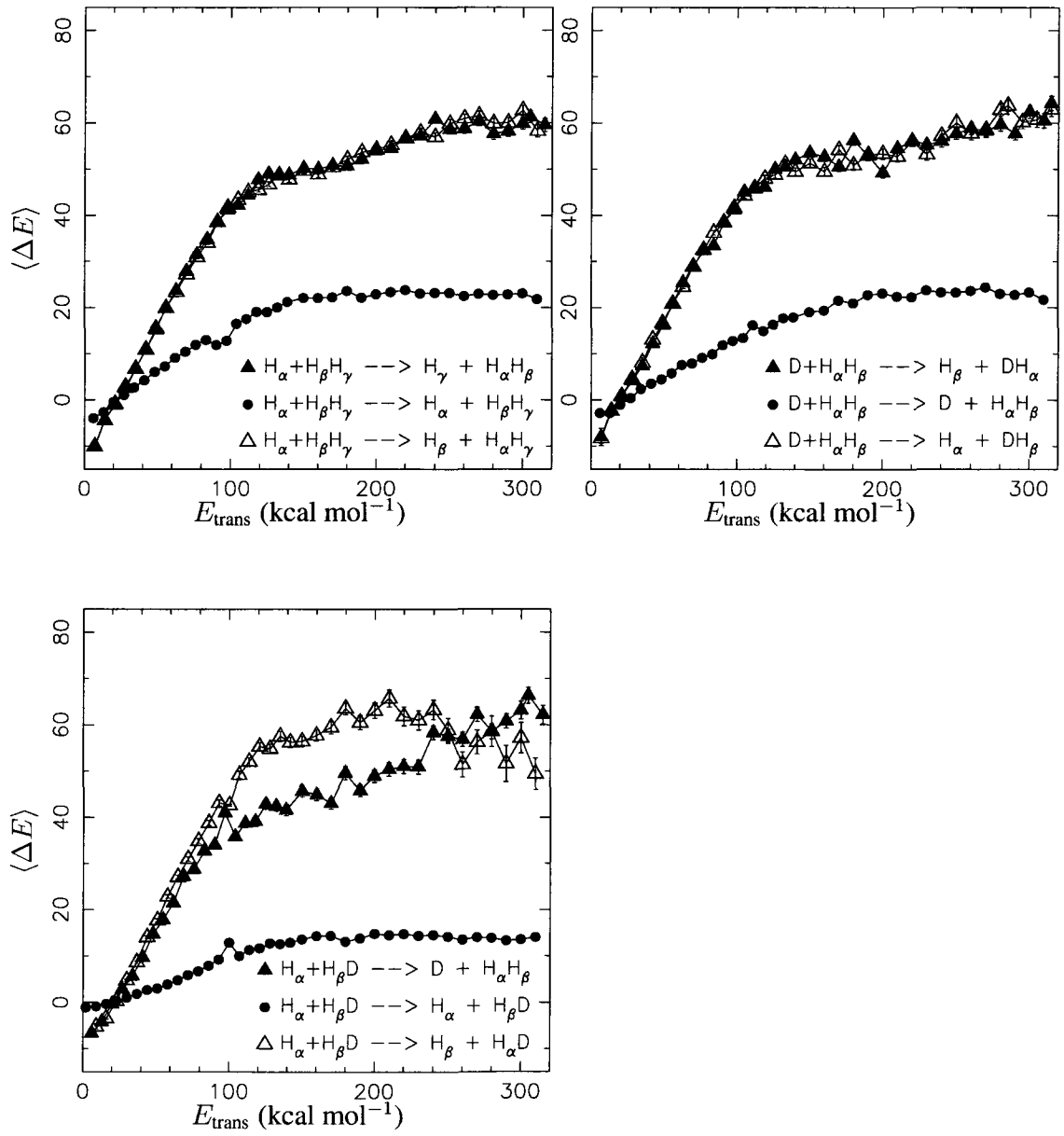

Figure 5.7: Average energy transfer, as in Figure 5.6, but for (0,8).

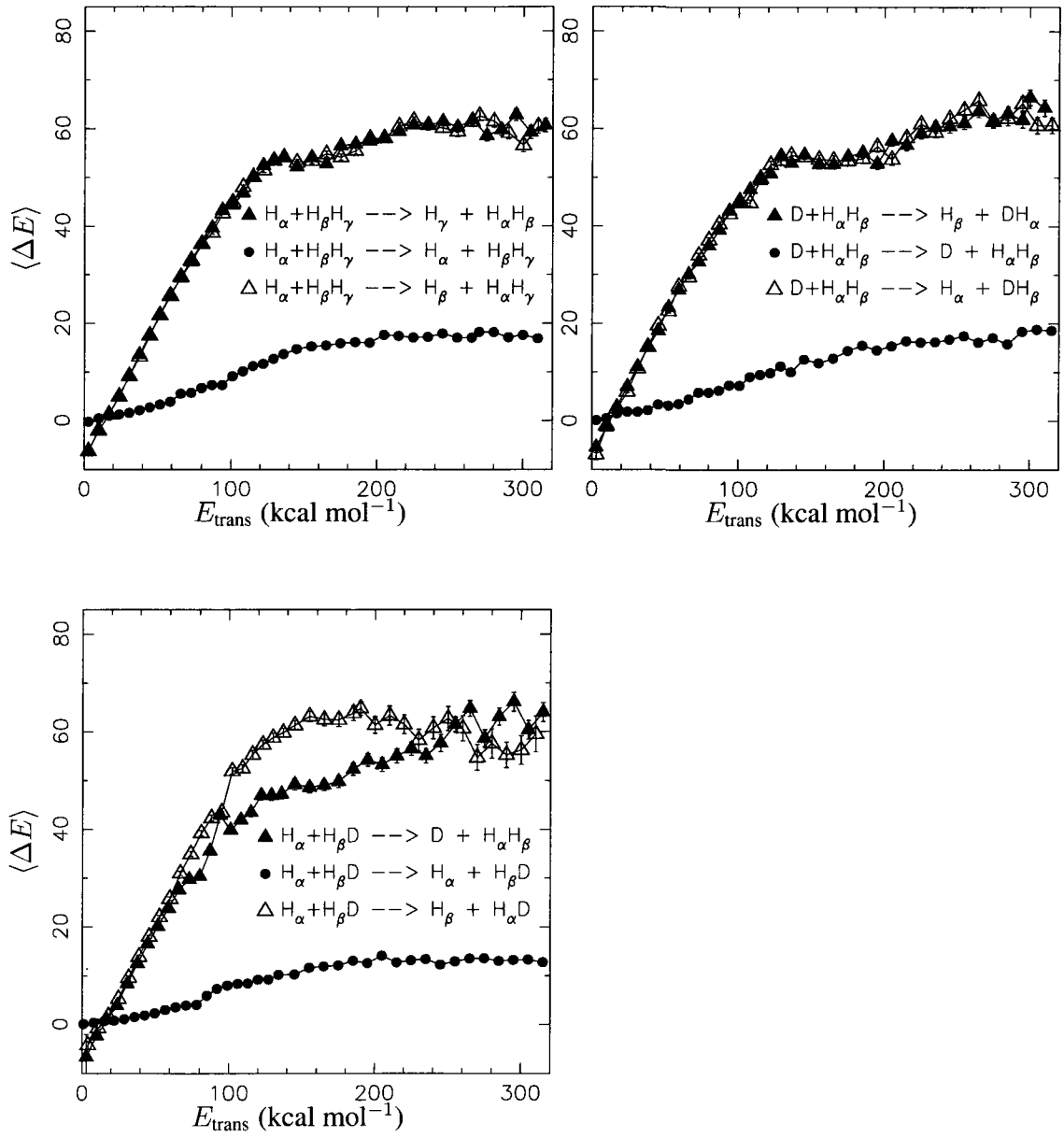

Figure 5.8: Average energy transfer, as in Figure 5.6, but for (1,0).

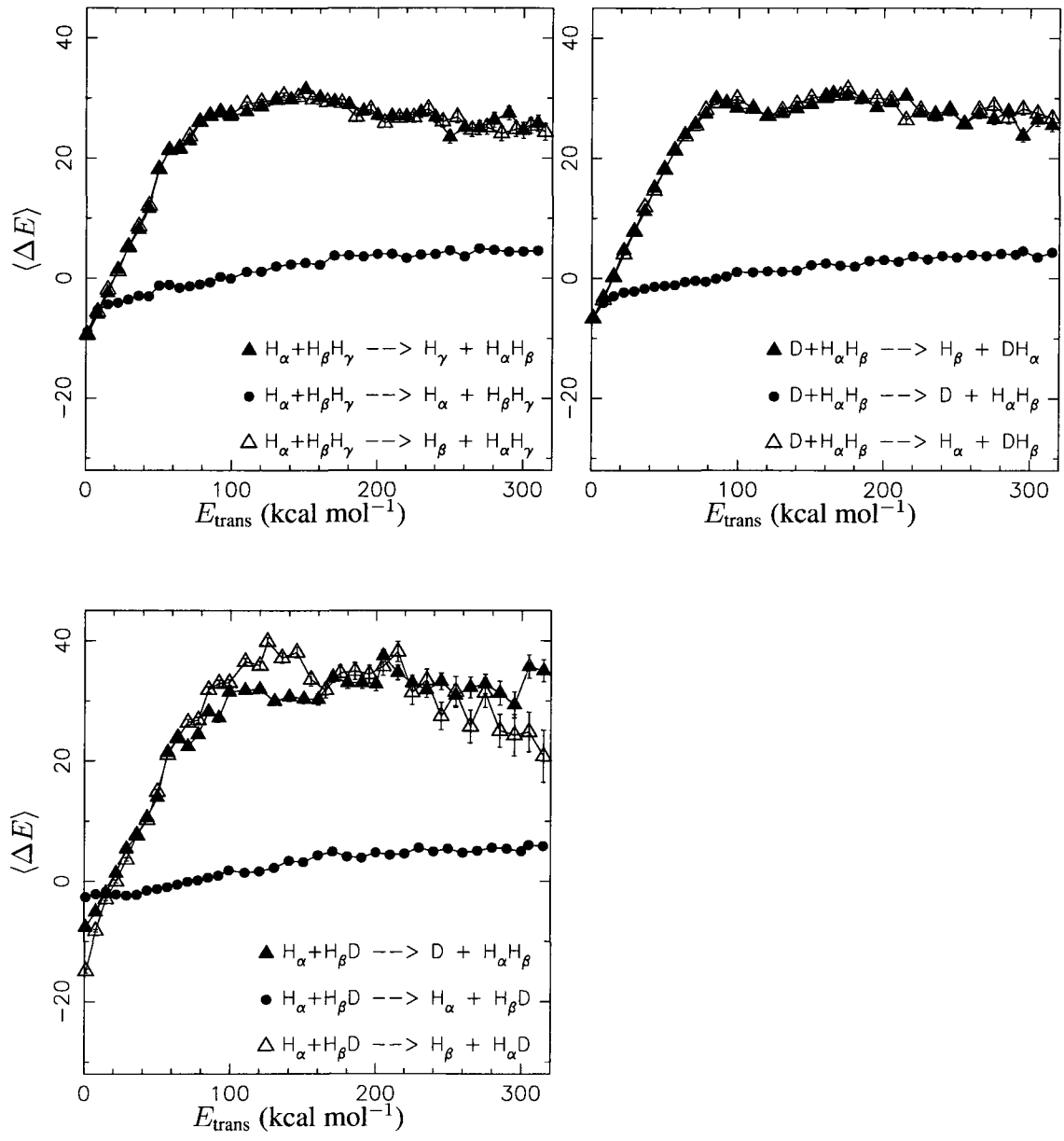

Figure 5.9: Average energy transfer, as in Figure 5.6, but for (5,0).

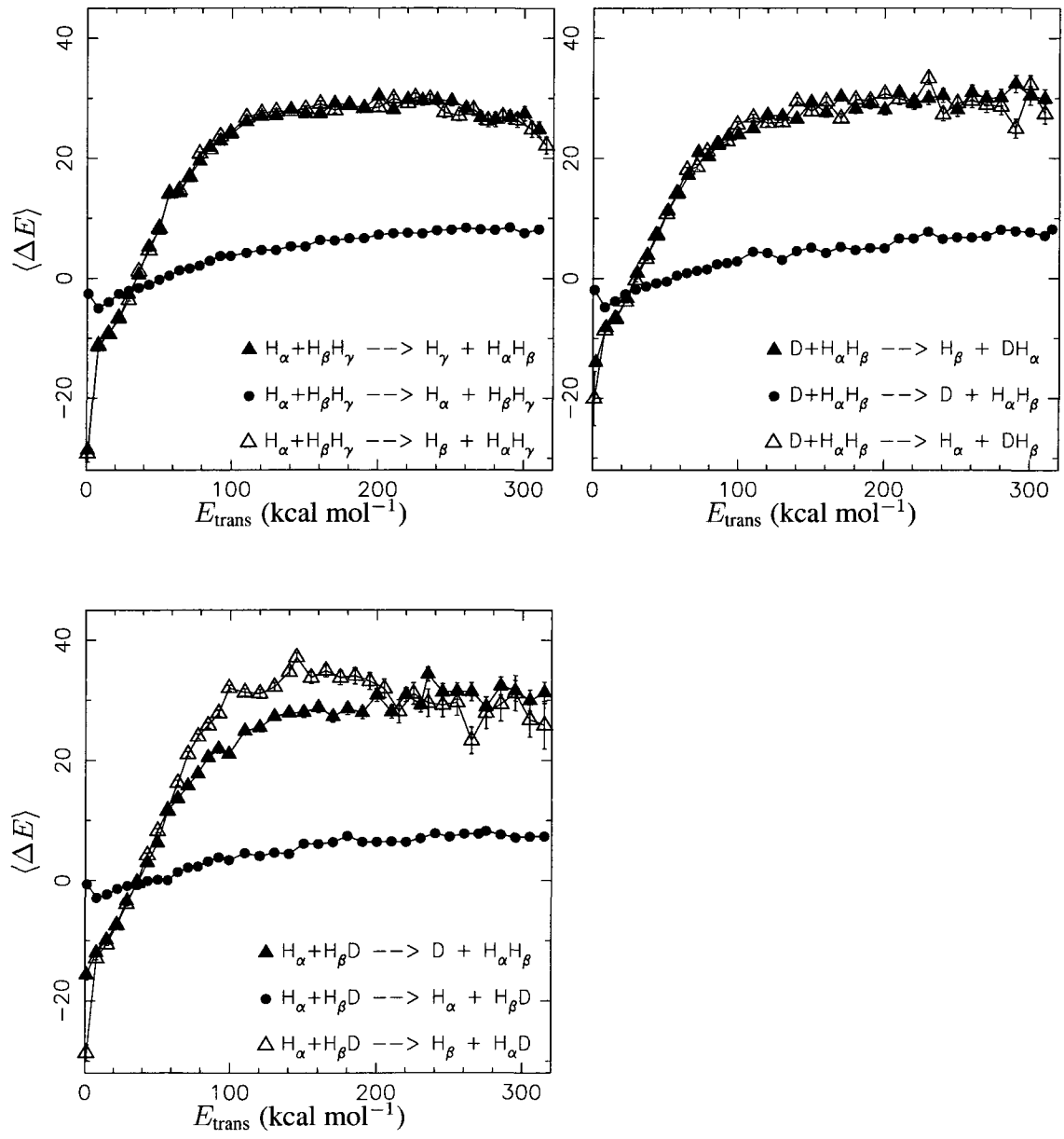

Figure 5.10: Average energy transfer, as in Figure 5.6, but for H + H_2(2,14), D + H_2(2,14), and H + HD(2,16).

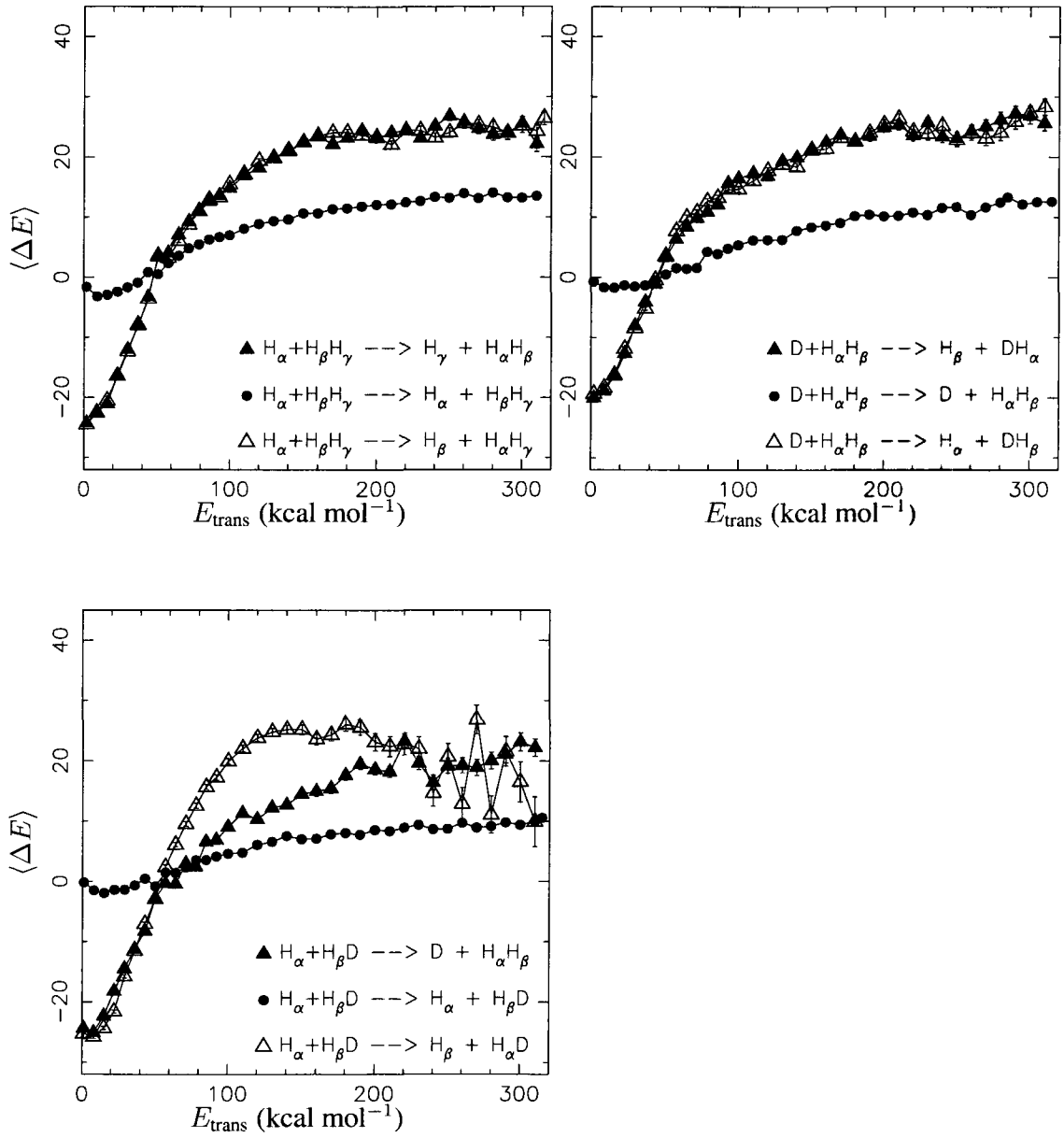

Figure 5.11: Average energy transfer, as in Figure 5.6, but for H + H_2(0,20), D + H_2(0,20), and H + HD(0,24).

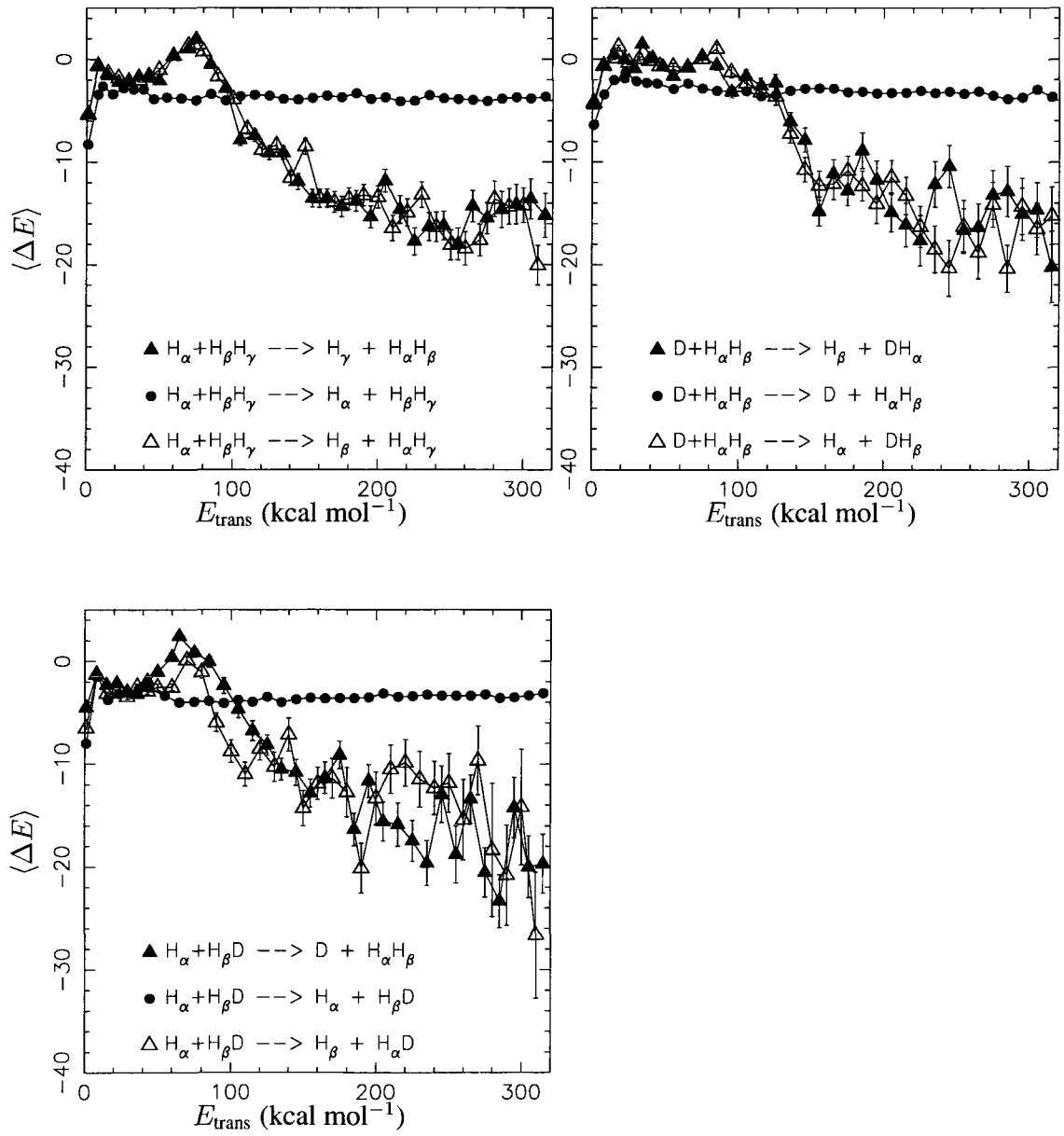

Figure 5.12: Average energy transfer, as in Figure 5.6, but for H + H_2(12,0), D + H_2(12,0), and H + HD(14,0).

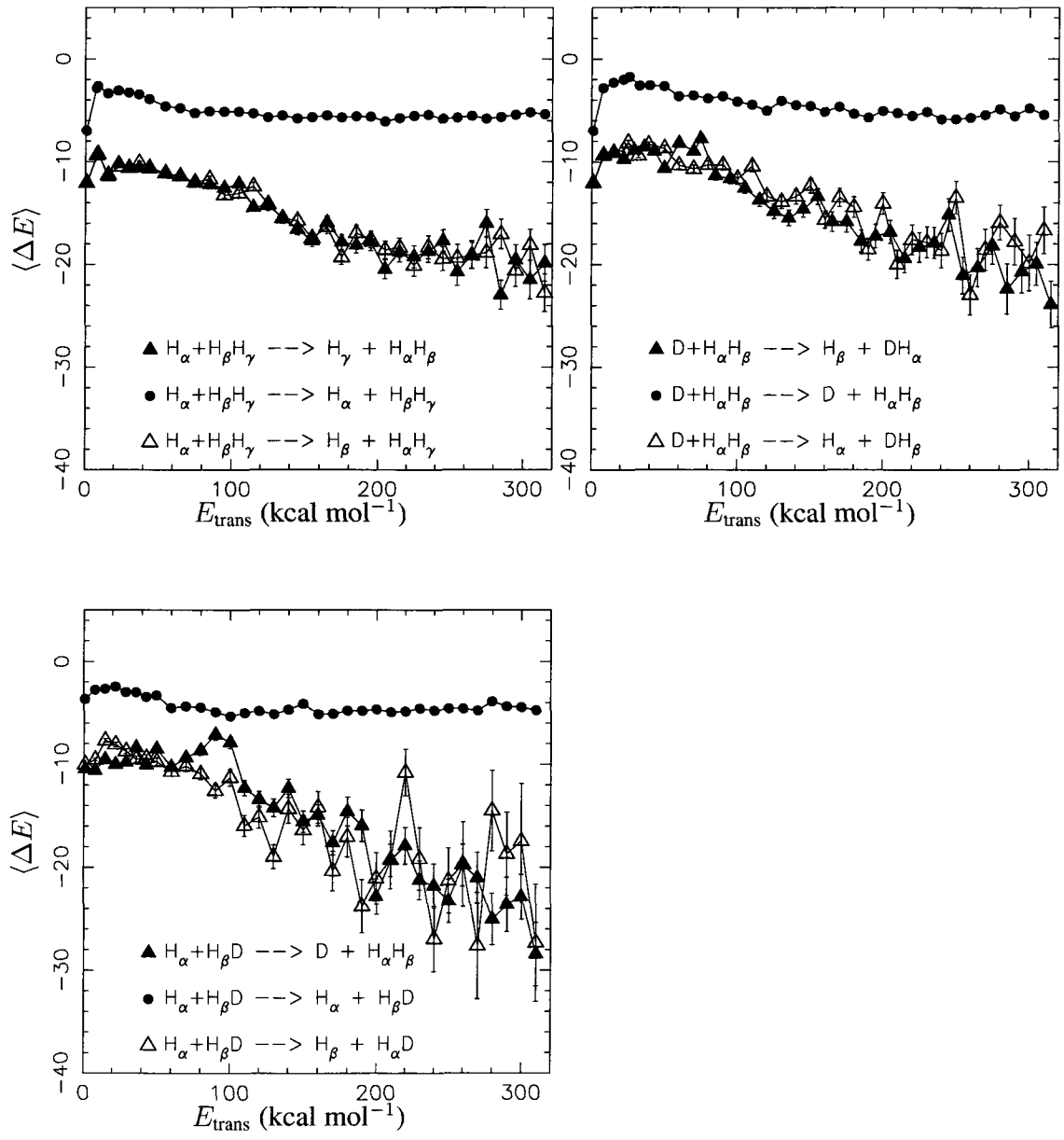

Figure 5.13: Average energy transfer, as in Figure 5.6, but for H + H_2(5,24), D + H_2(5,24), and H + HD(8,24).

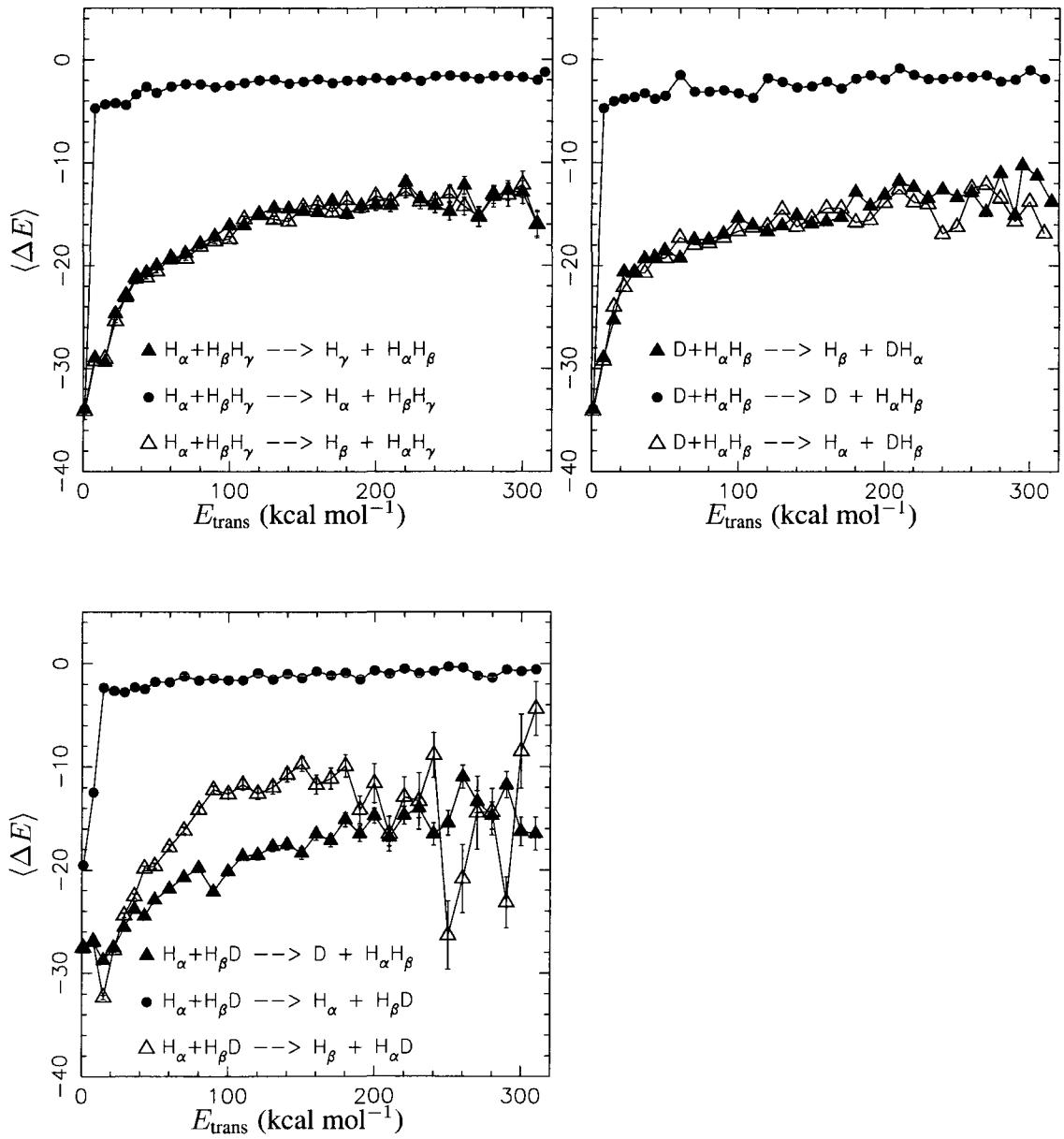

Figure 5.14: Average energy transfer, as in Figure 5.6, but for H + H_2(0,32), D + H_2(0,32), and H + HD(0,37).

Chapter 6

Competition among processes

To provide insights into the general behaviour of a gas consisting of molecular and atomic hydrogen, the relative importance of each process is considered. Because the calculation of the rate coefficients performed in this study assumes an equilibrium distribution of translational energies, only a master equation study can quantitatively determine the importance of each process in a real gas, so an attempt is made here to qualitatively predict the role the H + HD and D + H_2 systems may play in a neutral interstellar environment.

Many regions of the interstellar medium are not in thermal equilibrium; however, cold and warm neutral matter regions, with temperatures near 100 K and 8000 K, respectively (due to [CII] and Lyman α cooling, with variations due to pressure differences) may exist for long periods in local thermal equilibrium. These regions, along with cold molecular clouds, are the primary places in which molecular hydrogen can be found; warmer regions tend to be ionized by the processes that are heating them [79]. As quantum effects are important in the temperatures typical of cold molecular clouds ($\sim$ 10 K), it does not make sense to attempt to analyze the behaviour of these regions in a quasiclassical study. Shocked regions are another matter: they exist far from thermal equilibrium, and may be free of ionizing radiation. These vary enough in the details of energy distribution that they must be considered on a case–by–case basis, and are beyond the scope of this work. Hence the choice has been made in this section to use thermal rate coefficients as the basis for analysis.

It will be assumed that where total nonreactive rate coefficients are presented or dis-

cussed, they exclude any contributions from elastic collisions (defined in Section 2.3).

6.1 States with low internal energy

From the ground state, inelastic nonreactive energy transfer is generally the most important process (Figure 6.1). For H + H_2, the total nonreactive rate coefficient is greater than that of total exchange across all temperatures. Near 10000 K, the nonreactive rate coefficient is double that of exchange; both will be significant in models. Above 3000 K and below 30000 K, the rate coefficients for exchange and nonreactive energy transfer of H + H_2 have a greater relative difference than at temperatures between those two, and nonreactive processes will dominate over exchange or collision–induced dissociation (CID). Although the high and low temperature trends for D + H_2 are similar to those of H + H_2, exchange becomes a slightly more important process near 10000 K, rather than 30000 K. CID does not start to become important until 50000 K, and is an order of magnitude smaller than nonreactive energy transfer even at 100000 K.

For H + HD(0,0), the rate coefficients for both exchange channels (for which the dynamical thresholds are observed to be 7 kcal mol^{-1} for exchange to H_2 and 8 kcal mol^{-1} for exchange to HD) are small relative to those for nonreactive energy transfer (no observed threshold) at low to moderate temperatures. At higher temperatures, exchange remains unlikely relative to nonreactive energy transfer, as may be seen in Appendix B, Table B.1. Exchange to HD is more likely than exchange to H_2 below the temperature at which CID becomes important is reached; as temperature is increased above this, the rate coefficients for the two exchange channels converge to similar values. It is observed for other states of low internal energy that exchange to H_2 is favoured at lower temperatures, while exchange to HD is favoured at high temperature. It is also observed that for $j = 0$ states of H + HD, rate coefficients for CID tend to increase at the expense of rate coefficients for exchange to HD more than at the expense of the rate coefficients for exchange to H_2. The competition between exchange and dissociative channels from H + HD(0,0) may be seen in the bottom left panel of Figure 6.1, as the rate

coefficients for exchange to H_2 increase slightly from lower temperatures to 100000 K, while the rate coefficients for exchange to HD decrease and the rate coefficients for CID increase by a relatively large amount over the same temperature range.

Total rate coefficients from the (0,8) states, displayed in Figure 6.2, are qualitatively similar to those from the (0,0) states, with a few differences. There is a small enhancement of the rate coefficients for exchange relative to the rate coefficients for nonreactive energy transfer in $H + H_2(0,8)$ and $D + H_2(0,8)$ relative to the corresponding rate coefficients for $H + H_2(0,0)$ and $D + H_2(0,0)$. At 100 K, the rate coefficient for nonreactive energy transfer of H + HD(0,8) is smaller by a factor of 1000 than is that for H + HD(0,0), though the rate coefficients differ by no more than a factor of two for temperatures above 1000 K.

Although all transitions were endoergic (or "upward") in the case of (0,0), transitions from the (0,8) states may be exoergic (or "downward"). Rate coefficients for the upward and downward processes are given in Figure 6.3. For $H + H_2$ and $D + H_2$, exoergic transitions are favoured heavily at temperatures below 5000 K, while endoergic transitions become more important above this. For $H + H_2$, nonreactive and exchange rate coefficients are similar at low temperatures, but this is not the case for $D + H_2$, which has consistently larger exchange rate coefficients at most temperatures. In all cases, upward nonreactive transitions are the leading processes at 100000 K, while downward nonreactive transitions dominate at 100 K.

The rate coefficients for H + HD(0,8) are divided neatly into pairs: both the nonreactive rate coefficients as functions of temperature are qualitatively and quantitatively similar, as are the upward exchange functions, and the downward exchange functions. Although one in each pair might be an order of magnitude greater than the other at any given temperature, the two functions in each pair are qualitatively similar to each other in terms of temperature dependence.

The rate coefficients from (1,0) are qualitatively like those from (0,0), but are larger, as seen in Figure 6.4. Compared to those from (0,8), the rate coefficients for downward exchange from (1,0) for all systems are enhanced considerably over the corresponding downward nonre-

active rate coefficients. Upward H + HD nonreactive transitions dominate at low temperature. For the (1,0) state of all systems at high temperature, there is competition among the CID, upward exchange, and downward nonreactive processes.

6.2 States with internal energy near 55 kcal mol^{-1}

As the internal energy of the target molecule increases, nonreactive energy transfer ceases to be the sole dominant process at low temperature, as the exchange reactions become probable at lower translational energies. This is illustrated by the behaviour of the rate coefficients from the (5,0) states, as displayed in Figure 6.6. From H + H_2(5,0), exchange is favoured at temperatures below 20000 K, with nonreactive transfer favoured above that. From D + H_2(5,0), there is a greater relative gap between exchange and nonreactive rate coefficients, so exchange is favoured below 30000 K. As was the case for low energy states, this is the temperature regime in which dissociation begins to become important, indicating that the reduction in exchange rate coefficients is due primarily to the increase in dissociation.

H + HD(5,0) differs in that there are two separate exchange processes. Nonreactive energy transfer is more likely than either of the exchange channels; however, the sum of the rate coefficients for exchange is greater than the rate coefficients for nonreactive energy transfer below the temperature regime at which CID is important. It is observed in Figure 6.7 that the upward and downward nonreactive rate coefficients converge above 4500 K, for all systems.

Although the rate coefficients for the H + HD(5,0)$\rightarrow$H + HD exchange reaction decrease as temperature is raised to 100000 K, the rate coefficients for the H + HD(5,0)$\rightarrow$D + H_2 exchange reaction increase. This increase in rate coefficients for exchange to H_2 at the highest temperatures does not occur for the other states near 55 kcal mol^{-1}, but it is observed in H + HD(14,0) and other purely vibrationally excited states.

The total of the rate coefficients for processes from H + H_2(2,14), D + H_2(2,14), and H + HD(2,16) are given in Figure 6.8. These are qualitatively similar to those of the (5,0) rate coefficients, except that exchange is here dominant at higher temperatures. A departure from

the behaviour of (5,0) is shown in Figure 6.9, in which it can be seen that the upward exchange rate coefficients from D + H_2(2,14) are several times greater than those of H + H_2(2,14) at and above 10000 K. This is in contrast to the reactions of the (5,0) states, for which the relative difference is approximately a factor of two.

Among states with internal energy near 55 kcal mol^{-1}, exchange is dominant over the other processes at higher temperatures for those states with more rotational energy than for those with more vibrational energy. The rate coefficients from H + H_2(0,20), D + H_2(0,20), and H + HD(0,24) given in Figure 6.10, taken in conjunction with Figure 6.6 and Figure 6.8, support this. In Figure 6.10, it can be seen that even with two channels for exchange from H + HD(0,24), each is competitive with nonreactive energy transfer at all energies. When rate coefficients are calculated separately for exoergic and endoergic processes, as in Figure 6.11, it can be seen that at all temperatures considered but the few highest, collisions of both H and D with H_2 favour downward exchange over any other process. At the highest temperatures considered, the rate coefficients for nonreactive energy transfer are the greatest of all because of competition between the CID and exchange channels.

6.3 States with energy near 109.5 kcal mol^{-1}

The role of nonreactive energy transfer is greatly diminished for states with internal energy near 109.5 kcal mol^{-1}. For H + H_2(12,0), D + H_2(12,0), and H + HD(14,0), total rate coefficients for nonreactive energy transfer do not exceed those of either exchange and CID at any temperature, as illustrated in Figure 6.12. CID becomes important from these states at temperatures as low as 4500 K. The difference between total exchange and nonreactive rate coefficients is greater for D + H_2(12,0) than for H + H_2(12,0), as was the case for D + H_2(5,0) and H + H_2(5,0), due mostly to an enhancement of exchange rate coefficients in the D + H_2 system at moderate temperatures. This is a result of the fact that the cross sections for exchange to HD are greater than those for exchange to H_2 at all translational energies below approximately 40 kcal mol^{-1} (see Figure 5.5).

The total upward and downward rate coefficients, given in Figure 6.13, qualitatively resemble those of (5,0). The upward and downward nonreactive rate coefficients begin to converge at high temperature, with the downward slightly exceeding the upward due to the greater number of available low energy states and competition between upward transitions and the CID channel. Upward nonreactive rate coefficients at low energy are reduced relative to those of (5,0).

For H + HD(14,0), downward exchange to HD is important at low to moderate temperatures, as it was for H + HD(5,0). However, the upward rate coefficients are reduced in importance relative to those of H + HD(5,0), and downward exchange from H + HD(14,0) to H_2 takes on increased importance at all temperatures.

The systems H + H_2(5,24) and its isotopic analogues are to their purely vibrational counterparts what H + H_2(2,14) and its isotopic equivalents are to their purely vibrational counterparts. In Figure 6.14 it can be seen that the exchange channel takes on greater importance relative to the nonreactive channel for states with both vibrational and rotational energy. Indeed, as was the case for the states near 55 kcal mol^{-1}, it may be seen that an increase in rotational energy increases the relative importance of the exchange channel. The difference between the rate coefficients for exchange of D + H_2(5,24) and those for exchange of H + H_2(5,24) is not so pronounced as it was for the states previously studied. As for the states with high, purely vibrational energy, nonreactive energy transfer from high energy states with both vibrational and rotational energy is never the most important process, though it competes with CID at high temperature. Rate coefficients for exchange from H + HD to D + H_2 and to H + HD are nearly equal at all temperatures.

For H + HD(8,24), all four rate coefficients (CID, nonreactive, exchange to H_2, and exchange to HD) are nearly equal to each other at temperatures around 7800 K. This is approximately the same temperature as that at which the CID and nonreactive rate coefficients for H + H_2(5,24) are equal to each other, and is somewhat higher than the temperature at which the CID and nonreactive rate coefficients for D + H_2(5,24) are equal to each other.

From H + H_2(0,32), D + H_2(0,32) and H + HD(0,37) at low temperature, the total rate coefficients for exchange are two orders of magnitude greater than the corresponding rate coefficients for nonreactive energy transfer (Figure 6.16). As for the other states with high internal energy, the relative difference in rate coefficients between high energy states is greater for D + H_2 than for H + H_2. There are again temperatures at which rate coefficients for all processes are nearly equal for H + HD, and are slightly less similar for H + H_2 and D + H_2. When the total rate coefficients are calculated separately for exoergic and endoergic processes (Figure 6.17), it can be seen that the endoergic nonreactive processes become the most important processes at high temperature in all systems, with exoergic nonreactive processes playing a role in H + HD as well. This is a deviation from what is generally observed for other high energy states studied, for which an increase in rotational energy increases the probability of exchange relative to nonreactive energy transfer. It also differs from the other high energy states in that the nonreactive exoergic processes are not the most favoured at the highest temperatures for H + H_2(0,32). As discussed in Section 4.3.2, rotational energy transfer from highly rotationally excited states is improbable relative to rotational energy transfer from other states. As transitions involving small changes in internal energy tend to be the greatest contributors to total cross sections, nonreactive energy transfer for H + H_2(0,32) and its isotopic analogues is expected to have less relative importance than for lower energy or vibrationally excited systems.

For the high energy purely rotational states of all three systems, a nearly linear relationship exists between the logs of the nonreactive rate coefficients and the logs of the corresponding temperatures. The approximation to linearity is even better for just the downward nonreactive rate coefficients (Figure 6.15). The best linear regression fits for downward rate coefficients are given in Table 6.1, fit to the functional form

$$\log_{10} \gamma(T) \simeq a \log_{10} T + c. \tag{6.1}$$

This equation is of similar functional form to the hard sphere rate equation

$$\gamma(T) = \left(\frac{8\pi k_B T}{\mu}\right)^{1/2} d^2 \tag{6.2}$$

$$\log_{10}\gamma(T) = \log_{10}\left(\left(\frac{8\pi k_B}{\mu}\right)^{1/2} d^2\right) + \frac{1}{2}\log_{10} T \tag{6.3}$$

Most of these fits are improved by excluding rate coefficients below 600 K; however, all of the fits are good ($R^2 > 0.95$) even with the inclusion of low temperature values.

Other functional forms are possible for fitting rate coefficients. The reactive hard sphere (Arrhenius) model gives

$$\gamma(T) = \pi d^2 \left(\frac{8k_B T}{\pi\mu}\right)^{1/2} e^{-E_a/k_B T} \tag{6.4}$$

$$\log_{10}\gamma(T) = \log_{10}\left(\left(\frac{8\pi k_B}{\mu}\right)^{1/2} d^2\right) + \frac{1}{2}\log_{10} T + \frac{-E_a}{k_B T}, \tag{6.5}$$

which differs from the equation for rate coefficients for simple hard sphere collisions by the $\frac{-E_a}{k_B T}$ term. This term represents the fact that only collisions which occur at a total energy above the activation energy E_a can lead to a reactive outcome. However, for states with internal energy near that required for dissociation, there are few transitions from these states which will have nonzero activation energies, meaning that the simple hard sphere model may be appropriate. Additionally, the exchange and CID processes tend to dominate at lower impact parameters: most of the contribution to nonreactive rate coefficients comes from trajectories at high impact parameters. Thus, the attractive nature of the surface, which is neglected in the hard sphere model, is less important to the rate coefficients for nonreactive processes than for exchange or CID.

Martin and Mandy used a related functional form

$$\log_{10}\gamma(T) = a + b\log_{10} T' + c(\log_{10} T')^2 - d\left(\frac{1}{T'} - 1\right), \tag{6.6}$$

where in this case a, b, c, and d are free parameters, and T' is a reduced temperature ($T' = T/4500$ K) [80]. This functional form was designed to ensure more accurate parametrized

fits of the data in that study, partly as a result of the fact that the parametrized versions of the rate coefficients obey microscopic reversibility as a result of the $\frac{1}{T'}$ term. Although the functional form of Martin and Mandy is more suitable to fits of rate coefficients in general, the near–linearity of the log–log relationship between total rate coefficients and temperature for nonreactive transitions at high energy (and correspondingly good R^2 values for the fits made using the hard sphere model) makes the hard sphere model a suitable choice for these rate coefficients. The parameters for some of the fits obtained in Martin and Mandy, 1995 [80] are given in Table 6.2. Because the values of $\log_{10} T'$ range from -0.87 at 600 K to 0.65 at 20000 K, the term which contributes most significantly to each state–to–state rate coefficient is the value a. Therefore, the most significant contributors to the overall rate coefficients are those transitions with relatively high values of the parameter a. It can be seen from the state–to–state rate coefficients in Table 6.2 that the magnitude of the parameters c and d is small for the most significant contributors to total rate coefficients at most temperatures. Therefore, the c and d terms in a fit using the functional form of Equation 6.6 are small for total nonreactive rate coefficients from states with high internal energy.

The best fits to the linear model (for hard spheres, Equation 6.2) occur for H + H_2(5,24) and its isotopic analogues, with temperatures below 600 K excluded. The slopes (a values) of these fits match each other within 4%, and the R^2 values are all 0.998 or greater. The slopes for the purely rotationally excited states at low temperature vary considerably, but when low temperature rate coefficients are excluded, the slopes for each system match each other closely. The slopes for the purely vibrationally excited states where temperatures below 600 K are included vary the most among those studied. Of the fits performed, the fits for the purely vibrationally excited states have the worst R^2 values. Inclusion of the lower temperature rate coefficients for purely vibrationally excited states improves both the agreement between slopes and the R^2 values. Equation 6.1 could be used successfully to represent nonreactive rate coefficients for high energy states at temperatures at or above 600 K; however, these results should not be extrapolated to lower temperatures.

Matching terms between the hard sphere rate coefficient equation (Equation 6.2) and the linear functional form used (Equation 6.1), it may be possible to gain some insight into the fitting parameters in Table 6.1. If the hard sphere model were an accurate representation of the underlying dynamical processes, then

$$a = 0.5 \tag{6.7}$$

and

$$c = \log_{10}\left(\frac{8\pi k_B}{\mu}\right)^{1/2} d^2. \tag{6.8}$$

The temperature coefficients a in the fits are close to 1.25 for the initial states with rotational energy, while the purely vibrationally excited states have a terms closer to 1.75. The rate coefficients for nonreactive energy transfer have a much stronger temperature dependence than the hard sphere model would suggest. Because the H + H_2 potential energy surface is attractive, and because trajectories which result in nonreactive energy transfer may occur at impact parameters greater than those for which hard sphere collisions may occur, long–range interactions can result in a stronger temperature dependence than the hard sphere model predicts.

Assuming that the H atoms are hard spheres with radii of 0.529 Å (the Bohr radius), it is possible to calculate hard sphere rate coefficients using Equation 6.2. Hard sphere rate coefficients are placed alongside the QCT rate coefficients calculated in this study for selected states in Table 6.3. The QCT rate coefficients are smaller than the hard sphere rate coefficients by a factor as great as 16 at 1000 K. There is better agreement between the QCT and hard sphere rate coefficients for initial states with more vibrational energy. The greatest relative difference between QCT and hard sphere rate coefficients at 100000 K is a factor of 2.4.

As the temperature is increased, there is less time during the course of a collision for long–range interactions to occur, so only those trajectories which occur at small impact parameter contribute to the QCT rate coefficients. This fact should reduce the QCT rate coefficients relative to the hard sphere rate coefficients at high temperatures. It may be that the observed decline in rate coefficients for exchange at high temperature (c.f. Figure 6.12) is not due solely

to competition with CID; rather, some trajectories which would result in exchange at a low translational energy do not have sufficient time at a high translational energy to undergo either reaction or CID, resulting in a nonreactive collision.

Table 6.1: Linear regression fits and R^2 values for total downward rate coefficients for non-reactive (inelastic) energy transfer from states with high internal energy. The functional form chosen is $\log_{10}\gamma(T) \simeq a\log_{10}T + c$, with free parameters a and c. Fits are included for all temperatures T at which rate coefficients were calculated, and for temperatures above 600 K, below which QCT rate coefficients are not expected to be valid.

System	all T			$T \geq 600$ K		
	a	c	R^2	a	c	R^2
H + H_2(12,0)	1.78	20.7	0.970	1.71	20.1	0.959
D + H_2(12,0)	1.75	20.7	0.965	1.67	20.0	0.947
H + HD(14,0)	1.93	22.1	0.971	1.91	22.0	0.962
H + H_2(5,24)	1.12	14.7	0.995	1.19	15.3	0.997
D + H_2(5,24)	1.22	15.8	0.998	1.22	15.7	0.999
H + HD(8,24)	1.14	15.0	0.995	1.23	15.9	0.999
H + H_2(0,32)	1.12	15.0	0.980	1.32	17.0	0.998
D + H_2(0,32)	0.989	13.8	0.954	1.31	17.0	0.993
H + HD(0,37)	1.09	14.9	0.989	1.21	16.1	0.994

Table 6.2: Selected parameters for fitted rate coefficients from Martin and Mandy, 1995 [80], for nonreactive energy transfer from states with high internal energy. Mandy and Martin used the functional form $\log_{10}\gamma(T) = a + b\log_{10}T' + c(\log_{10}T')^2 - d\left(\frac{1}{T'} - 1\right)$ (where $T' = T/4500$ K) to fit the rate coefficients for temperatures between 450 K and 20000 K.

State	a	b	c	d
H + H_2(12,0)→H + H_2(12,2)	-9.564	0.287	-5.800×10^{-2}	1.400×10^{-2}
H + H_2(5,24)→H + H_2(6,22)	-10.359	0.177	-1.800×10^{-2}	4.02×10^{-2}
H + H_2(0,32)→H + H_2(1,30)	-10.499	0.142	-0.133	8.220×10^{-2}
H + H_2(12,0)→H + H_2(11,2)	-10.656	0.991	0.157	-4.770×10^{-2}
H + H_2(0,32)→H + H_2(0,30)	-10.705	1.320	-0.440	7.080×10^{-2}
H + H_2(5,24)→H + H_2(5,22)	-11.233	2.198	-1.336	-0.174
H + H_2(5,24)→H + H_2(6,20)	-11.255	0.932	-0.254	5.740×10^{-2}

Table 6.3: Rate coefficients for total nonreactive energy transfer from states with internal energy near that required for dissociation, for both the current QCT results and using a hard sphere model. All rate coefficients are in $\log(\gamma)$ ($cm^3s^{-1}molec^{-1}$).

System	1000 K	
	QCT	hard sphere
H + H_2(12,0)	$3.23 \times 10^{-10} \pm 2.2 \times 10^{-12}$	8.86×10^{-10}
D + H_2(12,0)	$2.49 \times 10^{-10} \pm 3.0 \times 10^{-12}$	7.23×10^{-10}
H + HD(14,0)	$3.73 \times 10^{-10} \pm 4.1 \times 10^{-12}$	8.41×10^{-10}
H + H_2(5,24)	$8.94 \times 10^{-10} \pm 4.8 \times 10^{-12}$	7.50×10^{-10}
D + H_2(5,24)	$7.26 \times 10^{-11} \pm 4.0 \times 10^{-12}$	6.13×10^{-10}
H + HD(8,24)	$1.76 \times 10^{-10} \pm 6.8 \times 10^{-13}$	7.67×10^{-10}
H + H_2(0,32)	$3.90 \times 10^{-11} \pm 2.8 \times 10^{-13}$	5.64×10^{-10}
D + H_2(0,32)	$2.89 \times 10^{-11} \pm 2.2 \times 10^{-13}$	4.61×10^{-10}
H + HD(0,37)	$7.56 \times 10^{-11} \pm 3.8 \times 10^{-13}$	5.23×10^{-10}

System	10000 K	
	QCT	hard sphere
H + H_2(12,0)	$1.21 \times 10^{-9} \pm 6.0 \times 10^{-12}$	2.80×10^{-9}
D + H_2(12,0)	$9.02 \times 10^{-9} \pm 8.1 \times 10^{-12}$	2.29×10^{-9}
H + HD(14,0)	$1.27 \times 10^{-9} \pm 9.5 \times 10^{-12}$	2.66×10^{-9}
H + H_2(5,24)	$6.87 \times 10^{-9} \pm 1.7 \times 10^{-12}$	2.37×10^{-9}
D + H_2(5,24)	$5.31 \times 10^{-10} \pm 2.6 \times 10^{-12}$	1.94×10^{-9}
H + HD(8,24)	$9.32 \times 10^{-10} \pm 4.1 \times 10^{-12}$	2.43×10^{-9}
H + H_2(0,32)	$6.12 \times 10^{-10} \pm 1.5 \times 10^{-12}$	1.78×10^{-9}
D + H_2(0,32)	$4.89 \times 10^{-10} \pm 2.2 \times 10^{-12}$	1.46×10^{-9}
H + HD(0,37)	$5.13 \times 10^{-9} \pm 2.5 \times 10^{-12}$	1.67×10^{-9}

System	100000 K	
	QCT	hard sphere
H + H_2(12,0)	$5.68 \times 10^{-9} \pm 1.2 \times 10^{-10}$	8.86×10^{-9}
D + H_2(12,0)	$4.22 \times 10^{-9} \pm 1.5 \times 10^{-10}$	7.23×10^{-9}
H + HD(14,0)	$5.66 \times 10^{-9} \pm 9.4 \times 10^{-11}$	8.41×10^{-9}
H + H_2(5,24)	$3.40 \times 10^{-9} \pm 3.3 \times 10^{-11}$	7.50×10^{-9}
D + H_2(5,24)	$2.55 \times 10^{-9} \pm 4.8 \times 10^{-11}$	6.13×10^{-9}
H + HD(8,24)	$4.19 \times 10^{-9} \pm 7.0 \times 10^{-11}$	7.67×10^{-9}
H + H_2(0,32)	$3.10 \times 10^{-9} \pm 3.0 \times 10^{-11}$	5.64×10^{-9}
D + H_2(0,32)	$2.44 \times 10^{-9} \pm 4.3 \times 10^{-11}$	4.61×10^{-9}
H + HD(0,37)	$2.31 \times 10^{-9} \pm 4.5 \times 10^{-11}$	5.23×10^{-9}

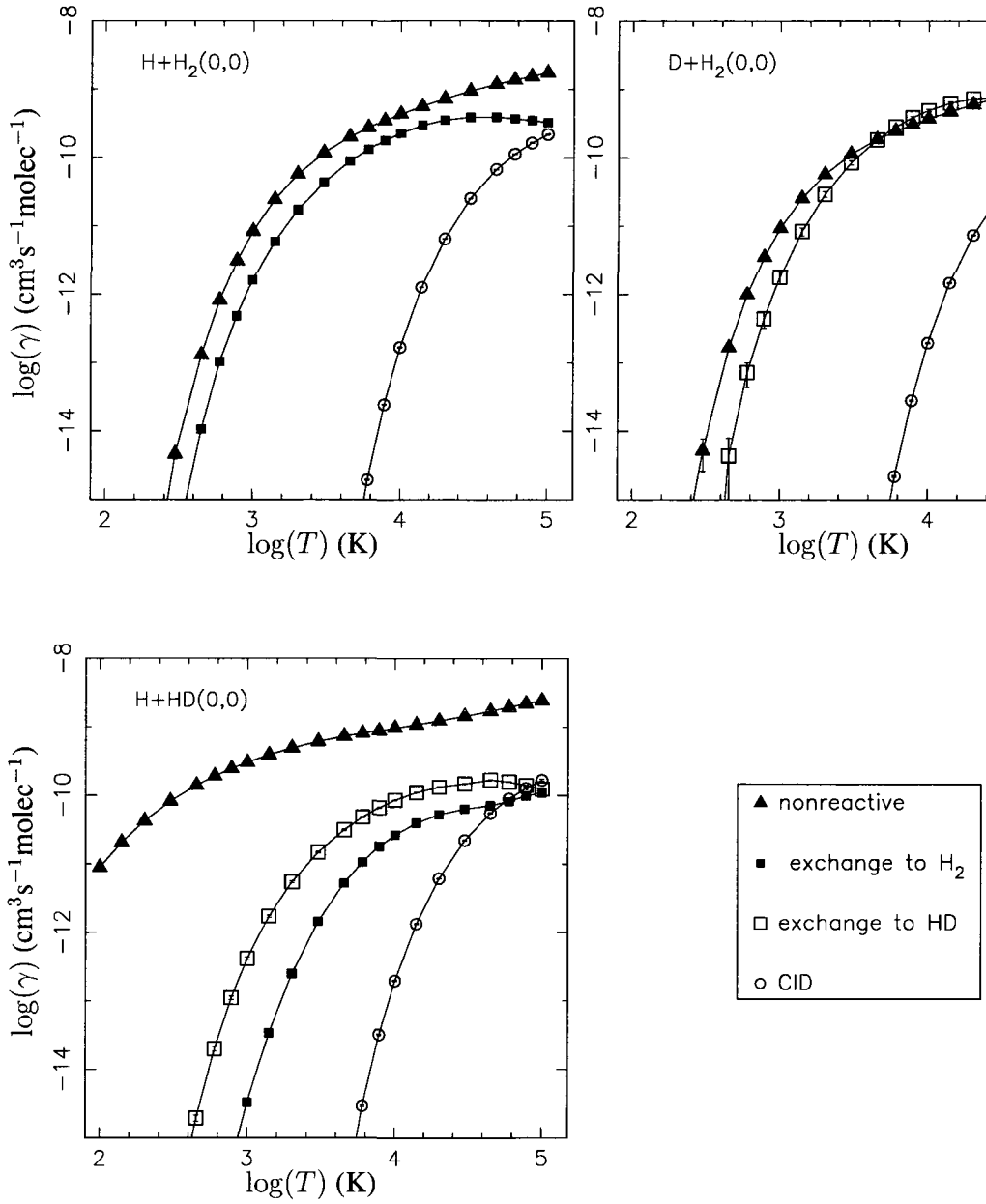

Figure 6.1: Total rate coefficients for nonreactive energy transfer, exchange, and CID from H + H_2(0,0), D + H_2(0,0), and H + HD(0,0).

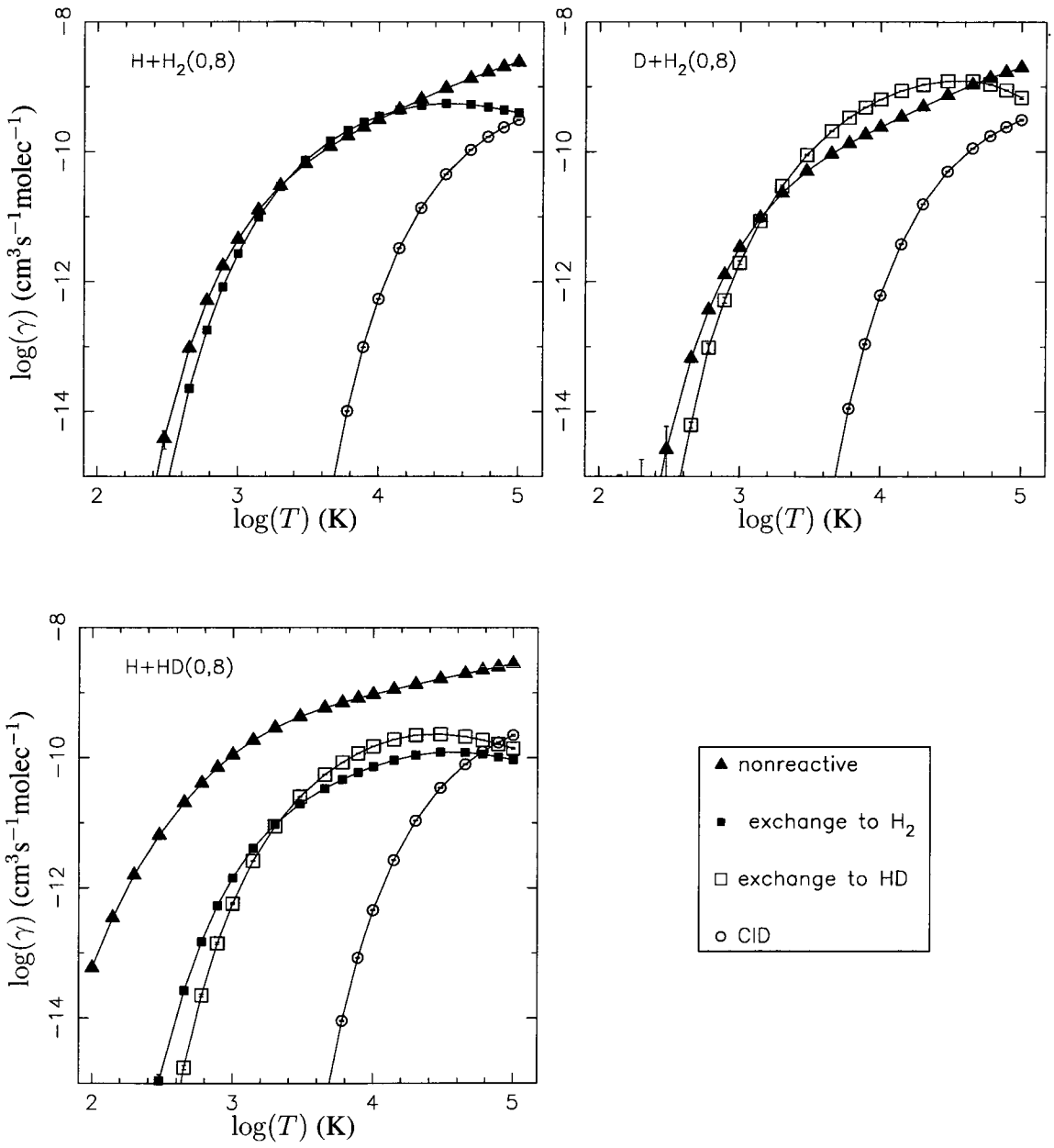

Figure 6.2: As in Figure 6.1, total rate coefficients from (0,8).

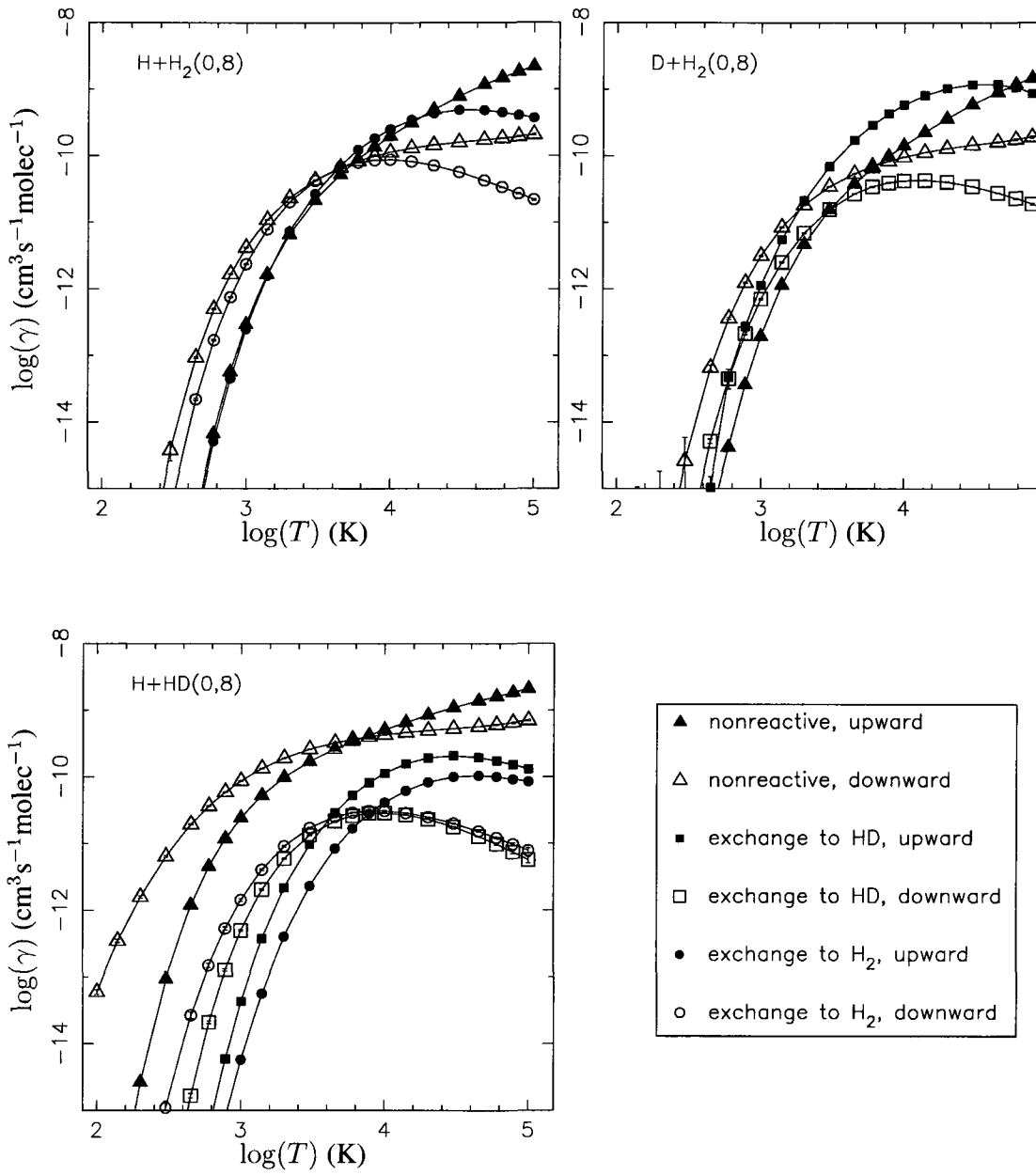

Figure 6.3: Total rate coefficients for transitions from (0,8), split into upward and downward components. An upward trajectory is considered to be one in which the product molecule has at least 3.5% more internal energy than had the initial state; a downward trajectory is considered to have at least 3.5% less energy than the initial state. Nearly isoergic transfers, those involving products with internal energy within 3.5% that of the initial state, are not included.

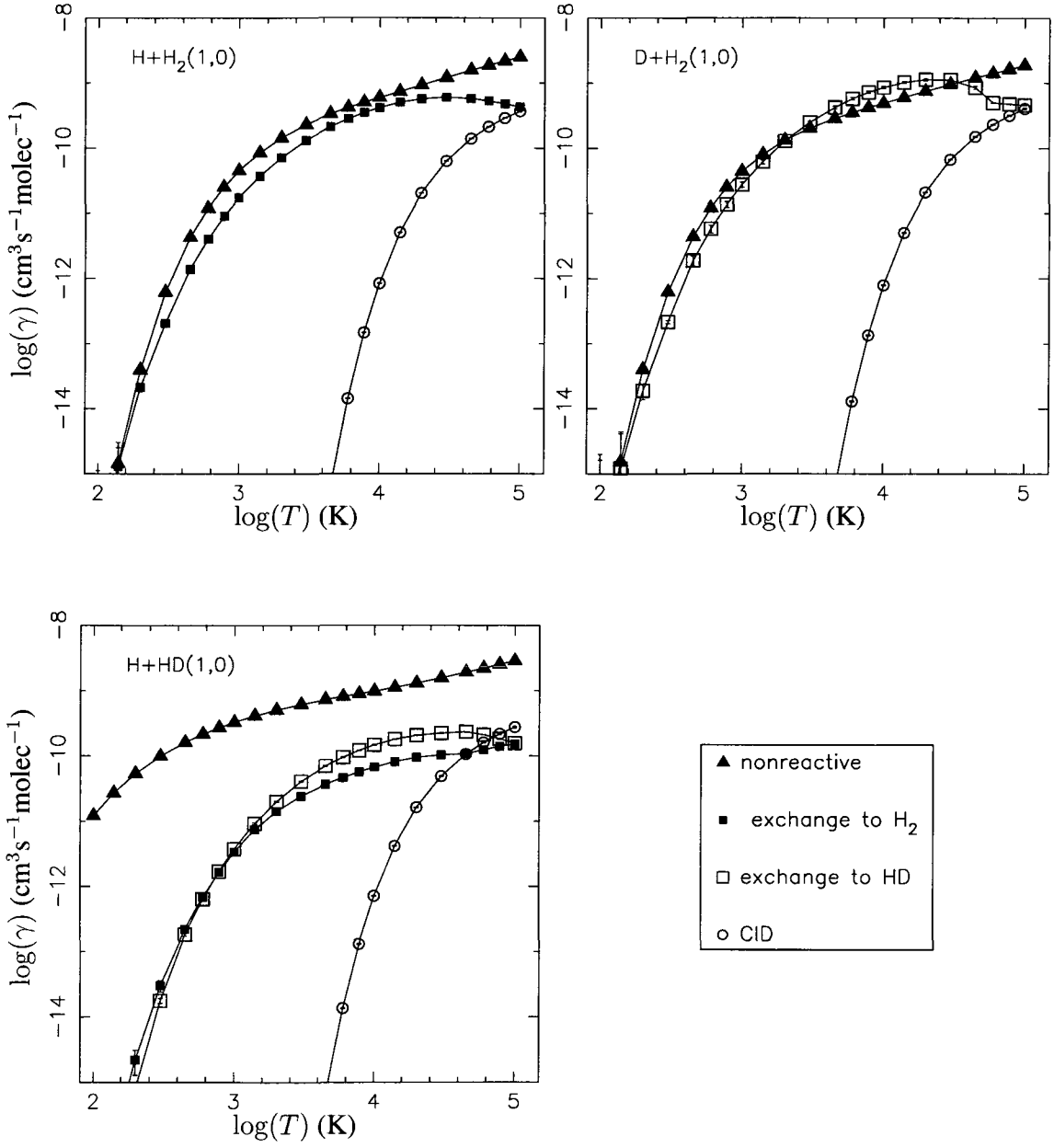

Figure 6.4: As in Figure 6.1, total rate coefficients from (1,0).

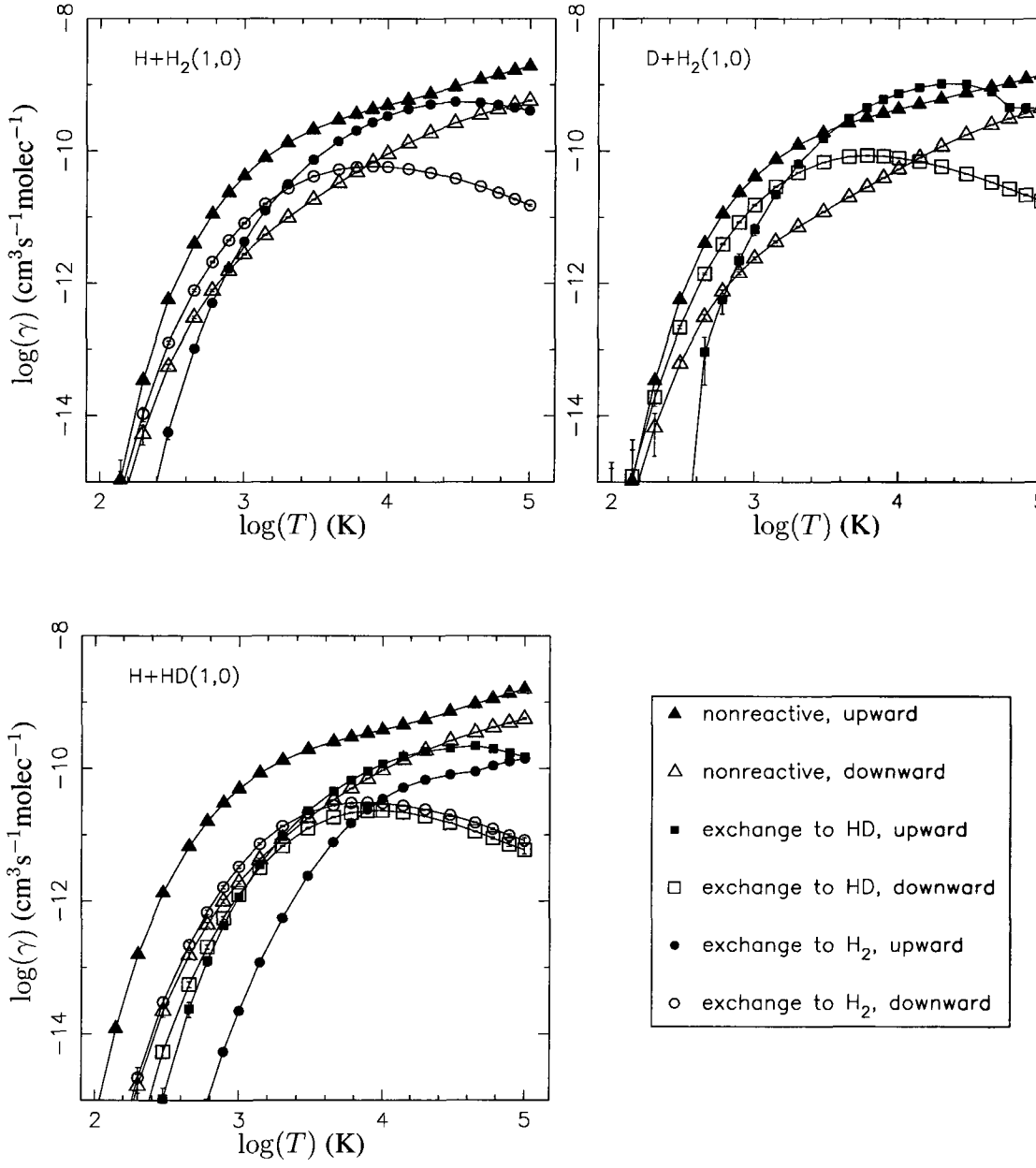

Figure 6.5: Total rate coefficients split into upward and downward components, as in Figure 6.3, but for (1,0).

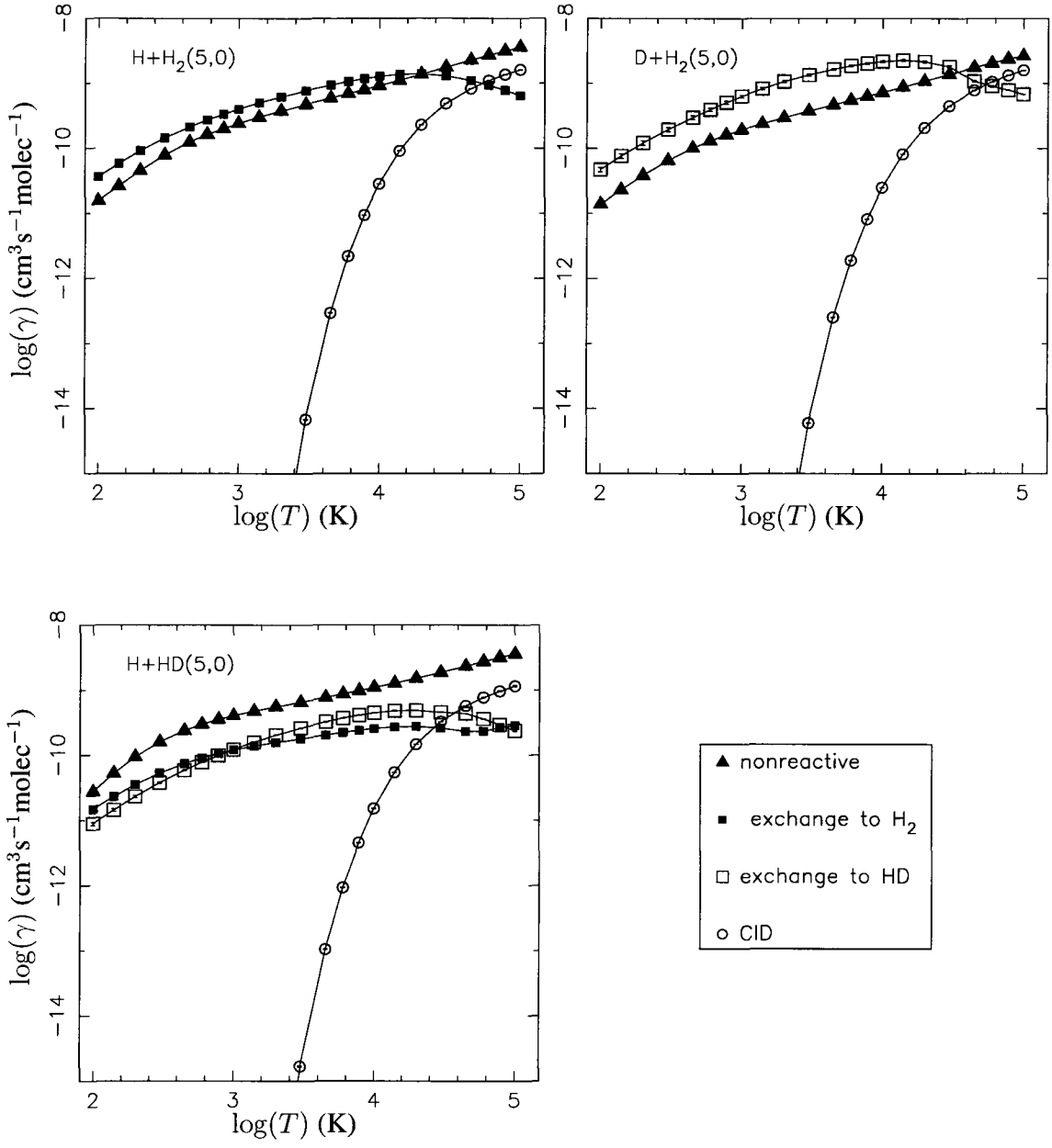

Figure 6.6: As in Figure 6.1, total rate coefficients from (5,0).

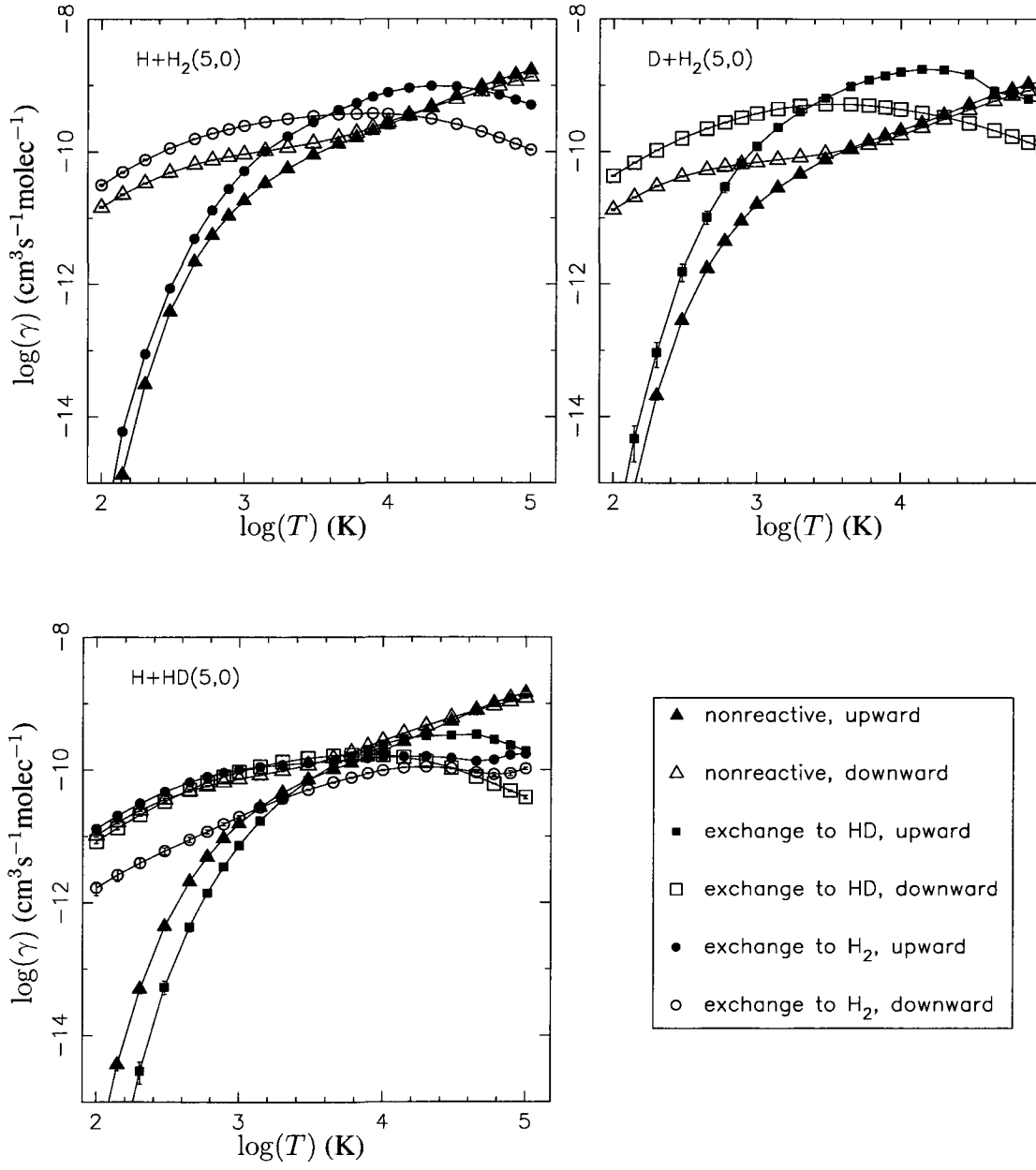

Figure 6.7: Total rate coefficients split into upward and downward components, as in Figure 6.3, but for (5,0).

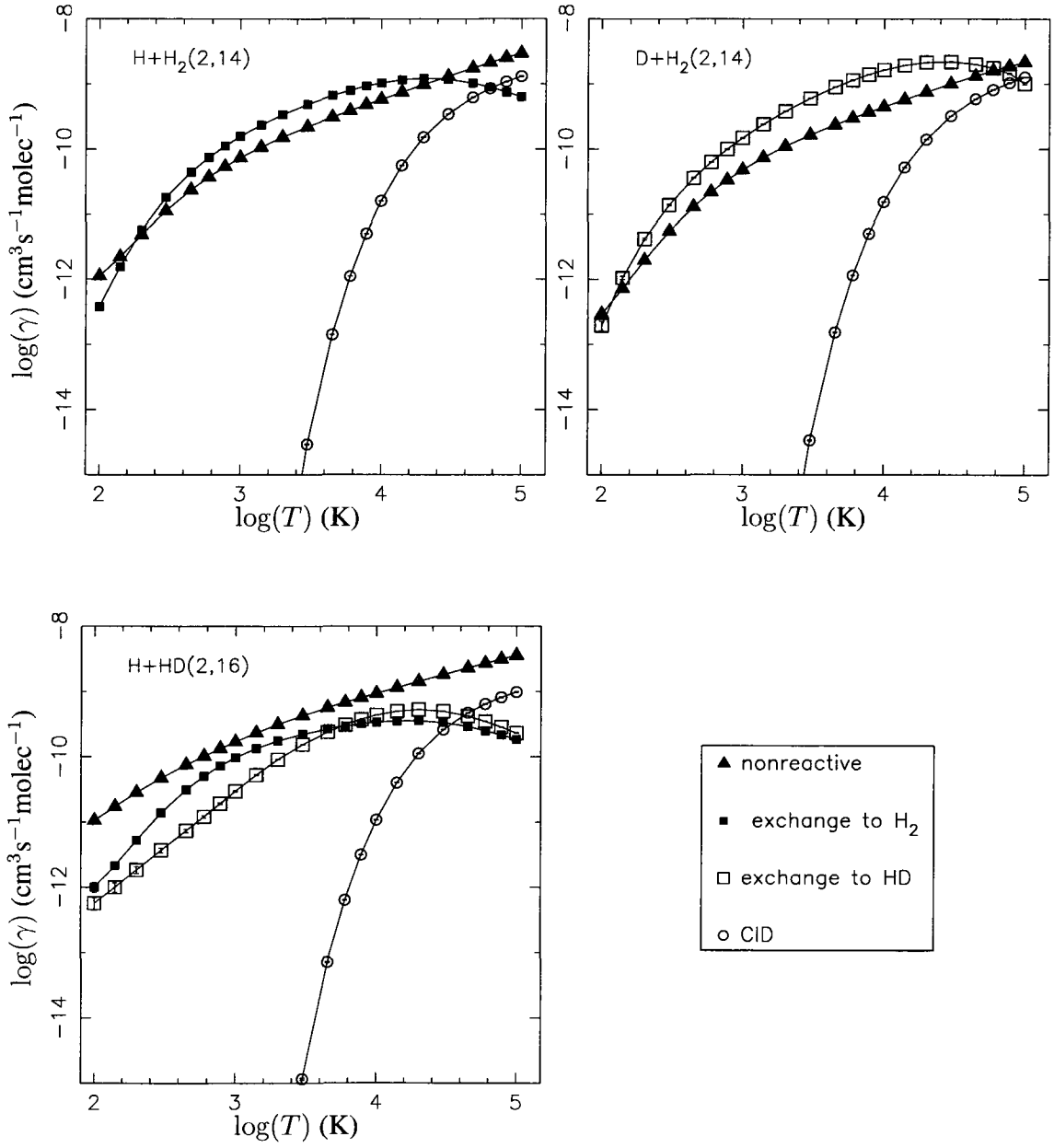

Figure 6.8: As in Figure 6.1, total rate coefficients from H + H_2(2,14), D + H_2(2,14), and H + HD(2,16).

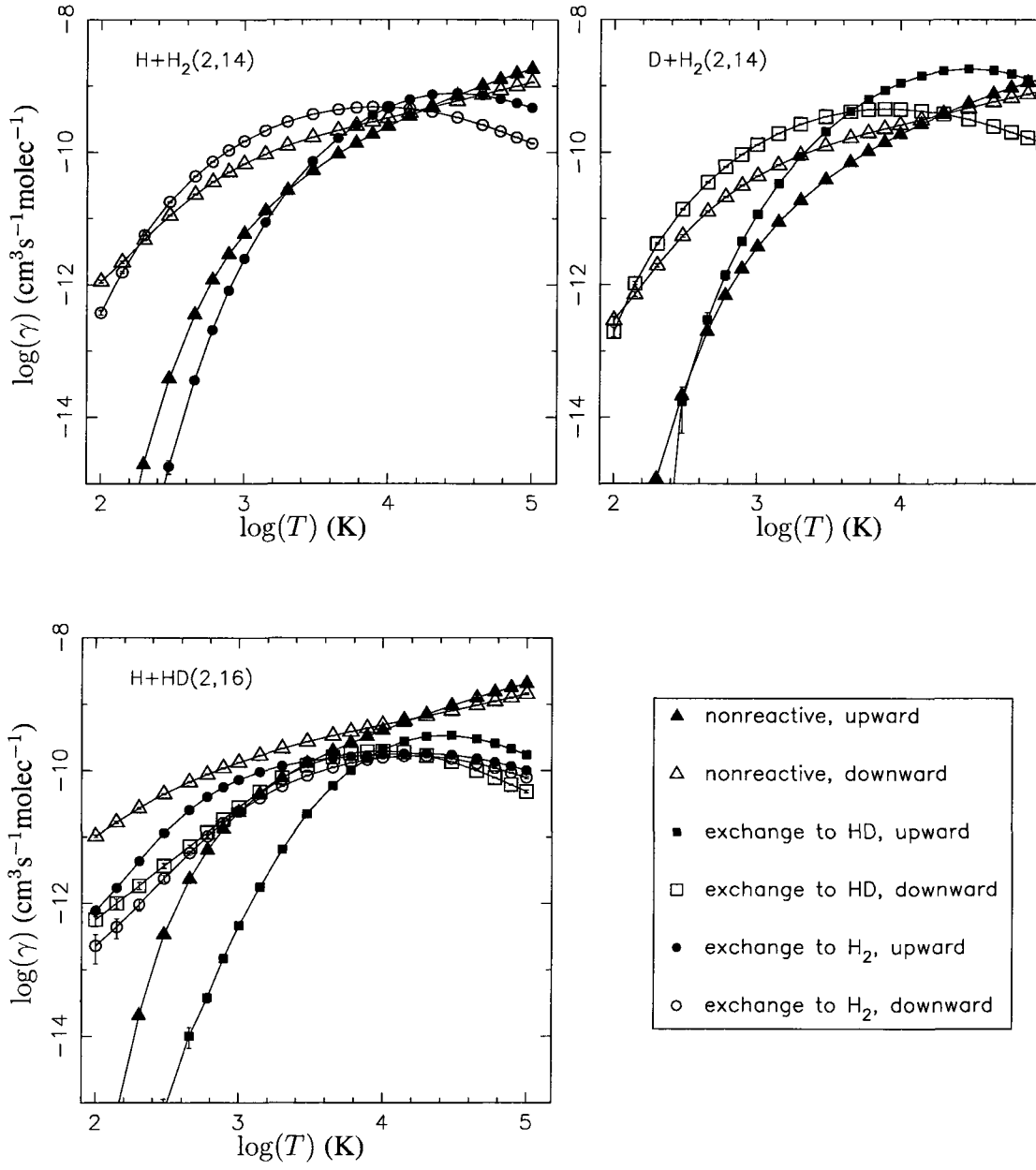

Figure 6.9: Total rate coefficients split into upward and downward components, as in Figure 6.3, but for H + H_2(2,14), D + H_2(2,14), and H + HD(2,16).

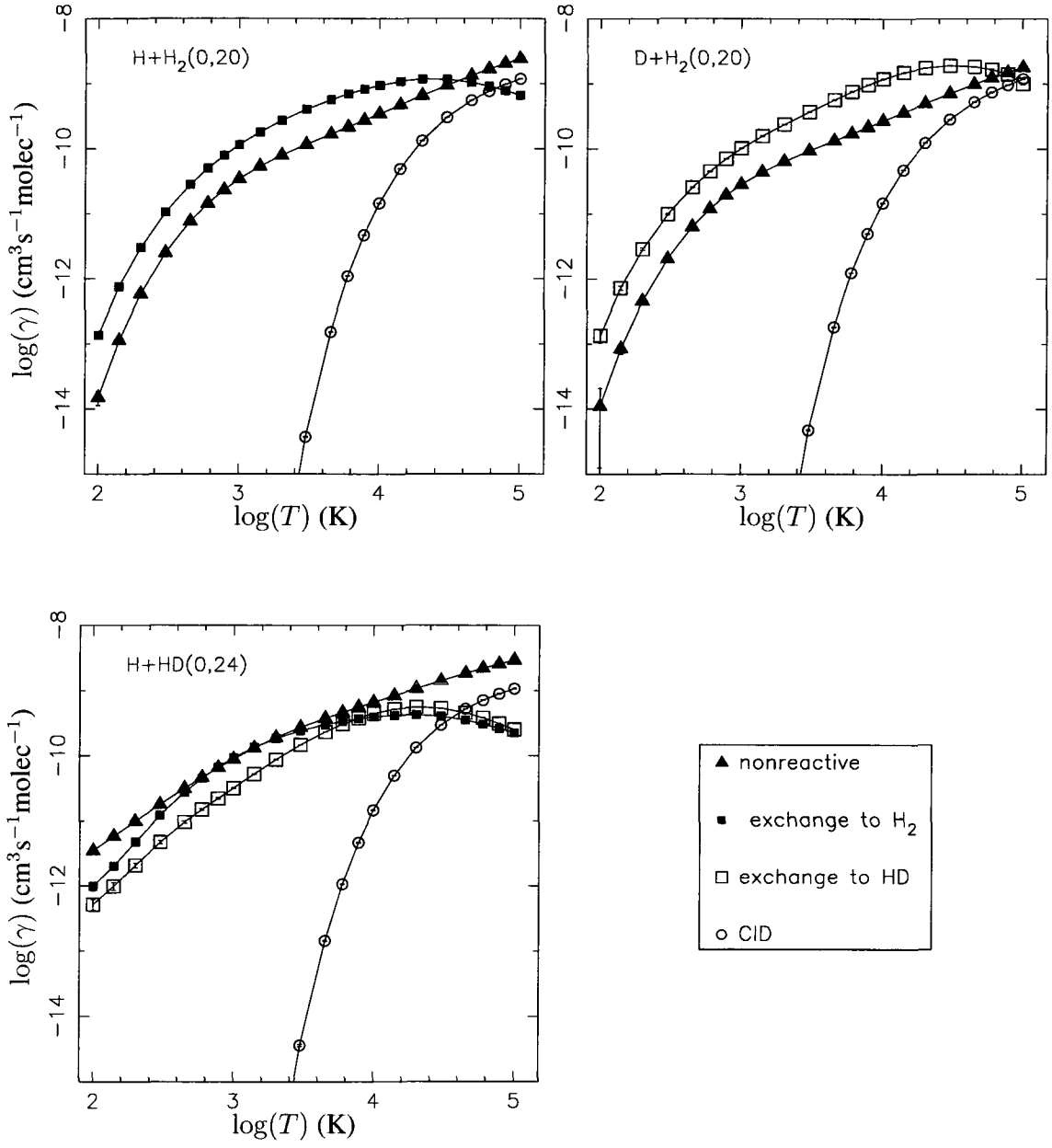

Figure 6.10: As in Figure 6.1, total rate coefficients from H + H_2(0,20), D + H_2(0,20), and H + HD(0,24).

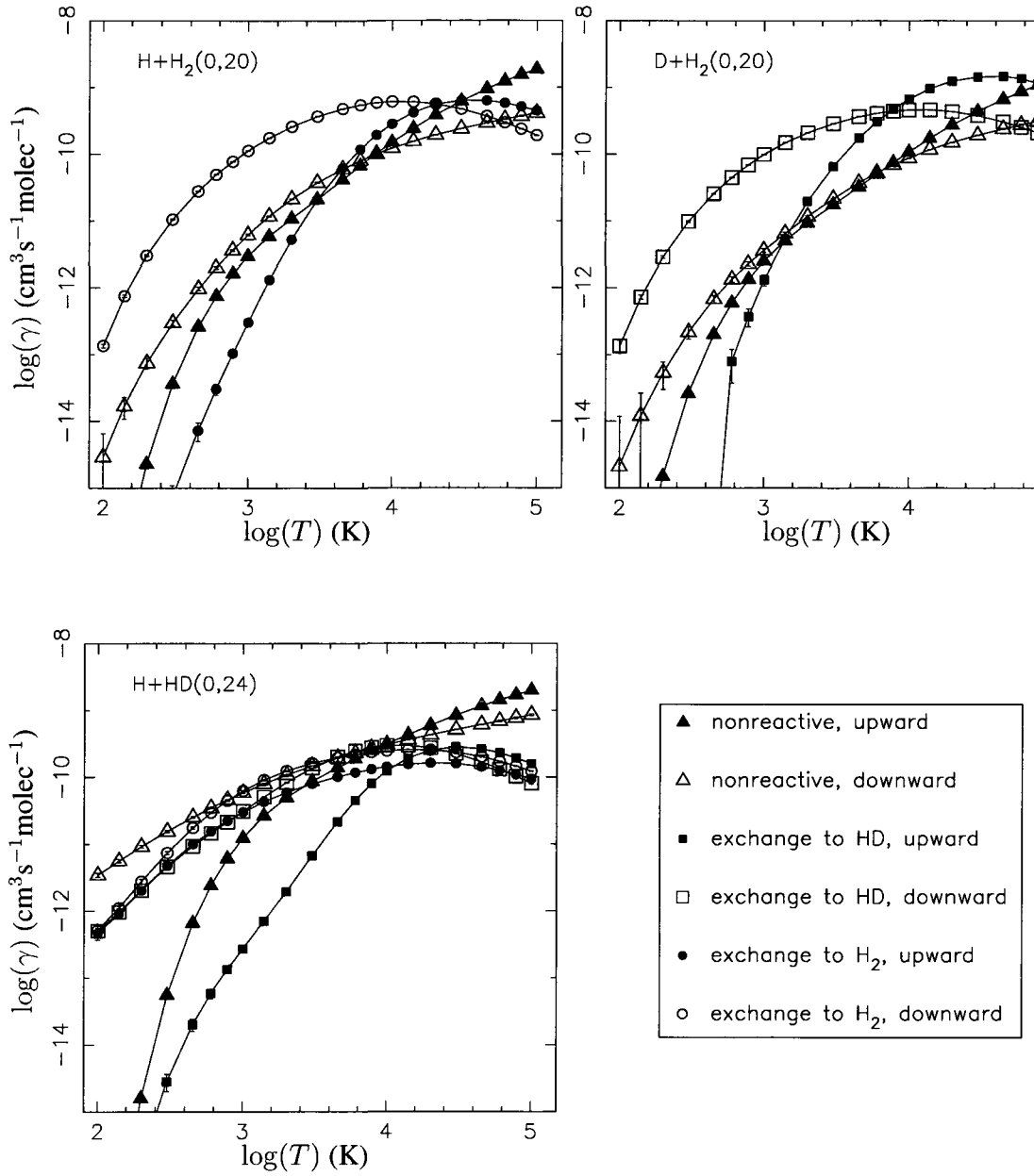

Figure 6.11: Total rate coefficients split into upward and downward components, as in Figure 6.3, but for H + H_2(2,14), D + H_2(2,14), and H + HD(2,16).

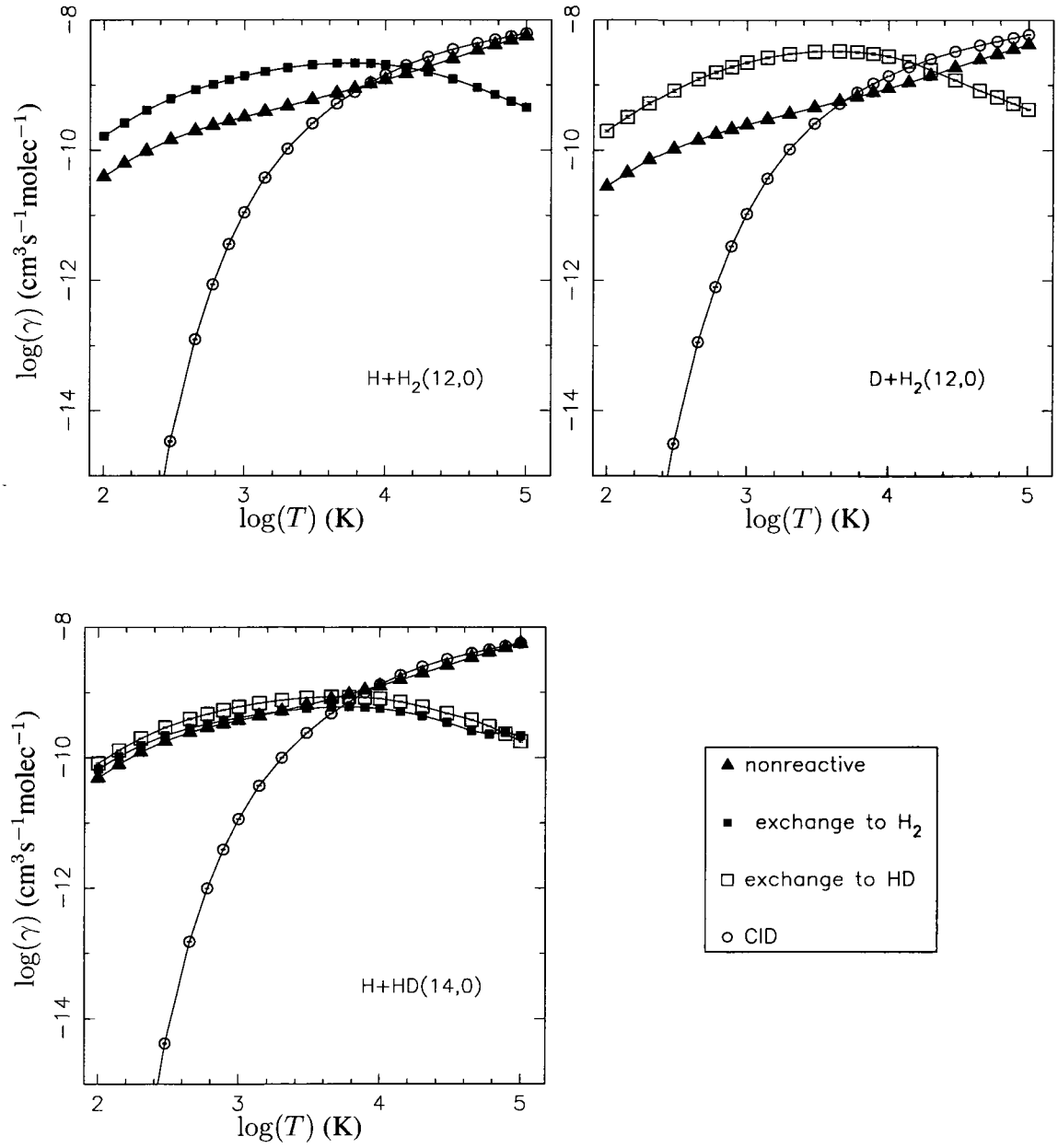

Figure 6.12: As in Figure 6.1, total rate coefficients from H + H_2(12,0), D + H_2(12,0), and H + HD(14,0).

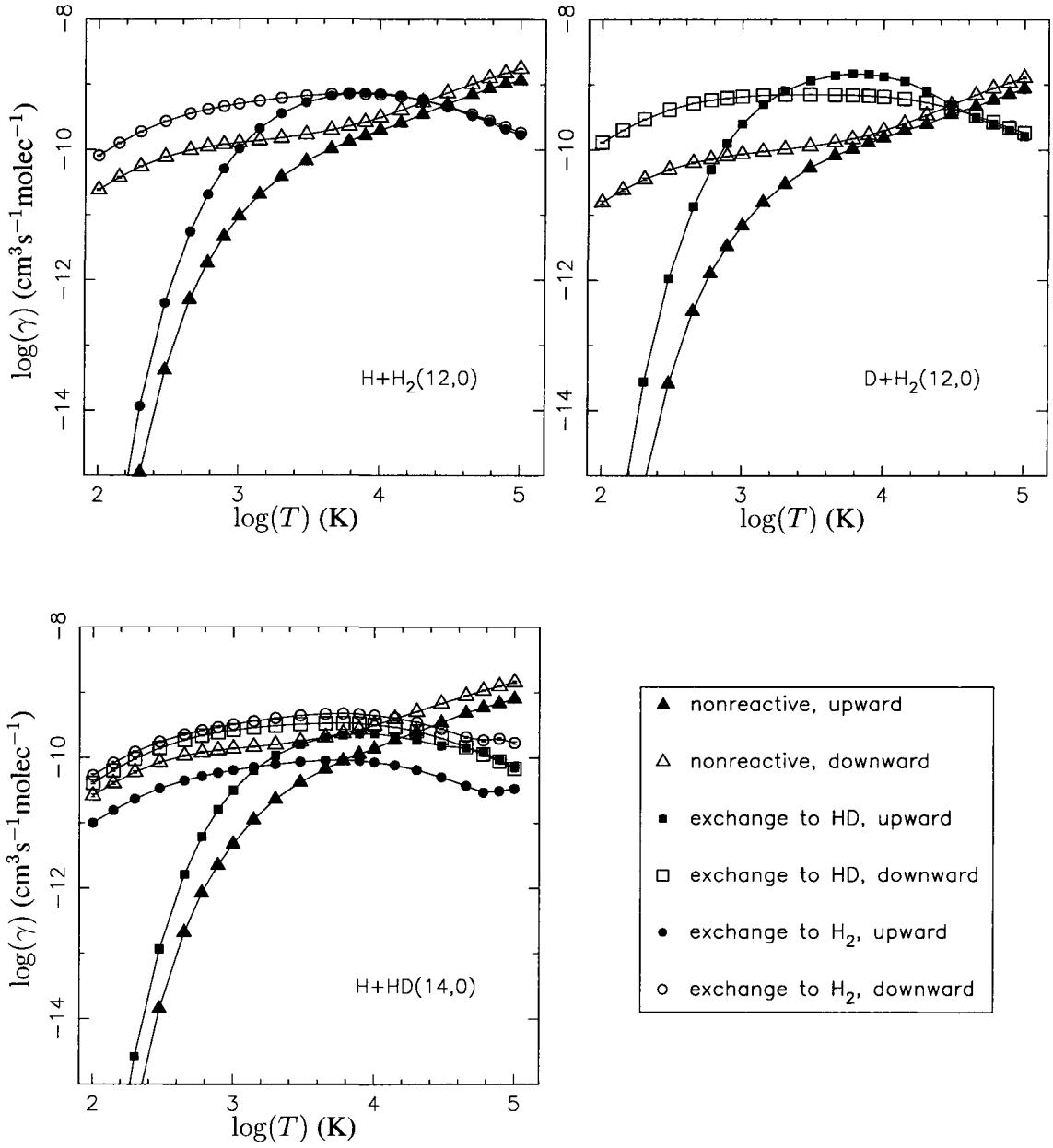

Figure 6.13: Total rate coefficients split into upward and downward components, as in Figure 6.3, but for H + H_2(12,0), D + H_2(12,0), and H + HD(14,0).

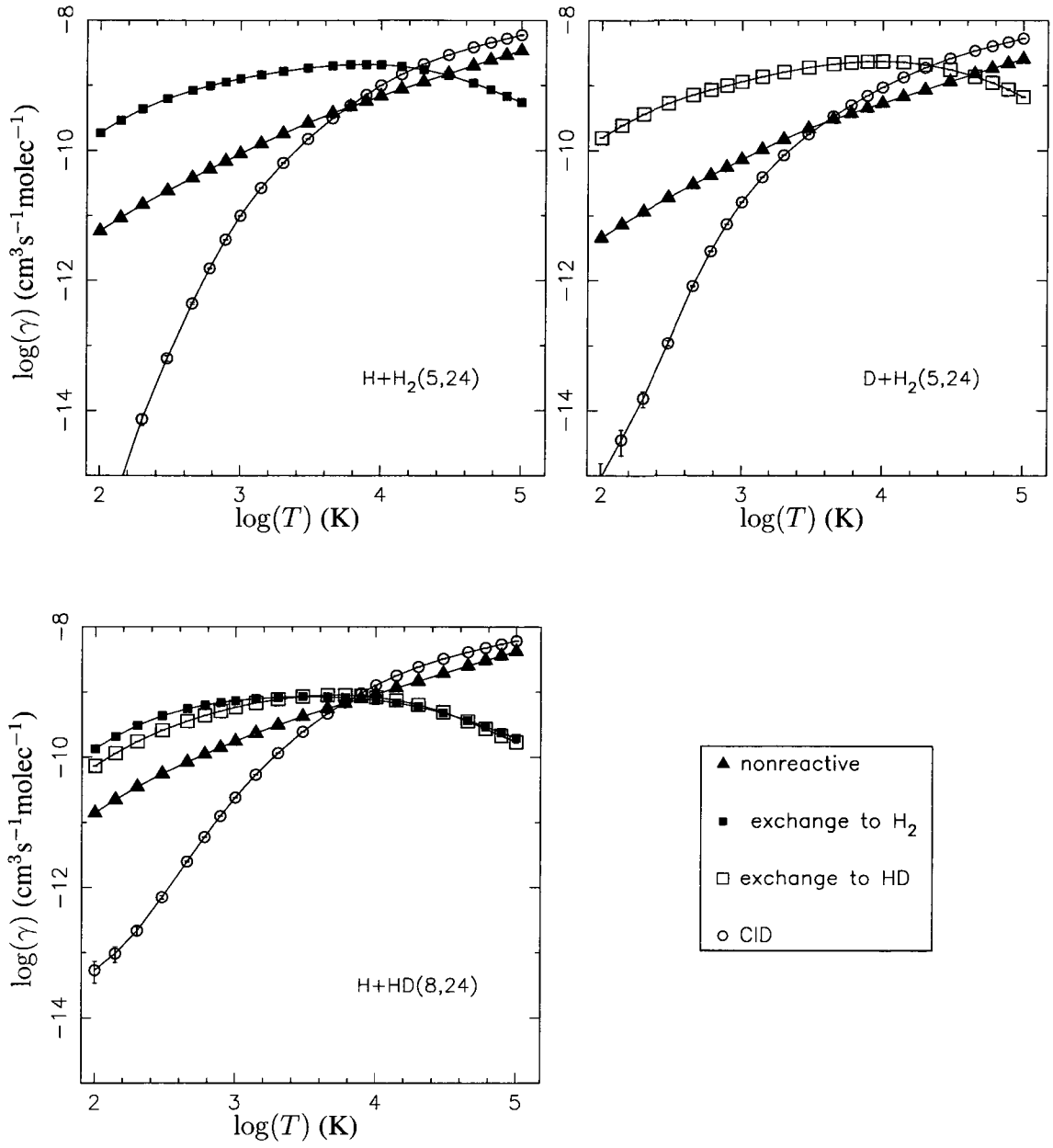

Figure 6.14: As in Figure 6.1, total rate coefficients from H + H_2(5,24), D + H_2(5,24), and H + HD(8,24).

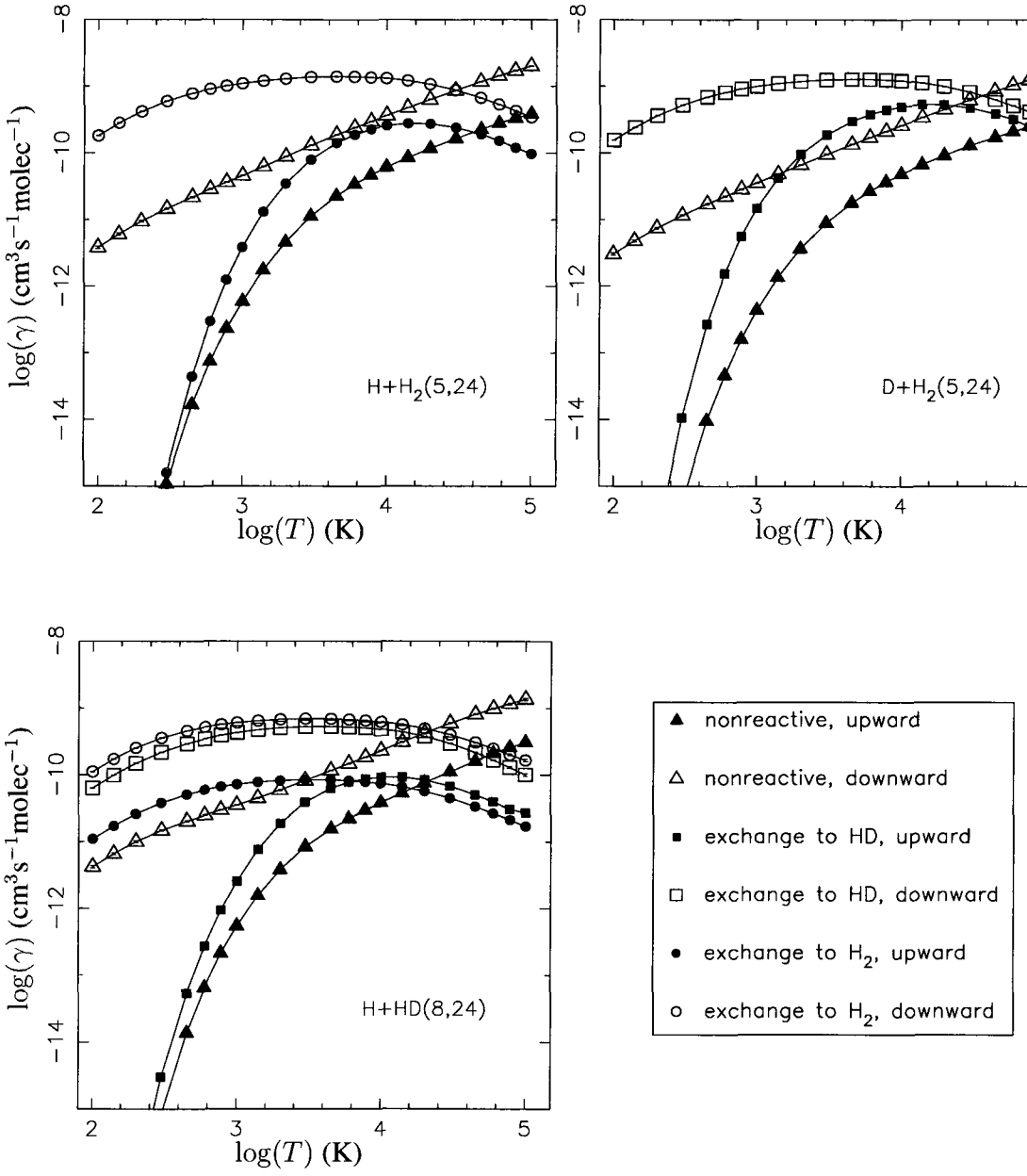

Figure 6.15: Total rate coefficients split into upward and downward components, as in Figure 6.3, but for H + H_2(5,24), D + H_2(5,24), and H + HD(8,24).

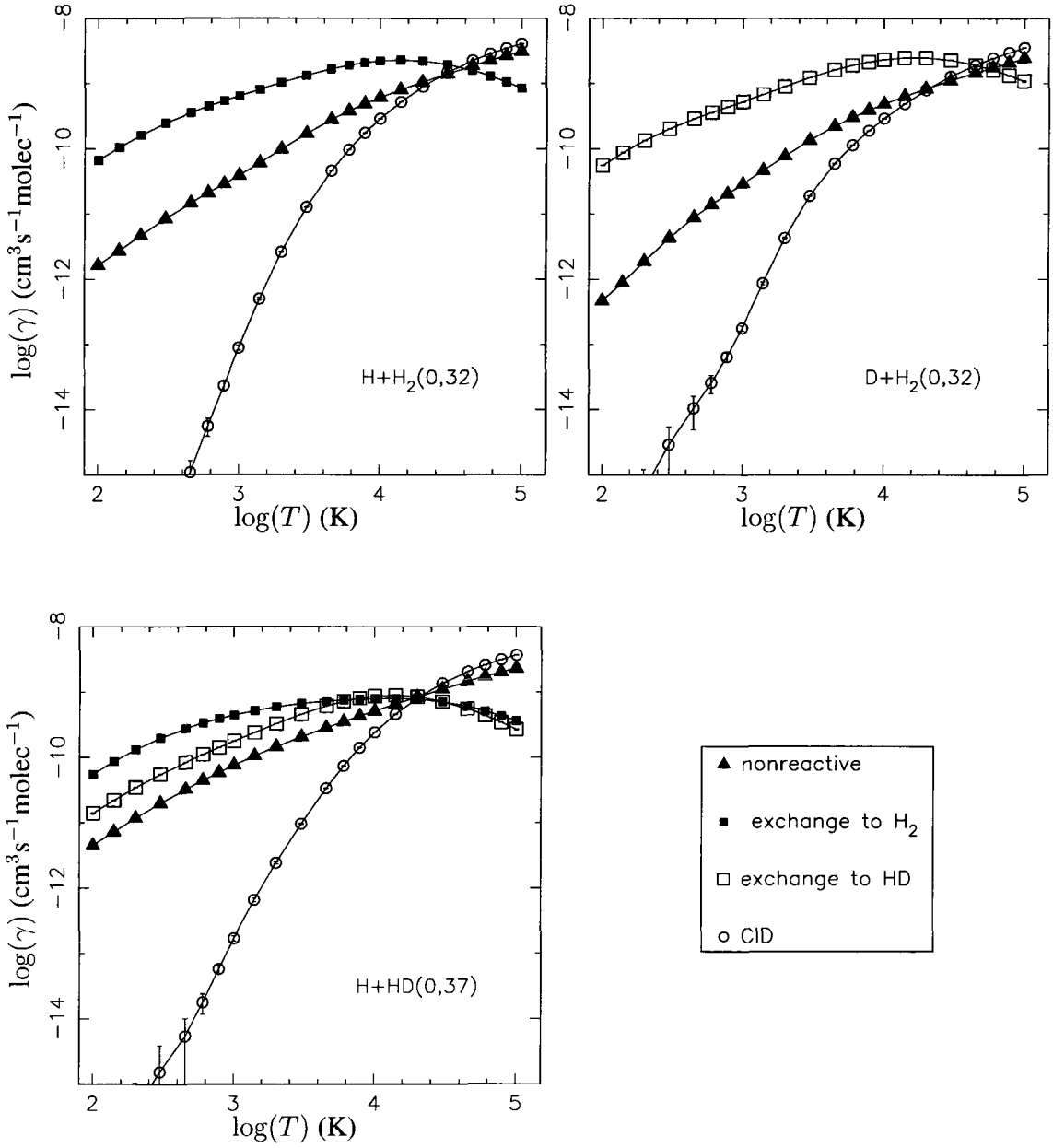

Figure 6.16: As in Figure 6.1, total rate coefficients from H + H_2(0,32), D + H_2(0,32), and H + HD(0,37).

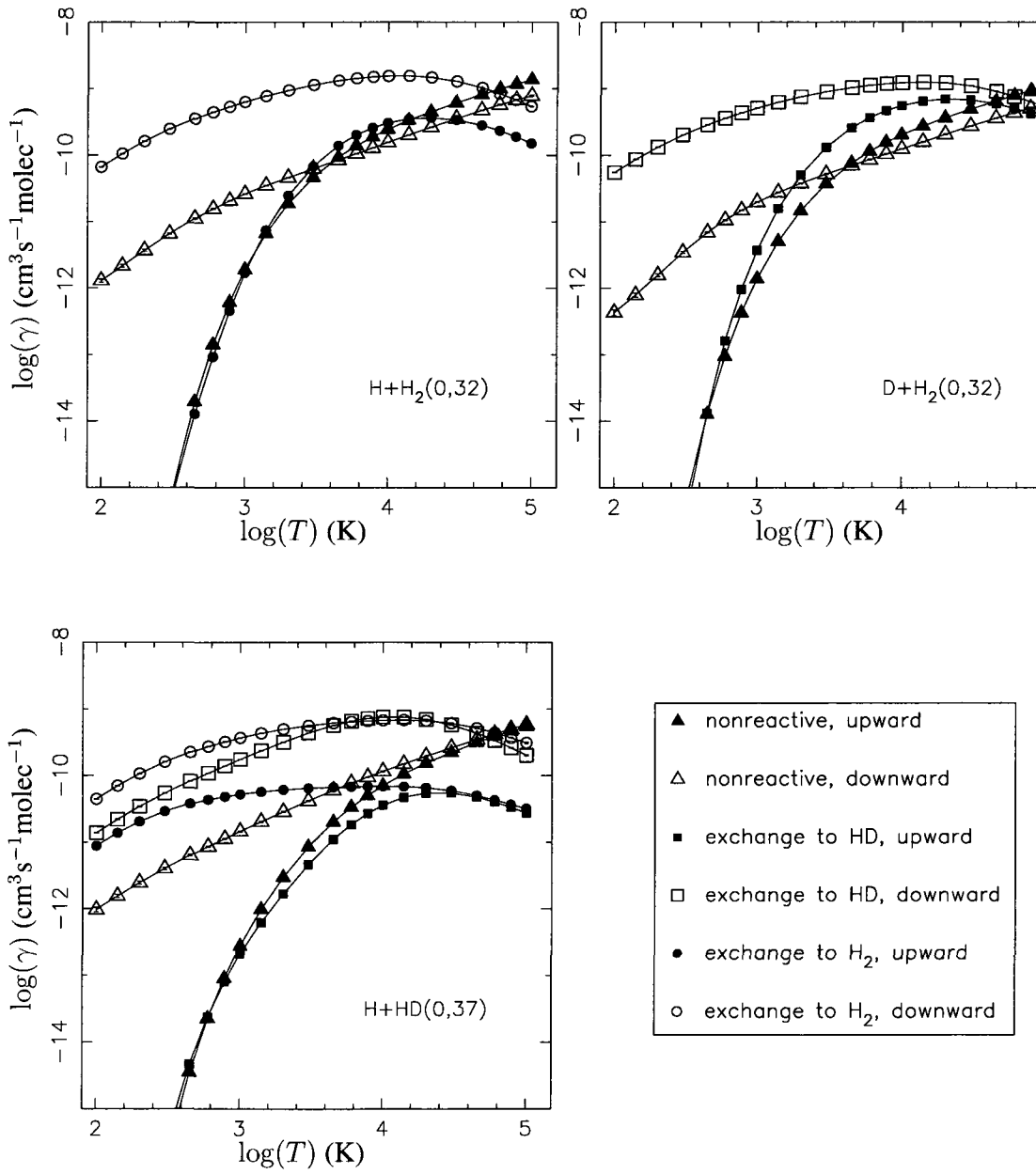

Figure 6.17: Total rate coefficients split into upward and downward components, as in Figure 6.3, but for H + H_2(0,32), D + H_2(0,32), and H + HD(0,37).

Chapter 7

Future directions

The primary motivation of this study is astrophysical, to obtain the cross sections and rate coefficients calculated here in order to integrate them into existing models of interstellar gases or planetary atmospheres. The most obvious future use of this data is in such applications.

Additionally, many questions pertaining to details of the dynamical behaviour of the systems under examination remain.

For systems with total energy slightly greater than that required for dissociation, it would be useful to understand precisely why the opacity functions for CID are greatest at an impact parameter near that corresponding to the outer turning point of the molecule, as opposed to an impact parameter corresponding to the centre of the molecular bond. A similar result is true for exchange reactions: exchange is most likely when the collider is aimed at the outer turning point. Is this because there is a greater chance of a close encounter between nuclei at this distance: do such trajectories tend to lead to compact configurations? A further analysis of the opacity functions for these processes would aid in answering these questions. Three–dimensional visualization of representative collisions may be beneficial for this purpose.

Further investigation into the apparent dynamical elevation of threshold for nonreactive energy transfer and exchange reactions is also warranted, especially since these thresholds have in previous studies been implicated in reducing QCT rate coefficients relative to accurate QM rate coefficients. Although the rate coefficients for the D + H_2 exchange reaction calculated in this study are greater than the corresponding quantum mechanical rate coefficients calculated

on the CCI surface because of the Born–Oppenheimer corrections made in the quantum calculations, it is desirable to understand the origins of the dynamical threshold elevation because of their potential applicability to systems involving heavier atoms, which may not have significant Born–Oppenheimer corrections. The rate coefficients for both nonreactive energy transfer and exchange reactions at lower temperatures could be improved both by determining these thresholds and by simulating many trajectories at low translational energies in 0.1 kcal mol^{-1} or smaller intervals, rather than the 1 kcal mol^{-1} intervals used in this study.

Some method of compensating for the Born–Oppenheimer approximation in the QCT method would be highly beneficial. This approximation makes the biggest difference between QCT and quantum mechanical results at most temperatures. With the number of trajectories computed in this study, the standard deviations of the rate coefficients are small. The roughly 3% difference which results from applying the Born–Oppenheimer correction at 2000 K is enough to shift the QM results from being significantly higher to being significantly lower than the QCT results. Perhaps an attempt could be made to systematically quantify the effect of the Born–Oppenheimer approximation on cross sections or rate coefficients. This could be accomplished by studying more massive isotopes of hydrogen, as in the studies of $D+D_2$, $^3H+^3H_2$, and so on. A scale factor $f(E_v, E_j, \mu)$, similar to a steric factor, might be applied to QCT results for collisions for systems with mass μ, vibrational energy E_v, and rotational energy E_j. For systems with high mass, the scale factors would be close to 1, but the scale factors would be greater than 1 for $H + H_2$, $D + H_2$, and H + HD. Such a scale factor might then be related to Equation 1.5 in Section 1.1.1.

Many of the arguments made in this work depend upon the mechanisms for energy transfer, either insertion or abstraction, and how the effectiveness of each mechanism is affected by the speed of the collider, and in particular, the total collision time. The collision times used here were estimates. It may be illuminating to gather data on the average collision times for various processes and attempt to correlate those to the trajectory results which follow. Calculation of the opacity functions for the state–to–state and total processes discussed may give

further information about each mechanism.

Certain collisions are more important than others. In particular, accurate determination of the dynamical thresholds of various processes is important. A finer translational energy grid near the energetic threshold for CID would help in the calculation of rate coefficients for CID. For nonreactive energy transfer and exchange, more trajectories at low translational energies for downward transitions would be useful because of the application of microscopic reversibility to the rate coefficients.

Bibliography

[1] V. AQUILANTI, M. BARTOLOMEI, D. CAPPELLETTI, E. CARMONA–NOVILLO, and F. PIRANI, **J. Chem. Phys. 117**, 615 (2002).

[2] M. MEUWLY and J. M. HUTSON, **PCCP 2**, 441 (2000).

[3] R. D. LEVINE and R. B. BERNSTEIN, **Molecular Reaction Dynamics**, p. 210, Clarendon Press, 1974.

[4] F. J. AOIZ, L. BANARES, and V. J. HERRERO, **Int. Rev. Phys. Chem. 24**, 119 (2005).

[5] I. N. LEVINE, **Quantum Chemistry**, p. 345, Prentice–Hall, Inc., Englewood Cliffs, New Jersey, 4 edition, 1991.

[6] D. W. SCHWENKE, **J. Phys. Chem. A 105**, 2352 (2001).

[7] B. C. GARRETT and D. G. TRUHLAR, **J. Chem. Phys. 82**, 4543 (1985).

[8] M. E. MANDY, P. G. MARTIN, and W. J. KEOGH, **J. Chem. Phys. 100**, 2671 (1994).

[9] M. E. MANDY and P. G. MARTIN, **J. Chem. Phys. 97**, 265 (1992).

[10] D. W. SCHWENKE, **J. Chem. Phys. 89**, 2076 (1988).

[11] S. LEPP and J. M. SHULL, **ApJ 270**, 578 (1983).

[12] J. E. DOVE, A. C. M. RUSK, P. H. CRIBB, and P. G. MARTIN, **ApJ 318**, 379 (1987).

[13] E. HABART, M. WALMSLEY, L. VERSTRAETE, S. CAZAUX, R. MAIOLINO, P. COX, F. BOULANGER, and G. PINEAU DES FORÊTS, **Space Science Reviews 119**, 71 (2005).

[14] F. BERTOLDI, R. TIMMERMANN, D. ROSENTHAL, S. DRAPATZ, and C. M. WRIGHT, **Astron. Astrophys. 346**, 267 (1999).

[15] M. TREFLER and H. P. GUSH, **Phys. Rev. Lett. 20**, 703 (1968).

[16] A. DALGARNO and E. L. WRIGHT, **ApJ 174**, L49 (1972).

[17] A. LIPOVKA, R. NÚÑEZ-LÓPEZ, and V. AVILA-REESE, **MNRAS 361**, 850 (2005).

[18] C. PARKINSON, J. MCCONNELL, L. BEN JAFFEL, A.-T. LEE, Y. YUNG, and E. GRIFFIOEN, **Icarus 183**, 451 (2006).

[19] H. R. MAYNE and J. P. TOENNIES, **J. Chem. Phys. 75**, 1794 (1981).

[20] H. BUCHENAU, J. P. TOENNIES, J. ARNOLD, and J. WOLFRUM, **Ber. Bunsen-Ges. Phys. Chem. 94**, 1231 (1990).

[21] F. LONDON, **Probleme der modernen Physik**, 1928.

[22] M. KARPLUS, R. N. PORTER, and R. D. SHARMA, **J. Chem. Phys. 43**, 3259 (1965).

[23] F. J. AOIZ, L. BANARES, T. DIEZROJO, V. J. HERRERO, and V. S. RABANOS, **J. Phys. Chem. 100**, 4071 (1996).

[24] B. LIU, **J. Chem. Phys. 58**, 1925 (1973).

[25] R. B. BERNSTEIN and R. D. LEVINE, **Chem. Phys. Lett. 29**, 314 (1974).

[26] A. KUPPERMANN, G. C. SCHATZ, and M. BAER, **J. Chem. Phys. 65**, 4596 (1976).

[27] G. C. SCHATZ and A. KUPPERMANN, **J. Chem. Phys. 65**, 4668 (1976).

[28] P. SIEGBAHN and B. LIU, **J. Chem. Phys. 68**, 2457 (1978).

[29] D. G. TRUHLAR and C. J. HOROWITZ, **J. Chem. Phys. 68**, 2466 (1978).

[30] D. G. TRUHLAR and C. J. HOROWITZ, **J. Chem. Phys. 71**, 1514 (1979).

[31] A. I. BOOTHROYD, W. J. KEOGH, P. G. MARTIN, and M. R. PETERSON, **J. Chem. Phys. 104**, 7139 (1996).

[32] Y. SUN and A. DALGARNO, **ApJ 427**, 1053 (1994).

[33] T. J. PARK and J. C. LIGHT, **J. Chem. Phys. 94**, 2946 (1991).

[34] S. L. MIELKE, G. C. LYNCH, D. G. TRUHLAR, and D. W. SCHWENKE, **J. Phys. Chem. 98**, 8000 (1994).

[35] B. C. GARRETT and D. G. TRUHLAR, **Proc. Nat. Acad. Sci. 76**, 4755 (1979).

[36] B. C. GARRETT and D. G. TRUHLAR, **J. Chem. Phys. 72**, 3460 (1980).

[37] B. C. GARRETT, D. G. TRUHLAR, A. J. C. VARANDAS, and N. C. BLAIS, **Int. J. Chem. Kinet. 18**, 1065 (1986).

[38] H. R. MAYNE and J. P. TOENNIES, **J. Chem. Phys. 73**, 217 (1980).

[39] H. R. MAYNE and J. P. TOENNIES, **J. Chem. Phys. 74**, 1017 (1981).

[40] E. B. GORDON, B. I. IVANOV, A. B. PERMINOV, V. G. BALALAEV, A. N. PONOMAREV, and V. V. FITATOV, **Chem. Phys. Lett. 58**, 425 (1978).

[41] V. B. ROZENSHTEIN, Y. M. GERSHENZON, A. V. IVANOV, S. D. IL'IN, S. I. KUCHERYAVII, and S. Y. UMANSKII, **Chem. Phys. Lett. 121**, 89 (1985).

[42] T. DREIER and J. WOLFRUM, **Int. J. Chem. Kinet. 18**, 919 (1986).

[43] A. J. C. VARANDAS, **Molec. Phys. 53**, 1303 (1984).

[44] A. J. C. VARANDAS, F. B. BROWN, C. A. MEAD, D. G. TRUHLAR, and N. BLAIS, **J. Chem. Phys. 86**, 6258 (1987).

[45] F. J. AOIZ, V. J. HERRERO, and V. SAEZ, **Chem. Phys. Lett. 161**, 270 (1989).

[46] F. J. AOIZ, V. J. HERRERO, and C. S. RABANOS, **J. Chem. Phys. 97**, 7423 (1992).

[47] F. J. AOIZ, H. K. BUCHENAU, V. J. HERRERO, and C. S. RABANOS, **J. Chem. Phys. 100**, 2789 (1994).

[48] M. MLADENOVIC, M. ZHAO, D. G. TRUHLAR, D. W. SCHWENKE, Y. SUN, and D. J. KOURI, **J. Phys. Chem. 92**, 7035 (1988).

[49] J. C. MICHAEL and J. R. FISHER, **J. Phys. Chem. 94**, 3318 (1990).

[50] J. V. MICHAEL, J. R. FISHER, J. M. BOWMAN, and Q. Y. SUN, **Science 249**, 269 (1990).

[51] N. C. BLAIS, M. S. ZHAO, D. G. TRUHLAR, D. W. SCHWENKE, and D. J. KOURI, **Chem. Phys. Lett. 166**, 11 (1990).

[52] S. L. MIELKE, R. S. FRIEDMAN, D. G. TRUHLAR, and D. W. SCHWENKE, **Chem. Phys. Lett. 188**, 359 (1992).

[53] W. J. KEOGH, A. I. BOOTHROYD, P. G. MARTIN, S. L. MIELKE, D. G. TRUHLAR, and D. W. SCHWENKE, **Chem. Phys. Lett. 195**, 144 (1992).

[54] D. A. V. KLINER, D. E. ADELMAN, and R. N. ZARE, **J. Chem. Phys. 95**, 1648 (1991).

[55] K. D. RINNEN, D. A. V. KLINER, and R. N. ZARE, **J. Chem. Phys. 91**, 7514 (1989).

[56] R. S. BLAKE, K. D. RINNEN, D. A. V. KLINER, and R. N. ZARE, **Chem. Phys. Lett. 153**, 365 (1988).

[57] D. A. V. KLINER, K. D. RINNEN, and R. N. ZARE, **Chem. Phys. Lett. 166**, 107 (1990).

[58] D. A. V. KLINER and R. N. ZARE, **J. Chem. Phys. 92**, 2107 (1990).

[59] S. TAKADA, A. OHSAKI, and H. NAKAMURA, **J. Chem. Phys. 96**, 339 (1992).

[60] D. E. ADELMAN, N. E. SHAFER, D. A. V. KLINER, and R. N. ZARE, **J. Chem. Phys. 97**, 7323 (1992).

[61] D. NEUHAUSER, R. S. JUDSON, D. J. KOURI, D. E. ADELMAN, N. E. SHAFER, D. A. V. KLINER, and R. N. ZARE, **Science 257**, 519 (1992).

[62] A. I. BOOTHROYD, W. J. KEOGH, P. G. MARTIN, and M. R. PETERSON, **J. Chem. Phys. 95**, 4343 (1991).

[63] L. BANARES, F. J. AOIZ, and V. J. HERRERO, **Phys. Scr. 73**, C6 (2006).

[64] S. L. MIELKE, B. C. GARRETT, and K. A. PETERSON, **J. Chem. Phys. 116**, 4142 (2002).

[65] S. L. MIELKE, K. A. PETERSON, D. W. SCHWENKE, B. C. GARRETT, D. G. TRUHLAR, J. V. MICHAEL, M. C. SU, and J. W. SUTHERLAND, **Phys. Rev. Lett. 91**, 063201 (2003).

[66] M. HANKEL, S. C. SMITH, R. J. ALLAN, S. K. GRAY, and G. G. BALINT-KURTI, **J. Chem. Phys. 126**, 164303 (2006).

[67] P. J. KUNTZ, E. M. NEMETH, J. C. POLANYI, S. D. ROSNER, and C. E. YOUNG, **J. Chem. Phys. 44**, 1168 (1966).

[68] J. ESPINOSA-GARCIA, **J. Phys. Chem. A 105**, 134 (2001).

[69] Y. S. M. WU, A. KUPPERMANN, and J. B. ANDERSON, **PCCP 1**, 929 (1999).

[70] J. L. SCHREIBER, PhD thesis, University of Toronto, 1973.

[71] M. E. MANDY, Master's thesis, University of Toronto, 1980.

[72] M. G. KENDALL and A. STUART, **The Advanced Theory of Statistics**, volume 2, C. Griffin: London, 4 edition, 1979.

[73] M. E. MANDY and G. J. MCNAMARA, **J. Phys. Chem. A 110**, 422 (2005).

[74] J. E. DOVE, M. E. MANDY, N. SATHYAMURTHY, and T. JOSEPH, **Chem. Phys. Lett. 127**, 1 (1986).

[75] J. E. DOVE, M. E. MANDY, V. MOHAN, and N. SATHYAMURTHY, **J. Chem. Phys. 92**, 7373 (1990).

[76] J. E. DOVE and H. TEITELBAUM, **Chem. Phys. 40**, 87 (1979).

[77] E. ROUEFF and D. R. FLOWER, **MNRAS 305**, 353 (1999).

[78] J. I. STEINFELD, J. S. FRANCISCO, and W. L. HASE, **Chemical Kinetics and Dynamics**, chapter 8, p. 218, Prentice-Hall, Inc., 2 edition, 1999.

[79] A. G. G. M. TIELENS, **The Physics and Chemistry of the Interstellar Medium**, chapter 2, Cambridge University Press, The Edinburgh Building, Cambridge CB2 2RU, UK, 2005.

[80] P. G. MARTIN and M. E. MANDY, **ApJ 455**, L63 (1995).

Appendix A

Energy levels of H_2 and HD

Table A.1: Internal energies (kcal mol^{-1}) for selected states of H_2 and HD. The energy at infinite separation is 109.5 kcal mol^{-1}.

H_2 state	(0,0)	(1,0)	(5,0)	(12,0)	(0,8)
E_{int}	6.225	18.127	59.118	104.332	17.811
H_2 state	(2,14)	(0,20)	(5,24)	(0,32)	
E_{int}	57.052	61.169	110.185	110.754	
HD state	(0,0)	(1,0)	(5,0)	(14,0)	(0,8)
E_{int}	5.404	15.793	52.358	104.542	14.239
HD state	(2,16)	(0,24)	(8,24)	(0,37)	
E_{int}	53.202	63.609	109.914	110.306	

Table A.2: Internal energies (kcal mol^{-1}) for states of H_2 and HD below 1 eV (23.06 kcal mol^{-1}). The energy at infinite separation is 109.5 kcal mol^{-1}.

H_2 state	(0,0)	(0,1)	(0,2)	(0,3)	(0,4)	(0,5)	(0,6)	(0,7)
E_{int}	6.225	6.563	7.238	8.242	9.567	11.201	13.130	15.339
H_2 state	(0,8)	(0,9)	(1,0)	(1,1)	(1,2)	(1,3)	(1,4)	(1,5)
E_{int}	17.811	20.528	18.127	18.449	19.090	20.043	21.301	22.852
HD state	(0,0)	(0,1)	(0,2)	(0,3)	(0,4)	(0,5)	(0,6)	(0,7)
E_{int}	5.404	5.659	6.168	6.296	7.930	9.171	10.643	12.336
HD state	(0,8)	(0,9)	(0,10)	(0,11)	(1,0)	(1,1)	(1,2)	(1,3)
E_{int}	14.239	16.342	18.633	21.101	15.792	16.037	16.523	17.249
HD state	(1,4)	(1,5)	(1,6)	(1,7)				
E_{int}	18.209	19.396	20.803	22.421				

Table A.3: Nuclear separation in angstroms at the turning points for selected (v, j) states of H_2 and HD, given as inner–outer.

H_2	(0,0) 0.63–0.88	(1,0) 0.57–1.01	(5,0) 0.47–1.41	(12,0) 0.42–2.37	(0,8) 0.67–0.93
H_2	(2,14) 0.63–1.26	(0,20) 0.83–1.12	(5,24) 0.72–2.01	(0,32) 1.10–1.46	
HD	(0,0) 0.64–0.87	(1,0) 0.58–0.99	(5,0) 0.48–1.34	(14,0) 0.42–2.38	(0,8) 0.67–0.90
HD	(2,16) 0.64–1.22	(0,24) 0.85–1.12	(8,24) 0.64–2.18	(0,37) 1.11–1.45	

Table A.4: Times for movement to the centre of mass for head–on ($b = 0$) non–interactive collisions of H + H_2 and isotopic analogues at selected translational energies. This provides a way of gauging the amount of interaction time available to these systems. Times are in 10^{-16} s.

E_{trans} (kcal mol^{-1})	H + H_2	D + H_2	H + HD
1	1984	2429	2104
10	627	768	665
50	281	343	298
100	198	243	210
200	140	172	149
300	115	140	121

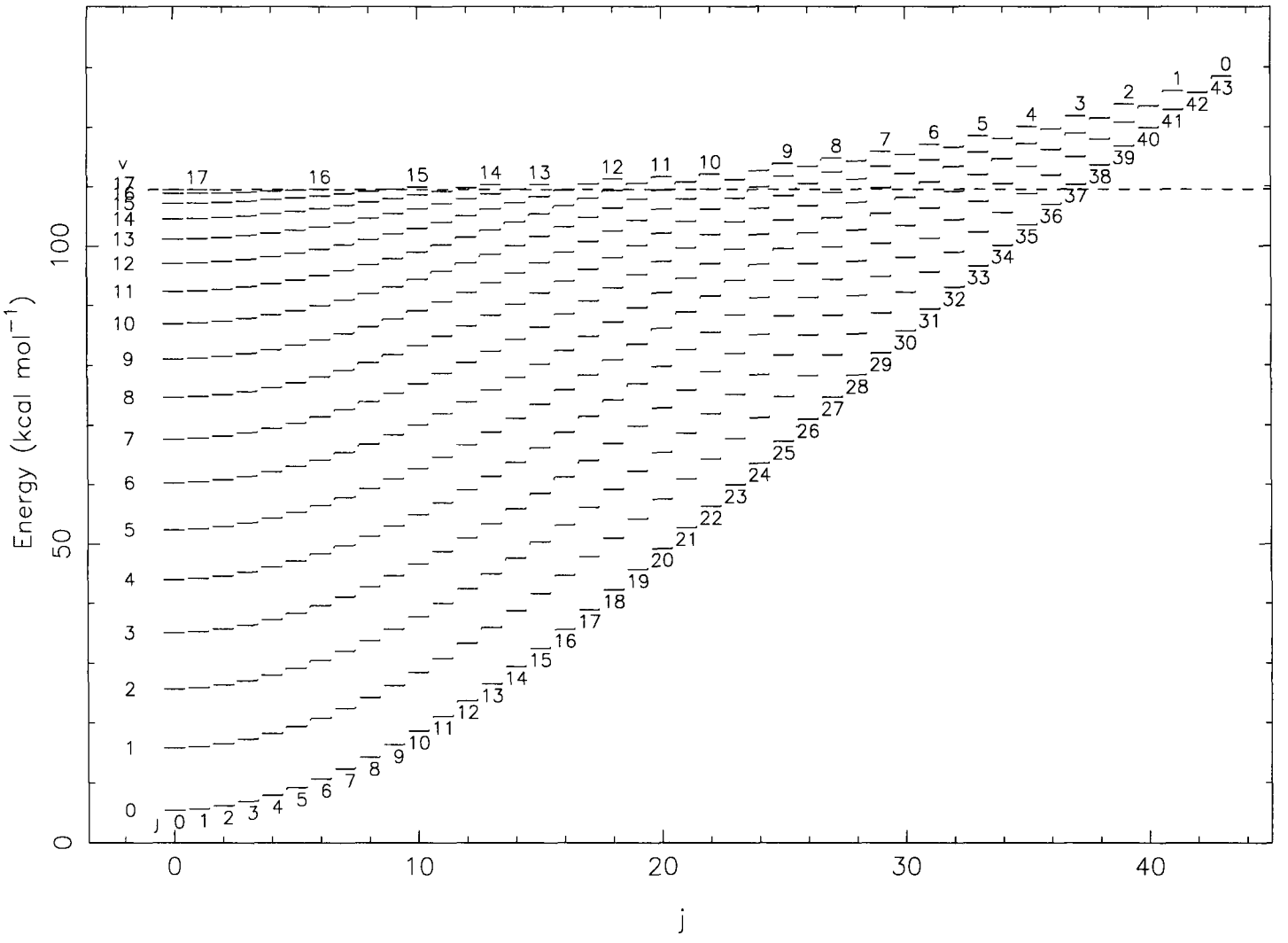

Figure A.1: HD energy levels. Vibrational manifolds are labelled down the left hand side and across the top, while rotational levels are indicated by numbers beneath the $(0, j)$ states. The dotted line indicates the dissociation energy. States above the dissociation energy are called quasibound: although classically bound, they have only finite lifetimes from a quantum perspective.

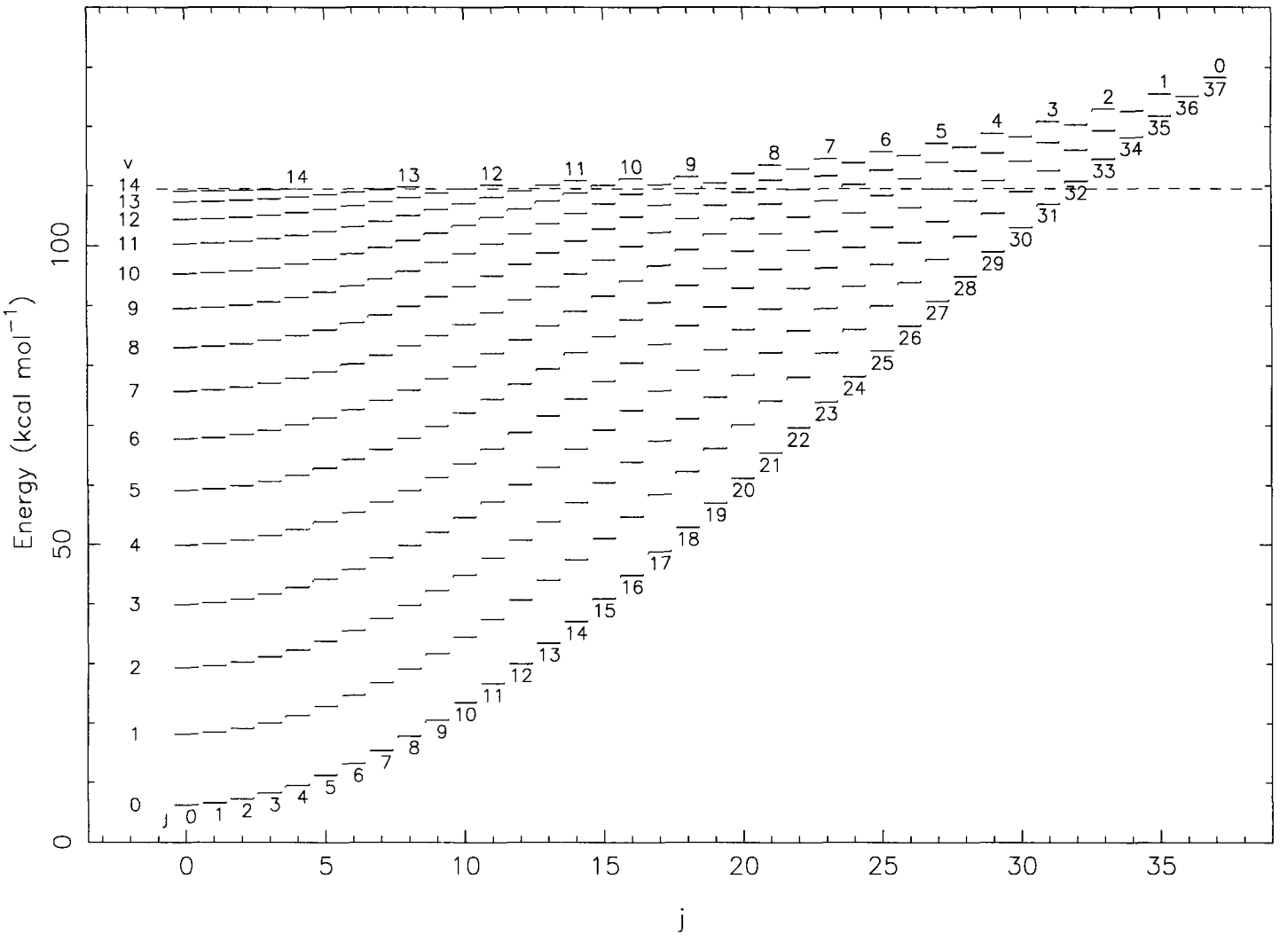

Figure A.2: As in Figure A.1, but for H_2.

Appendix B

Outcome counts of selected batches of trajectories

Table B.1: Number of trajectories per 1000 leading to nonreactive energy transfer, exchange outcomes, and CID for H + H_2(0,0), D + H_2(0,0), and H + HD(0,0). Column headers are translational energies in kcal mol^{-1}. Row headers are impact parameter strata. Within each stratum, counts are divided into nonreactive energy transfer (denoted n.r.), exchange to H_2 (denoted ex. H_2), exchange to HD (denoted ex. HD), and CID.

		H + H_2(0,0)					D + H_2(0,0)					H + HD(0,0)				
		6	10	55	110	300	6	10	55	110	300	6	10	55	110	300
< 0.5 Å	n.r.	84.7	401	234.3	212.8	180.7	278	443	179	122.1	67	854	780	243	285.3	338
	ex. H_2	0	213.3	747.3	786	364.7						0	65	215	180	214
	ex. HD						0	268	810	877.1	556	0	96	536	533.9	108
	CID	0	0	0	0.1	454	0	0	0	0.1	377	0	0	0	0.7	340
< 1.0 Å	n.r.	0	343.3	470.3	576.5	752	25	398	374	479.4	695	828	897	577	245.5	894
	ex. H_2	0	48	424	316	4.7						0	18	138	107.3	15
	ex. HD						0	76	537	458.7	45	0	10	243	138.2	3
	CID	0	0	0	0	74.3	0	0	0	0	158	0	0	0	0.4	53
< 1.5 Å	n.r.		16	330	373	298.3		55	390	415.7	369	778	809	790	787.1	639
	ex. H_2		0	74	25.8	0						0	0	30	5.2	0
	ex. HD							0	104	62.2	0	0	0	8	0	0
	CID		0	0	0	0		0	0	0	0	0	0	0	0	0
< 2.0 Å	n.r.			1.7	1.7	2.7			0	4.4	3	444	500	207	101.1	16
	ex. H_2			0	0	0						0	0	0	0	0
	ex. HD								0	0	0	0	0	0	0	0
	CID			0	0	0			0	0	0	0	0	0	0	0
< 2.5 Å	n.r.											19	10			
	ex. H_2											0	0			
	ex. HD											0	0			
	CID											0	0			

Table B.2: As in Table B.1, but for H + H_2(5,0), D + H_2(5,0), and H + HD(5,0).

		H + H_2(5,0)					D + H_2(5,0)					H + HD(5,0)				
		6	10	55	110	300	6	10	55	110	300	6	10	55	110	300
< 0.5 Å	n.r.	250	229.3	130.3	134.7	152.3	213.7	179	114.4	79.7	52.7	358	295	163	180	215
	ex. H_2	702.7	750	865	770.3	206.7						227	261	214	232	123
	ex. HD						753	811	882.7	792.3	267	395	431	622	486	39
	CID	0	0	2.6	93.3	641	0	0	1.1	127.3	680.3	0	0	0	102	621
< 1.0 Å	n.r.	254	250.7	194.7	266	436.3	218	207.3	146.2	179.7	325.3	388	308	219	309	488
	ex. H_2	688	720	803.2	555.7	42.3						223	257	245	233	39
	ex. HD						740.7	775.3	852.7	616.7	92.3	365	423	535	330	4
	CID	0	0	0.5	175.3	508	0	0	0.4	202.3	574.3	0	0	0	127	467
< 1.5 Å	n.r.	273	251.3	334.7	435.7	617.3	215.7	207.7	263.3	384.3	548	420	412	452	559	753
	ex. H_2	598.7	666	625.1	327.7	0						230	217	240	192	1
	ex. HD						694.3	736.3	714.5	388.3	1	308	341	290	114	0
	CID	0	0	0	174.7	284.3	0	0	0	201.3	373.3	0	0	0	120	172
< 2.0 Å	n.r.	248.3	277	400.7	419.7	459.3	229	250	413.9	426.7	464	584	580	639	566	503
	ex. H_2	507.3	502.3	308.1	69.3	0						182	198	124	61	0
	ex. HD						592.7	555.7	368.5	105	0	139	123	58	15	0
	CID	0	0	0	132.7	60.7	0	0	0	160.7	110.7	0	0	0	53	27
< 2.5 Å	n.r.	194.7	204.7	136.5	117	61	227.3	250	157	142	91.7	376	17	141	128	68
	ex. H_2	174.7	133.3	23.7	0	0						102	0	29	7	0
	ex. HD						212.7	160.3	32.5	4	0	5	0	0	1	0
	CID	0	0	0	8	0	0	0	0	9	0.3	0	0	0	1	1
< 3.0 Å	n.r.	0.3	0				2.3	0				14		2	0	0
	ex. H_2	0	0									1		0	0	0
	ex. HD						0	0				0		0	0	0
	CID	0	0				0	0				0		0	0	0